Applied Science Dept.

JOURNAL OF THE AERONAUTICAL SCIENCES

VOLUME 23 JANUARY, 1956 NUMBER 1

V. 23. 1956

ST. LOUIS JAN 23 1956 PUBLIC LIBRARY

CONTENTS

A Salute to Hugh L. Dryden 1

The Development of Turbulent Boundary Layers ..... D. A. SPENCE 3

Interaction of a Shock Wave with a Thermal Boundary Layer .. WAYLAND C. GRIFFITH 16

An Investigation on Fully Developed Turbulent Flows in a Curved Channel ..... SALAMON ESKINAZI AND HSUAN YEH 23

Boundary-Layer Measurements in Hypersonic Flow ..... F. K. HILL 35

Some Effects of Viscosity on Wing-Body Interference at $M = 1.9$ ..... T. R. RHEES AND W. P. CRENSHAW 43

Analysis of the Plastic Collapse of a Cruciform Column with Initial Twist, Loaded in Compression ..... J. F. BESSELING 49

System Mode Shapes in the Flutter of Compressor Blade Rows ..... FRANK LANE 54

The Determination of Temperature, Stresses, and Deflections in Two-Dimensional Thermoelastic Problems ..... BRUNO A. BOLEY 67

Compressibility Effects on Secondary Flows ..... H. G. LOOS 76

Readers' Forum 81–96

A600604

Published by

INSTITUTE OF THE AERONAUTICAL SCIENCES, INC.

JOURNAL OF THE AERONAUTICAL SCIENCES

Editor: W. R. SEARS
Director, Graduate School of Aeronautical Engineering, Cornell University

Associate Editor: ROBERT R. DEXTER *Managing Editor:* RITA J. TURINO
Editorial Assistant: CAROLINE TAYLOR

Editorial Committee

Aerodynamics and Fluid Mechanics
Holt Ashley
H. Julian Allen
Dean R. Chapman
Francis H. Clauser
Hugh L. Dryden
John C. Evvard
Antonio Ferri
Alexander Flax
Wallace D. Hayes
R. T. Jones
Carl Kaplan
H. W. Liepmann
C. C. Lin
H. F. Ludloff
Harold Luskin
Clark B. Millikan
C. D. Perkins
H. J. E. Reid
George S. Schairer
G. B. Schubauer
John Stack
Theodore Theodorsen
Arthur N. Tifford
Th. von Karman

Flight Testing
R. R. Gilruth
Melvin N. Gough
W. L. Howland
W. F. Milliken, Jr.

Rotating Wing Aircraft
F. B. Gustafson
K. H. Hohenemser
Bartram Kelley
R. B. Maloy
Ralph McClarren
R. H. Miller
R. H. Prewitt
Igor I. Sikorsky

Structures
John E. Duberg
N. J. Hoff
Samuel Levy
J. F. McBrearty
W. Ramberg
E. E. Sechler
F. R. Shanley
C. R. Strang
S. Timoshenko

Meteorology
C. F. Brooks
D. M. Little
F. W. Reichelderfer
K. C. Spengler

Vibration and Flutter
Lee Arnold
M. A. Biot
R. L. Bisplinghoff
Harold A. Cheilek
I. E. Garrick
Martin Goland

Aircraft Design
W. E. Beall
E. H. Heinemann
Hall L. Hibbard
Richard Hutton
C. L. Johnson
A. A. Kartveli
E. G. Stout
F. K. Teichmann
Robert J. Woods

Electronics
Welcome W. Bender
K. C. Black
M. V. Kiebert, Jr.
David S. Little
S. B. Rogers
Paul Rosenberg
L. M. Sherer

Physiologic Problems
H. G. Armstrong
Louis H. Bauer
Robert J. Benford
W. Randolph Lovelace, II
Ross A. MacFarland

Flight Propulsion
William Bollay
George W. Brady
R. P. Kroon
Frank E. Marble
Abe Silverstein
Martin Summerfield
E. S. Taylor

Instruments
Allan G. Binnie
Charles H. Colvin
Frank R. Cook
C. S. Draper
S. G. Eskin
C. F. Savage
R. C. Sylvander

SUBSCRIPTION RATES

JOURNAL OF THE AERONAUTICAL SCIENCES, Published Monthly.—United States and Possessions: 1 Year, $15.00; Single Copies, $1.50. Foreign Countries Including Canada (American Currency Rates): 1 Year, $16.00; Single Copies, $1.50.

AERONAUTICAL ENGINEERING REVIEW, Published Monthly.—United States and Possessions: 1 Year, $3.00; Single Copies, $0.50. Foreign Countries Including Canada (American Currency Rates): 1 Year, $3.50; Single Copies, $0.50.

Notices of change of address should be sent to the Institute at least 30 days prior to actual change of address.

Manuscripts for publication, proofs, and all correspondence should be addressed to the Editorial Office of the JOURNAL.

Correspondence regarding subscriptions may be addressed to the Editorial Office of the JOURNAL OF THE AERONAUTICAL SCIENCES, 2 East 64th Street, New York 21, N.Y., or to the Publication Office, 20th and Northampton Sts., Easton, Pa.

© *Copyright, 1956, by the Institute of the Aeronautical Sciences, Inc.*

Entered as Second Class Matter at the Post Office, Easton, Pa., May 1, 1937. Acceptance for mailing at a special rate of Postage provided for in the Act of August 24, 1912. Authorized April 29, 1937.

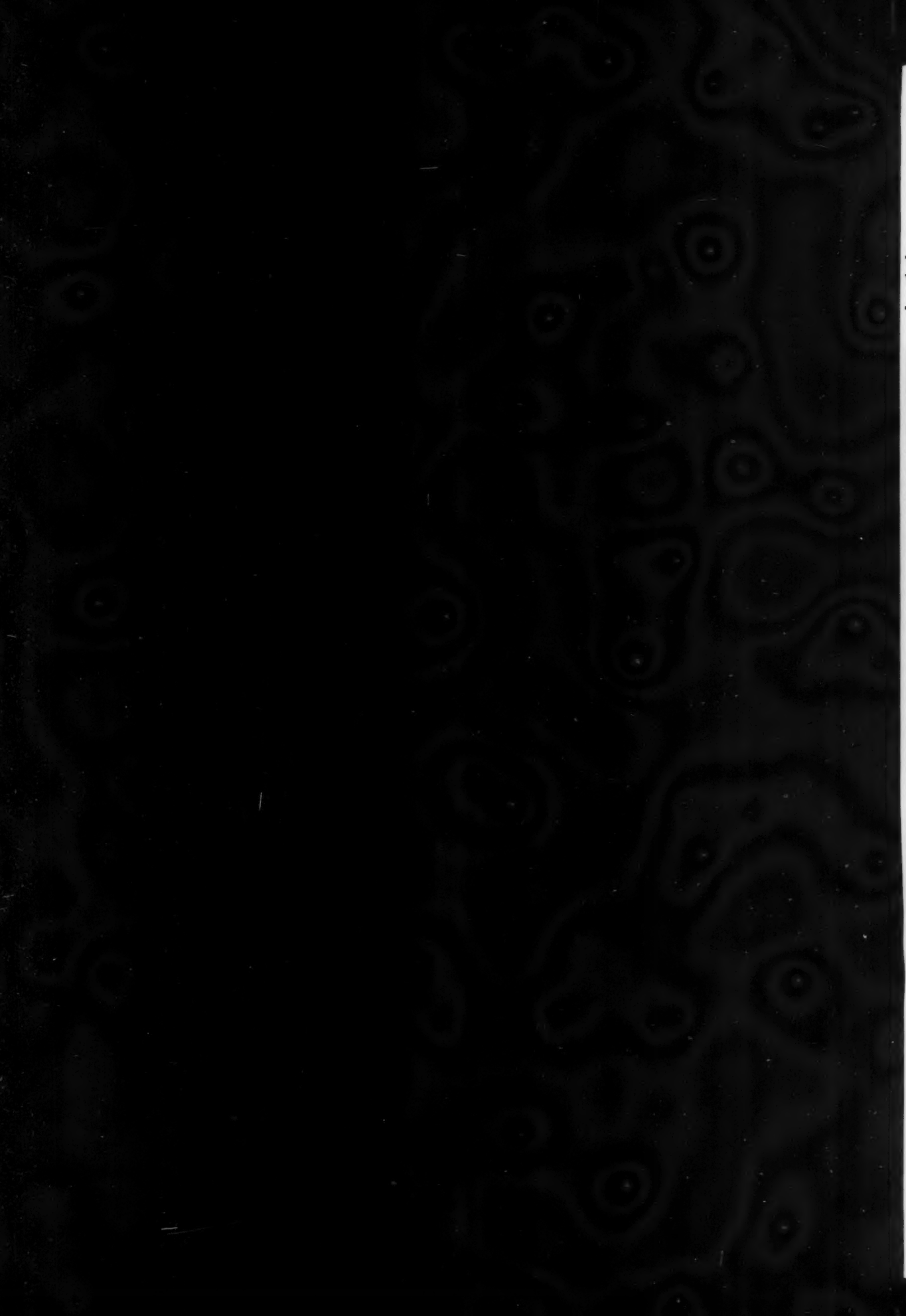

Ref. 629.1
Shelved w. 050

JOURNAL OF THE AERONAUTICAL SCIENCES

VOLUME 23 JANUARY, 1956 NUMBER 1

Hugh L. Dryden, Director of the National Advisory Committee for Aeronautics, served as President of the IAS in 1943. Before joining the NACA in 1947, the noted physicist had been with the National Bureau of Standards 29 years. At the age of 21, he became Chief of its Aerodynamics Section and later was successively Chief of the Mechanics and Sound Division, Assistant Director, and Associate Director.

Born in Pocomoke City, Md., in 1898, Dr. Dryden was graduated from Johns Hopkins University in 1916 and obtained his Ph.D. in physics and mathematics in 1919. He has six honorary degrees. An Honorary Fellow of the IAS and a Fellow of the Royal Aeronautical Society, he delivered the second Wright Brothers Lecture in 1938 and the Wilbur Wright Memorial Lecture of the RAeS in 1949. Recently, Dr. Dryden was named the Wright Brothers Medalist for 1955, having previously been awarded the Daniel Guggenheim Medal in 1950 and the Sylvanus Albert Reed Award in 1940. He was President of the Washington Academy of Sciences in 1946. He has served the U.S. Government on numerous scientific advisory committees, including AGARD, the Scientific Advisory Board of the Air Force, and the Research and Development Board of the Department of Defense. For his aid in developing guided missiles, Dr. Dryden was awarded the Medal for Freedom and the Presidential Certificate of Merit.

A Salute to Hugh L. Dryden . . .

There are many reasons why members of this organization are indebted to the NACA's director. As a Charter Member, a Past President, a long-time Council Member, and an active participant in many IAS affairs, Dr. Dryden has made long and notable contributions to the work of the Institute.

In one area in particular he has left an indelible mark. For the past 15 years, he has been Editor of the JOURNAL OF THE AERONAUTICAL SCIENCES. His sound judgment

and wise guidance in the selection and preparation of its papers for publication have put the JOURNAL in the forefront of the world's scientific publications. He has been assisted by editorial committees in the several technical fields and by a competent staff, but he has been largely responsible for the technical material that has appeared between the familiar blue covers since 1942.

A simple scanning of all the papers that have come to hand in the past 12 years or so would have provided an almost full-time job for an ordinary man. But Dr. Dryden is not an ordinary man. In his deceptively easy-going and quiet way, he runs a wide variety of operations in the national defense network. Outside of NACA, he is an active member of an astounding number of boards and committees. He is U.S. representative to AGARD and seldom misses any important gathering of aeronautical scientists and physicists around the world. And yet, with all his commitments, he has always found time to look over JOURNAL papers, confer with our editors, and correspond with authors on technical questions.

But Hugh Dryden, as a human being, has physical limits. He can handle only so much at a time. A year or more ago, he let us know that he must, of necessity, reduce his total load and asked us to seek a replacement for him on the JOURNAL. We accepted his suggestion with reluctance, but circumstances left us no choice.

Working closely with Dr. Dryden, we have selected a new Editor for the JOURNAL. He has been on our editorial committees for a long time. He has been closely associated with Dr. Dryden on the JOURNAL and in many other capacities. He knows most of our staff people, and he knows how we work. We all feel that the selection of Dr. William Sears of Cornell will pose no transitional problems as he takes over the editorship on January first.

It is with great reluctance that we accept Hugh Dryden's resignation, but we speak for the entire membership in extending to him our thanks for the magnificent job he has done with the JOURNAL. He has set and has maintained a standard of excellence that will be difficult to surpass in the future.

At the same time, we pledge to Dr. Sears the maximum of staff assistance and cooperation as he takes on his new assignment. We anticipate a continuation of JOURNAL activity on the level at which Dr. Dryden has placed it. We look forward to many years of this new relationship.

S. P. J.

This also appeared as an Editorial, Aeronautical Engineering Review, pp. 24, 25, December, 1955.

. . . and a

"Welcome Aboard"

to the new

Editor of the *Journal*

William R. Sears

William R. Sears, FIAS, has been Director of the Graduate School of Aeronautical Engineering at Cornell University since 1946. Born in Minneapolis in 1913, he was graduated from the University of Minnesota in 1934 with a degree in aeronautical engineering and earned his Ph.D. at California Institute of Technology in 1938. From 1934 to 1939, he was a wind-tunnel assistant, instructor, and assistant professor at Caltech. He then joined Northrop Aircraft, Inc., as a consulting engineer and was chief aerodynamicist when he left the company for Cornell. Dr. Sears is a member of the IAS Meetings Committee and the Editorial Committee (Aerodynamics) of the *Journal of the Aeronautical Sciences*. He has served as a member of the USAF Scientific Advisory Board, the Naval Research Advisory Board, and the NACA Subcommittee on Fluid Mechanics.

SEP 13 1957

The Development of Turbulent Boundary Layers

ST. LOUIS PUBLIC LIBRARY SEP 27 1957

D. A. SPENCE*

Cambridge University Aeronautics Laboratory

SUMMARY

The structure of several recently measured sets of velocity profiles in quasi-two-dimensional turbulent boundary layers is examined. It is shown that the inner one-fifth of each profile is well represented, independently of pressure gradient, by the universal logarithmic law that was observed by Ludwieg and Tillmann.[2] An adequate expression for the velocity in the outer four-fifths of the layer is provided by the well-known power law $u/U = (y/\delta)^n$. The significance of the composite type of profile obtained from the two laws is discussed in the light of Townsend's[3] work on the eddy structure of the boundary layer on a flat plate.

The logarithmic expression for velocity is substituted into the equation of motion at height $y = \theta$ from the surface, at which height it is still valid. (θ = momentum thickness.) With an approximation suggested by Schubauer and Klebanoff's[1] measurements for the term that involves shear stress, this leads to an equation for the variation of the form parameter $\gamma = (u/U)_{y=\theta}$. γ is a simple function of the usual parameter $H = \delta^*/\theta$, and the equation could be put into the form

$$\theta(dH/dx) = [-(\theta/U)(dH/dx)]\phi(H) + c_f^{3/2}\psi(H)$$

(c_f = skin-friction coefficient). This is rather similar to the form assumed by von Doenhoff and Tetervin[6] in their semi-empirical investigation in 1943, but c_f occupies a different position.

When used with the momentum equation and a skin-friction relation, the form parameter equation enables one to calculate θ, H, c_f, and the detailed profile shape. Predictions have been found to agree well with experiment. A simple method of step-by-step integration which does not require knowledge of velocity derivatives is outlined, and the effect of variations in initial conditions can be examined rapidly. The ultimate separation point appears to depend rather sensitively on the value of H at transition, but, broadly speaking, the equation predicts separation when the external velocity has fallen to between one-half and two-thirds of its value at transition.

(1) INTRODUCTION

TURBULENT BOUNDARY LAYERS play a governing role in almost all the phenomena of low-speed aerodynamics, and attempts to predict their growth and separation have been made by many workers in the past 20 years. These have for the most part been semi-empirical, the underlying turbulent mechanism being too complicated for exact analysis in the foreseeable future, and despite the work done so far the problem remains very formidable. Nevertheless, one is now able to select a starting point for a mathematical investigation with more physical justification than hitherto, in the light of recently reported experimental investigations on different aspects of the problem by Schubauer and Klebanoff,[1] Ludwieg and Tillmann,[2] and Townsend.[3]

Ludwieg and Tillmann's main conclusion was that approximately the inner one-fifth of the boundary layer (excluding the viscous sublayer) has a velocity profile of logarithmic form, independent of pressure gradient and characterized by the friction velocity $u_\tau = \sqrt{(\tau/\rho)}$ (τ = skin friction). It is shown here that Schubauer and Klebanoff's profiles and others obtained earlier in England by Fage[4] support this law. They also exhibit, in the outer four-fifths of the layer, dependence on the single form parameter H, as had formerly been suggested for the whole of the boundary layer by Gruschwitz[5] and by von Doenhoff and Tetervin.[6] The fundamental work of Townsend on the structure of turbulent shear flows provides a physical picture into which one can fit the composite form that velocity profiles are now seen to have.

It is shown that by substitution of this form into the equation of motion, with a slight further appeal to experiment regarding the distribution of shear stress, an equation is obtained for the variation of the form parameter $H = \delta^*/\theta$. In conjunction with this equation and an expression for skin friction, the momentum integral equation of von Kármán[7] may be solved for the growth of the thicknesses δ^* and θ, and the velocity profiles and separation point can be predicted.

(2) LIST OF SYMBOLS

x, y	= coordinates parallel and normal to surface in plane of free stream
u, v	= mean velocity components in x, y directions
U	= free-stream velocity at edge of boundary layer
p, P	= static pressure inside and at edge of boundary layer
$\overline{u'^2}$, $\overline{u'v'}$	= components of Reynolds stress
μ, ρ, ν	= viscosity, density, kinematic viscosity
τ, τ_w	= shear stress, shear stress at wall
c_f	= local skin-friction coefficient = $\tau_w/(1/2)\rho U^2$
u_τ	= friction velocity = $(\tau_w/\rho)^{1/2}$
δ	= thickness of boundary layer
δ^*	= displacement thickness = $\int_0^\delta \left(1 - \frac{u}{U}\right) dy$
θ	= momentum thickness = $\int_0^\delta \frac{u}{U}\left(1 - \frac{u}{U}\right) dy$
ϵ	= energy thickness = $\int_0^\delta \frac{u}{U}\left(1 - \frac{u^2}{U^2}\right) dy$
R_θ	= Reynolds Number based on momentum thickness = $U\theta/\nu$

Received September 30, 1954.

* Now at the Royal Aircraft Establishment, Farnborough, Hampshire, England.

The author wishes to thank Dr. J. H. Preston for suggesting this work and for much valuable advice; he also wishes to thank Dr. G. K. Batchelor and Prof. H. B. Squire for helpful discussions. An earlier version of the paper was presented as Report No. 14,162 to the Aeronautical Research Council, July, 1951.

y^*, θ^* = yu_τ/ν, $\theta u_\tau/\nu$, respectively
f, F = universal functions for inner and outer parts of velocity profile
H = δ^*/θ } form parameters for velocity profile
γ = $(u/U)_{y=\theta}$ }
Φ, Ψ = functions occurring in form parameter equation
$\phi(H), \psi(H)$ = functions defined in Eq. (48)
A, B = constants in universal logarithmic velocity profile, = 2.5, 5.5, respectively
k = constant defined in Eq. (32)
α = constant defined in Eq. (33)
$Z(k, \gamma)$ = function defined in Eq. (35)
$\chi(\gamma)$ = $1.797\ (1.22 + \gamma)^{1.017}\ (0.82 - \gamma)^{0.683}$ [Eq. (44)]
0 = suffix referring to initial values
$\theta^{(1)}$ = momentum thickness calculated with H constant
$\theta^{(2)}$ = correction to $\theta^{(1)}$ to take account of variation in H
ΔH = $H - H_0$

(3) General Equations

(3.1) *Equation of Motion*

With the coordinate system defined in Section (2), the mean equations of motion and of continuity for steady two-dimensional incompressible flow in the boundary layer on a wall of (zero or) moderate curvature are normally taken as

$$u(\partial u/\partial x) + v(\partial u/\partial y) = U(dU/dx) + (1/\rho)\,(\partial/\partial y)\,[\mu(\partial u/\partial y) - \rho\,\overline{u'v'}] = U(dU/dx) + (1/\rho)(\partial\tau/\partial y) \quad (1)$$

where

$$\tau = \mu(\partial u/\partial y) - \rho\,\overline{u'v'}$$

is the shear stress, and

$$\partial u/\partial x + \partial v/\partial y = 0 \quad (2)$$

The boundary conditions are $u = v = \overline{u'v'} = 0$ at $y = 0$, $u = U(x)$ at $y = \delta(x)$. (δ is a function of x which depends on the solution.)

Quite apart from the complication of nonlinearity, these equations are essentially inadequate, since the relation between the Reynolds stress $-\rho\,\overline{u'v'}$ and the distribution of mean velocity is unknown. Any physical assumption on which a mathematical solution can be based is ultimately a hypothesis regarding this unknown relation.

(3.2) *Momentum, Skin-Friction, and Form Parameter Equations*

Integrating Eq. (1) with respect to y from 0 to δ, we obtain

$$d\theta/dx + (H + 2)\,(\theta/U)\,(dU/dx) = \tau_w/\rho U^2 \quad (3)$$

where θ, H, τ_w are as defined in Section (2). This is von Kármán's momentum-integral equation. If the boundary-layer approximations are refined to take account of transverse pressure variations and of the Reynolds stress $\overline{u'^2}$ which occurs in the full equations of motion, one must add to the right-hand side of Eq. (3) the terms

$$-\frac{1}{\rho U^2}\frac{d}{dx}\int_0^\delta (P - p)\,dy, \qquad \frac{1}{U^2}\frac{d}{dx}\int_0^\delta \overline{u'^2}\,dy \quad (4)$$

respectively (where P, p are the static pressures at the edge of and inside the boundary layer). Except near separation or in regions of large surface curvature, these may safely be neglected.

Two auxiliary equations between θ, H, and c_f are required in the solution of Eq. (3):

(a) A skin-friction relation of the type

$$c_f = f(R_\theta, H) \quad (5)$$

for which Squire and Young[8] have given the equation

$$c_f = 2\,(3.59 + 2.56 \log_e R_\theta)^{-2} \quad (6)$$

(which does not depend on H); and for which Ludwieg and Tillmann[2] have given the equation

$$c_f = 0.246\ (10)^{-0.678H}\ (R_\theta)^{-0.268} \quad (7)$$

(b) A form parameter relation for the variation of H. Most recent workers have attempted to find such a relation in the form

$$\theta(dH/dx) = [-(\theta/U)\,(dU/dx)]\,\Phi - \Psi \quad (8)$$

where Φ and Ψ depend on H and c_f and are both positive. Φ represents the tendency of the boundary layer toward separation in an adverse pressure gradient, and Ψ corresponds to flow on a flat plate without pressure gradient.

Forms for Φ and Ψ were found empirically by von Doenhoff and Tetervin:[6]

$$\left.\begin{aligned}\Phi &= e^{4.68(H-2.975)}\,c_f^{-1}\\ \Psi &= -2.035\,(H - 1.286)e^{4.68(H-2.975)}\end{aligned}\right\} \quad (9)$$

A slight modification of their equation was given later by Garner.[9] At this stage c_f was assumed to depend only on R_θ, but more recently Zaat[10] and Maskell[11] have produced modifications that take into account the extra dependence of c_f on H as found by Ludwieg and Tillmann.†

† *Energy Equation*

Another approach due to Tetervin and Lin[17] uses the energy equation

$$\frac{d\epsilon}{dx} + \frac{3\epsilon}{U}\frac{dU}{dx} = \frac{2}{\rho U^2}\int_0^\delta \frac{u}{U}\frac{\partial\tau}{\partial y}\,dy$$

[where ϵ is the energy thickness defined in Section (2)]. This is the second ($m = 0$, $n = 1$) of a series of relations obtained by multiplying the equation of motion [Eq. (1)] by $y^m u^n$ before integrating with respect to y from 0 to δ. The first ($m = n = 0$) is the momentum equation. The assumption of a power law for the velocity profile—which is shown in the next section to be inadequate—reduces the energy equation to the form (8) and concentrates the remaining empiricism into the integral on the right-hand side. Tetervin and Lin were unable to find a satisfactory expression for τ from theoretical reasoning, but a form for Eq. (8) has since been derived on somewhat similar lines by Rubert and Persh,[18] using Schubauer and Klebanoff's measurements. More recently Rotta[19] has also published an energy equation method, which like the present paper uses both "inner" and "outer" laws for velocity distribution, and it appears very promising.

The form parameter equations derived by these authors give reasonable agreement with the data from which they were derived, but one must make two reservations in regard to their somewhat empirical approach. Firstly, the forms chosen for Φ and Ψ may omit parameters that become significant only outside the Reynolds Number range covered by the data. Secondly, too much weight may have been attached to the values of H which were correlated. The value obtained from a measured velocity profile is fairly sensitive to errors in profile shape, especially when these occur close to the wall (where, moreover, measurements are least certain). In this paper no attempt is made to correlate measured values of H and dH/dx, but instead the form parameter equation is based on experimental knowledge of the velocity profile itself.

(4) Velocity Profiles

(4.1) *Functional Form of Profiles*

Turbulent velocity profiles typically show a sharp rise close to the wall which gives way abruptly to a more gradual rise through the outer four-fifths of the boundary layer. It had been argued from their similar appearance that they approximate to a one-parameter family, which could be written

$$\frac{u}{U} = F\left(\frac{y}{\theta}, H\right) \tag{10}$$

F being a universal function common to all boundary layers, θ the momentum thickness (chosen for this representation rather than the total thickness δ because its value is more precise), and H the form parameter δ^*/θ. Other characteristics of the velocity profile can of course be used instead of H for the second argument of F; in this paper it proves to be more convenient in deriving the form parameter equation [Section (5)] to use the parameter

$$\gamma = (u/U)_{y=\theta} = F(1, H) \tag{11}$$

which was defined by Ludwieg and Tillmann. (A similar parameter $\eta = 1 - \gamma^2$ was used by Gruschwitz[5]). Recently, however, Clauser[21] has obtained results that cast some doubt on the universality of Eq. (10).

Von Doenhoff and Tetervin[6] and Schubauer and Klebanoff have obtained experimentally sets of curves of u/U against H for $y/\theta = 1/2, 1, 2, \ldots$ which support the use of Eq. (10). Both sets of curves have been found by the author to agree very closely with the power law interpolation.

$$u/U = (y/\delta)^n \tag{12}$$

for which

$$\theta/\delta = n/(n+1)(2n+1) \tag{13}$$

$$H = 2n + 1 \tag{14}$$

$$\gamma = [(H-1)/H(H+1)]^{(1/2)(H-1)} \tag{15}$$

and the velocity profile in the form (10) becomes

$$u/U = \gamma(y/\theta)^{(1/2)(H-1)} \tag{16}$$

In Fig. 1 the justification for using the expression (15) for γ is demonstrated by plotting it against H together with a large number of experimental values of $(u/U)_{y=\theta}$. Equally good experimental agreement could be shown for the corresponding curves with $y = 2\theta, 3\theta, \ldots$.

However Ludwieg and Tillmann's measurements made in the turbulent region closest to the wall show that this representation is not adequate for the whole boundary layer. They found that profiles just outside the laminar sublayer could be written

$$u/u_\tau = A \log (yu_\tau/\nu) + B \tag{17}$$

independently of the pressure gradient existing in the outside stream. Here $u_\tau = \sqrt{\tau/\rho}$ is the friction velocity, and the constants A, B have values previously observed in the boundary layer on a flat plate—namely,

$$A = 2.5, \quad B = 5.5 \tag{18}$$

Independent verification of this law from two published sets of data is described in Section (4.3).

In the laminar sublayer itself the profile may be written

$$u/u_\tau = yu_\tau/\nu \tag{19}$$

since $\rho u_\tau^2 = \mu(\partial u/\partial y)_{y=0}$. The junction between the regions of linear and of logarithmic velocity is given approximately by the equation

$$u/u_\tau = y^* = 2.5 \log y^* + 5.5 \tag{20}$$

($y^* = yu_\tau/\nu$) whose roots are $y^* = 0.1, 11.7$. The larger is appropriate since it corresponds to $\partial^2 u/\partial y^2 < 0$—i.e., to a region in which the viscous shear stress $\mu(\partial u/\partial y)$ is decreasing.†

In practice the transition from laminar to turbulent flow takes place through an intermediate layer in which the profile may be expected to be expressible in the same functional form as both Eqs. (17) and (19)—namely,

$$u/u_\tau = f(y^*) \tag{21}$$

where f is a universal function. Thus in the inner part of the boundary layer there exists a dynamical similarity characterized by conditions at the wall and independent of pressure gradient. This is of a different kind from the similarity expressed by Eq. (10). Figure 2 shows several sets of data plotted logarithmically in this universal form, and in Fig. 3 the composite nature of some velocity profiles obtained by Brebner and Bagley[12] is illustrated by plotting experimental points together with the "inner" and "outer" analytic expressions. The slight discrepancy in the fit in the outer part of each profile would be overcome if the exponent of the power law were chosen so as to make H for the complete interpolated profile agree with the

† This agrees with a criterion given by Fediaveski,[20] that at the outer edge of the laminar sublayer u and y should correspond to a critical Reynolds Number somewhere between 100 and 150. Taking $y^* = 11.7$,

$$uy/\nu = (u/u_\tau)(u_\tau y/\nu) = (11.7)^2 = 137$$

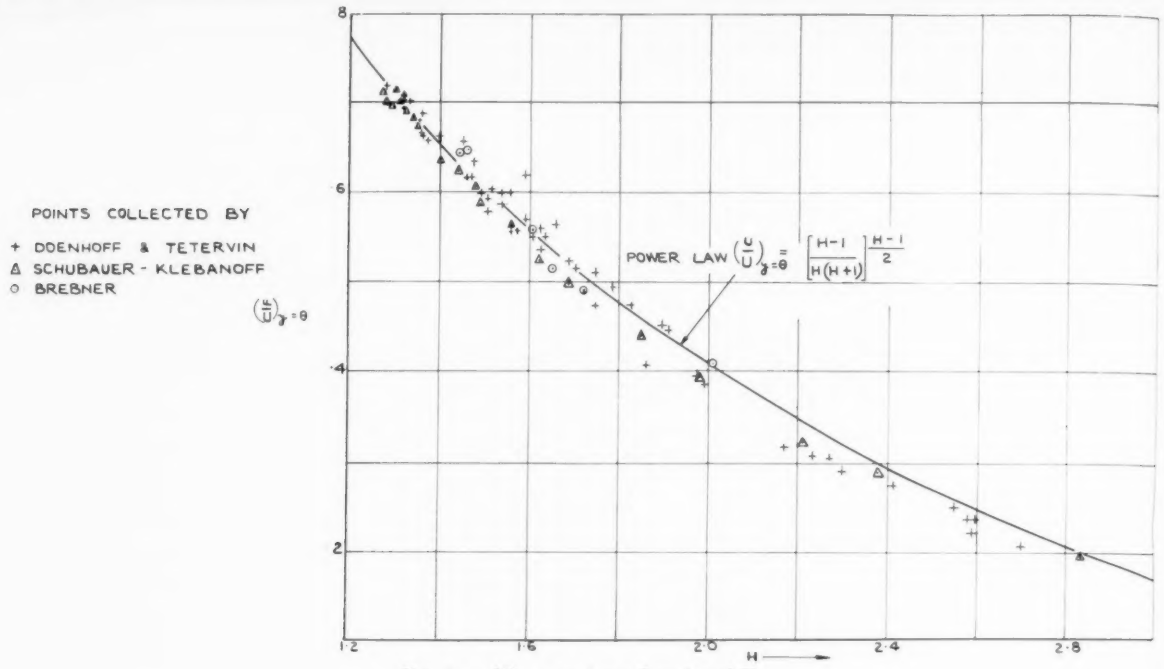

FIG. 1. u/U at $y = \theta$ as a function of H.

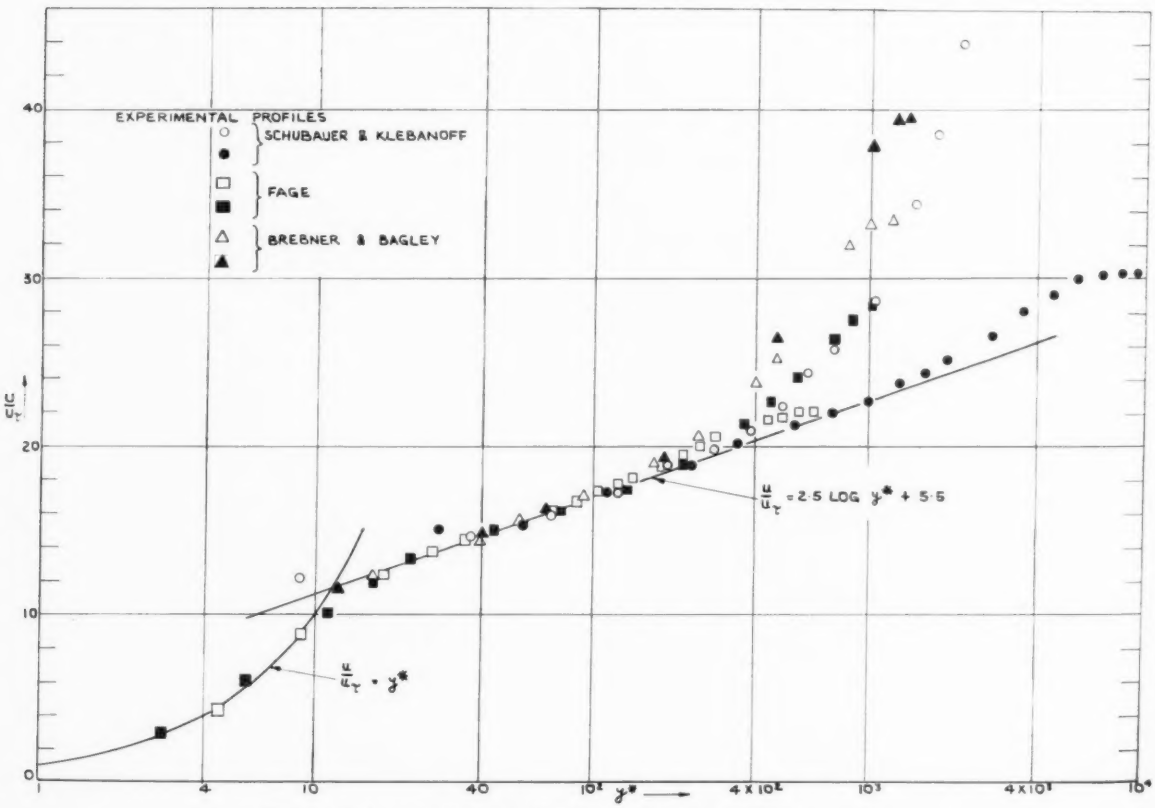

FIG. 2. Universal velocity profile $u/u_\tau = f(y^*)$ plotted logarithmically.

EXPERIMENTAL POINTS.	$\frac{x}{c}$	$10^3 \times \frac{\theta}{c}$	H	$\frac{U_\tau}{U_0}$
◁	·400	2·491	1·474	·0445
▷	·795	3·939	1·655	·0285
▽	·951	5·369	2·009	·0155

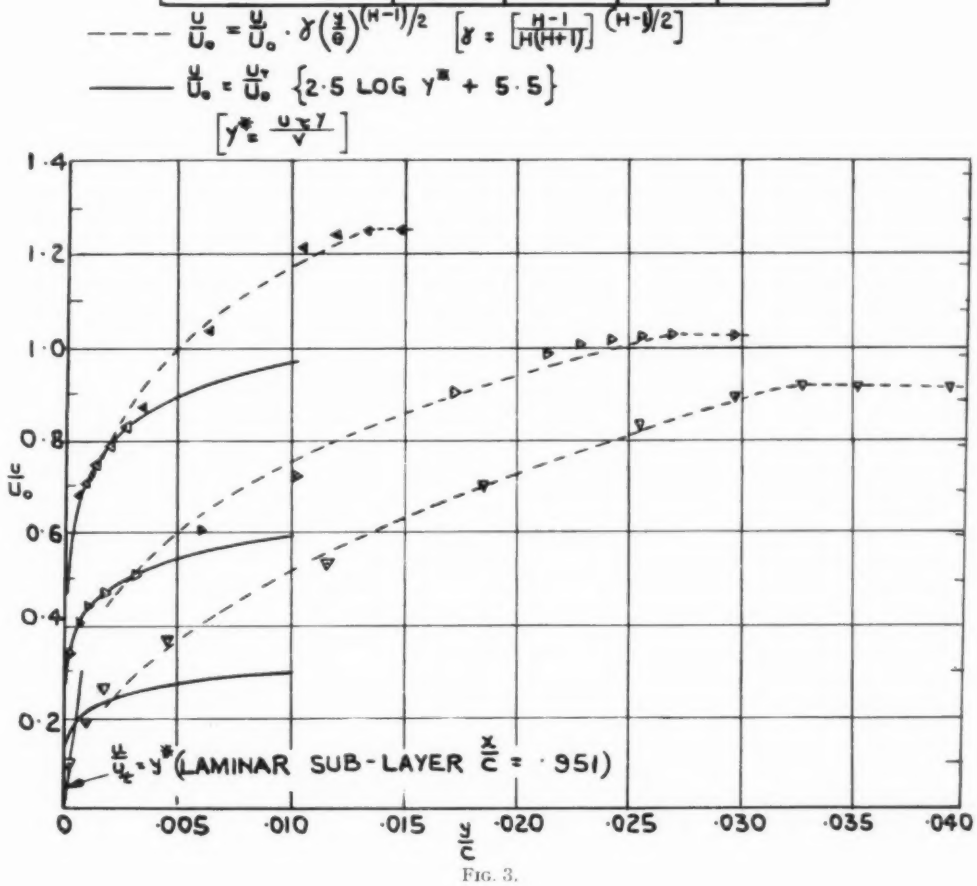

FIG. 3.

experimental value $H_{exp.}$—i.e., if it were slightly higher than (1/2) ($H_{exp.}$ − 1) which has been used.

(4.2) *Eddy Structure of the Boundary Layer*

A tentative interpretation of the two velocity distribution laws [Eqs. (10) and (20)] is possible in the light of Townsend's[3] model of the flow in a boundary layer without longitudinal pressure gradient. The turbulent motion in that case falls into eddy systems of successively diminishing size and increasing wave number. From the mean flow energy is transferred to the largest system of eddies, which occupies the outer part of the boundary layer and is responsible for the entrainment of new fluid by which the boundary layer spreads. From this system energy is transferred to the system the next order of magnitude smaller and so on until ultimately it is dissipated close to the wall by very small scale eddies. One might guess that in the pressure gradient case Eq. (10) describes the velocity profile in the part of the boundary layer in which the largest scale eddies predominate, since these are most directly related to the main flow. U is then an appropriate representative velocity, and δ might be interpreted as a length scale characteristic of the largest eddies. The equation takes account of the upstream history of the layer by means of the form parameter H, which must therefore play a part in determining the geometrical structure of the largest eddy system.

The universal form of Eq. (20), on the other hand, suggests dynamical similarity of the turbulent motion in the inner part of the boundary layer, where the flow is strongly influenced by the presence of the wall. For this region, Townsend found that length scales derived from the eddy viscosity and the local turbulent intensity were comparable with distance from the wall. u_τ is then an appropriate representative velocity, and yu_τ/ν is a measure of dimensionless distance from the wall. (u_τ is of course indirectly determined by the up-

EXPERIMENTAL POINTS	x (FEET)	$\frac{u_\tau}{U}$
⊕	17·5	·033
▽	19·5	·0305
+	21·5	·0255
△	23·5	·020
⊥	24·5	·0145
×	25·4	·0095

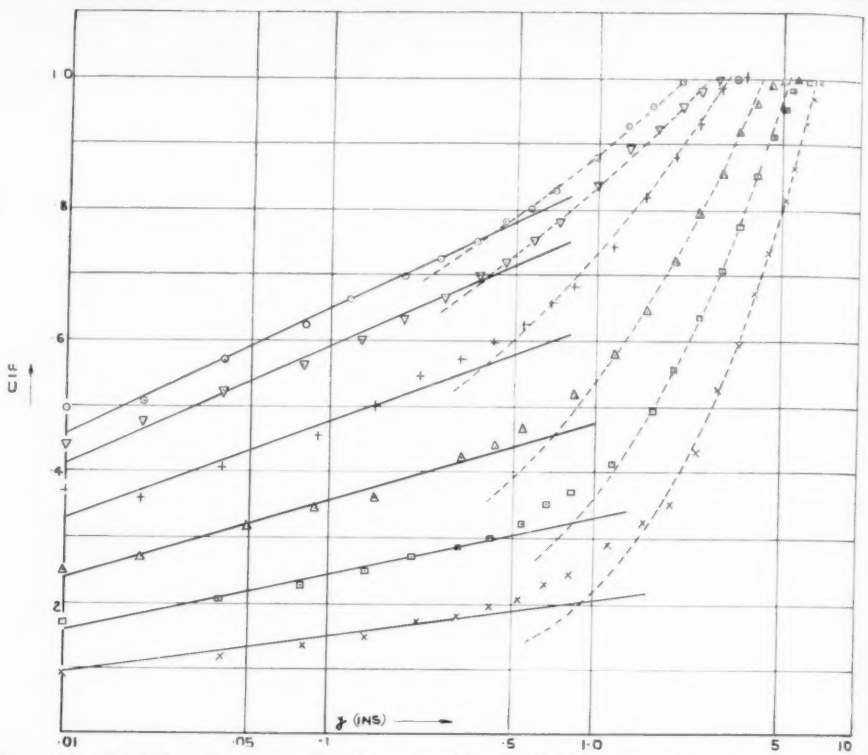

FIG. 4. Schubauer-Klebanoff velocity profiles plotted logarithmically. Solid lines are $u/U = (u_\tau/U)(A \log y^* + B)$. Broken lines are power laws.

EXPERIMENTAL POINTS	$\frac{x}{c}$	$\frac{u_\tau}{U_0}$
▽	·403	·054
+	·504	·049
○	·605	·045
×	·706	·0425
△	·807	·0385
□	·956	·0335

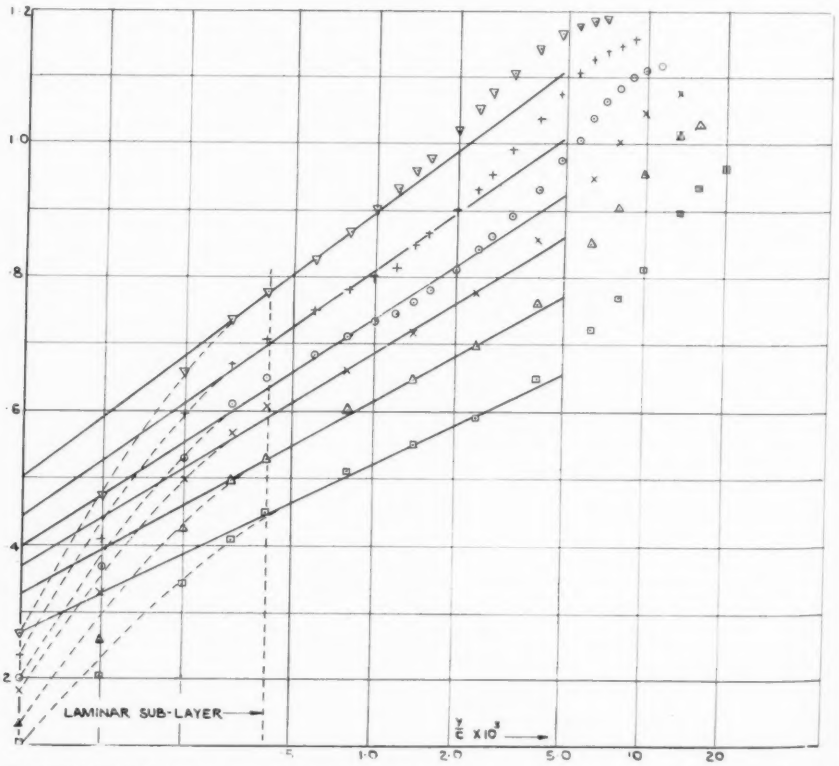

FIG. 5. Fage's velocity profiles plotted logarithmically ($U_0 c/\nu = 1.67 \times 10^6$). Solid lines are $u/U_0 = (u_\tau/U_0)(A \log y^* + B)$.

stream history of the layer and, in turn, influences indirectly the outer part of the layer further downstream.)

(4.3) *Verification of Logarithmic Law in a Pressure Gradient*

Two sets of velocity profiles not used by Ludwieg and Tillmann have been plotted logarithmically to examine the validity of their expression (17) in strong pressure gradients. These were obtained (a) by Schubauer and Klebanoff[1] in 1950 at the Bureau of Standards and (b) by Fage[4] in 1930 at the National Physical Laboratory. In each case it was found that the profiles could be well fitted for some distance out from the wall, by members of the family of lines

$$u/U = (u_\tau/U)\left\{2.5 \log\left[(u_\tau/U)\,(Uy/\nu)\right] + 5.5\right\} \quad (22)$$

which is characterized by the single parameter u_τ/U. The results are shown in Figs. 4 and 5, respectively, exponential curves corresponding to power law velocity distributions in the outer part of the layer also being shown in Fig. 4. The points closest to the wall in this figure tend to lie above the straight lines. This may be due to the fact that the velocities were not corrected either for the displacement of the effective center of the pitot tube or for turbulence. The measurements did not reach into the laminar sublayer since the Reynolds Number was above 10^7. In Fage's measurements at a lower Reynolds Number the sublayer is easily recognized.

(4.4) *Skin Friction*

The examples given in Section (4.3) have shown it possible to obtain values for u_τ/U, regarded simply as a parameter, for which Eq. (22) adequately describes the inner velocity profiles. However the precise relation of the values thus obtained to the skin-friction coefficient remains to be demonstrated. It is well established that for boundary layers on flat plates this relation is

$$\tau_w = \rho\, u_\tau^2 \quad (23)$$

and indeed theoretical arguments have been given to explain this in terms of the mixing length $l = 0.4y$(e.g., reference 13).

However these assume the shear stress to be constant across the relevant part of the boundary layer. This is certainly not the case when there is a longitudinal pressure gradient,† for by putting $y = 0$ in the equation of motion (1) we obtain

$$(\partial\tau/\partial y)_{y=0} = -\rho U(dU/dx) \quad (24)$$

Nevertheless, the available evidence seems on the whole to support the hypothesis that u_τ is related to skin friction by Eq. (23) as before. This would be expected from the argument of Section (4.2). The difficulty in confirming it is that none of the velocity profiles were obtained in conjunction with an entirely reliable method of measuring skin friction. Ludwieg and Tillmann used a heat-transfer method, but direct force measurements would be more desirable.

Figures 6 and 7 show the skin friction obtained by means of Eq. (23) from the u_τ/U values which fit the velocity profiles of references 1 and 4, together with values obtained (a) by evaluation of the terms on the left-hand side of the momentum equation (3), (b) from the skin-friction formulas (6) and (7), and (c) by measurement.

With the momentum equation, discrepancies occur close to separation. Clauser[21] has shown that these may be due to three-dimensional effects; in addition, the extra terms [Eq. (4)] are no longer negligible. The Ludwieg-Tillmann formula gives good agreement throughout, but the Squire-Young formula, since it has no form parameter dependence, does not predict the decrease in skin friction close to separation. Of the direct measurements, Fage's (Fig. 7) made with a Stanton tube in the sublayer, give good agreement, but the measurements in Fig. 6 lie considerably above the curves otherwise derived. Schubauer and Klebanoff deduced c_f by a steep extrapolation from rather scattered and probably high measurements of $\overline{u'v'}$, some of which are shown in Fig. 8, and it seems possible that the discrepancy could be completely explained by the inherent uncertainties in the method.

(5) Form Parameter Equation

Using the information on velocity profiles presented in the previous section, an equation for the variation of the form parameter γ in an adverse pressure gradient may now be derived by formulating the equation of motion at height $y = \theta$. At this height the logarithmic representation [Eq. (17)] is still valid; the only awkward term is the shear stress gradient $(\partial\tau/\partial y)_{y=\theta}$, but this is relatively small and may be dealt with by an approximation suggested by Schubauer and Klebanoff's measurements of $-\overline{u'v'}$. The equation for γ which is obtained is equivalent to an equation for H because of the relation (15).

Near the wall $u = u_\tau f(y^*)$. Writing for convenience $df/dy^* = f'$, $du_\tau/dx = u_\tau'$,

$$\partial u/\partial x = u_\tau' f + (yu_\tau/\nu)u_\tau' f' = u_\tau'(f + y^* f')$$

$$\partial u/\partial y = (u_\tau^2/\nu)f'$$

By continuity $\partial u/\partial x = -\partial v/\partial y$; moreover $v = 0$ when $y = 0$ so that

$$v = -u_\tau' \int_0^y (f + y^* f')\, dy$$

$$= -\frac{u_\tau' \nu}{u_\tau} \int_0^{y^*} (f + y^* f')\, dy^*$$

Therefore

† Even for a flat plate, if the profile (22) is substituted into the equation of motion [Eq. (1)], one finds that $\partial\tau/\partial y$ is proportional to du_τ/dx, which is always negative. Mixing length theories in any case are no longer generally accepted.

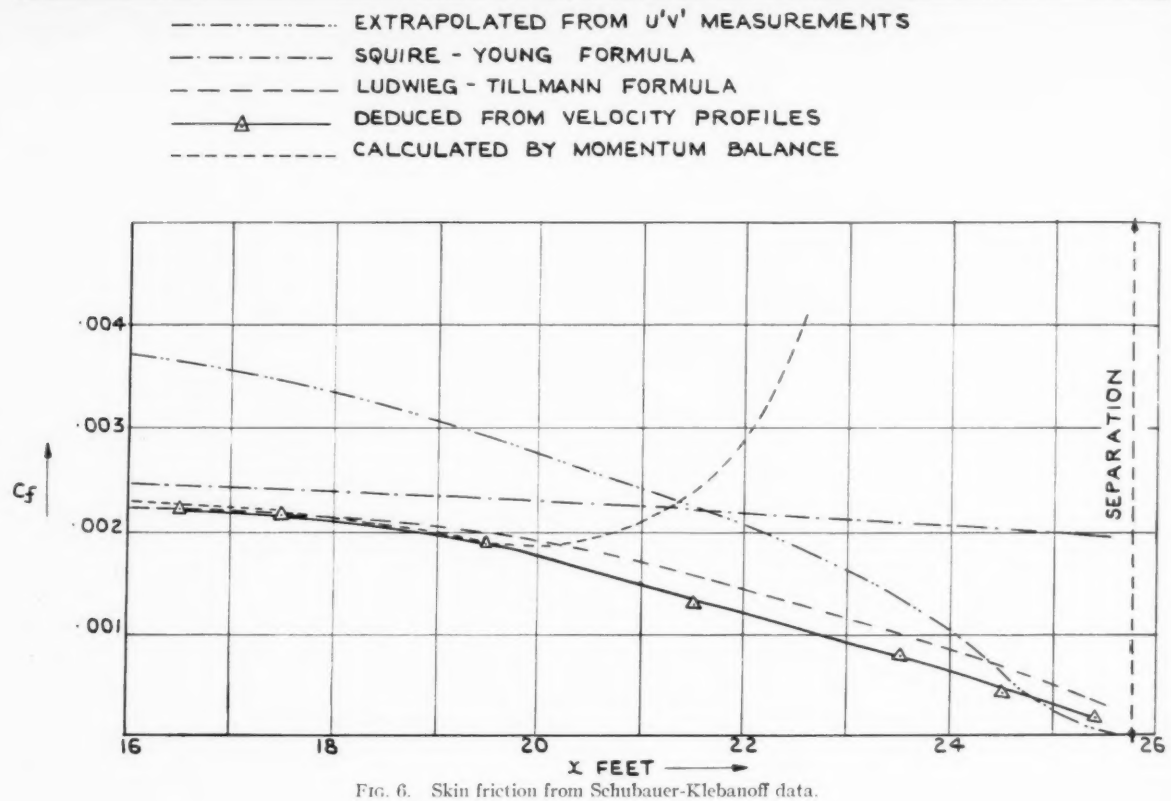

FIG. 6. Skin friction from Schubauer-Klebanoff data.

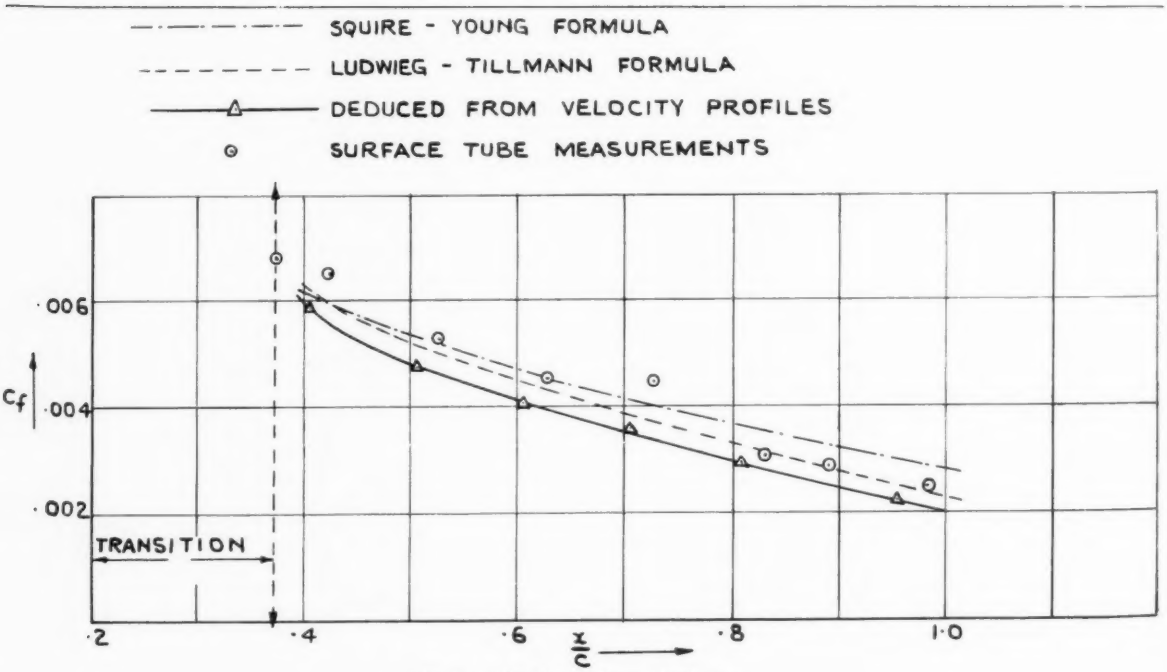

FIG. 7. Skin friction from Fage's data.

$$u\frac{\partial u}{\partial x} + v\frac{\partial u}{\partial y} = u_\tau u_\tau' \times \left[f(f + y^* f') - f' \int_0^{y^*} (f + y^* f')\, dy^* \right]$$

Integrating the last term by parts and using $f(0) = 0$, the expression reduces to

$$u(\partial u/\partial x) + v(\partial u/\partial y) = u_\tau u_\tau' f^2(y^*) \qquad (25)$$

At height $y = \theta$ Eq. (1) thus becomes

$$u_\tau u_\tau' f^2(\theta^*) = U(dU/dx) + (\partial/\partial y)(\tau/\rho)_{y=\theta} \qquad (26)$$

We now calculate the term on the left-hand side of Eq. (26). $f(\theta^*)$ is found from the relation

$$\gamma = (u_\tau/U) f(\theta^*) \qquad (27)$$

which is obtained by putting $y = \theta$ in Eq. (21), and $u_\tau \div u_\tau$ is found by differentiating with respect to x the equivalent relation

$$\gamma = (u_\tau/U)[A \log (u_\tau\theta/\nu) + B] \qquad (28)$$

where, as before, $A = 2.5$, $B = 5.5$. (Here $\gamma' = d\gamma/dx$, $\theta' = d\theta/dx$.) This gives

$$\left(1 + \frac{Au_\tau}{\gamma U}\right)\frac{u_\tau'}{u_\tau} = \frac{\gamma'}{\gamma} + \frac{U'}{U} - \frac{Au_\tau}{\gamma U}\frac{\theta'}{\theta} \qquad (29)$$

In practice the term $Au_\tau/\gamma U \ll 1$ and may be neglected in the parentheses on the left. The term θ'/θ is found from the momentum equation (3), divided throughout by θ:

$$\theta'/\theta = (1/\theta)(u_\tau/U)^2 - (H + 2)(U'/U) \qquad (30)$$

and altogether Eq. (26) may be written

$$\gamma\gamma' - \frac{A\gamma}{\theta}\left(\frac{u_\tau}{U}\right)^3 = \frac{U'}{U}\left[1 - (H+2)\frac{Au_\tau}{U}\gamma - \gamma^2\right] + \frac{\partial}{\partial y}\left(\frac{\tau}{\rho U^2}\right)_{y=\theta} \qquad (31)$$

To simplify this equation empirically, two slowly varying quantities may be replaced by constants to be fitted from experimental results:

(a) $(H + 2)$ increases while u_τ/U decreases, and we write

$$(H + 2)A(u_\tau/U) = 2k \qquad (32)$$

where k is a constant of the order of 0.1 or 0.2.

(b) $(\partial/\partial y)\ [\tau/(\rho U^2)]_{y=\theta}$ is a small fraction of $-(1/U)\ (dU/dx)$ which is the gradient of $\tau/(\rho U^2)$ at $y = 0$, as may be seen from the shear stress profiles in the Schubauer-Klebanoff boundary layer (Fig. 8). However as x increases and with it H and the quantity $(1 - 2k\gamma - \gamma^2)$, the gradient of $\tau/\rho U^2$ at $y = \theta$ becomes a progressively larger fraction of $-(1/U)\ (dU/dx)$, and we write empirically

$$(\partial/\partial y)\ [\tau/(\rho U^2)]_{y=\theta} = -\alpha(1 - 2k\gamma - \gamma^2)\ (U'/U) \qquad (33)$$

where α is a constant to be found from experiment.

With these approximations Eq. (31) becomes

$$(1 - \alpha)\ (U'/U) - [(\gamma\gamma')/(1 - 2k\gamma - \gamma^2)] = -[\gamma/(1 - 2k\gamma - \gamma^2)]\ (A/\theta)\ (u_\tau/U)^3 \qquad (34)$$

Solution of Eq. (34) involves the following function:

$$Z(k, \gamma) = [(1 + k^2)^{1/2} + (k + \gamma)]^{(1+k^2)^{1/2}+k} \div [(1 + k^2)^{1/2} - (k + \gamma)]^{(1+k^2)^{1/2}-k} \qquad (35)$$

Differentiating logarithmically

$$(1/Z)\ (dZ/d\gamma) = -2(1 + k^2)^{1/2}\ [\gamma/(1 - 2k\gamma - \gamma^2)] \qquad (36)$$

Thus Eq. (34) may be written

$$\frac{1}{2(1 + k^2)^{1/2}}\frac{1}{Z}\frac{dZ}{dx} + (1 - \alpha)\frac{1}{U}\frac{dU}{dx} = -\frac{\gamma}{1 - 2k\gamma - \gamma^2}\frac{A}{\theta}\left(\frac{u_\tau}{U}\right)^3 \qquad (37)$$

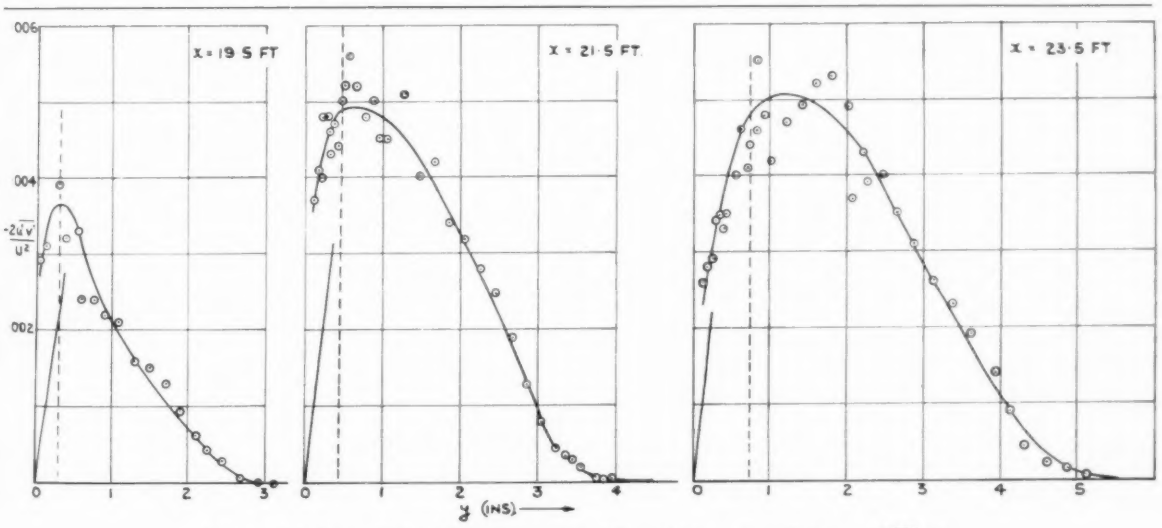

FIG. 8. Schubauer-Klebanoff measurements of Reynolds' stress coefficient $-2\overline{u'v'}/u^2$.

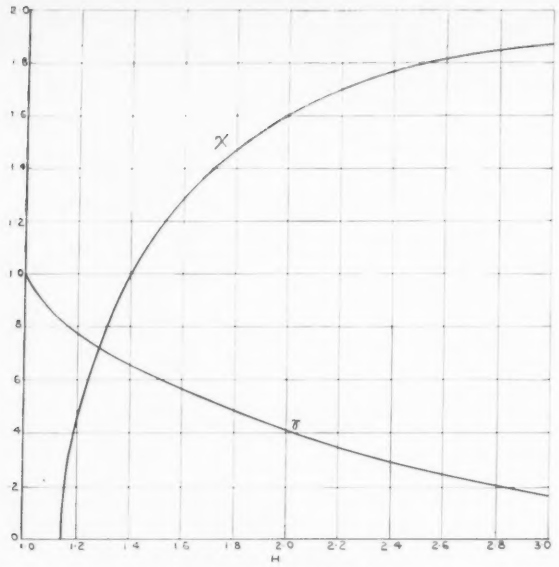

FIG. 9. γ [Eq. (15)] and χ [Eq. (44)] plotted as functions of H.

(5.1) *Evaluation of k, α*

At this stage it is convenient to fit the constants k, α from experiment. To do this we consider cases in which the right-hand side of Eq. (37) is small compared with either of the terms on the left-hand side. These correspond to cases where the same is true of the momentum equation (3)—i.e., to strong adverse pressure gradients in which the turbulent layer has had some distance to develop beyond transition so that $1/\theta$ is not too large. The solution of Eq. (37) may then be written

$$U^n Z = \text{constant} \tag{38}$$

where

$$n = 2(1 + k^2)^{1/2}(1 - \alpha) \tag{39}$$

The relation (38) was therefore tested for $k = 0, 0.05, \ldots, 0.25$ by plotting experimental values of $\log Z$ (which may be computed as a function of H) against $\log U$ for a large amount of data obtained from references 1, 5, 6, and 15. For each value of k approximately parallel lines resulted for all the data in regions sufficiently far from transition. The slope of these lines gave the power n, which depended on the particular k. The values ultimately chosen were $k = 0.2$, $n = 2.4$, ($\alpha = -0.18$) although a virtually identical result would be obtained from $k = 0.05$, $n = 1.8$, and the latter might, on physical grounds, seem more probable since it corresponds to $\alpha > 0$.

(5.2) *Solution of Eq. (37) with k = 0.2, α = −0.18*

To solve the full Eq. (37), we find K, m such that

$$\gamma/(1 - 2k\gamma - \gamma^2) \doteqdot K Z^m \tag{40}$$

over the relevant range of H, which is about 1.3 to 1.8 ($\gamma = 0.4$ to 0.7). With $K = 0.625$, $m = -5/3$, Eq. (40) is accurate to within 3 or 4 per cent, and with this approximation Eq. (37) may be written (using $A = 2.5$)

$$(5/12)(1/Z)(dZ/dx) + (1/U)(dU/dx) = -1.328\, Z^{-5/3}(1/\theta)(u_\tau/U)^3 \tag{41}$$

$4\, U^4 Z^{5/3}$ is an integrating factor, and the equation is

$$(d/dx)(U^4 Z^{5/3}) = -5.312(U^4/\theta)(u_\tau/U)^3 \tag{42}$$

Integrating Eq. (42) with respect to x, from a point $x = 0$ where $Z = Z_0$, $U = U_0$, and using a nondimensional velocity $\bar{U} = U/U_0$

$$\bar{U}^4 Z^{5/3} = Z_0^{5/3} - 5.312 \int_0^x \frac{\bar{U}^4}{\theta}\left(\frac{u_\tau}{U}\right)^3 dx \tag{43}$$

This may be put into a slightly neater form by defining a function

$$\chi = 1.797\, Z^{5/6} = 1.797\,(1.22 + \gamma)^{1.017}(0.82 - \gamma)^{0.683} \tag{44}$$

The constant 1.797 has been chosen so that $\chi = 1$ when $H = 1.4$, which is a typical starting value for turbulent boundary-layer calculations. χ and γ are shown as functions of H in Table 1 and in Fig. 9.

In terms of χ, Eq. (43) becomes

$$\bar{U}^4 \chi^2 = \chi_0^2 - 17.16 \int_0^x \frac{\bar{U}^4}{\theta}\left(\frac{u_\tau}{U}\right)^3 dx \tag{45}$$

or, when the integral on the right is small enough

$$\bar{U}^2 \chi = \chi_0 - \frac{8.58}{\chi_0}\int_0^x \frac{\bar{U}^4}{\theta}\left(\frac{u_\tau}{U}\right)^3 dx \tag{46}$$

In particular for $H_0 = 1.4$

$$\bar{U}^2\chi = 1 - 8.58\int_0^x \frac{\bar{U}^4}{\theta}\left(\frac{u_\tau}{U}\right)^3 dx \tag{47}$$

The general form parameter equation [Eq. (45)], or the special form [Eq. (46) or (47)], may now be solved in conjunction with the momentum equation (3) and a skin-friction relation to give θ, H, and c_f. In the next section a procedure for this solution is described.

In passing it may be noted that the basic differential equation [Eq. (41)] is in fact of the expected form (8),

TABLE 1

H	γ	$\gamma^{1.705}$	χ
1.0	1.000	1.000	
1.1	0.855	0.765	
1.2	0.773	0.646	0.452
1.3	0.708	0.555	0.783
1.4	0.653	0.483	1.000
1.5	0.604	0.424	1.161
1.6	0.559	0.370	1.288
1.7	0.518	0.326	1.391
1.8	0.479	0.284	1.477
1.9	0.443	0.249	1.548
2.0	0.408	0.217	1.608
2.1	0.376	0.189	1.660
2.2	0.346	0.162	1.703
2.3	0.318	0.142	1.742
2.4	0.291	0.122	1.769
2.5	0.267	0.105	1.795
2.6	0.243	0.089	1.818
2.7	0.222	0.077	1.835
2.8	0.202	0.065	1.848
2.9	0.184	0.056	1.860
3.0	0.167	0.048	1.870

since Z may be written as a function of H only, and

$$dZ/dx = (dZ/dH)\,(dH/dx)$$

If the functions

$$\left.\begin{aligned}\phi(H) &= 2.4\,Z/(dZ/dH)\\ \psi(H) &= 3.187\,Z^{-2/3}/(dZ/dH)\end{aligned}\right\} \quad (48)$$

are defined, the equations may be written

$$\theta(dH/dx) = [-(\theta/U)\,(dU/dx)]\phi(H) - c_f{}^{3/2}\psi(H) \quad (49)$$

Z is an increasing function of H, so dZ/dH is positive and ϕ and ψ are positive, as expected.

(6) Procedure for Numerical Solution

For a given velocity distribution the momentum equation and Eq. (45), in conjunction with a relation for c_f, form a pair of simultaneous equations. They may be solved successively for θ and H, respectively, with any desired accuracy by an iterative process when the starting values θ_0 and H_0 are given. The momentum equation is first solved with H constant, $= H_0$. θ and u_τ/U as obtained from this solution are used to calculate the integral in Eq. (45), which leads to the variation of $\chi(H)$ and therefore of H. The correction that must be applied to θ because of the departure of H from H_0 in the momentum equation is then found by a variational method. Repetition of the process is unnecessary, since the integral in the form parameter equation is strongly convergent and receives almost all its contributions from a region where $H = H_0$ very closely.

(6.1) *Use of Momentum Equation*

Immediately behind transition the three terms of the momentum equation [Eq. (3)] are comparable in size, and c_f must be known accurately in order to calculate θ. In this region H has values of the same order as those encountered on a flat plate (i.e., about $H = 1.4$), and the Squire-Young and Ludwieg-Tillmann skin-friction formulas, Eqs. (6) and (7), respectively, agree with each other, but as H rises towards separation Eq. (7) gives lower values than Eq. (6). However it is then no longer necessary to know c_f very accurately, since it has become much smaller than the other terms in the equation. In fact accuracy is gained rather than lost by using a formula that overestimates skin friction, since this partly compensates for leaving out the pressure gradient and $\overline{u'^2}$ terms which are no longer negligible. For this reason the Squire-Young formula has been used for the present calculation.†

† The author has since found that extremely accurate values of θ are given by the simpler formula

$$\theta U^4\left(\frac{U\theta}{\nu}\right)^{0.2} = \text{const.} + 0.0106\int_0^x U^4\,dx$$

This is obtained by taking $\tau_w/\rho U^2 = 0.00883\,(U\theta/\nu)^{-0.2}$, which fits the Squire-Young formula very closely, and $H = \text{constant} = 1.5$, in the momentum equation. A similar formula, with slightly different constants, was obtained empirically in reference 11.

Suppose that solving the momentum equation with constant $H = H_0$ gives a value $\theta^{(1)}$. Then

$$(d\theta^{(1)}/dx) + (H_0 + 2)\,(\theta^{(1)}/U)\,(dU/dx) = \tau_w/(\rho U^2) \quad (50)$$

where $\tau_w/(\rho U^2)$ is a function of $U\theta^{(1)}/\nu$.

The solution of Eq. (50) is

$$\theta^{(1)}U^{H_0+2} = \theta_0 + \int_0^x \frac{\tau_w}{\rho U^2}\,U^{H_0+2}\,dx \quad (51)$$

$\theta^{(1)}$ may readily be obtained stepwise from this equation, splitting the range into intervals x_i to x_{i+1} (not necessarily equal) and evaluating the integral as

$$\sum_i \left(\frac{\tau_w}{\rho U^2}\right)_i \int_{x_i}^{x_{i+1}} U^{H_0+2}\,dx \quad (52)$$

where $[\tau_w/(\rho U^2)]_i$ is the mean value of the (slowly-varying) function over an interval, estimated from the preceding step and subsequently adjusted if necessary. Except at the beginning of the calculation large steps may be used (e.g., 0.05 × the chord of an airfoil).

Now suppose $\theta = \theta^{(1)} + \theta^{(2)}$, where $\theta^{(2)} \ll \theta^{(1)}$, is the solution of the momentum equation when the correct $H = H_0 + \Delta H$, say, is used. The momentum equation, Eq. (3), may then be written

$$(d/dx)\,(\theta^{(1)} + \theta^{(2)}) + (\Delta H + H_0 + 2) \times [(\theta^{(1)} + \theta^{(2)})/U]\,(dU/dx) = \tau_w/(\rho U^2) \quad (53)$$

$\tau_w/(\rho U^2)$ being in this case a function of $U(\theta^{(1)} + \theta^{(2)})/\nu$. But this function varies slowly and is almost the same as the right-hand side of Eq. (50).

Thus, equating the left-hand side of Eq. (50) to the left-hand side of Eq. (53),

$$(d\theta^{(2)}/dx) + (H_0 + 2)\,(\theta^{(2)}/U)\,(dU/dx) = -\Delta H[(\theta^{(1)} + \theta^{(2)})/U]\,(dU/dx) \doteq -\Delta H(\theta^{(1)}/U)\,(dU/dx) \quad (54)$$

$\theta_0{}^{(2)} = 0$, therefore

$$\theta^{(2)}U^{H_0+2} = -\frac{1}{H_0+2}\int_{x=0} \theta^{(1)}\Delta H\,d\,(U^{H_0+2}) \quad (55)$$

The integral here is again evaluated as a Riemann sum—namely,

$$-\frac{1}{H_0+2}\sum_i \theta_i{}^{(1)}\Delta H_i\,(U_{i+1}^{H_0+2} - U_i^{H_0+2}) \quad (56)$$

where $\theta^{(1)}$ and ΔH_i are mean values. We find in actual calculations that the assumption $\theta^{(2)} \ll \theta^{(1)}$ is well justified. A higher approximation could now be obtained by including $\theta^{(2)}$ obtained from Eq. (55) in the right-hand side of Eq. (54), but this is scarcely necessary.

The integration just outlined has the advantage of not involving velocity derivatives, which are difficult to obtain accurately.

(6.2) *Transition Conditions*

The theory of this paper is applicable only to boundary layers in which the turbulence is fully developed.

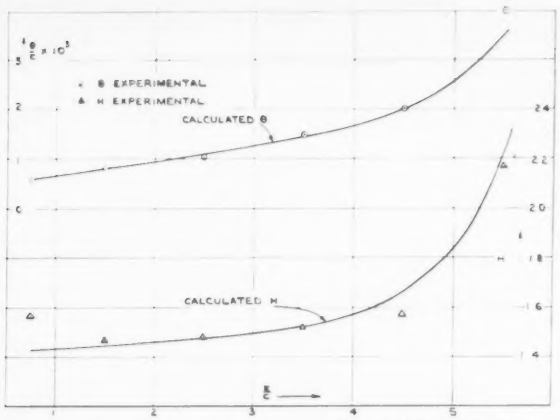

FIG. 10. Growth of boundary layer on NACA 65(216)-222 Airfoil ($\alpha = 10.1°$, $R = 2.64 \times 10^6$).

On an airfoil transition to this state from that of purely laminar flow occupies a finite region and may be brought about in several ways, notably (a) by free transition, in which a disturbance—either inherent in the laminar boundary layer or arising from the surface or the outside stream—is amplified, or (b) by "bubble" transition, in which the laminar layer separates and subsequently breaks down, reattaching when it is fully turbulent.

Unfortunately there is no hope at present of predicting the transitional flow with any precision, and one can only proceed on the assumption of abrupt transition. In this case θ is continuous, and for θ_0 we use the laminar flow value, as calculated, for instance, from the Thwaites[14] formula

$$\theta^2 = 0.45\, \nu\, U^{-6} \int U^5\, dx \tag{57}$$

The calculated distribution of θ in the turbulent layer is relatively insensitive to θ_0 except very close to the starting point, and good agreement with experiment is invariably achieved, even when the location of transition is a little uncertain. The choice of H_0 is more difficult. Experience has shown the calculated distribution of H to depend rather sensitively on the initial value, and indeed this is not surprising on physical grounds. It is also fairly sensitive to the exact location of transition. At high Reynolds Numbers a laminar boundary layer cannot advance far against an adverse pressure gradient, and the best assumption to make in the absence of more precise information would seem to be that transition occurs at the point of maximum velocity.

The criterion in selecting H_0 is then that it should lead to the correct values of H some distance downstream when the boundary-layer calculation is begun at the assumed transition point. Thus inaccuracy in locating the transition position is to some extent compensated by the choice of H_0. For all the available data in references 5, 6, 12, 15, and 16 for airfoils on which one would expect free transition to occur—i.e., on relatively thick airfoils or on thin airfoils at low incidence—the value

$$H_0 = 1.4 \tag{58}$$

has been found to lead to good agreement with observed distributions of H. For thin airfoils at high incidences, when the transition is predominantly of type (b), it seems likely from an examination of the data in reference 15 that a smaller value of H_0 than 1.4 must be used. (This might be expected from consideration of the velocity profiles in a turbulent jet from which the boundary layer is then formed.) However, insufficient evidence is available as yet from which to select a value for H_0; and the value chosen is likely to be affected by a change in the assumed transition point. In this case the laminar separation point seems more appropriate than the velocity peak.

(6.3) *Separation*

The presence of a form parameter factor, given by the authors either as $10^{-0.678H}$ or as $\gamma^{1.705}$, in the Ludwieg-Tillmann skin-friction formula indicates a rapid decrease in c_f as H increases (i.e., as γ decreases) which ultimately results in separation. $\gamma^{1.705}$ is shown as a function of H in Table 1. Gruschwitz[5] gave $1 - \gamma^2 = 0.8$ as a separation criterion; this corresponds to $H \doteqdot 2$. It now seems likely that separation always takes place within the range $2.0 < H < 2.8$. The criterion cannot be defined more precisely, but a comparatively narrow range of x corresponds to this range of H because of the steep gradient dH/dx at high H, which is found experimentally and in calculations using Eq. (45).

(6.4) *Comparison of Results with Experiment and with Reference 6*

The result of applying the calculation method to two interesting cases is shown in Figs. 10 and 11. For the NACA 65(216)-222 airfoil shown in Fig. 10 the agreement is very satisfactory. Equally good results were

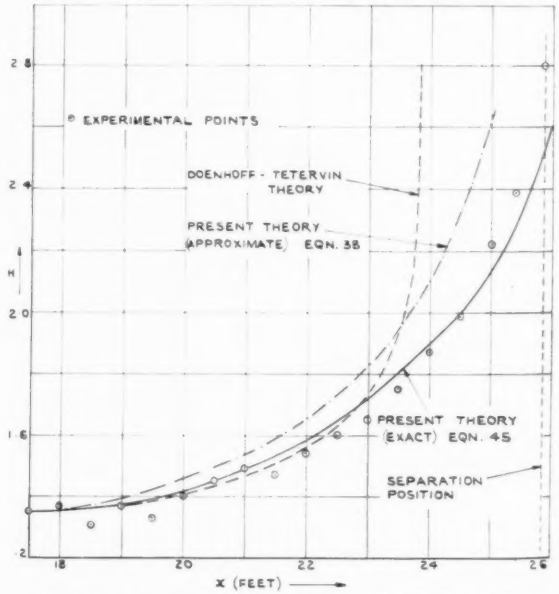

FIG. 11. Growth of H on Schubauer-Klebanoff airfoil.

obtained by von Doenhoff and Tetervin,[6] but their computation was a great deal more laborious than the present in which only 24 steps were used.

Figure 11 shows the results of applying both methods to the calculation of H for the airfoil of reference 1. Here the solution of Eq. (45) agrees very well with the experimental points, whereas von Doenhoff and Tetervin's equation predicts separation considerably further forward. The approximate solution given by Eq. (38) has been calculated also and lies midway between the other two curves.

(6.5) *Reynolds Number Dependence of Solutions*

On an airfoil with a prescribed distribution of (falling) velocity and a fixed transition point increase of Reynolds Number has the effect at each x of decreasing θ, increasing R_θ, and therefore decreasing $\tau_w/\rho U^2$. Because of the negative power of $\tau_w/\rho U^2$ occurring in the coefficient Φ when von Doenhoff and Tetervin's equation is written in the form (9), the equation then predicts more rapid growth of H and forward movement of separation with increasing Reynolds Number. This is the opposite of what would be expected but explains why the equation predicts separation too far forward on the Schubauer-Klebanoff airfoil where the Reynolds Number of 1.4×10^7 was well outside the range of the data used in deriving the equation. The present method predicts a decrease in the growth of H as Reynolds Number increases, the correcting integral in Eq. (45) becoming larger with decreasing θ.

(7) Conclusions

(1) Further confirmation has been found for Ludwieg and Tillmann's result that close to a wall velocity profiles are of the universal form

$$u/u_\tau = f(yu_\tau/\nu) \tag{21}$$

(2) von Doenhoff and Tetervin's statement that profiles form a one-parameter family is approximately true in the outer part of the boundary layer but must be qualified by the fact that Eq. (21) holds close to the wall. When the form parameter and skin-friction coefficient are known, the entire profile may be constructed exactly.

(3) An equation for the growth of the form parameter was derived in Section (5) with little further appeal to experiment. This predicts boundary-layer growths in good agreement with experiment in the cases tried, and, since its functional form was derived theoretically, it is a suitable basis into which empirical refinements might be introduced as more experimental information becomes available.

(4) In Section (6) a simple numerical method was outlined for integrating the equations without using velocity derivatives, which tend to introduce errors. The method enables one to examine rapidly the effect of variations in the initial conditions and in particular it is found that:

(a) As a general rule, the separation of the boundary layer is produced by the rise in pressure beyond the transition point and occurs when $(U_S/U_T)^2$ is somewhere between 1/3 and 1/2. (Here S, T refer to separation and transition, respectively.)

(b) Nevertheless the separation position depends fairly sensitively on the value of H at transition. The best value for this which can be suggested at present is 1.4.

(c) Increase in overall Reynolds Number should delay separation in an adverse gradient. The opposite of this is predicted by the von Doenhoff-Tetervin theory.

(d) Increase in the initial thickness of the boundary layer should bring separation forward.

References

[1] Schubauer, G. B., and Klebanoff, P. S., *Investigation of Separation of the Turbulent Boundary Layer*, NACA Report 1030, 1950.

[2] Ludwieg, H., and Tillmann, W., *Investigation of the Wall Shearing Stress in Turbulent Boundary Layers*, NACA TM 1285, 1950.

[3] Townsend, A. A., *The Structure of the Turbulent Boundary Layer*, Proc. Camb. Phil. Soc., Vol. 47, No. 2, pp. 375–395, 1951.

[4] Fage, A., *Profile and Skin Friction Aerofoil Drags*, R & M 1852, 1938.

[5] Gruschwitz, E., *Die Turbulente Reibungsschicht in ebener Strömung bei Druckabfall und Druckanstieg*, Ing. Archiv II, pp. 321–326, 1931.

[6] von Doenhoff, A. E., and Tetervin, N., *Determination of General Relations for the Behaviour of Turbulent Boundary Layers*, NACA Report 772, 1943.

[7] von Kármán, Th., *Turbulence and Skin Friction*, Journal of the Aeronautical Sciences, Vol. 1, No. 1, pp. 1–20, 1934.

[8] Squire, H. B., and Young, A. D., *The Calculation of the Profile Drag of Aerofoils*, R & M 1838.

[9] Garner, H. C., *The Development of Turbulent Boundary Layers*, R & M 2133, 1944.

[10] Zaat, J. A., *Revised Methods for Routine Calculations of Laminar and Turbulent Boundary Layers of Two Dimensional Incompressible Flows*, National Luftvaartlaboratorium (Amsterdam), Report F79, 1951.

[11] Maskell, E. C., *Approximate Circulation of the Turbulent Boundary Layer in Two-Dimensional Incompressible Flow*, RAE Report Aero 2443, 1951.

[12] Brebner, G. G., and Bagley, J. A., *Pressure and Boundary Layer Measurements on a Two-Dimensional Wing at Low Speed*, R & M 2886, 1952.

[13] Goldstein, S., Ed., *Modern Developments in Fluid Dynamics*, Vol. II, Chap. 8, Clarendon Press, 1938.

[14] Thwaites, B., *Approximate Calculation of the Laminar Boundary Layer*, Aero Quart I, pp. 245–280, 1949.

[15] von Doenhoff, A. E., and Tetervin, N., *Variation of Lift Coefficient with Reynolds Number*, NACA/CB/19, 1942.

[16] McCullough, G. B., and Gault, D. E., *Examples of Three Representative Types of Airfoil—Section Stall at Low Speed*, NACA TN 2502, 1951.

[17] Tetervin, N., and Lin, C. C., *A General Integral Form of Boundary Layer Equation for Incompressible Flow with an Application to the Calculation of the Separation Point of Turbulent Boundary Layers*, NACA TN 2158, 1950.

[18] Rubert, K. F., and Persh, J., *A Procedure for Calculating the Development of Turbulent Boundary Layers under the Influence of Adverse Pressure Gradients*, NACA TN 2478, 1950.

[19] Rotta, J., *Näherungsverfahren zur Berechnung Turbulenter Grenzschichten unter Benützung des Energiesatzes*, Mitteilungen Nr. 8, Max Planck Inst. fur Stromungsforschung, Gottingen, 1953.

[20] Fediaevski, K., *Turbulent Boundary Layer on an Aerofoil*, NACA TM 822, 1937.

[21] Clauser, F. H., *Turbulent Boundary Layers in Adverse Pressure Gradients*, Journal of the Aeronautical Sciences, Vol. 21, No. 2, pp. 91–108, February, 1954.

Interaction of a Shock Wave with a Thermal Boundary Layer*

WAYLAND C. GRIFFITH†
Princeton University

ABSTRACT

The interaction of a plane shock wave with a thermal boundary layer has been studied experimentally in the shock tube and a theory developed for those cases in which the shock is sufficiently strong and the heating small enough for the shock to extend clear to the surface. The experiment involves a technique of sliding a hot plate into the shock tube just before the shock arrives. The time required for establishment of steady conditions has been determined and the theory tested with experiments using shocks up to a pressure ratio of 1.36 and surface temperatures up to 80°C. The observed shape of the shock and pressure distribution along the surface agree well with predictions. When the speed of sound at the surface exceeds the shock velocity, pressure disturbances propagate ahead of the main wave and the total pressure rise extends over about two heated thicknesses. Finally, the possibility of extending the experimental results to more extreme conditions by an analogy with diffusion of gases is discussed.

INTRODUCTION

A PLANE SHOCK WAVE sweeping over a heated surface will encounter a thermal layer which disturbs the foot of the shock and thereby modifies the pressure distribution along the surface. Such a situation may be realized experimentally in the shock tube. If the air ahead of the shock is at rest relative to the surface, then viscous forces will probably have little effect on the flow initially, and the analytical problem becomes somewhat simpler than the shock–boundary-layer interaction commonly encountered in a wind tunnel.

For flows in which the air temperature varies only with distance from the surface two types of steady flow can be distinguished depending on whether the shock extends all the way to the surface or not. When the shock velocity U_s is greater than the speed of sound at the surface, the shock can reach the plate. When U_s is less than the local sound speed at the surface, on the other hand, the shock must vanish before reaching the plate and signals may propagate upstream ahead of the main wave in a manner similar to that observed with a laminar boundary layer.

Received October 1, 1954.

* Prof. Lester Lees suggested the ideas from which the theoretical treatment in this paper grew and was a frequent adviser during the course of the work. I should also like to express my thanks to the Guggenheim Aeronautical Laboratory, California Institute of Technology, for its hospitality during the summer of 1953 when much of the theory was worked out. The experimental part was done in the shock wave laboratory at Princeton with the support of ONR Contract N6ori-105, Task II. Reproduction, translation, publication, use and disposal, in whole or in part, by or for the United States Government is permitted.

† Assistant Professor of Physics, Palmer Physical Laboratory.

This paper presents experimental results on both types of flow and a theoretical treatment for those cases in which the amount of warming is rather small so that the shock is only slightly disturbed from its normal position. A linearized theory is developed, based on a method originated by Lighthill,[1] from which the shape of the shock and the flow field may be found. The problem is also closely related to several recent investigations on the interaction of sound and vorticity with a plane shock wave.[2, 3, 4] It has been found that the arrival of either small acoustic or shear waves at a plane shock produces both kinds of disturbance in the air downstream. In the present problem a steady state is imagined in which an enthalpy gradient generated by heating is convected through the shock, no sound waves being produced.

THEORY FOR SMALL AMOUNTS OF HEATING

The physical situation to be investigated is shown in Fig. 1. For convenience a coordinate system moving with the shock will be adopted so that the incoming flow has the constant velocity U_1 equal to the shock velocity U_s and an arbitrary temperature distribution $T(y)$. The x- and y-axes lie along the surface and undisturbed shock, respectively. The actual shock position resulting from the thermal layer is denoted by $B(y)$. The subscript 2 will be used to identify the downstream value of pressure P, density R, velocity components U, V, and speed of sound A which would result in the absence of any heating. We shall see that this state actually exists beyond about three thicknesses from the surface. Behind the curved portion of the shock the flow variables become $P_2 + p$, $R_2 + \rho$, $U_2 + u$, v, and $A_2 + a$.

Following Lighthill's treatment the two-dimensional nonviscous steady flow equations expressing conservation of mass, momentum, and energy are, for an ideal gas,

$$\frac{\partial}{\partial x} RU + \frac{\partial}{\partial y} RV = 0 \tag{1}$$

$$RU\frac{\partial U}{\partial x} + RV\frac{\partial U}{\partial y} + \frac{\partial P}{\partial x} = 0,$$

$$RU\frac{\partial V}{\partial x} + RV\frac{\partial V}{\partial y} + \frac{\partial P}{\partial y} = 0 \tag{2}$$

$$V\frac{\partial P}{\partial x} + V\frac{\partial P}{\partial y} = A^2\left(U\frac{\partial R}{\partial x} + V\frac{\partial R}{\partial y}\right) \tag{3}$$

If the perturbations p, ρ, etc., are assumed to be small when the heating is small, Eqs. (1) to (3) are greatly simplified. Elimination of ρ and u in favor of p and v yields

$$(1 - M_2^2)\,(\partial p/\partial x) = R_2 U_2\,(\partial v/\partial y) \tag{4}$$

$$\partial p/\partial y = -R_2 U_2 (\partial v/\partial x) \tag{5}$$

These may be written in the form of the Cauchy-Riemann relations if a set of reduced coordinates are used. Let

$$\left.\begin{aligned} p^* &= \sqrt{1 - M_2^2}\; p/\gamma P_2 \qquad & v^* &= M_2^2 v/U_2 \\ x^* &= x/\sqrt{1 - M_2^2} & y^* &= y \end{aligned}\right\} \tag{6}$$

Then

$$\partial p^*/\partial x^* = \partial v^*/\partial y^*, \qquad \partial p^*/\partial y^* = -(\partial v^*/\partial x^*) \tag{7}$$

Therefore p^* and v^* are derivable from a potential $\phi(x^*, y^*)$ such that

$$p^* = \partial\phi/\partial x, \qquad v^* = \partial\phi/\partial y \tag{8}$$

A solution to Laplace's equation must now be chosen which will satisfy the boundary conditions along the shock and at the surface. The pressure immediately behind the shock may be determined from the appropriate shock wave equation since the state of the gas upstream is completely specified by P_1, U_1, and $T(y)$. According to the initial assumptions $T(y)$ may be written

$$T(y) = T_1[1 + T'(y)],\ T' \ll 1 \tag{9}$$

The local Mach Number of the incoming flow becomes

$$M = M_1\,(1 - T'/2) \tag{10}$$

It is understood that even for weak shocks M must be greater than one everywhere so that a shock can exist. The pressure ratio across a shock is

$$P/P_1 = [2\gamma M^2 \cos^2\sigma - (\gamma - 1)]/(\gamma + 1) \tag{11}$$

where σ is the angle between the flow and the normal to the shock. Ignoring the effect of the slight inclination of the shock and using Eq. (10) one finds

$$p = -[2\gamma/(\gamma + 1)]P_1 M_1^2 T'(y), \qquad x = 0 \tag{12}$$

In the course of the solution this condition will be applied on the y-axis rather than on the actual shock. Presumably a correction to the result thus obtained could be made, but in view of the success of the simple theory such an extension seems unnecessary.

The second requirement on the flow solution is that the vertical velocity component vanishes at the surface. The boundary conditions to be met are therefore given by Eqs. (12) and (13).

$$v = 0, \qquad y = 0 \tag{13}$$

A distribution of sources of strength $g(y)$ along the y-axis provides the necessary change in the basic flow so the potential function is taken to be

$$\phi = \frac{1}{2\pi}\int_{-\infty}^{+\infty} g(\eta)\,\ln\,[x^{*2} + (y - \eta)^2]d\eta \tag{14}$$

Flow parallel to the surface at $y = 0$ is assured if an image flow is added in the lower half plane with $g(-y) = g(y)$. This gives for the reduced pressure

$$p^* = \frac{1}{\pi}\int_{-\infty}^{+\infty} \frac{g(\eta)x^*d\eta}{x^{*2} + (y - \eta)^2} \tag{15}$$

Along the y-axis this expression reduces to $p^*(0, y) = g(y)$—i.e., the source distribution is directly proportional to the excess temperature in the thermal layer. The actual pressure change is found from Eqs. (6) and (12) to be

$$p = -[2\gamma/\pi(\gamma + 1)]P_1 M_1^2 x^* \int_{-\infty}^{+\infty} \frac{T'(\eta)d\eta}{x^{*2} + (y - \eta)^2} \tag{16}$$

Since the experimental arrangement described later makes use of a Mach-Zehnder interferometer, data are obtained on the density field rather than the pressure field. Variations from the uniform state in region 2 will result both from distortion of the shock and directly from the initial heating. According to the second law of thermodynamics

$$ds = [C_V/p]dp - [C_p/\rho]d\rho \tag{17}$$

so that in first approximation

$$\rho/R_2 = p/\gamma P_2 - (S - S_2)/C_p \tag{18}$$

Here $S - S_2$ is the entropy change from heating plus the difference between the entropy rise through the inclined shock and through the undisturbed shock. The latter difference is small compared to the effect of heating and may be safely omitted in the remainder of this work.† Accordingly, Eq. (18) becomes

$$\rho = R_2\,[p/\gamma P_2 - T'(y)] \tag{19}$$

An equation for the actual shock position $B(y)$ may be obtained from the vertical velocity component v at $x = 0$. Consider a segment of the shock inclined at an angle σ to the vertical where the flow is deflected through an angle θ as shown in Fig. 2. Since only the component of velocity normal to the shock is altered by the shock, the angle σ must be given by

$$\sigma = v(0, y)/[U_1 - V_2 - u(0, y)] \tag{20}$$

and θ is

$$\theta = v(0, y)/[U_2 + u(0, y)] \tag{21}$$

The two angles are related by the shock wave relation

† The fact that the entropy change across an inclined portion of the shock and that across the straight part differ by a negligible amount for the conditions postulated here follows from consideration of the dependence of entropy rise upon shock inclination, σ (defined in Fig. 2). Since $S_2 - S_1 \propto \ln\,(p_2/p_1) + \gamma\,\ln\,(\rho_2/\rho_1)$ and each of these terms varies as $M^2\cos^2\sigma$, the effect of shock inclination will be of second order in σ when σ is small, so that

$$\cos^2\sigma = 1 - \sigma^2 + \ldots .$$

$$\tan\theta/\tan\sigma = [M^2\cos^2\sigma - 1] \div \{M^2[(1/2)(\gamma+1) - \cos^2\sigma] + 1\} \quad (22)$$

For small deflections it is possible to show with the use of Eq. (10) that

$$u(0, y) = [2U_1/(\gamma+1)M_1^2]\, T'(y) \quad (23)$$

and therefore u may be omitted from Eq. (20) for σ whenever the shock is strong enough for $M_1^2 - 1 \gg T'$. Finally, $B(y)$ is given by

$$B(y) = \int \sigma dy \doteq \frac{1}{U_1 - U_2}\int v(0, y)dy = \frac{U_2}{(U_1 - U_2)M_2^2}\,\phi(0, y) + \text{const.} \quad (24)$$

This result completes the formal development of the linearized theory, since the only remaining information needed to compare predictions with experiment is the initial temperature distribution $T(y)$. This may be computed from the theory of heat conduction if the initial conditions are known, and the calculated values can be checked experimentally with the interferometer.

Experimental Technique

The shock tube is well suited for experiments of the sort needed in a study of the interaction of a shock wave and a purely thermal layer. Since the principles in the theory and operation of the shock tube are doubtless familiar by now, only those special features of the Princeton tube which are pertinent to this study will be described. In all of the experiments reported here the downstream section, or channel, was open to the atmosphere and the chamber pumped up to some higher pressure.

The most satisfactory method found for generating a thermal layer has been to preheat a steel plate and slide it into the test section just before the tube is fired.† For moderate temperatures immersing the plate in a tray of hot water gives good results. Some heat escapes in wiping the plate dry and passing it into the dark house but reproducible results are achieved with careful timing. In a typical run with the plate initially at 100° C. a temperature of 80°C. was measured in the gas at the surface from the interferogram. A low surface heat-transfer coefficient might also be significant in accounting for this diminution in temperature.

A plate 1/2 in. by 4 in. by 24 in. was bevelled at one end so that part of the incident shock could be sliced off and advance undisturbed except by the thermal layer. A sketch of the test section with the plate fully inserted is shown in Fig. 3. For experiments with heated plates the test surface faces down so that strong convection currents are not set up, while for cooled plates the test surface is put in facing up. Some of the warm air flows around the tip of the wedge but the velocities are rather small and little air escapes. At the back the mounting block for the guides acts as a dam so that no convection occurs.

Once the hot plate is in place the gas is warmed largely by heat conduction. Since the heat capacity of steel is enormous compared to that of air it is likely that the plate temperature changes very little during the interval before the shock arrives. Accordingly, the transient one-dimensional heat flow solution for conduction from a surface at constant temperature T_w into a semi-infinite medium initially at T_1 should give a good approximation to the actual temperature distribution. The solution is expressed in terms of the error integral.

$$(T - T_1)/(T_w - T_1) = 1 - 2/\sqrt{\pi}\int_0^{y/\sqrt{4Kt}} e^{-z^2}\,dz = 1 - \text{erf}(y/\sqrt{4Kt}) \quad (25)$$

The thermal diffusivity K is 0.03 in.²/sec. for air. Taking the quantity $\sqrt{4Kt}$ as a characteristic length y_0 in the heated region, one finds that for $y_0 = 3/4$ in. the time required is ≈ 5 sec. This is a reasonable interval with which to work.

Before the tube is actually fired a sequence timer turns on a number of circuits involved in measuring the shock speed and obtaining the interferogram. One minute elapses between the instant when a switch starts the timer and a signal light goes on indicating that the tube is ready to fire. Six seconds before the lamp goes on the camera shutter opens with a loud click. This click is used as the signal for the man in the dark house to slide the hot plate, which he has just received through a slit from outside the house, into the shock tube. Then there is enough time to jump back and cover the ears. The plate must be removed soon after the experiment is over because thermal stresses produced in the observation windows create a spurious fringe shift.

A test of the assumptions leading to Eq. (25) is made in Fig. 4 by plotting the relative temperature rise against distance from the surface for four different plate temperatures. Since no attempt was made to measure the time of heating accurately the curves are fitted at $(T - T_1)/(T_w - T_1) = 1/2$ and y_0 computed accordingly. The resulting times agree as well as expected with the estimated intervals during the actual experiments. The shape of the experimental distribution agrees well with the error function so y_0 can be chosen as the unit of distance. It serves as a very handy measure of the actual thickness of the thermal layer. Values of $(T - T_1)/(T_w - T_1)$ at $(1/2)y_0$, y_0, and $2y_0$ are 0.4795, 0.1573, and 0.0047, respectively. The energy conducted beyond $2y_0$ amounts to less than 1/4 per cent of the total and may be safely omitted from numerical calculations.

Comparison of Theory and Experiment

A series of interferograms have been obtained for a variety of temperatures and heating times with shock strengths of $P_2/P_1 \doteq 1.17$, 1.30, and 1.36. Fig. 5

† This technique was first used in this laboratory by D. R. White and Walker Bleakney, who heated the plate with a blowtorch.

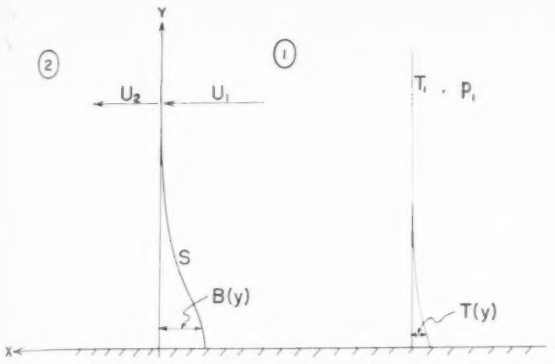

FIG. 1. Nomenclature used in describing the thermal layer and flow field for a coordinate system moving with the shock wave. The initial temperature is assumed to vary only with y and the pressure to be constant everywhere. The subscripts 1 and 2 refer to conditions before and behind the undisturbed shock far from the surface.

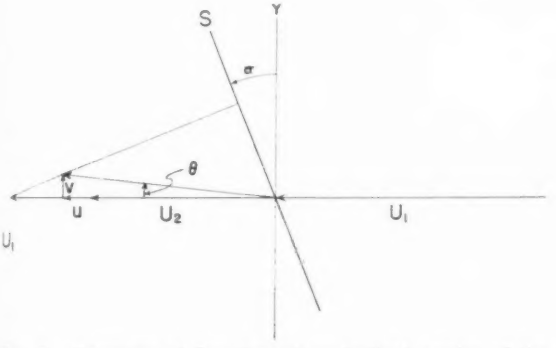

FIG. 2. Geometry of flow through an inclined portion of the shock.

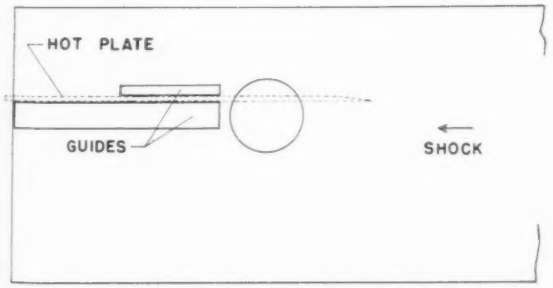

FIG. 3. Test section of the shock tube showing location of the plate for an experiment in which the shock travels about 6 in., or $8y_0$, before the interferogram is taken. For a heated plate the experiment is conducted on the bottom surface to avoid the effects of convection.

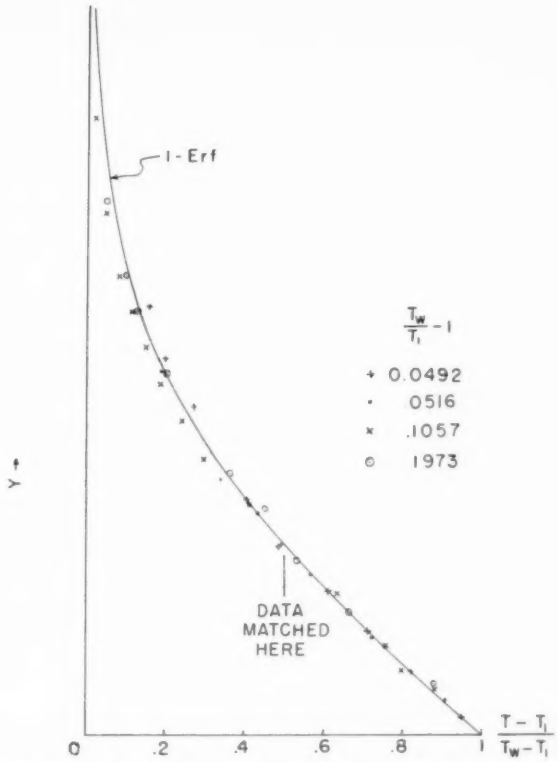

FIG. 4. Relative temperature distribution in the thermal layer as a function of distance y from the surface for several different plate temperatures. The solid curve is the error function of Eq. (25). The experimental data are matched at $(T - T_1)/(T_w - T_1) = 1/2$ and the actual distributions are seen to be very close to the curve.

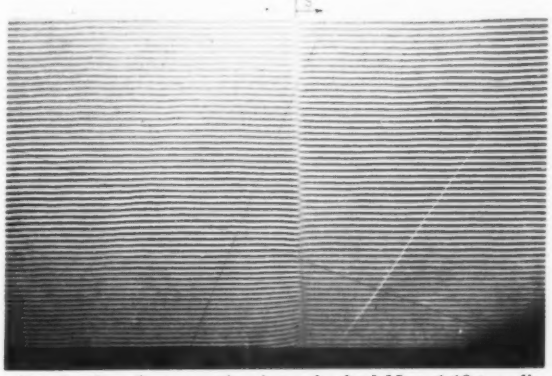

FIG. 5. Interferogram showing a shock of $M_1 = 1.12$ traveling to the right over a thermal layer in which $T_w - T_1 = 20.7°C$. The distance y_0 is actually 0.38 in. The crowding of fringes in the thermal layer ahead of the shock and the asymptotic approach to parallel flow behind are clearly discernible.

shows the fringe pattern when $P_2/P_1 = 1.297$ and $T_w - T_1 = 20.7°C$. The shape of the shock wave and the density along the surface are especially convenient properties to compare with the theory. To be sure that the pattern observed is actually a steady one a set of pictures were taken with the plate inserted various distances into the tube. It appears that after the shock travels about ten y_0 no further changes in the flow occur. Usually y_0 was around 3/4 in. and the tip of the plate 14 in., or 20 y_0, beyond the point of observation.

Some simplification in the numerical work is achieved by replacing the distribution of Eq. (25) with a function that is explicitly integrable. The parabola

$$T'(y)_{\text{para.}} = (T_w/T_1 - 1)\,(1 - y/1.65y_0)^2 \quad (26)$$

matches the error integral very closely as may be seen in Fig. 6. To test the sensitivity of the predicted value to the form of the temperature distribution a linear variation possessing the same total energy will also be included in the calculations

$$T'(y)_{\text{lin.}} = (T_w/T_1 - 1)\,(1 - y/1.10y_0) \quad (27)$$

The shape of the shock wave is, from Eqs. (14), (24), and (26),

$$B(y) = -\frac{2U_1\sqrt{1 - M_2^2}}{\pi(\gamma + 1)\,(U_1 - U_2)}\left(\frac{T_w}{T_1} - 1\right) \times \int_{-1.65y_0}^{+1.65y_0}\left(1 \mp \frac{\eta}{1.65\eta_0}\right)^2 \ln\,(y - \eta)d\eta + \text{const.} \quad (28)$$

The upper sign must be used for $\eta > 0$ and the lower sign for $\eta < 0$. In terms of the reduced variable $y' = y/1.65y_0$ the integral gives

$$B(y) = \frac{2U_1\sqrt{1 - M_2^2}}{\pi(\gamma + 1)\,(U_1 - U_2)}\left(\frac{T_w}{T_1} - 1\right) 1.65y_0 \times \left[\frac{1}{3}(1 + y')^3 \ln\,(1 + y') + \frac{1}{3}(1 - y')^3 \times \ln|1 - y'| - 2y'\left(\frac{1}{3} + \ln y'\right)\right] \quad (29)$$

The additive constant has been chosen to make $B(0) = 0$. The shock is perpendicular to the surface at $y = 0$ since the existence of a temperature gradient upstream does not affect the local requirement of outflow parallel to the surface. As $y \to \infty$, $B(y) \propto \ln y$, a familiar feature of a linearized theory. Fig. 7 shows the predicted values from the parabolic and linear temperature distributions and the results of several experimental observations. The x-dimension in physical space has been expanded relative to the y-dimension to bring out more clearly any departure from the theory that may exist. The parabolic and linear temperature distributions give shock shapes which are almost indistinguishable. A cubic equation for T' shows no significant departure from these results either. One may conclude that the shock shape is relatively insensitive to changes in the profile of the thermal layer.

The experimental results include three runs with a cooled layer as well as several when the plate was heated. For the smaller amounts of heating, $T_w/T_1 - 1 < 0.07$, good agreement is found with the theory for all three shock strengths. More heating produces a greater deflection of the shock as may be seen from the results for $P_2/P_1 = 1.17$ and $T_w/T_1 - 1 \cong 0.11$. Recalling the assumption made in deriving Eq. (24) for $B(y)$ that $M_1^2 - 1 \gg T'$, such an increase in the observed deflection is reasonable. As long as $M_1^2 - 1 > 2T'$ we may conclude that the first-order theory for the shock location serves very well.

The theoretical pressure distribution is found from Eqs. (16) and (26):

$$p = -[2\gamma/\pi(\gamma + 1)]M_1^2P_1(T_w/T_1 - 1)I(x^*, y) \quad (30)$$

where

$$I(x^*, y) = x^*\int_{-1.65y_0}^{+1.65y_0}\frac{(1 \mp \eta/1.65y_0)^2\,d\eta}{x^{*2} + (y - \eta)^2} \quad (31)$$

Along the surface integration gives

$$I(x^*, 0) = 2\left[1 - \frac{x^{*2}}{(1.65y_0)^2}\right]\tan^{-1}1.65y_0/x^* - [2x^*/1.65y_0]\left\{\ln\left[1 + \left(\frac{1.65y_0}{x^{*2}}\right)\right] - 1\right\} \quad (32)$$

Since the same integral I appears in the formula for density a convenient check on the theory is made by comparing the calculated value of I with that from analysis of the interferograms. A question arises over choice of the origin in this case. One can argue either that the y-axis in the theory should coincide with the undisturbed shock or that the point $x = 0$, $y = 0$ in the theory should coincide with the actual foot of the shock. With either choice it is clear that some part of the flow field will not match in this first-order theory and the immediate problem becomes one of making the most useful choice. For comparing surface pressures only, the second alternative seems more logical and Fig. 8 is plotted accordingly. An interesting conclusion is that the disturbed region extends only about two heated thicknesses downstream even for shocks of pressure ratio 1.36. As in the case of the shock shape very little difference was noted between the predictions of the parabolic and linear temperature distributions.

The entire pressure field has been computed for the linear case and a contour plot is shown at the right in Fig. 9. The numbers on the contours are values of the integral I in Eq. (30), they apply whenever the original assumptions are valid so that an affine transformation of the x-coordinate by the factor $\sqrt{1 - M_2^2}$ gives the theoretical flow field for all such cases. The scale in Fig. 9 has been chosen to fit the particular case when $P_2/P_1 = 1.36$, so that the result can be easily compared with one of the experiments used in Figs. 7 and 8. The drawing on the left was obtained from an interferogram in which $(T_w/T_1 - 1) = -0.067$.

Cases Where the Shock is Separated from the Surface

So far the discussion has dealt exclusively with cases

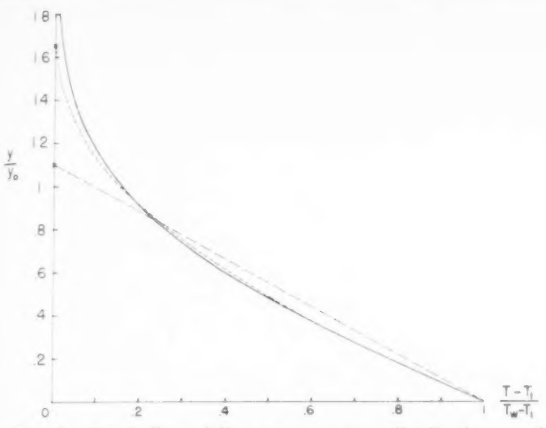

FIG. 6. Parabolic and linear temperature distributions used to facilitate calculation and test the effect of temperature profile on shock shape and surface pressure. The distributions are chosen to have the same energy as the original profile.

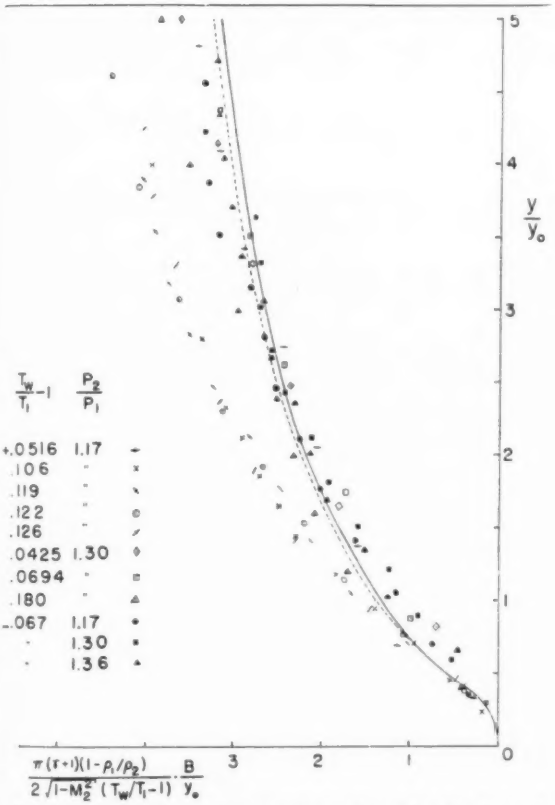

FIG. 7. Comparison of theory and experiment for the shape of the shock wave $B(y)$. The x-coordinate includes a dimensionless scale factor which should make all shocks identical according to the theory. Little difference exists between the shape predicted from the parabolic distribution and that from a linear distribution. Experimental data for $T_w/T_1 - 1 < 0.07$, $M > 1.07$ show satisfactory agreement with theory while greater heating at the same shock strength produces relatively more distortion of the shock. The theory is therefore reliable so long as $M_1^2 > 2[(T_w/T_1) - 1]$.

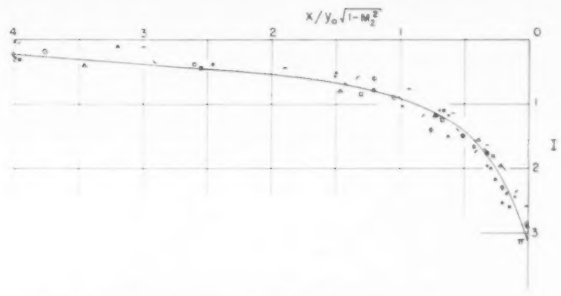

FIG. 8. Surface pressure distribution expressed in terms of the integral I in Eq. (30). The symbols are the same as those in Fig. 7. No detectable difference between the parabolic and linear solutions existed in this case. The pressure ratio across the foot of the shock is less than P_2/P_1 for a heated layer, more for a cooled one. The rate of approach to the final pressure P_2 depends on the thickness of the heated layer y_0 and on $\sqrt{1-M_2^2}$. The quantity increases with increasing shock strength; at $M_1 = 1.16$, $\sqrt{1-M_2^2} = 0.5$, so that the disturbed region extends only about $2y_0$ along the surface.

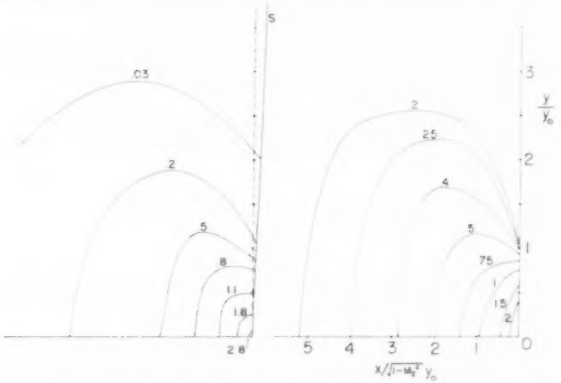

FIG. 9. Comparison of experimental and theoretical pressure fields when $P_2/P_1 = 1.36$. The drawing on the left was obtained from an interferogram in which $T_w/T_1 - 1 = -0.067$, that is, the plate was cooled so as to retard the foot of the shock. The theoretical distribution on the right may be applied to other shock strengths with an affine transformation by the factor $\sqrt{1-M_2^2}$ in the x-dimension.

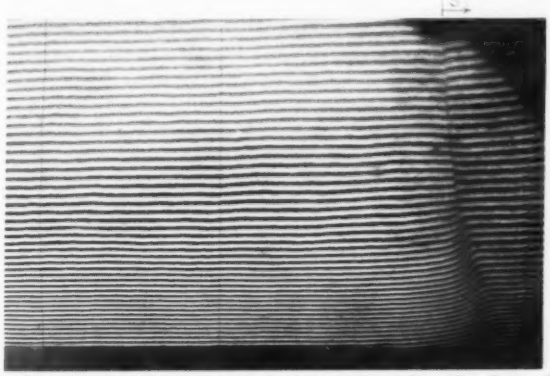

FIG. 10. Interferogram of the interaction when the thermal layer is so hot that the shock does not extend all the way to the surface. The shock strength is $P_2/P_1 = 1.169$; $T_w - T_1 = 58.5°$ C. The surface pressure distribution for this picture is given by the triangles in Fig. 11.

for which the shock is strong enough to extend clear to the wall—i.e., $M_1^2 > T_w/T_1$. When this condition no longer holds, flow at the wall becomes subsonic relative to the shock and pressure disturbances propagate ahead of the main wave. Fig. 10 shows an example of such a situation. A shock of strength $P_2/P_1 = 1.169$ (Mach Number 1.070) is seen sweeping over a thermal layer whose maximum temperature $T_w - T_1 = 58.5°C$.

A sequence of pictures, of which Fig. 10 is one, taken after the shock traveled different distances along the plate, shows that a steady pattern exists here also. This may seem rather surprising in view of the fact that the entire field is influenced by any acoustic signal. Nevertheless, some damping mechanism apparently acts with great rapidity to establish the steady flow pattern. The approach to equilibrium can be followed by studying just the pressure distribution along the plate, since attainment of a steady surface pressure understandably is observed to be accompanied by steady conditions everywhere. Fig. 11 is a graph of surface pressure when a shock of $M = 1.070$ has advanced various distances from the leading edge of the plate. These distances are 0, $1.8y_0$, $6.5y_0$, $14.6y_0$, $22y_0$, and $30y_0$. The shock decays very rapidly at first and a continuous compression takes its place. As time goes by the front broadens to about $2y_0$ and approximately half the total pressure rise occurs at a constant gradient of $dp/dx = (P_2 - P_1)/y_0$. An unexpected feature is the absence of any detectable signal upstream of $x = 0.9y_0$ and the sharp rise thereafter.

The shock appears to vanish at $1.35y_0$ from the surface. The distance at which the shock velocity just equals the local speed of sound in the undisturbed thermal layer is only $0.24y_0$, indicating that the air has already been set in motion at least $1.35y_0$ from the surface before the shock arrives. Experiments under a variety of conditions suggest that the features observed here are common to all such interactions with moderate shock strengths and heating.

No theoretical solution has been worked out for the configuration just described. The problem is considerably more difficult than that attempted in the first part of this paper because of the mixed subsonic and supersonic flows. The methods of transonic small disturbance theory could be applied but the limitation to both weak shocks and small heating might reduce the value of the solution in relation to the work involved. As will be pointed out in the following section, quite different effects may be anticipated under more extreme conditions than those discussed so far.

Discussion

A study of the interaction of very strong shocks with thermal layers having a temperature rise of a 100°C. or more offers a logical continuation of the present work. Hess[5] has discussed some of the general features of the flow one might expect to encounter. If, for example, the stagnation pressure of the air in the thermal layer is less than the pressure behind the undisturbed shock

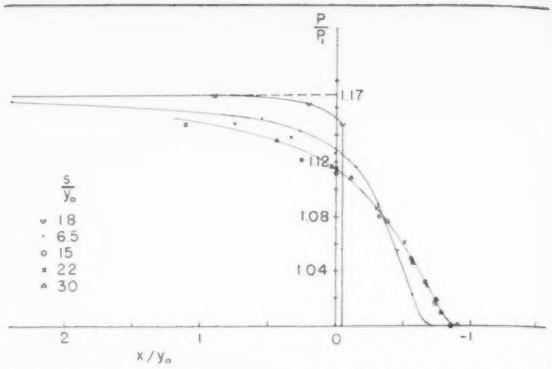

Fig. 11. Surface pressures on a plate (for the same conditions as those in Fig. 10) showing the approach to a steady distribution as the shock proceeds. The distance s is measured from the tip of the plate to the undisturbed shock.

wave, then steady flow of the type discussed so far is impossible. The warm air must pile up somehow behind the foot of the shock in an ever-increasing volume. Hess points out that a quasi-stationary situation may arise under certain conditions. Suppose that the thermal layer is semi-infinite in extent so that the interaction begins at a definite instant. Transient effects certainly predominate initially, but after a long time the bubble of dead air will have a volume proportional to the length of hot air enveloped by the shock and therefore a linear dimension proportional to the square root of the time. A quasi-stationary pattern may thus appear. A small region at the front of the bubble must be excluded, since the thickness of the layer is assumed to be constant with time.

The locus of points in the T_w/T_1 vs. M_1 plane, for which the pressure behind the undisturbed shock just equals the stagnation pressure of the gas in the thermal layer, is found by equating the pressure rise across a shock of Mach Number M_1 to that in a deceleration from velocity U_1 and temperature T_w to rest. A few values are given in Table 1 for $\gamma = 1.4$. The maximum Mach Number for which a steady flow is possible with the shock detached from the surface is 1.328. Stronger shocks either extend to the surface or form bubbles, depending on the surface temperature. Likewise, steady interactions of the type investigated earlier may be expected only for temperature ratios below 1.765.

The experimental technique devised for the moderate temperatures and pressures used so far seems to be unsuitable for investigation of the stagnation region. Some difficulty arises in protecting the observation windows from thermal strains without destroying the two-dimensional character of the flow while the pressures associated with shocks faster than $M = 1.25$

(*Continued on page 66*)

Table 1

M_1	1.2	1.3	1.328	2	3
T_w/T_1	2.39	1.84	1.765	1.30	1.18

Values of the shock Mach Number and wall temperature for which the pressure behind the undisturbed shock just equals the stagnation pressure of the flow at T_w.

An Investigation on Fully Developed Turbulent Flows in a Curved Channel*

SALAMON ESKINAZI† AND HSUAN YEH‡
The Johns Hopkins University

SUMMARY

Measurements of turbulent properties have been made on a fully developed, plane incompressible flow in a curved channel between circular, concentric walls. Comparison with the flow in a straight channel of the same Reynolds Number shows strong influence of curvature of the mean flow on mean velocity, turbulence intensity, scale, and spectrum. The influence of curvature is discussed on the basis of turbulent energy equations.

LIST OF SYMBOLS

d	= width of straight and curved channel
	= $r_o - r_i$ in curved channel
F	= spectrum
k_1	= one-dimensional wave number
L	= integral scale, defined in Section (4-8)
n	= frequency
p	= fluctuating pressure
P	= mean pressure
P_t	= mean total pressure
(Pr)	= turbulence production
$(Pr)_*$	= $\nu(Pr)/U_*^4$
r	= radius, radial direction in cylindrical coordinates
r_i	= radius of inner wall
r_0	= radius at which $\tau = 0$
r_o	= radius of outer wall
u, v, w	= fluctuating velocities along x, y, z in straight channel or along ϕ, r, z in curved channel
$\bar{u}, \bar{v}, \bar{w}$	= root mean square values of u, v, w
U, V, W	= mean velocities along x, y, z in straight channel or along ϕ, r, z in curved channel
U_*	= $\sqrt{\tau_{wall}/\rho}$
x	= longitudinal (streamwise) coordinate of straight channel
y	= lateral coordinate perpendicular to wall in straight channel. Distance from the wall in both curved and straight channels
z	= coordinate perpendicular to x and y in straight channel or to ϕ and r in curved channel.
ϕ	= tangential (streamwise) direction in cylindrical coordinates
λ	= microscale, defined in Section (4-7)
τ	= shear stress
ρ	= density
μ	= viscosity
ν	= kinematic viscosity

Subscripts

Av	= spatial average
i	= at inner wall
m, max	= maximum
0	= at outer wall

A bar on top denotes temporal average.

Received November 3, 1954.

* This work was sponsored by the Office of Naval Research through Contract Nonr-248(33) and under the contract directorship of Dr. G. F. Wislicenus. The authors wish to thank Dr. Francis H. Clauser and Dr. Stanley Corrsin for their interest and discussions.

† Formerly, Research Associate, Department of Mechanical Engineering, The Johns Hopkins University. Now, Associate Professor, Department of Mechanical Engineering, Syracuse University.

‡ Associate Professor of Mechanical Engineering.

(1) INTRODUCTION

THE TWO-DIMENSIONAL FULLY DEVELOPED turbulent flow in a curved passage between two concentric, circular walls (Fig. 1) has been investigated by Wattendorf.[1] In Wattendorf's investigation the (temporal) mean velocity and pressure were measured. When one compares the turbulent mean velocity profile across a curved channel with that across a straight channel, one finds a remarkable difference even if the curved channel has a mild curvature, while the laminar flow would show practically the same velocity distribution in the two channels. Thus in Fig. 2 the temporal mean velocity as a ratio to its spatial average (U/U_{Av}) across a straight channel is compared with the same quantity across a curved channel of $r_i/r_0 = 0.9$. The theoretical laminar solutions for the two channels show a difference so small that the same U/U_{Av} curve can be used to represent both. For turbulent flows, however, measurements in the two channels of the same Reynolds Number (74,200 based on the half width of the channel in the present investigation) show a distinct difference—the curved channel has a more equalized velocity distribution accompanied by a smaller peak velocity U_{max}/U_{Av}. A more meaningful comparison is perhaps the distribution of angular momentum $(Ur)/(Ur)_{Av}$, Fig. 3. For the straight channel the plot of $(Ur)/(Ur)_{Av}$ is of course the same as that of U/U_{Av}. Again there is practically no difference in the distribution of $Ur/(Ur)_{Av}$ across the curved and straight channels if the flow is laminar. For turbulent flows, the angular momentum is much more uniform in the curved than in the straight channel. In fact, in about half of the width of the curved channel the mean flow is practically the same as that of a potential flow. Since the mean velocity distribution is determined by the turbulence characteristics of the flow, we have here conclusive evidence that even a mild curvature of the mean flow influences the turbulence quantities to a significant extent.

This paper presents results of an investigation on a curved channel of $r_i/r_0 = 0.9$. Measurements were taken on the turbulence intensity, shear, scale, and energy spectrum as well as mean velocity. The mean velocity is compared with the results on similar channels by Wattendorf.[1] The turbulence quantities are com-

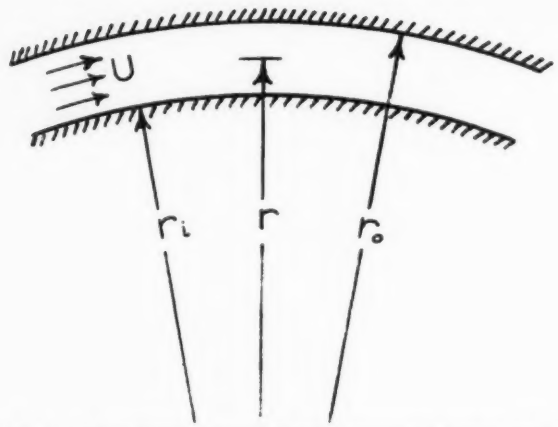

FIG. 1. Plane curved channel between concentric circular walls ($r_i/r_0 = 0.9$).

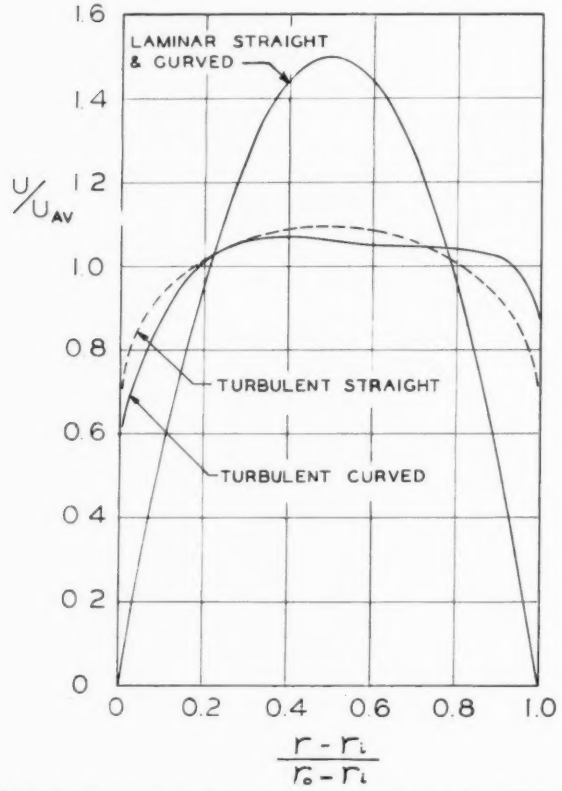

FIG. 2. Comparison of mean velocity distribution in straight and curved channels ($r_i/r_0 = 0.9$ for curved channel).

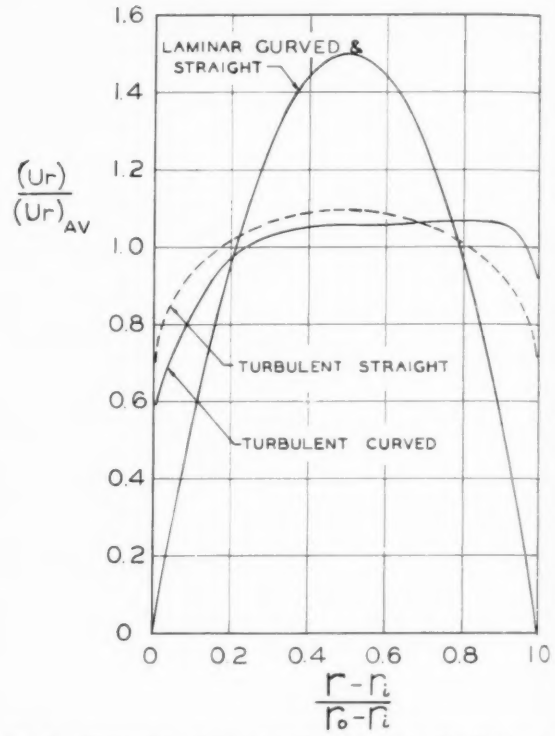

FIG. 3. Comparison of mean angular momentum distribution in straight and curved channels ($r_i/r_0 = 0.9$ for curved channel).

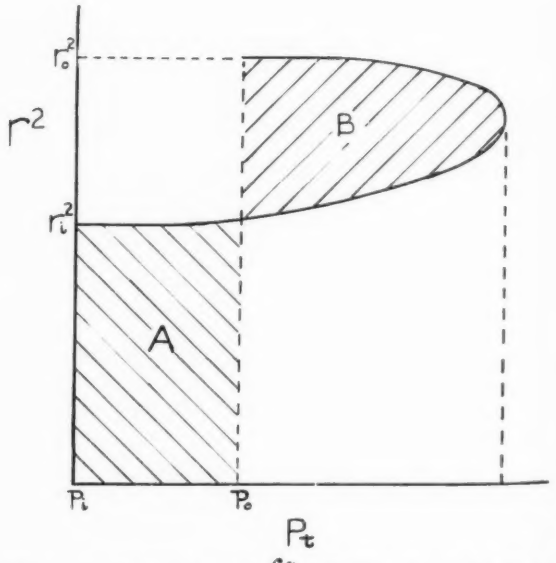

FIG. 4. Showing the integral $\int_{ri}^{r_0} r^2 dP_t$ across a curved channel.

pared with both the results in the straight channel of this experiment and the results of a straight channel reported by Laufer.[2] Finally, the influence of curvature is discussed on the basis of turbulent energy equations.

The main part of this paper is a summary of two separate reports of limited circulation.[3, 4] However, a few interpretations, including Section (5) of this paper, are new.

(2) Analytical Considerations

We let ϕ, r, z be the cylindrical coordinates along tangential, radial, and axial directions, respectively; U, V, W, be the (temporal) mean velocity components along ϕ, r, z, respectively; and u, v, w be the turbulent velocity components along ϕ, r, z, respectively. In a two-dimensional curved channel of Fig. 1 in which the flow has reached a fully developed state, we assume (a) $V = W = 0$; (b) $\partial/\partial z = 0$; and (c) the velocities are independent of ϕ. The Reynolds equations along the directions of r, ϕ, z then become:

$$(d/dr)(\overline{uv}) + (2\overline{uv}/r) = -(1/\rho)[\partial P/(r\partial\phi)] + \nu\{(d^2U/dr^2) + [(1/r)(dU/dr)] - (U/r^2)\} \quad (1)$$

$$(d/dr)(\overline{v^2}) - (U^2/r) - (\overline{u^2}/r) + (\overline{v^2}/r) = -(1/\rho)(\partial P/\partial r) \quad (2)$$

$$(d/dr)(\overline{vw}) + (\overline{vw}/r) = 0 \quad (3)$$

Eq. (3) together with the boundary conditions $\overline{vw} = 0$ at $r = r_i$ and $r = r_0$ requires that $\overline{vw} = 0$ throughout the channel. Eq. (1) can be written

$$(r/\rho)(\partial P/\partial\phi) + (\partial/\partial r)(r^2\overline{uv}) = \nu(\partial/\partial r)[r^3(\partial/\partial r)(U/r)] \quad (4)$$

Differentiating Eq. (2) with respect to ϕ, we have

$$\partial^2 P/(\partial\phi\partial r) = \partial^2 P/(\partial r\partial\phi) = 0$$

Hence $\partial P/\partial\phi$ is independent of r. Eq. (4) can thus be integrated with respect to r to form

$$\mu r(\partial/\partial r)(U/r) - \rho\overline{uv} = (1/2)(\partial P/\partial\phi) + (C/r^2) \quad (5)$$

where C is the constant of integration.

Eq. (2) cannot be easily integrated across the channel. However, by considering a mean total pressure P_t such that

$$P_t = P + (1/2)\rho(U^2 + \overline{u^2} + \overline{v^2} + \overline{w^2}) \quad (6)$$

where P is the mean static pressure, Eq. (2) becomes

$$[1/(2r^2)](\partial/\partial r)[r^2(U^2 + \overline{u^2} - \overline{v^2})] = (1/\rho)(\partial P_t/\partial r) + (1/2)(\partial/\partial r)(\overline{w^2})$$

Multiplying this equation by r^2 and integrating across the channel from the inner wall $r = r_i$ to any other radius $r = r$, we obtain

$$\frac{1}{2}\rho U^2 = (P_t - P_i) - \frac{\rho}{2}(\overline{u^2} - \overline{v^2} + \overline{w^2}) - 1/r^2 \int_{r_i}^{r} [2(P_t - P_i) - \rho\overline{w^2}]r\,dr \quad (7)$$

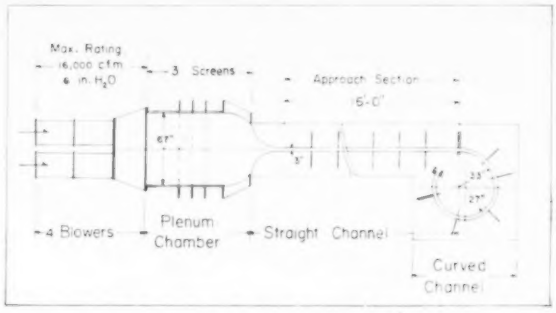

Fig. 5. Assembly of the Wind Tunnel

where P_i is the mean pressure at the inner wall. Thus the mean velocity U can be evaluated from the measurements of P_t and turbulence intensities. In particular, we have, since $U = \overline{u^2} = \overline{v^2} = \overline{w^2} = 0$ at $r = r_0$,

$$\int_{P_i}^{P_0} r^2\,dP_t = \rho\int_{r_i}^{r_0}\overline{w^2}\,r\,dr \quad (8)$$

where P_0 is the mean pressure at the outer wall. The integral on the left-hand side of Eq. (8) is the area A minus the area B in Fig. 4. Eq. (8) vanishes identically if the channel is straight.

The turbulent energy equation for incompressible flows in the fully developed curved channel is[3]

$$\overline{uv}\left(\frac{\partial U}{\partial r} - \frac{U}{r}\right) + \frac{1}{r}\frac{\partial}{\partial r}\left[r\overline{v\left(\frac{u^2 + v^2 + w^2}{2} + \frac{p}{\rho}\right)}\right] = \nu\left(\overline{u\nabla^2 u} + \overline{v\nabla^2 v} + \overline{w\nabla^2 w} - \frac{\overline{u^2}}{r^2} - \frac{\overline{v^2}}{r^2} + \frac{2}{r^2}\overline{u\frac{\partial v}{\partial\phi}} - \frac{2}{r^2}\overline{v\frac{\partial u}{\partial\phi}}\right) \quad (9)$$

where

$$\nabla^2 = (\partial^2/\partial r^2) + [(1/r)(\partial/\partial r)] + [(1/r^2)(\partial^2/\partial\phi^2)] + (\partial^2/\partial z^2)$$

The first term represents the production of turbulent energy. The second term represents the diffusion of turbulent energy and the transfer of energy due to the action of fluctuating pressure gradients. The last term can be identified as the transport of the turbulent energy by the viscous forces and dissipation of turbulent energy to heat.[5]

(3) Test Equipment

(3-1) *The Wind Tunnel*

The wind tunnel was designed for maximum velocities in the neighborhood of 100 ft. per sec. Two banks of blowers, each bank consisting of two blowers in series, were used to supply the flow. Each blower has a maximum rating of 4,000 cu. ft. per min. and a static head of 3 in. of water. The blowers discharged the air into a plenum chamber 60 in. high and 67 in. wide (Fig. 5). The interior of the plenum chamber is equipped with three screens with different solidity. A fourth screen of low solidity was located at the discharge of the blowers.

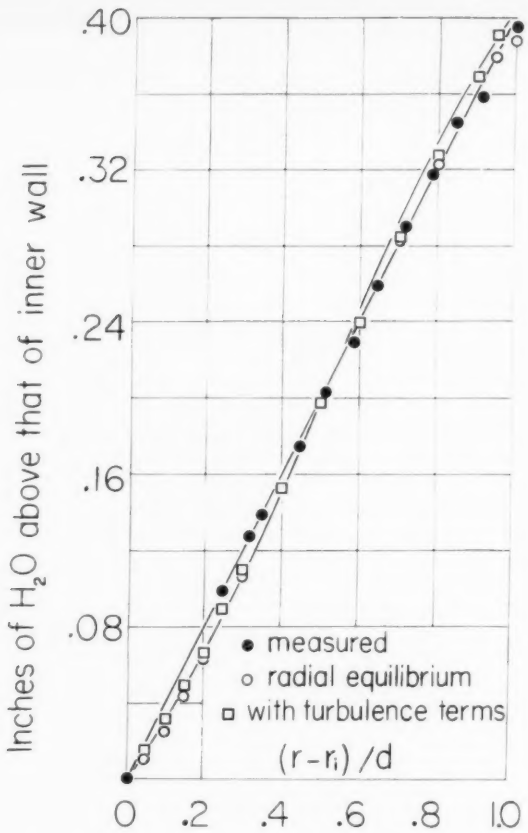

Fig. 6 Radial static pressure distribution in curved channel.

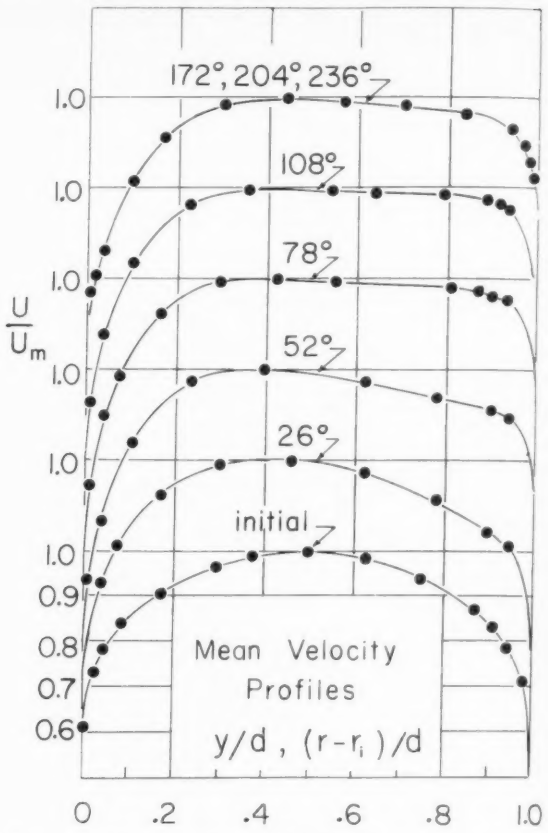

Fig. 7. Dimensionless Velocity Distributions.

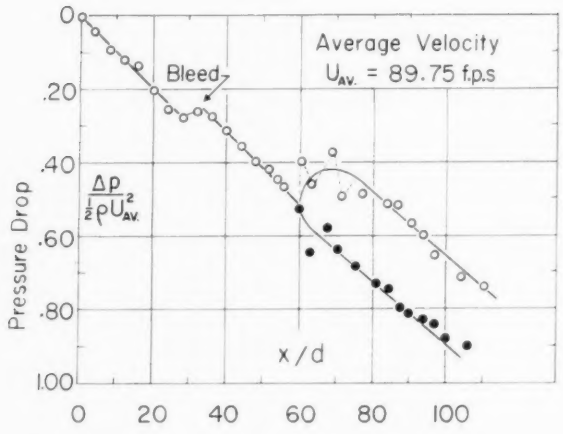

Fig. 8. Static Pressure along Length of Channel

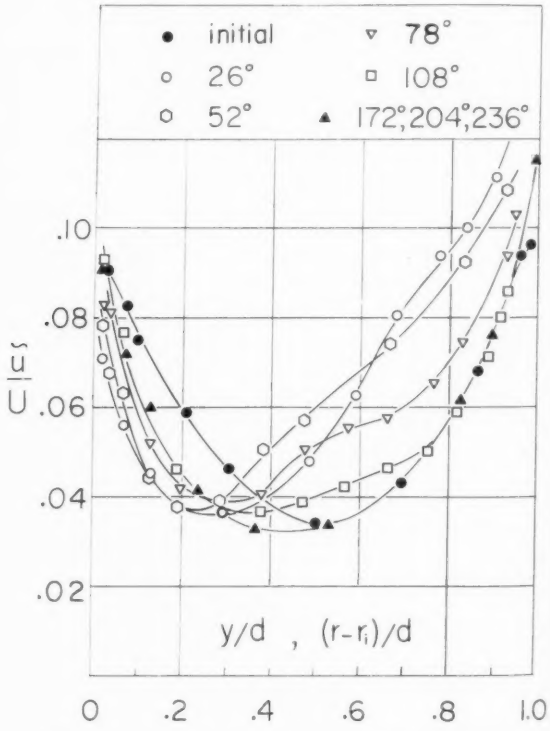

Fig. 9. Local Intensity of Turbulence.

A vertical and a lateral contraction followed the plenum chamber to meet the dimensions of the test section. The dimensions of the straight approach section are 3 in. wide, 46½ in. high, and 16 ft. long. The width and the height of the channel remains constant up to the exit. An aspect ratio of 15.5 to 1 was chosen in order to ensure two-dimensionality in the major middle portion of the channel. Halfway downstream of the inlet of the straight parallel section, 1- by 3-in. slots are located on the channel ceiling and floor in order to evacuate the boundary layer already developed there. This bleeding helps to establish two-dimensional flow in the curved section of the channel.

The walls in the straight parallel section are made of 1/2-in. plywood with a plastic surface finish. In order to establish a fully developed flow at the end of the straight parallel section, it was necessary to make the walls 16 ft. long or 64 duct widths.

The curved section has the same height and width as the approach section. The walls are made of rolled sheet metal # 16 gage. In order to accommodate an arc of more than 360° in the curved section, it was necessary to make the radius of curvature of the outer wall in the first quadrant 36 in. and that of the remaining curved portion 30 in. Subsequently it was found that only 300° of curved wall was necessary in these experiments, because the fully developed state occurred about the end of the second quadrant. As compared with the original design shown in Fig. 5, this simplified many problems associated with the proper discharge of air. In the equilibrium section of the curved channel, r_0, the radius of the outside wall is 30 in. and r_i, the radius of the inner wall, is 27 in. Hence $r_i/r_0 = 0.9$.

The maximum (temporal) mean velocity at the end of the straight parallel section is 98.36 ft. per sec., and the Reynolds Number based on this velocity and the half width of the channel is 74,200.

(3-2) *The Hot-Wire Anemometer Equipment*

Tungsten wires 0.00030 in. in diameter were used in these experiments.[6] The hot-wire anemometer set was designed and built to handle wires with time constant up to 2 millisec. Using an approximately 1 millisec. wire in the actual flow conditions, the overall frequency response is flat from 10 to 5,000 cycles per sec. The set contains two separate bridges and two separate compensating amplifiers. This eliminates signal coupling when two wires are used at the same time. An adding and subtracting circuit similar to the one used by Kovasznay[7] was used.

Time derivatives of the fluctuating quantities were measured with an electronic differentiator. All mean-square values of the turbulent fluctuating quantities were measured through a thermocouple unit. The compensation was calibrated with a square wave input to the wire.

The frequency analysis of the turbulent fluctuating quantities was made with a Hewlett-Packard wave analyzer. In order to obtain mean-square values of the voltage associated with a band width at a given frequency, the output circuit of the wave analyzer was altered. The output was fed directly into a thermocouple, bypassing the rectifier at the output of the wave analyzer.

(4) Results

(4-1) *Mean Velocity and Mean Pressure Across the Channel*

The distribution of the mean total pressure P_t across the channel was measured with a boundary-layer type of Pitot tube of small aperture. The closest distance that could be measured near the wall with this probe was 0.020 in. The mean static pressure across the channel can be obtained by substituting Eq. (6) into Eq. (7) with the result:

$$P = P_i + \frac{1}{r^2}\int_{r_i}^{r} (P_t - P_i)2r\,dr - \rho w^2 - \frac{\rho}{r^2}\int_{r_i}^{r} w^2\,r\,dr \quad (10)$$

If we neglect the turbulence terms, Eq. (10) reduces to

$$P = P_i + \frac{1}{r^2}\int_{r_i}^{r} (P_t - P_i)2r\,dr$$

This equation was derived and used by Wattendorf.[1]

In the present investigation, calculated values of P including and neglecting the turbulence terms are compared with the measured values using a static probe. At the inner and outer walls P was measured by static holes. The results are plotted in Fig. 6. It can be seen that the turbulence terms become significant only in the immediate neighborhood of the two walls.

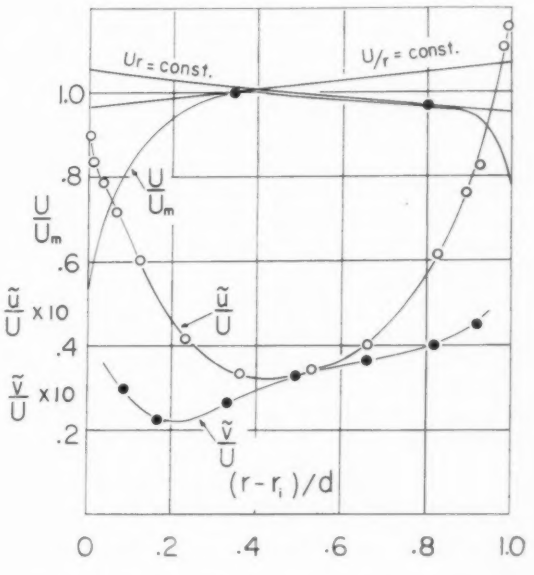

Fig. 10. Mean Velocity and Turbulence Level at Fully Developed Curved Section.

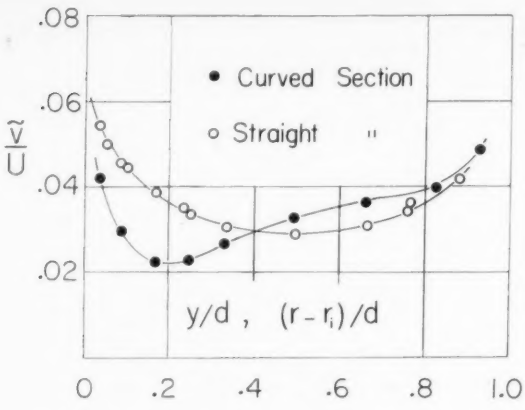

Fig. 11. Comparison of $\frac{\tilde{v}}{U}$ in Fully Developed Straight and Curved Sections.

The distribution of mean velocity as a ratio of the maximum mean velocity (U/U_{max}) in the fully developed section is in good agreement with the experimental results by Wattendorf.[1] A comparison of the velocity distributions as they proceed around the curved section are plotted in Fig. 7. The symmetrical profile labeled 0° corresponds to the fully developed straight section, and the profile closest to the top of Fig. 7 represents the velocity distribution at three consecutive stations in the curved channel at 172°, 204°, and 236°. The experimental data show that the flow in the curved channel has reached equilibrium at 172°. This checks the results of Wattendorf. [The turbulent intensity shows the same evidence and this fact is discussed in Section (3-3).] Velocity measurements at three vertical stations showed that two dimensionality existed.

(4-2) *Pressure Drop Along the Channel*

The drop of wall static pressure along the channel is shown in Fig. 8. The level of the static pressure is arbitrarily considered to be zero at the beginning of the straight "approach" section. The static pressure drop is expressed as a ratio to the dynamic head based on the spatial average velocity in the channel.

The effect of boundary-layer bleeding [see Section (3-1)] can be seen in the static pressure drop a little after the mid-length of the straight channel. The entrance to the curved channel begins at $x/d = 60$. At this point, the static pressure drop divides into two separate curves: an upper curve for the outer wall and a lower curve for the inner wall. The abscissa in the curved region represents actual arc length $r\phi$ of each wall. Since the pressure drop $\partial P/\partial\phi$ is the same for both walls, the slope $\partial P/r\partial\phi$ is not the same for the two walls.

(4-3) *Turbulence Intensities $\tilde{u}/U$ and $\tilde{v}/U$*

Measurements on local turbulence intensities $\tilde{u}/U$ and $\tilde{v}/U$ were made in the fully developed straight and curved sections, as well as in the transition region in between. The results are shown in Figs. 9, 10, and 11. One foot ahead of the entrance to the curved section (labeled by 0° in Fig. 9), $\tilde{u}/U$ is symmetrical with respect to the center of the channel. In the first 26° of transition from straight to curved section, $\tilde{u}/U$ shows considerable increase near the outer wall and a decrease near the inner wall. As the flow proceeds in the transition region a tendency to restore $\tilde{u}/U$ to its original distribution can be noticed. Finally, in the fully developed curved section, the values of $\tilde{u}/U$ in the inner half of the channel are still smaller than those in the straight section, while the values in the immediate vicinity of the outer wall are higher than those in the straight section. Measurements of $\tilde{u}/U$ at the three stations 172°, 204°, and 236° show a variation not more than experimental accuracy. Hence the flow settles down to an essentially fully developed pattern after an arc of 172°. This was in agreement with the mean velocity measurements as discussed in Section (3-1).

The turbulence intensity $\tilde{v}/U$ was measured with an X-meter. Fig. 11 shows that curvature has a similar effect on v/U as on $\tilde{u}/U$.

(4-4) *Shear Stress*

Eq. (5) can be written

$$\tau = \tau_t + \tau_l = (1/2)\,(\partial P/\partial\phi) + (C/r^2) \qquad (11)$$

where τ is the total shear stress, $\tau_t \equiv -\rho\overline{u\bar{v}}$ is the turbulent shear stress, and $\tau_l \equiv \mu r(\partial/\partial r)\,(U/r)$ is the laminar shear stress. Except in the immediate vicinity of the walls, τ_l is negligible when compared to τ_t. If r_n is the radius at which $\tau = 0$, the constant C in the above equation can be evaluated and the equation becomes,

$$\tau = -(1/2)\,(\partial P/\partial\phi)\,[(r_n/r)^2 - 1] \qquad (12)$$

From the measured values of r_n and $\partial P/\partial\phi$, τ is plotted against $(r - r_i)/(r_0 - r_i)$ in Fig. 12. The absolute values of τ at the two walls are

$$\tau_i/\rho U_{max}^2 = 0.00139$$

at the inner wall and

$$\tau_0/\rho U_{max}^2 = 0.00248$$

at the outer wall.

The turbulent shear stresses measured by an X-meter showed the consistent tendency that its absolute value is less than that calculated from Eq. (12). This tendency has also been observed in the measurements of turbulent shear stresses in the straight section. It might be added that in Laufer's experiments on straight channels the measured $\overline{u\bar{v}}$ for the highest Reynolds Number of 61,600 was almost 30 per cent lower than the values calculated from the pressure drop, although the agreement was good for lower Reynolds Numbers.

(4-5) *The Location of Zero Shear Stress*

Wattendorf found that the radius r_n for zero shear stress corresponds neither to the point at which $d(Ur) \div$

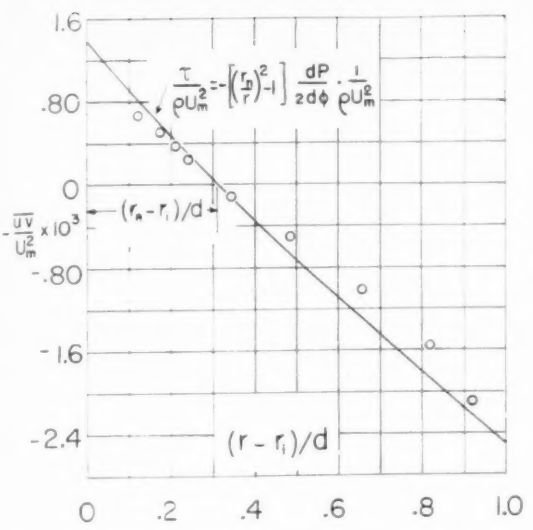

Fig. 12. Shear Stress Distribution across Fully Developed Curved Section.

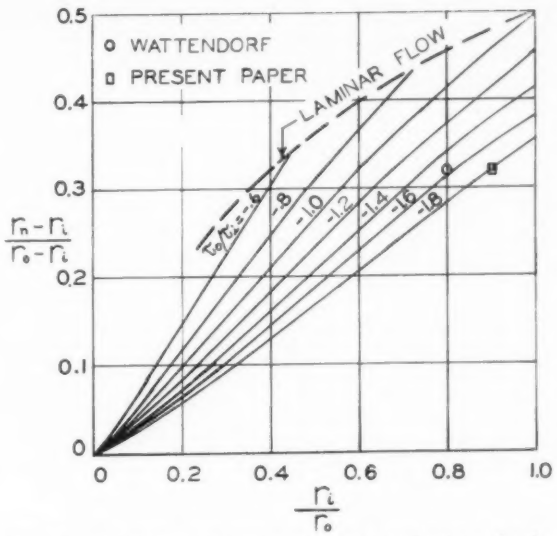

FIG. 13. The location of zero τ as functions of r_o/r_i and r_i/r_o.

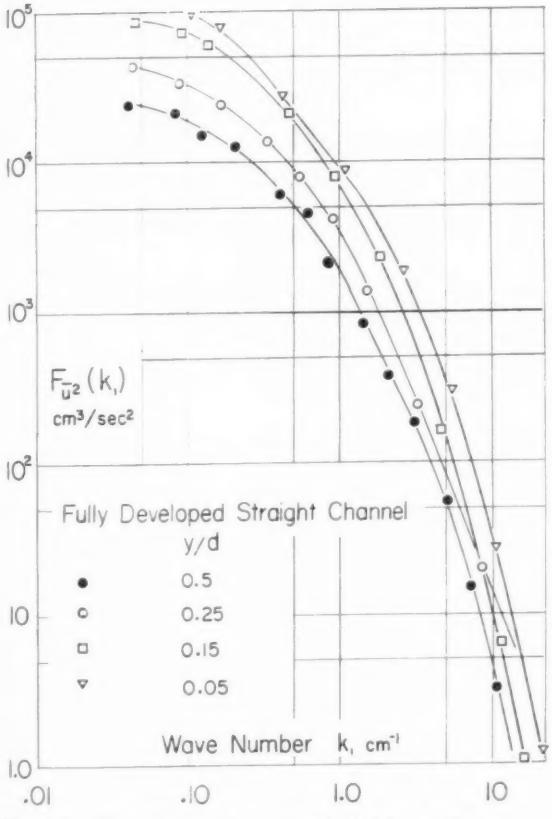

Fig. 14. Spectrum of u in straight section.

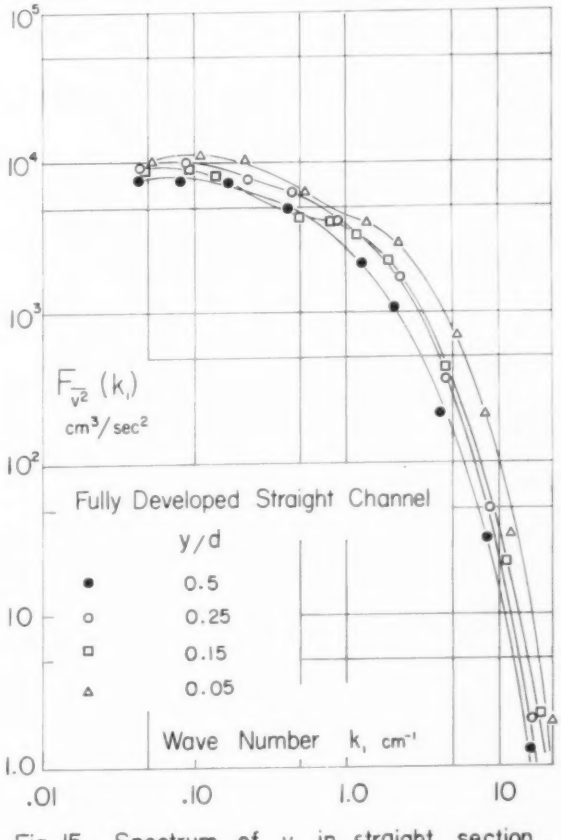

Fig. 15. Spectrum of v in straight section.

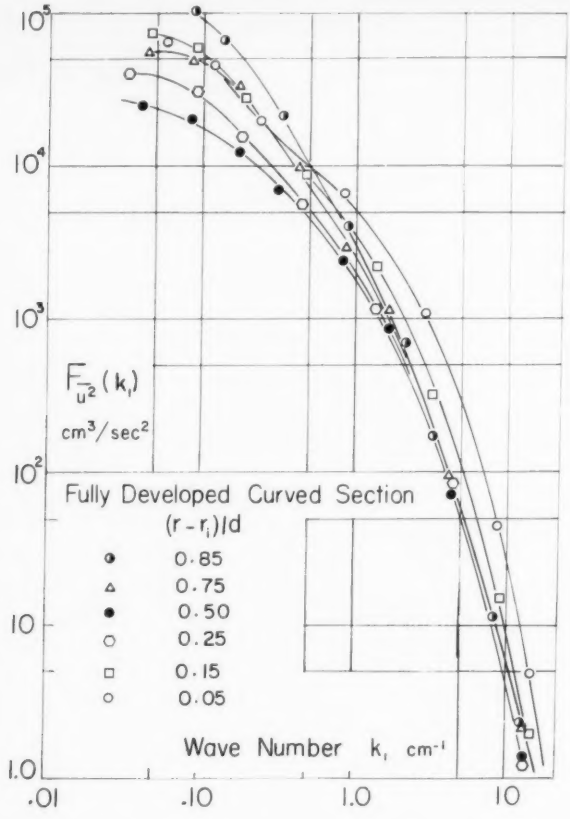

Fig. 16. Spectrum of u in curved section.

$dr = 0$ nor to the point at which $d(U/r)/dr = 0$. The same observation appeared to be also true in this investigation. Without attempting to predict the value of r_n, one can instead relate r_n to the wall shear stresses in the following way. From Eq. (12) we get

$$\tau_0 = -(1/2)\,(\partial P/\partial\phi)\,[(r_n/r_0)^2 - 1] \text{ at outer wall}$$

$$\tau_i = -(1/2)\,(\partial P/\partial\phi)\,[(r_n/r_i)^2 - 1] \text{ at inner wall}$$

From these two equations one can solve for the location of zero τ, expressed by the ratio $(r_n - r_i)/(r_0 - r_i)$, as a function of τ_0/τ_i and r_i/r_0. The result is

$$\frac{r_n - r_i}{r_0 - r_i} = \left[\sqrt{\frac{(\tau_0/\tau_i) - 1}{(\tau_0/\tau_i) - (r_i/r_0)^2}} - 1\right] \Big/ [(r_0/r_i) - 1] \tag{13}$$

In this investigation,

$$r_i/r_0 = 0.9$$

$$\tau_0/\tau_i = -1.784$$

$$(r_n - r_i)/(r_0 - r_i) \approx 0.32$$

In Wattendorf's channel II

$$r_i/r_0 = 0.8$$

$$\tau_0/\tau_i = -1.49$$

$$(r_n - r_i)/(r_0 - r_i) \approx 0.32$$

That $(r_n - r_i)/(r_0 - r_i)$ in both cases happens to be about 0.32 must be considered as a coincidence.

In both Wattendorf's investigation and the present one, the absolute magnitude of τ_0/τ_i for turbulent flows in curved channels between smooth walls is larger than 1. However, τ_0/τ_i for laminar flows is always less than 1 in absolute magnitude. The dotted line in Fig. 13 is obtained from the theoretical solutions of laminar flows. It can be expected that this line sets the limit for the family of curves for turbulent flows between curved walls of the same roughness.

(4-6) *Spectrum of $\overline{u^2}$ and $\overline{v^2}$*

The one-dimensional energy spectra of $\overline{u^2}$ and $\overline{v^2}$ at various distances from the walls in the straight and the curved channels are shown in Figs. 14 to 17. In these figures the abscissa is k_1 or the one-dimensional wave number in the direction of the mean flow U. The fact that $\overline{v^2}$-spectra of Fig. 17 show a marked influence of curvature will be discussed in Section (5).

Figs. 18 to 21 show the distribution of $n^2F(n)$ as a function of n. These curves are used for the calculation of microscales. (See next section).

(4-7) *Microscale*

The microscales λ_x, λ_y in the fully developed straight section and λ_ϕ, λ_r in the fully developed curved section

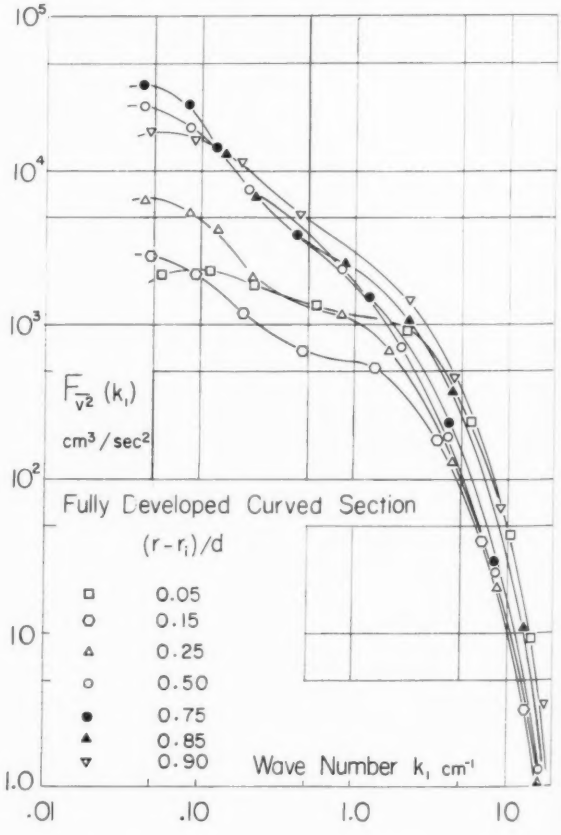

Fig. 17. Spectrum of v in curved section.

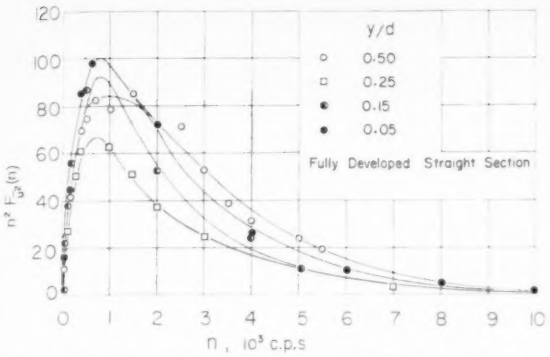

Fig. 18 . Second moment of u spectrum in straight section

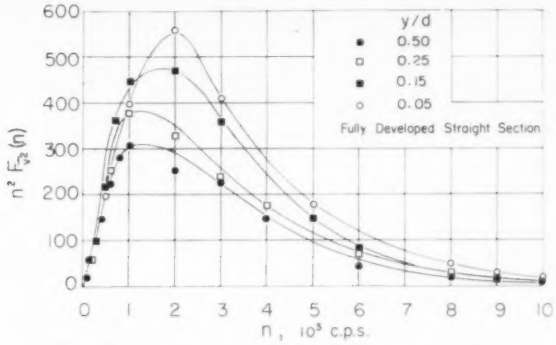

Fig. 19. Second moment of v spectrum in straight section

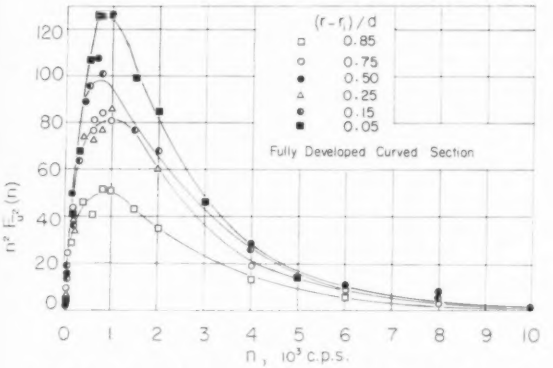

Fig. 20 . Second moment of u spectrum in curved section

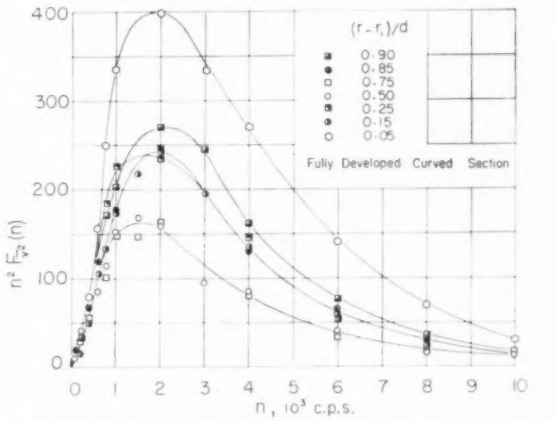

Fig. 21. Second moment of v spectrum in curved section

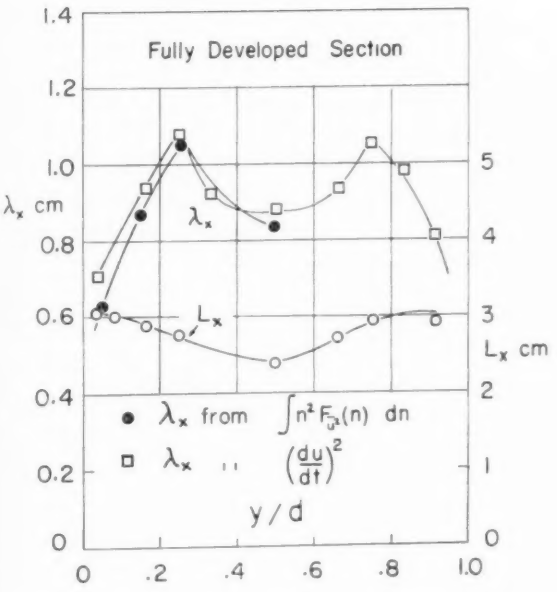

Fig. 22 . Scales of turbulence in straight section

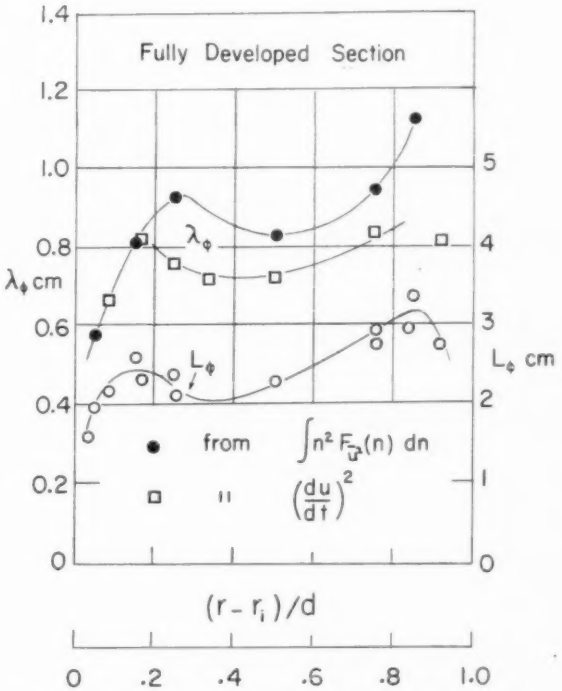

Fig. 23. Scales of turbulence in curved section.

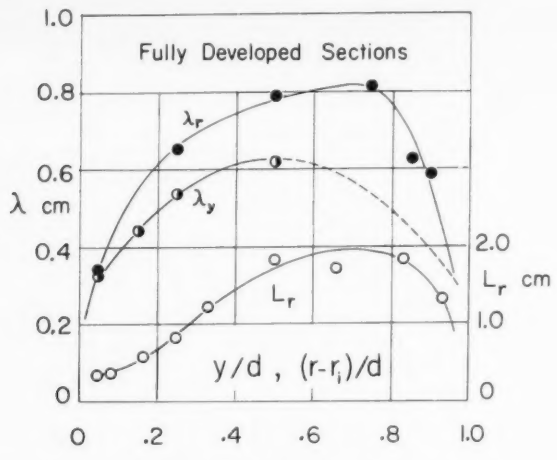

Fig. 24. Transversal and radial scales of turbulence.

are defined as:

$$\overline{(\partial u/\partial x)^2} = \overline{u^2}/\lambda_x^2$$

$$(1/2)\ \overline{(\partial v/\partial x)^2} = \overline{v^2}/\lambda_y^2$$

$$\overline{[\partial u/(r\partial\phi)]^2} = \overline{u^2}/\lambda_\phi^2$$

$$(1/2)\ \overline{[\partial v/(r\partial\phi)]^2} = \overline{v^2}/\lambda_r^2$$

The microscales can be obtained experimentally in the following manner first suggested by Townsend.[8] Assuming Taylor's hypothesis holds, we can write $\partial/\partial x = (1/U)\ (\partial/\partial t)$ for the straight section and $\partial/(r\partial\phi) = (1/U)\ (\partial/\partial t)$ for the curved section. Thus,

$$\overline{(\partial u/\partial x)^2} = (1/U^2)\ \overline{(\partial u/\partial t)^2}$$

and so on. In this investigation, $\overline{(\partial u/\partial t)^2}$ in the fully developed straight and curved sections was measured by an electronic differentiation circuit.

A second method of obtaining the microscale is based on the fact that the space correlation function R is the Fourier transform of the one-dimensional energy spectrum $F(n)$. Hence

$$\frac{1}{\lambda_x^2} = \left(\frac{\partial^2 R_x^u}{\partial x^2}\right)_{x=0} = \frac{4\pi^2}{U^2}\int_0^\infty n^2\ F_{u^2}(n)dn$$

$$\frac{2}{\lambda_y^2} = \left(\frac{\partial R_x^v}{\partial x^2}\right)_{x=0} = \frac{4\pi^2}{U^2}\int_0^\infty n^2\ F_{v^2}(n)dn$$

with similar expressions for λ_ϕ and λ_r. The distribution of $n^2F(n)$ has been given in Figs. 18 to 21; from these figures microscales were calculated.

Figs. 22 and 23 show the four microscales as functions of distances from the walls. The two methods of obtaining λ_x and λ_ϕ show substantial agreement, especially for λ_x. In the fully developed curved section, λ_ϕ decreases in the inner half and increases in the outer half of the channel, when compared to λ_x of the fully developed straight section. On the other hand, λ_r of the curved section is larger than λ_y of the straight section for the major portion of the channel, except near the inner wall where they are equal. The values of λ/d are approximately three times larger than those of Laufer's straight channel at a Reynolds Number of 61,600.

(4-8) *Integral Scales of Turbulence*

The integral scales L_x, L_y in the fully developed straight channel and L_ϕ, L_r in the fully developed curved channel are defined as follows:

$$L_x = \int_0^\infty R_x^u\, dx;\quad L_y = \int_0^\infty R_x^v\, dx$$

$$L_\phi = \int_0^\infty R_\phi^u\, rd\phi;\quad L_r = \int_0^\infty R_\phi^v\, rd\phi$$

The integral scales were estimated by a simple, approximate method based on the compensated and uncompensated values of the hot-wire signal.[2] The results are shown in Figs. 22 to 24. The method used is less justifiable for L_y and L_ϕ, the values of which are included merely as an indication of the trend. The effect of curvature on integral scales is just about the same as that on the microscale. A second method of estimating the integral scale is the extrapolation of the energy spectrum to zero frequency. The values obtained in this manner are not represented here, but their magnitude and trend are consistent with those shown in Figs. 22 to 24. The average ratio of L/d is the same as that found by Laufer in his straight channel of Reynolds Number 61,600.

(4-9) *Similarity Considerations*

It is well known that in the vicinity of walls, a universal curve of U/U_* vs. yU_*/ν holds for all Reynolds Numbers and even for different types of flows. Fig. 25 shows such curves near the two walls of the curved channel as well as near the wall of the straight channel. For $25 < yU_*/\nu < 200$ (y is the distance from the wall for all three cases), all curves follow the same logarithmic law

$$U/U_* = A\ \log_{10}(yU_*/\nu) + B \qquad (14)$$

The constants A and B are 5.03 and 6.5, respectively. The three curves branch out at $yU_*/\nu \approx 200$. The distribution represented by Eq. (14) is very close to other experiments[9] for the range of yU_*/ν considered above.

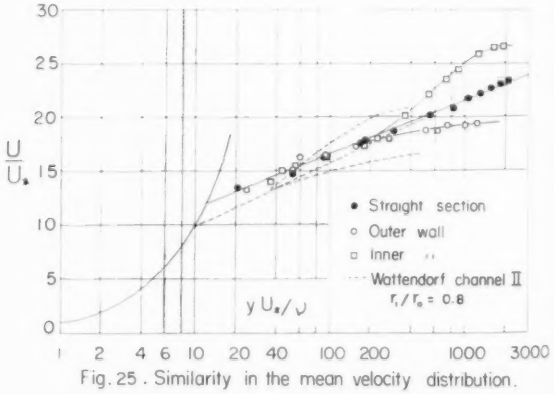

Fig. 25. Similarity in the mean velocity distribution.

The dotted curve in Fig. 25 is taken from Wattendorf's channel II of $r_i/r_0 = 0.8$. It is seen that considerable discrepancy exists between Wattendorf's data and the present measurements. From the point of view of dimensional analysis, near the wall U not only depends on y, ν and wall shear stress but also on the radius of curvature r. It is therefore to be expected that U_*/U is a function not only of yU_*/ν but also of y/r or perhaps of some combinations of the two. Such functional relationships are however not obvious at present.

Beyond the neighborhood of the walls, the similarity of the mean velocity for all Reynolds Numbers can be expressed for the case of a straight channel in the form

$$(U_{max} - U)/U_* = f(y/d)$$

Wattendorf[1] extended this concept to a curved channel and investigated the function

$$[(Ur)_{max} - Ur] \Big/ r\sqrt{\frac{1}{\rho}\frac{\partial P}{r_p \partial \phi} b_p} = f\left(\frac{y_p}{b_p}\right) \qquad (15)$$

where r_p is the radius of the reference point at which $(Ur) = (Ur)_{max}$, b_p is the distance from the reference point to the two walls, and y_p is the distance from the reference point. Plotted in this form Wattendorf showed that the mean velocity distributions on both sides of the reference point for two curved channels of different curvatures could all be reduced into a single curve. However, this curve differs distinctly from a corresponding plot of the velocity distribution of a straight channel. This is hardly surprising, for as pointed out in Section (1), a prominent feature of curved channel flow is a more equalized velocity distribution in the middle of the channel. Hence it is not to be expected that the same functional relation such as Eq. (15) can exist in both curved and straight channel flows.

Values of $\tilde{u}/U_*$ and $\tilde{v}/U_*$ near the walls are plotted against yU_*/ν in Fig. 26. It appears that as far as turbulence quantities are concerned, no similarity exists between the neighborhoods of the inner and the outer walls of a curved channel and the straight wall.

(4-10) *Turbulent Energy Production*

From the turbulent energy equation, Eq. (9), the production of turbulent energy of a two-dimensional fully developed flow in a curved channel is

$$(Pr) = \overline{uv}[(dU/dr) - (U/r)] \qquad (16)$$

This term can be made dimensionless by defining

$$(Pr)_* \equiv (\nu/U_*^4)\,[(dU/dr) - (U/r)] \qquad (17)$$

The major portion of this production occurs in a region close to the wall. This region, which includes the laminar sublayer, is characterized by a universal law of U/U_* vs. yU_*/ν. Since U/r in this region is small compared to dU/dr, we can write

$$(Pr)_* \approx (\nu/U_*^4)\,(dU/dy) \qquad (18)$$

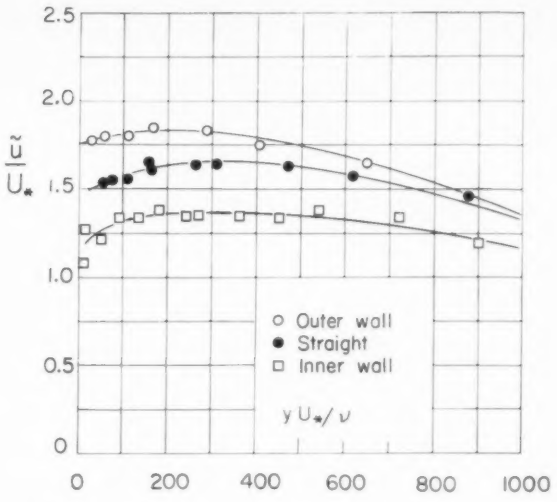

Fig. 26. Similarity in the turbulence intensity.

near the wall. Eq. (18) is an exact relation for a straight channel. Let us now consider two regions near the wall.

(a) For $25 < yU_*/\nu < 200$, Fig. 25 shows that Eq. (14) holds. Differentiating Eq. (14) with respect to y, we obtain

$$(\nu/U_*^2)\,(dU/dy) = 0.4343A/(yU_*/\nu)$$

In this region, $\overline{uv}/U_*^2$ is practically a constant and equal to unity. Hence

$$(Pr)_* = 0.4343A/(yU_*/\nu) \qquad (19)$$

(b) In the laminar sublayer corresponding roughly to $yU_*/\nu < 10$,

$$(\nu/U_*^2)\,(dU/dy) = 1$$

Hence
$$(Pr)_* = \overline{uv}/U_*^2 \qquad (20)$$

In Fig. 27 $(Pr)_*$ for the curved and straight channels in this investigation is obtained from Eq. (19) and plotted as a solid line. For comparison, Laufer's data on pipe flows[10] are plotted as dotted lines. The curves representing Eq. (19) or (20) are of course not valid in the neighborhood of $y_*U/\nu \approx 10$.

(5) Influence of Curvature on Turbulent Channel Flows[11]

Consider first the fully developed turbulent flow in a *straight* channel. The energy equations for the fluctuation components $\overline{u^2}$, $\overline{v^2}$, $\overline{w^2}$ are

$$[\overline{uv}(dU/dy)] + (1/2)\,(d\overline{vu^2}/dy) = -(1/\rho)\,[\overline{u(\partial p/\partial x)}] + \nu\overline{u\nabla^2 u} \qquad (21)$$

$$(1/2)\,(d\overline{v^3}/dy) = -(1/\rho)\,[\overline{v(\partial p/\partial y)}] + \nu\overline{v\nabla^2 v} \qquad (22)$$

$$(1/2)\,(d\overline{vw^2}/dy) = -(1/\rho)\,[\overline{w(\partial p/\partial z)}] + \nu\overline{w\nabla^2 w} \qquad (23)$$

The sum of these three equations is the total turbulent energy equation.[2]

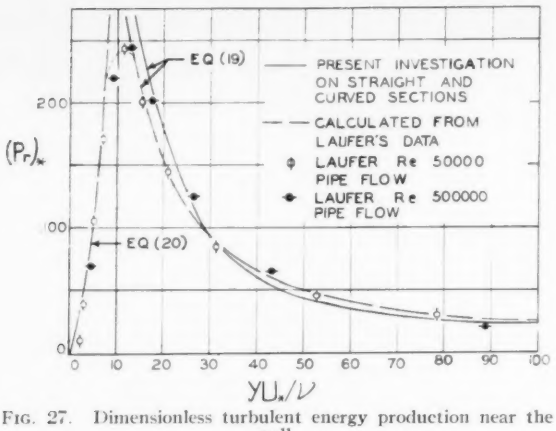

FIG. 27. Dimensionless turbulent energy production near the wall.

$$\overline{uv}\frac{dU}{dy} + \frac{d}{dy}\left[\overline{v\left(\frac{u^2+v^2+w^2}{2}+\frac{p}{\rho}\right)}\right] = \nu(\overline{u\nabla^2 u} + \overline{v\nabla^2 v} + \overline{w\nabla^2 w}) \quad (24)$$

Taking Eq. (21) as an example, the first term represents the production of $\overline{u^2}$ due to the action of Reynolds stress on the mean velocity gradient, the second term represents the diffusion of $\overline{u^2}$ by v, the third term represents an energy exchange which produces other fluctuating components, and the last term represents the transport by the viscous forces and the dissipation. A *negative* sign for the first term corresponds to a *positive* turbulent energy production and vice versa.

Based on Eqs. (21) to (24), one can draw the following conclusions for a *straight* channel.[12]

(a) The entire turbulent energy production goes directly to the longitudinal fluctuation $\overline{u^2}$.

(b) The other two fluctuation components ($\overline{v^2}$ and $\overline{w^2}$) receive their energy from $\overline{u^2}$ by action of the pressure fluctuation.

(c) Since $\overline{uv}$ is negative when dU/dy is positive and vice versa, the product $(\overline{uv})dU/dy$ is always negative. Hence turbulent energy is produced through the entire width of the channel, except at the channel center where it is zero.

Let us now consider a fully developed *curved* channel as described in this paper. The turbulent energy equations for the three fluctuation components are[3]

$$\overline{uv}\frac{dUr}{rdr} + \frac{1}{2}\frac{d\overline{rvu^2}}{r\,dr} + \frac{\overline{u^2v}}{r} = -\frac{1}{\rho}\overline{u\frac{\partial p}{r\partial\phi}} + \nu\left(\overline{u\nabla^2 u} - \frac{\overline{u^2}}{r^2} + \frac{2}{r^2}\overline{u\frac{\partial v}{\partial\phi}}\right) \quad (25)$$

$$-2\overline{uv}\frac{U}{r} + \frac{1}{2}\frac{d\overline{rv^3}}{rdr} - \frac{\overline{u^2v}}{r} = -\frac{1}{\rho}\overline{v\frac{\partial p}{\partial r}} + \nu\left(\overline{v\nabla^2 v} - \frac{\overline{v^2}}{r^2} - \frac{2}{r^2}\overline{v\frac{\partial v}{\partial\phi}}\right) \quad (26)$$

$$(1/2)\,[(d\overline{rvw^2})/(r\,dr)] = -(1/\rho)\,[\overline{w(\partial p/\partial z)}] + \nu(\overline{w\nabla^2 w}) \quad (27)$$

The sum of these three equations is the total turbulent energy equation which is just Eq. (9).

From Eqs. (25) to (27) and Eq. (9), we can draw the following conclusions for a *curved* channel:

(a) Turbulent energy is produced directly not only on $\overline{u^2}$ but also on $\overline{v^2}$.

(b) Since the point of zero $\overline{uv}$ does not coincide with the point of zero $d(Ur)/dr$ [see Section (4-5)], there is a region between these two points in which the product $\overline{uv}d(Ur)/dr$ is positive. In the present investigation, the value of $(r - r_i)/(r_0 - r_i)$ for $\overline{uv} = 0$ is 0.32 and that for $d(Ur)/dr = 0$ is 0.8. Between these two points is a region, occupying 48 per cent of the width of channel, in which turbulent energy on $\overline{u^2}$ is being *suppressed* by Reynolds stress working on the mean momentum gradient. However, nature seems to come to the rescue by providing a flat momentum profile (Fig. 3) so that the amount of suppression in this region is small when compared to the turbulence production outside of this region.

(c) The total energy production on all fluctuation components is $\overline{uv}r\,d(U/r)/dr$. In the present investigation, U/r reaches a peak at $(r - r_i)/(r_0 - r_i) \approx 0.27$. Hence for $(r - r_i)/(r_0 - r_i)$ between 0.27 and 0.32, or about 5 per cent of the channel width, the total fluctuation energy is being suppressed by the action of Reynolds stress working on the gradient of U/r.

(d) The transfer of energy between $\overline{u^2}$ and $\overline{v^2}$ is not only due to the pressure fluctuation but also due to the term $\overline{u^2v}/r$ appearing in both Eq. (25) and Eq. (26) but in opposite sign.

(e) The most important influence of curvature is perhaps the $\overline{v^2}$-production term $-\overline{uv}\,U/r$ in Eq. (26). Near the inner wall $\overline{uv}$ is negative, resulting in a positive sign of this term. This means a suppression of $\overline{v^2}$. Near the outer wall $\overline{uv}$ is negative, thus giving rise to a production of $\overline{v^2}$. Hence the radial movement of the fluctuations is suppressed near the inner wall but excited near the outer wall. This checks the stability criterion first suggested by Rayleigh.[13, 1] According to this criterion, a fluid particle near the outer wall, upon being displaced to a larger radius, will possess a larger momentum (Ur) than its new neighbors. The centrifugal force of the displaced particle will be greater than the centripetal pressure gradient existing at its new location, and the particle will therefore tend to displace to a still larger radius. Thus a radial displacement is unstable near the outer wall. Conversely, it is stable near the inner wall. It should be noted, however, that Rayleigh's criterion is based on the sign of $d(Ur)/dr$, whereas the direct production (or suppression) of $\overline{v^2}$ is based on the sign of $\overline{uv}$.

(f) The production of turbulent energy is usually associated with eddies of large size or of small wave numbers. The fact that $\overline{v^2}$ is suppressed near the inner wall should reflect in a lack of $\overline{v^2}$ energy in the low wave number range. That this is actually the case is shown remarkably in Fig. 17.

(*Continued on page 75*)

Boundary-Layer Measurements in Hypersonic Flow*

F. K. HILL†

The Johns Hopkins University

SUMMARY

Experimental data are presented on boundary-layer formation, heat transfer, and skin-friction coefficient at Mach Numbers of 8.25 and 9.0. The boundary-layer measurements were made on the wall of a conical nozzle in the presence of a favorable pressure gradient and several rates of heat transfer. The Reynolds Number based on momentum thickness varied from 1,500 to 3,500. Comparison is made with data at lower Mach Numbers and with the semiempirical theory of von Kármán. The existing data up to Mach Numbers of nine indicate agreement to within 5 per cent when compared with a form of the Wilson theory, but it is clear that the effects of heat transfer and pressure gradients present problems which require extensive study and experiment in the future.

SYMBOLS

C_f = local skin-friction coefficient
C_F = mean skin-friction coefficient
M = Mach Number
P = pressure
Pr = Prandtl Number
R = radius of nozzle at test station
Re = Reynolds Number
T = temperature
Te = equilibrium temperature
To' = total temperature at test station
Ty = static temperature at y
U = velocity in x direction
q = $(1/2)(\rho_\infty U_\infty^2)$
r = recovery factor
y, x = coordinates normal to wall and along the nozzle axis
γ = ratio of specific heats
δ = boundary-layer thickness
δ^* = displacement thickness
λ = molecular mean free path
μ = viscosity
ν = μ/ρ
ρ = density
τ = shearing stress
θ = momentum thickness

Subscripts

0 refers to stagnation condition
∞ refers to free stream
w refers to wall
h refers to pitot pressure
s refers to static pressure
δ_L refers to edge of laminar sublayer

INTRODUCTION

SINCE THE EARLY 1930's when von Kármán[1] discussed the importance in high-speed flows of turbulent as well as viscous shearing stresses, there have been many attempts to provide an adequate theory of turbulent boundary-layer formation in compressible flow. Although there is not, as yet, a completely satisfactory theory, a considerable body of data in the low supersonic range of Mach Numbers has been reported in the literature during recent years. Among the various theories proposed, and in some instances in the data as well, there have been rather large discrepancies. For example, Clauser[2] has discussed the inconsistencies which are known to exist in the results of extensive investigations of the characteristics of boundary layers formed in the presence of adverse pressure gradients and/or separation. Also, significantly, Chapman and Kester[3] and Coles[4] have pointed out that the numerous theories for skin-friction coefficients are quite discrepant at high Mach Numbers, especially those above 5. To a limited extent, recent work such as that reported by Coles[4, 5] has resolved some of these discrepancies by discussing the significance of certain boundary-layer parameters; experimental data at hypersonic Mach Numbers, $5 < M < 10$, which are now becoming available also assist in the clarification of the inconsistencies. This report presents data on the properties of boundary layers formed in the presence of flow at a free stream Mach Number of 9. It is apparent that in the study of hypersonic boundary layers the effects of viscosity, heat transfer, and compressibility are significant and must be clearly recognized in order to evaluate the measurements and correlate them with theory. The results are compared with those obtained at lower Mach Numbers where possible, although it is obvious that conditions of test here have not been idealized as well as can be done in conventional supersonic research where the number of flow variables may be restricted to a minimum. Heat transfer, Mach Number and pressure gradients are present, and the Reynolds Number range is limited. One of the consequences of operating at hypersonic Mach Numbers is to complicate the test conditions, but this in turn is helpful in directing attention to the parameters which are important and in leading to a clearer understanding of the problems involved.

EXPERIMENTAL CONDITIONS

The measurements reported here were made in a conical nozzle described elsewhere in the literature.[6] Pressure and temperature surveys were made across the nozzle at several stations in order to investigate the boundary layer formed on the nozzle wall. The two survey stations for which the data are presented were

Received October 7, 1954.

* This work was supported by the Bureau of Ordnance, Department of the Navy, under Contract NOrd 7386.

† Physicist, Applied Physics Laboratory.

near the nozzle exist where the pressure and Mach Number gradients were relatively small. Nitrogen gas, obtained commercially as Super Dry, was used and supplied to the tunnel settling chamber at pressures from 350 to 800 psig and heated to temperatures from 1,300 to 1,400°R. The inside of the nozzle, along which the boundary-layer measurements were made, had a smooth surface of electroformed nickel with surface irregularities of the order of 5μ in. The nozzle was constructed and mounted so that it could be rotated about its axis through any desired angle, without disturbing pressure or temperature probes mounted at fixed locations. A check was thus provided of complete axial flow symmetry. With nitrogen the nominal Mach Number of the tunnel at the exit was 9.1.

Since a nozzle boundary layer is being studied it is clear that there are several conditions different from the great majority of boundary-layer investigations which have been done in "two-dimensional" flow on a flat plate and with "zero" pressure gradient. In the present case the throat of the nozzle serves essentially as a source and produces almost ideally irrotational flow. There is no evidence of "cross-flow" or separation within the boundary layer. Since the nozzle conical surface is inclined 6° with respect to its axis, there is, of course, both a favorable pressure gradient as well as a Mach Number gradient along the nozzle axis. The pressure and Mach Number gradients are least at the nozzle exit and amount to 0.26 mm. Hg/in. and 3 per cent/in., respectively (P_0 = 600 psig case).

Data

One of the primary aims of this investigation was the determination of skin friction. Because of the relatively small scale of the tunnel (the exit diameter of the nozzle was 2 in.) a floating element technique for wall friction measurements was not feasible. The method used was that of deriving the wall shearing stress from the velocity profile by boundary-layer surveys of pitot pressure, static pressure, and total temperature. The data for one survey are shown in Figs. 1a and 1b. The supply conditions in this case were 600 psig and 1,360°R. Similar data for supply pressures of 400, 500, and 750 psig were recorded. A full discussion of the techniques of measurement is given elsewhere.[7]

The pitot pressures and static pressures were recorded by means of Statham pressure transmitters connected to string galvanometers and by conventional mercury manometers. When using the pressure transmitters the response of the entire electrical system was less than 10^{-3} sec. and it was found that pressure pulses of the order of 10^{-3} sec. could be resolved, although the overall response of the system was slower for gross pressure changes. In the data there was no evidence of pressure fluctuations or intermittent flow with time constants greater than the instrumentation response. Generally, conventional pitot probes were used (0.042 in. o.d., blunt tip); for positions close to the tunnel wall flattened probes of 0.008 in. overall thickness were used. A calculation of the molecular mean free path indicated that slip-flow conditions for the stream did not obtain in the "free stream" nor throughout the boundary layer—i.e., the Tsien[8] condition, $\lambda/\delta < 1/100$ was not violated. Surveys were made at Station A near the nozzle exist where $M \sim 9$ and at Station B two in. upstream where $M \sim 8.25$.

T_0' values shown for the total temperature surveys in Fig. 1b represent the probe readings corrected for the measured recovery factor of the probe itself. This factor varied from unity at $M = 0$ to 85 per cent at $M = 9$ with a slight dependence on stream density. Calibration curves for each set of test conditions were used to determine the true T_0'. The probe was made of ceramic tubing 0.058 in. in diameter at the tip, with 0.010-in. iron-constantan thermocouple wire inside and an exit to entrance duct ratio of 20 per cent. A thermocouple was placed in the wall to check the temperatures at the wall with the value extrapolated from the T_0' and T_y curves. Stabilization of this temperature indicated when the tunnel heat-transfer rates were constant.

Accuracy of the Data

The range of pressures and temperatures in hypersonic tunnels is large compared to that normally employed in supersonic work. In addition, because several new phenomena such as slip flow may enter, not only the accuracy of the measurements must be stated but also conditions of test must be defined. For pitot pressures at the test Stations A and B, the range of pressures was from 1.5 to 300 mm. Hg; the recording accuracy in absolute value was ±3 per cent and ±0.25 per cent, respectively. For static pressures the recording accuracy was ±3 per cent. In practice many runs were made at all supply conditions within the limits of the test conditions, so that the average values used are all believed to be within 1 per cent. The total temperature measurements plus the corrected recovery factor of the probe are accurate to 2 per cent, and in deriving velocity values from the temperature data the error is not greater than 1 per cent provided the flow is locally isentropic. Two other sources of error must be noted. The supply gas, when heated to 1360°R. prevents any measurable effects of condensation after expansion in the nozzle[9] but partially excites the first vibrational mode of nitrogen. A careful study of pitot pressure as a function of supply temperature was made and it was found that the relaxation time of N_2 under our test conditions affected the pressure recorded by the pitot probe by less than 1 per cent. (For extremely small bore pitot probes the effect was found to increase.) The second source of error likely to occur in hypersonic flow is that due to slip-flow and viscous effects on the pitot probes in the boundary layer, even though the gas as a whole exhibits no slip effects with respect to the tunnel wall under these test conditions. The probes are sufficiently small, so that very near the wall where the molecular mean free path is greatest a more critical evaluation must be made. At a distance

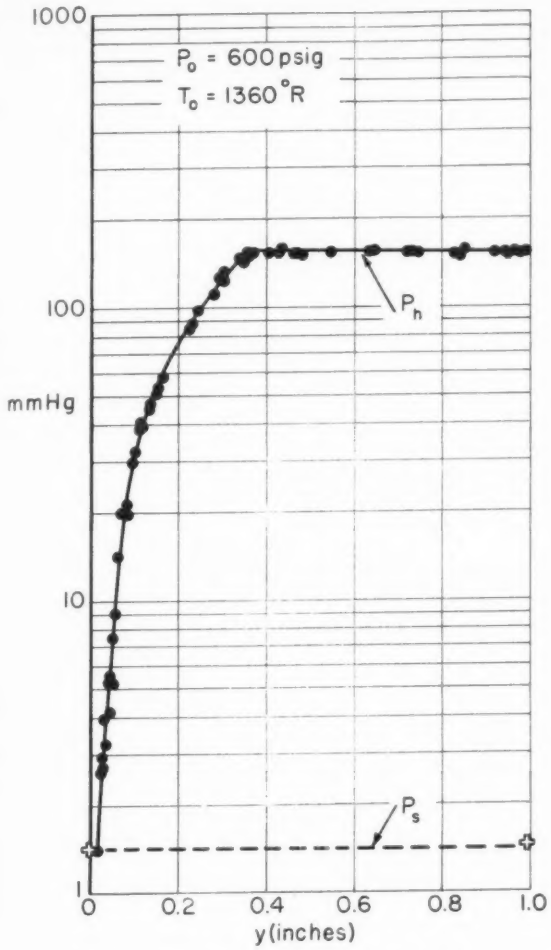

FIG. 1a. Pitot pressure vs. distance from wall.

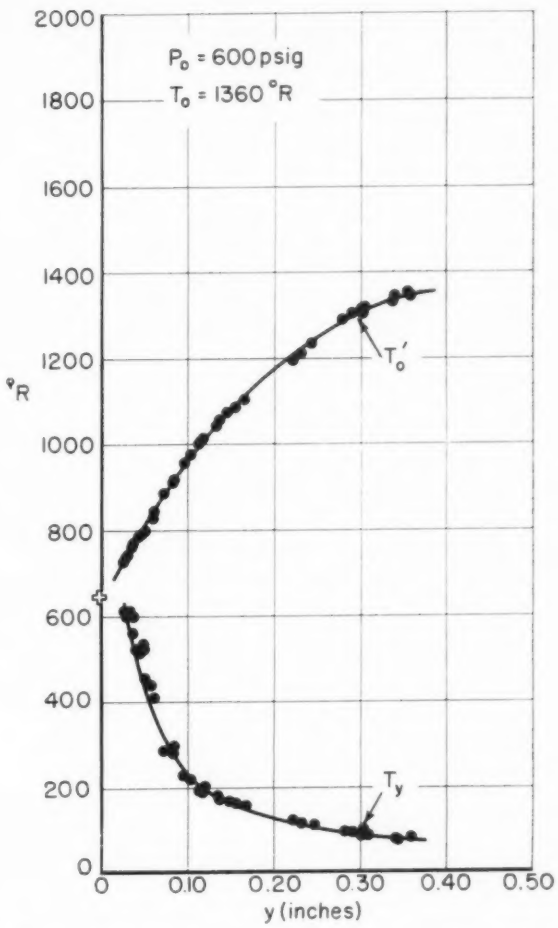

FIG. 1b. Total and stream temperature vs. distance from wall.

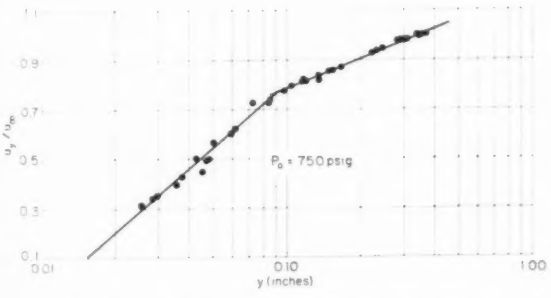

FIG. 2a. Velocity ratio vs. distance from wall.

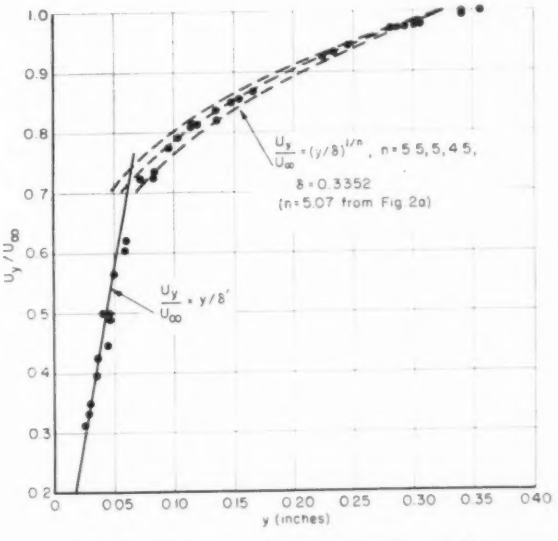

FIG. 2b. Velocity ratio vs. distance from wall.

TABLE 1
Boundary-Layer Parameters, Station A

P_0 (psig)	400	500	600	750
T_0 (°R.)	1,360	1,360	1,360	1,360
M_∞	8.99	9.04	9.07	9.10
T_∞(°R.)	79.24	78.42	77.93	77.44
Re_∞(/in.)	1.060×10^5	1.302×10^5	1.545×10^5	1.906×10^5
T_w(°R.)	601	625	645	673
ρ_w/ρ_∞	0.1318	0.1255	0.1208	0.1151
δ (in.)	0.3475	0.3406	0.3367	0.3352
θ (in.)	0.01175	0.01235	0.01235	0.0120
Re_θ	1,245	1,607	1,908	2,287
$\left(\nu \frac{u}{y}\right)_w \frac{\text{ft.}^2}{\text{sec.}^2}$	4.654×10^4	5.513×10^4	5.470×10^4	5.400×10^4

TABLE 2
Summary of Skin-Friction Measurements

M_∞	T_w/T_∞	Re_θ	C_f	C_f/C_{f_i}
8.99	7.68	1,245	7.899×10^{-4}	0.197
9.04	7.97	1,607	8.910	0.235
9.07	8.28	1,908	8.505	0.234
9.10	8.69	2,287	8.000	0.227
8.22	7.17	2,081	9.240	0.257
8.25	7.26	2,498	9.102	0.265
8.27	7.34	2,885	8.695	0.259
8.29	7.37	3,202	8.202	0.247
8.29	7.41	3,451	7.709	0.239

of 0.025 in. from the wall the ratio M/Re is 0.009. According to Kane and Maslach,[10] this would require a correction of less than 1 per cent. Their criterion for applicability of the Rayleigh formula is that if the ratio of Mach to Reynolds Number is less than 0.015 the correction is less than 1 per cent. In practice our measurements were limited to 0.020 in. from the wall so that it was concluded (for the nitrogen runs) the error due to viscous and slip effects was less than 1 per cent.

Numerical Results

Plots of the velocity in the boundary layer for four supply conditions at Station A and for five supply conditions at Station B were derived from the pressure and temperature data. The Rayleigh formula was used to compute Mach Number. Total temperatures together with tables[11] of isentropic flow with $\gamma = 1.4$ were used to calculate density and velocity as a function of distance from the wall. The results for one case are presented graphically in Figs. 2a and 2b. The transition from laminar to turbulent flow is apparent, and the laminar sublayer is significantly thicker in relation to the total boundary-layer thickness, δ, than in boundary layers at lower supersonic Mach Numbers. Other properties of the boundary layer have been found from these basic data. The momentum thickness, θ, is calculated from the expression

$$\theta(2R - \theta) = \int_{R-\delta}^{R} 2 \frac{\rho_y U_y}{\rho_\infty U_\infty} \left(1 - \frac{U_y}{U_\infty}\right) y \, dy \quad (1)$$

where R is the radius of the circular section at which the survey is made. The local coefficient of skin friction, C_f, is calculated from the usual formula relating shearing stress at the wall with the velocity gradient.

$$\tau_w = C_f[(1/2)\rho_\infty U_\infty^2] = \mu_w(\partial u/\partial y)_w \quad (2)$$

A summary of the significant parameters at Station A is given in Table 1, and in Table 2 the skin-friction data for both test stations is summarized. The incompressible skin-friction coefficient, C_{f_i}, is obtained from the Kármán-Schoenherr[1] relation, at comparable Re_θ and for zero heat transfer.

Analysis of Results

Universal Velocity Profiles

As pointed out in the introduction the original work of von Kármán introduced the concept of turbulent shearing stress into boundary-layer analysis and this was based on his well-known mixing length theory. The result of this concept for very high-speed flows was that near the wall the shearing stress would be laminar and proportional to $\mu(du/dy)$, while further from the wall the shearing stress would be predominantly turbulent and proportional to $\rho\overline{u'v'}$, u' and v' being the velocity fluctuations. When this is translated into velocity profiles the functions are of the form

$$U/U_\tau = y(U_\tau/\nu_w) \qquad \text{for laminar flow} \quad (3)$$

$$U/U_\tau = a + b \log [y(U_\tau/\nu_w)] \qquad \text{for turbulent flow} \quad (4)$$

where a and b are constants and u_τ is the friction velocity, $(\tau_w/\rho)^{1/2}$. These two equations have constituted the well-known universal velocity profiles for boundary layers, and provide a method which has been widely used in graphical plots of boundary-layer data. It has been particularly useful for (a) both two dimensional and axially symmetric flows and (b) flows with and without pressure gradients. It is, consequently, a very convenient way to show hypersonic boundary-layer data where the flow may be either axially symmetric or two-dimensional, and where pressure gradients and large heat-transfer rates may also be present.[12] In Fig. 3 such universal velocity profiles are shown for the Station A data and for the curves calculated from Eqs. (3) and (4) in which the values of the constants a and b were those derived by von Kármán.[1]

Several features of these velocity profiles are significant.

(1) The laminar region is relatively large (~15 per cent of total boundary-layer thickness) and the data scatter about the $U/U_\tau = y(U_\tau/\nu_w)$ line; if all four cases are superimposed the consistent random scatter about this line shows very clearly.

(2) In the turbulent region for the 500, 600 and 750 psig cases, the data show similar behavior with respect to the straight line represented by Eq. (4). There is a displacement above the line which is consistent with data reported by Lobb, Winkler and Persh[13] for Mach Numbers of 5 and 6.8. Their data represented boundary layers on the nozzle wall of the NOL hypersonic tunnel (two-dimensional case) in the presence of a favorable pressure gradient and with heat transfer. Their data showed a displacement upwards from the straight line with increasing heat-transfer rates and a constant displacement above the line with Mach Number. Our data at a nominal Mach Number of 9 are in agreement with these results, the turbulent portion being above the line by a smaller amount than the NOL data.

(3) The turbulent data shown in Fig. 3 for $P_0 = 400$ psig is clearly inconsistent with that taken at the other P_0 values. The reason for this is believed to be due to an incompletely developed turbulent boundary layer with the flow in the "transition" stage. This hypothesis is further borne out by the skin-friction data and is comparable to the findings of Coles.[5]

(4) For hypersonic Mach Numbers the transition from laminar to turbulent flow within the boundary layer is completed by a limiting value of (yU_τ/ν_w) of 20, whereas for low velocity flows the value[6] is near 50.

Heat-Transfer Rates

The heat-transfer rates for the four cases at Station A may be readily calculated from the data given in Table 1. The heat-transfer rate is defined as $(T_e - T_w)/T_\infty$, where T_e is the equilibrium temperature computed for zero heat transfer. This involves the assumption of a recovery factor. Two sets of values have been computed and are given in Table 3. The first is computed for the entire boundary layer with the recovery factor equal to $\sqrt{Pr}$ which is customarily associated with laminar flow.

$$r = \frac{T_e - T_\infty}{T_0 - T_\infty} \tag{5}$$

The second computation attempts to give the heat-transfer rate in the turbulent layer by taking the recovery factor equal to $\sqrt[3]{Pr}$ with Pr evaluated at $y = \delta_L$ and T_{δ_L} used in place of T_w.

With fully developed turbulent boundary layers in lower Mach Number supersonic flow the recovery factor is usually close to the $\sqrt[3]{Pr}$ and the heat-transfer rate is determined by using the wall temperature, T_w. This same calculation may be made for the present data from the numbers given in Tables 1 and 3, but has not been tabulated because it is felt this is not truly representative of the actual heat-transfer rates in hypersonic streams. The laminar sublayer is relatively so thick (15 per cent) that the physical process of heat transfer in hypersonic boundary layers may be different from boundary layers where turbulence predominates through 96 to 99 per cent of the total thickness.

TABLE 3
Heat-Transfer Rates at Station A, $M \sim 9$

P_0 (psig)	400	500	600	750
$\frac{T_e - T_w}{T_\infty}$	6.93	6.73	6.48	6.17
$\frac{T_e - T_{\delta_L}}{T_\infty}$	3.60	4.55	4.57	4.18

Pressure Gradient Effects

Since negative pressure gradients were present in this experimental work, and since in practical applications at hypersonic Mach Numbers similar pressure gradients will be encountered, the order of magnitude of these effects should be estimated. As is well known, from the two-dimensional momentum equation for boundary-layer flow,

$$\frac{d}{dx}\int_0^\delta \rho U(U_\infty - U)\,dy = \delta^* \frac{dP}{dx} + \tau_w \tag{6}$$

the local skin-friction coefficient may be expressed as

$$C_f = 2(d\theta/dx) + (1/q)(M^2 - 2 - \delta^*/\theta)\theta(dP/dx) \tag{7}$$

For zero pressure gradient the last term is zero and provides the usual expression for the flat plate case. For a first-order approximation this two-dimensional form may be applied to the present work, since both θ and δ^* are small compared to the cross-section radius and their variation with x is also small. Data were taken at several stations along the nozzle, and hence, values of $d\theta/dx$ and dP/dx are known. Thus, Eq. (7) may be evaluated numerically; for the $M = 9.07$ case at Station A the last term is approximately 1.70×10^{-4}, or 20 per cent of the C_f value, with the pressure independent term, $2(d\theta/dx)$, accounting for the remaining 80 per cent. To this extent, then, the pressure gradient may influence the rate of growth of the momentum thickness.

Ludwieg and Tillmann,[12] reporting turbulent measurements for incompressible flow with negative pressure gradients, showed a small C_f increase over the constant pressure case; Lobb et al.[13] do not attribute to the favorable gradients in their experiment a significant effect on their skin-friction coefficients. Chapman and Kester[3] have given specific data at $M = 1.92$ indicating that the turbulent skin friction is not significantly affected by pressure and Mach Number gradients numerically comparable to those obtaining for the present measurements, and Dhawan[19] has given some data at a low supersonic Mach Number indicating a small effect of pressure gradient on skin friction. The question of the effect of pressure gradients on skin-friction measurements requires further research, and it is important to emphasize that the present data were obtained in the

presence of favorable pressure gradients. It is anticipated that at high Mach Numbers practical applications will require skin-friction data under comparable conditions.

Skin Friction

In Table 2 the numerical values of skin-friction coefficients were given together with the corresponding Reynolds Numbers. The significant Reynolds Number for wall measurements against which skin friction is plotted may be based on momentum, displacement, or total boundary-layer thickness.† In Fig. 4 the data are plotted vs. Re_δ where the line representing turbulent flow has been derived from Eq. (4), with the velocity and viscosity terms written in terms of C_f and Re_δ.

$$(2/C_f)^{1/2} = a' + b' \log [Re_\delta (C_f)^{1/2}] \qquad (8)$$

and the laminar curve is derived from Eq. (3). The data points shown in Fig. 4 are connected by a smooth curve, since calculation of similar points at intermediate P_0 values indicates a variation as shown. The peak of the curve indicates the edge of the transition region and the Reynolds Number ($Re_\delta \sim 40{,}000$) at which the turbulent flow is fully developed. That the experimental points do not lie on the solid line, Eq. (8), as derived from Eq. (4) is not surprising, since the values of the constants a, b used were not originally determined under hypersonic conditions. Of even more significance, as pointed out by Chapman and Kester,[3] is the fact that the semiempirical mixing length theory of Prandtl and von Kármán does not provide additional constants of integration when applied to compressible flow in a boundary layer. Therefore, it does not seem pertinent to re-evaluate a and b from the present data. It is of more interest to plot C_f as a function of a Reynolds Number, Re_θ, whose significant length is momentum thickness. Data are available at lower Mach Numbers, both with and without pressure gradients, under conditions of natural and forced transition to turbulent flow and for both cylindrical and plane surfaces. Data from several sources[5, 13, 14] are compared with the results of the present report in Fig. 5. They indicate a decrease in skin-friction coefficient with increase in Mach Number. The data of Coles at low Mach Numbers are most readily comparable to the present work. The former indicate that a value of $Re_\theta = 2{,}000$ is needed to complete the transition to fully developed turbulent flow. At $M \sim 9$ our data show that a value of approximately 1,500 is required. This may be somewhat surprising because at the higher Mach Numbers the laminar sublayer is relatively thicker, and it might be expected that larger Re_θ values would be required to provide fully developed turbulent flow. However, as is clear from Fig. 2b, the turbulent layer follows a lower power law development, index $n \sim 5$, as compared to lower supersonic power law developments where the index has generally been found to lie between 7 and 9. Consequently the turbulent flow in hypersonic streams develops more rapidly to free-stream conditions than supersonic flows at lower Mach Number but higher Reynolds Number. The differences as well as the similarities of the various data must be taken into account when comparison is made, since these differences could contribute to the apparent scatter of the results.

Both the NOL and APL data are taken with moderately large heat-transfer rates. It must also be noted that the present data and that of Brinich and Diaconis[14] are taken on cylindrical surfaces, whereas for all the other data the flow was presumably two-dimensional. Another source of axial flow data is available as reported by Chapman and Kester[3] for Mach Numbers 0.81, 2.15, and 3.6. Their data are not shown on Fig. 5 because values of the momentum thickness were not included; their work gave the skin-friction measurements as a function of Reynolds Number based on model length. A rough computation, however, of the approximate range of Re_θ values of their experiment indicates that their data fall within the appropriate range of C_f values given in Fig. 5.

Fig. 5 shows the usual behavior of skin-friction coefficient as a function of Reynolds Number where the curves at constant Mach Number approximate the slope of the $M = 0$ line. At low supersonic Mach Numbers the ratio of C_F/C_{F_i} or C_f/C_{f_i} is generally independent of Reynolds Number, and it is useful therefore to plot C_F/C_{F_i} vs. M_∞. In Fig. 6 this has been done for the data shown in Fig. 5. The theory of Wilson,[15] which appears most applicable has been plotted for constant Reynolds Numbers.‡ Values of Re_θ of 2,000 and 7,000 were chosen to cover the range of interest in Fig. 5. Where possible, the data points shown in Fig. 6 were interpolated from Fig. 5 to give corresponding C_f/C_{f_i} at both Reynolds Numbers. In the case of the Chapman and Kester data, exact Re_θ values were not known, but the range of length Reynolds Numbers given and the fact that at lower Mach Numbers the C_f/C_{f_i} values are less dependent on Reynolds Number, justified including them. The data of Coles interpolated to $Re_\theta = 2{,}000$ are all above the curve, and this may reflect the test conditions where in this case the flow was still near or in the transition region. On the other hand his values at $Re_\theta = 7{,}000$ are in good agreement with the theory and the trend of the other experimental data.

The data at Mach Numbers above 5 show the effects of heat transfer and pressure gradients. These pa-

† Coles[18] has discussed the uniqueness of fully developed turbulent boundary layers and the correspondence between local friction coefficients and Re_θ.

‡ The expression for C_F given by Wilson is

$$\frac{\sin^{-1}\sqrt{\sigma}}{\sqrt{\sigma}}\left(1 + C_\theta \frac{\gamma - 1}{2} M_\infty^2\right)^{-1/2} \frac{0.242}{\sqrt{C_F}} = \log_{10}(C_F Re) - 0.768 \log_{10}\left(1 + C_\theta \frac{\gamma - 1}{2} M_\infty^2\right) \qquad (10)$$

where σ is a simple function of M_∞ and C_θ is taken as 0.88. In order to evaluate this in terms of Re_θ, the momentum equation, Eq. (8), with zero pressure gradient and two-dimensional flow was used.

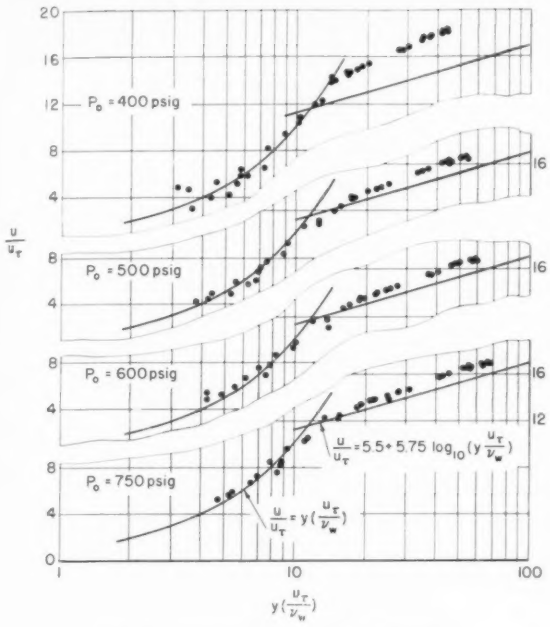

FIG. 3. Universal velocity distribution.

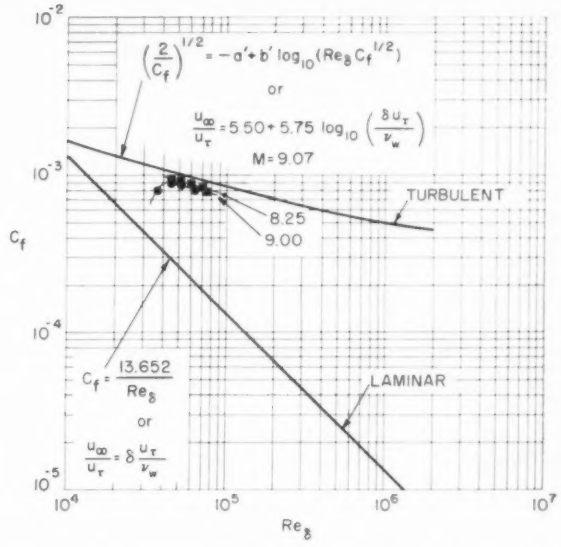

FIG. 4. Skin friction vs. Reynolds Number based on total boundary-layer thickness.

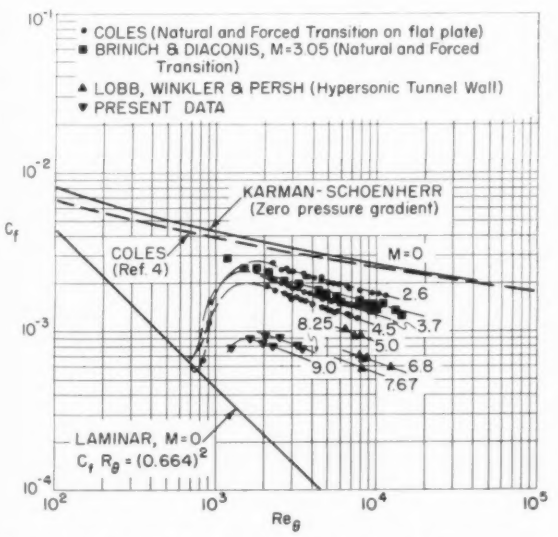

FIG. 5. Skin friction vs. Reynolds Number based on momentum thickness.

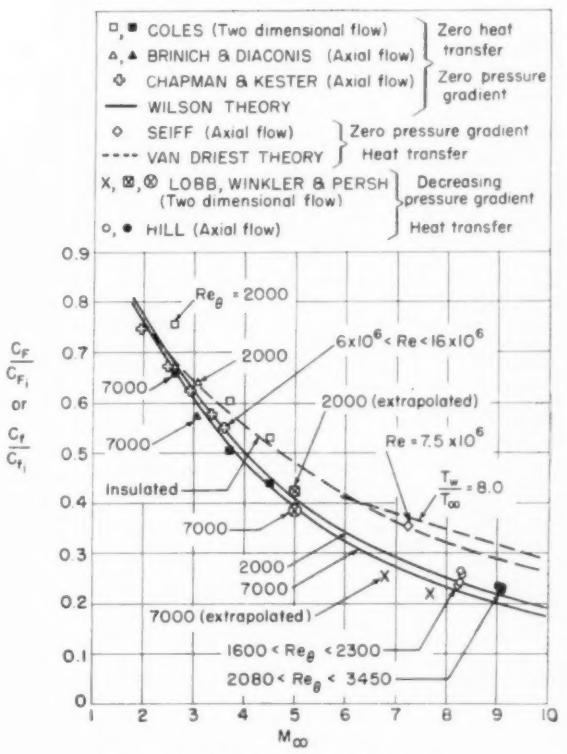

FIG. 6. Skin friction vs. Mach Number.

rameters need to be examined in more detail theoretically in order to see how they may influence skin friction. Two theoretical curves derived from the heat-transfer theory of Van Driest[16] have been plotted† in Fig. 6, and indicate the effects that heat transfer may have on skin friction at high Mach Numbers. The two cases chosen are, in Van Driest's notation, for the case where $T_w/T_\infty = 8.0$ and the insulated case where T_w/T_∞ varies from 21.0 at $M = 10$ to 1.8 at $M = 2$. The present data (see Table 2) shown near $M = 8.25$ and $M = 9$ correspond to T_w/T_∞ values of about 7.2 to 8.7. It is therefore evident that although the Van Driest theory predicts skin-friction values some 40 per cent higher than the data, the effect of heat transfer in his theory is commensurate with the difference between our measurements and the zero heat transfer theory (see Wilson). Seiff, as reported by Abbott,[17] has obtained skin-friction data at $M = 3.9$ and at $M = 7.25$ under conditions of very high heat-transfer rates. His data obtained by firing a cylinder upstream through a $M = 2$ air stream at $Re \sim 5$ to 7.5×10^6 indicate a much higher C_f, in fact in line with the Van Driest insulated case.

It may be concluded that for Mach Numbers up to 9 with low or moderate heat-transfer rates the coefficient of skin friction is known to within about 5 per cent from experimental measurements. At the higher Mach Numbers the effects of pressure gradients and heat transfer must be taken into account, and the need for adequate theoretical treatment of these effects is evident.

References

[1] Von Kármán, Th., *Turbulence and Skin Friction*, Journal of the Aeronautical Sciences, Vol. 1, No. 1, pp. 1–20, January, 1934.

[2] Clauser, Francis H., *Turbulent Boundary Layers in Adverse Pressure Gradients*, Journal of the Aeronautical Sciences, Vol. 21, No. 2, pp. 91–108, February, 1954.

[3] Chapman, Dean R., and Kester, Robert H., *Measurements of Turbulent Skin Friction on Cylinders in Axial Flow at Subsonic and Supersonic Velocities*, Journal of the Aeronautical Sciences, Vol. 20, No. 7, pp. 441–448, July, 1953.

[4] Coles, Donald, *Measurements in the Boundary Layer on a Smooth Flat Plate in Supersonic Flow. 1. The Problem of the Turbulent Boundary Layer*, JPL/CIT Report No. 20–69, June, 1953.

[5] Coles, Donald, *Measurements of Turbulent Friction on a Smooth Flat Plate in Supersonic Flow*, Journal of the Aeronautical Sciences, Vol. 21, No. 7, pp. 433–448, July, 1954.

[6] Faro, I. D. V., Small, T. R., and Hill, F. K., *Hypersonic Flow at a Mach Number of 10*, J. Appl. Phys., Vol. 22, No. 2, February, 1951.

[7] Faro, I. D. V., *Boundary Layer Measurements in Hypersonic Flow*, Paper presented at U.S. Navy Symposium on Aeroballistics, Laurel, Maryland, October, 1954.

[8] Tsien, Hsue-Shen, *Superaerodynamics, Mechanics of Rarefied Gases*, Journal of the Aeronautical Sciences, Vol. 13, No. 12, pp. 653–664, December, 1946.

[9] Faro, I. D. V., Small, T. R., and Hill, F. K., *Supersaturation of Nitrogen in a Hypersonic Wind Tunnel*, J. Appl. Phys., Vol. 23, No. 1, January, 1952.

[10] Kane, E. D., and Maslach, G. J., *Impact-Pressure Interpretation in a Rarefied Gas at Supersonic Speeds*, NACA TN 2210, October, 1950.

[11] Burcher, Marie A., *Compressible Flow Tables for Air*, NACA TN 1592, August, 1948.

[12] Ludwieg, H., and Tillmann, W., *Investigations of the Wall-Shearing Stress in Turbulent Boundary Layers*, NACA TM 1285, May, 1950. Translation of *Untersuchungen über die Wandschubspannung in Turbulenten Reibungsschichten*.

[13] Lobb, R. Kenneth, Winkler, Eva M., and Persh, Jerome, *Experimental Investigation of Turbulent Bounday Layers in Hypersonic Flow*, Institute of the Aeronautical Sciences, Preprint No. 452, Paper presented at 22nd Annual Meeting, January, 1954.

[14] Brinich, Paul F., and Diaconis, Nick S., *Boundary-Layer Development and Skin Friction at Mach Number 3.05*, NACA TN 2742, July, 1952.

[15] Wilson, Robert E., *Turbulent Boundary-Layer Characteristics at Supersonic Speeds—Theory and Experiment*, Journal of the Aeronautical Sciences, Vol. 17, No. 9, pp. 585–594, September, 1950.

[16] Van Driest, E. R., *The Turbulent Boundary Layer for Compressible Fluids on a Flat Plate with Heat Transfer*, North American Aviation, Inc., Report AL-1006, February, 1950.

[17] Abbott, Ira A., *Some Factors Contributing to Scale Effect at Supersonic Speeds*, AG8/M4, London AGARD Conference, September, 1953.

[18] Coles, Donald, *The Problem of the Turbulent Boundary Layer*, Zeitschrift für angewandte Mathematik und Physik, Vol. V, p. 181, 1954.

[19] Dhawan, Satish, *Direct Measurements of Skin Friction*, NACA Report 1121, 1953.

† Again Eq. (7) has been used with zero pressure gradient.

Some Effects of Viscosity on Wing-Body Interference at $M = 1.9$*

T. R. RHEES† AND W. P. CRENSHAW‡
University of Michigan

ABSTRACT

Interference pressure distribution data were obtained at $M = 1.9$ for the body of a flat rectangular wing-cylindrical body combination with a laminar boundary layer on the body. The results are compared with earlier experimental results obtained with a turbulent boundary layer on the body and with the linearized inviscid theory of NACA TN 2677.

The experimental results agree well with theory except for viscous effects not predicted by the theory.

Qualitative similarity of the shock-wave and laminar boundary-layer interaction to the two-dimensional case is noted.

Body lift loading due to interference for two configurations representing missiles with wings or control surfaces near the tail is discussed.

SYMBOLS

C_p = pressure coefficient, $(p - p_1)/[(\rho_1/2)V_1^2]$
M_1 = free-stream Mach Number
p = static pressure at any particular body orifice, lbs. per sq.ft.
p_1 = static pressure at any particular body orifice, body alone, lbs. per sq.ft.
R = radius of cylindrical body, in.
V_1 = free-stream velocity, ft. per sec.
X = distance from leading edge of wing, in.
α_B = body angle of attack, zero in all cases
α_W = angle of attack of the wing, radians
β = $\sqrt{M_1^2 - 1}$
θ = angle between meridional plane under consideration and the horizontal plane, deg.
ρ_1 = free-stream density, slugs per cu.ft.

(A) INTRODUCTION

IN THE PAST FEW YEARS there has been considerable experimental and analytic study of the two-dimensional problem of the interaction of a shock wave and the boundary layer on a flat surface. In practice, however, the configurations in which shock waves interact with boundary layers are generally three-dimensional. Wing-body combinations usually give rise to problems of the latter type.

Some of the methods that have been developed for computing the effects of wing-body interference on pressure distribution in a supersonic flow have been summarized and compared by Lawrence and Flax[1] and Phinney.[2] A method of solving a wide class of wing-body interference problems is presented by Nielsen and Pitts,[3] with a numerical application to the case of a flat rectangular wing mounted at an angle of attack on a cylindrical body at zero angle of attack. The extension of the method for the body at an angle of attack has been made by Bailey and Phinney[4] and by Pitts, Nielsen, and Gionfriddo.[5]

The experimental interference pressure distribution on the body of a wing-body combination in a supersonic flow differs from the theoretical inviscid pressure distribution due to two effects: (1) the presence of subsonic velocities in the boundary layer permits upstream propagation of pressure disturbances within the subsonic portion of the boundary layer, thus influencing the flow field ahead of the Mach cone whose apex is at the disturbance; and (2) the sharp pressure gradients that may exist in a supersonic stream can induce sizable cross flows in the three-dimensional boundary layer and even separation of the boundary layer.

For the particular wing-body combination used in this investigation, Bailey and Phinney[6, 7] have presented the theoretical inviscid interference pressure profiles on the body and experimental interference pressure profiles measured with a turbulent boundary layer on the body.

It was the purpose of this investigation to obtain the interference pressure profiles on the body with a laminar boundary layer on the fore body and to compare the results with the experimental results for the turbulent case[6, 7] and the theoretical pressure distribution predicted by the method of Nielsen.[3] In addition, it was desired to compare the predicted body lift due to interference for two possible wing-body configurations with the experimental force when the boundary layer on the body was laminar and when turbulent.

The Reynolds Number for these tests, based on a 2-in. model body diameter, was 7×10^5, which corresponds to an actual missile of 2-ft. diameter flying at Mach Number 1.9 at 90,000 ft.

(B) EQUIPMENT AND PROCEDURE

The experiments were conducted in the University of Michigan 8 by 13 in. Intermittent-Flow Supersonic Wind Tunnel,[8] Mach 1.9 channel.

Received December 6, 1954.

* This investigation was conducted at the University of Michigan Supersonic Wind Tunnel while the authors were continuing graduate study as part of the curriculum in Aeronautical Engineering of the U.S. Naval Postgraduate School, Monterey, Calif.

The authors are especially indebted to A. M. Kuethe, Felix Pawlowski Professor of Aerodynamics, and H. E. Bailey, Research Associate, Engineering Research Institute, for invaluable guidance and assistance.

† Lieutenant Commander, U.S. Navy.

‡ Lieutenant, U.S. Navy.

(1) *Description of Model*

The model consists of a cylindrical body and two half-wings, Fig. 1. The model is the same used by Bailey and Phinney[6, 7] except for use of a shorter nose piece, ensuring a laminar boundary layer on the body in the test region. Use of the same model permits a direct quantitative comparison between the results obtained for the laminar case and the results reported for the turbulent case.

The model body is a hollow circular cylinder, with a 2-in. outer diameter and a $1^1/_2$-in. inner diameter. The nose piece is $2^9/_{16}$ in. long and tapers to an inlet diameter of $1^5/_{16}$ in. The chord of the half-wings is 2 in. and the half-span is $2^1/_2$ in. The wing section is flat on one side and double-wedge shaped on the other, with a wedge angle of 10° at the leading and trailing edges.

The body contains 92 pressure orifices arranged in 21 meridional planes, with 1 in. between the orifices in each meridional plane. In the present investigation, 44 of the pressure orifices in the upper quadrant were used.

The two half-wings are rigidly supported by brackets outside the test section. The sealing of the wing-body juncture was accomplished by mechanical contact at flat spots on the side of the body. The maximum gap encountered was slightly greater than 0.008 in. at the leading edge of the wing.

The axial position of the body may be varied about $1^1/_2$ inches by axial movement of the strut attachment at the top of the tunnel. Since the half-wings are fixed with respect to the tunnel, this axial movement of the body permits the measurement of pressure profiles on the body in the presence of the wing. The axial position of the body and thus the orifice locations with respect to the leading edge of the wing was determined within ±0.003 in.

(2) *Instrumentation*

The static pressures were measured with mercury manometers which were photographed during the test run, permitting an accuracy in the measurements of 1 per cent of the ambient static pressure.

Schlieren photographs of each configuration were obtained.

A modified china-clay technique was used to illustrate the flow in the boundary layer close to the surface of the body. The drying time was controlled so that a dry film was obtained for the laminar boundary layer and a wet surface would aid in identifying a region of separation. The china-clay pattern was also useful in locating the traces of shock waves on the body and wing surfaces.

(3) *Experimental Procedure*

Prior to taking data, two runs were made with the body alone: (1) visual schlieren showed nose shock attached and no blocking; and (2) china-clay pattern indicated a laminar boundary layer over the fore part of the body.

For all runs, zero body angle of attack with respect to the free stream was maintained. Pressure data were obtained with the half-wings positioned at ±8.2° angle of attack. The variation of angle of attack setting between runs was negligible. Pressure data were also obtained for the body alone.

The china-clay pattern was checked on every run to ensure that the boundary layer ahead of the Mach helix originating at the juncture of the leading edge of the wing and the body remained laminar, and pressure readings in three meridional planes were plotted after each run to check immediately the reliability of the pressure data for that run.

(4) *Data Preparation*

The pressure measured at any one orifice with the body alone in the tunnel may be written

$$p_{\text{measured}} = p_{\text{body alone}} + \Delta p_{\text{induced}}$$

where $p_{\text{body alone}}$ is the pressure on the body alone in a uniform flow and is a function only of the geometry of the particular body and $\Delta p_{\text{induced}}$ is the incremental pressure induced on the body alone due to the wind-tunnel flow nonuniformities and is a function of the body geometry and the flow nonuniformities.

If the wing is introduced into the flow, the measured pressure becomes

$$p_{\text{measured}} = p_{\text{body alone}} + \Delta p'_{\text{induced}} + \Delta p_{\text{interference}}$$

where $p_{\text{body alone}}$ is as defined above, $\Delta p'_{\text{induced}}$ is the incremental pressure induced on the body in the presence of the wing due to the wind-tunnel flow nonuniformities, and $\Delta p_{\text{interference}}$ is the incremental pressure induced on the body in a uniform flow due to the presence of the wing. Uniform flow is the condition usually encountered in free flight but is extremely difficult to obtain in a wind tunnel.

Provided $\Delta p_{\text{interference}}$, $\Delta p_{\text{induced}}$, and $\Delta p'_{\text{induced}}$ are small quantities,

$$\Delta p_{\text{induced}} = \Delta p'_{\text{induced}}$$

so that a simple subtraction of the pressure on the body alone from the pressure on the body in the presence of the wing gives $\Delta p_{\text{interference}}$, which is the desired result.

Actually, there is some interaction between $\Delta p_{\text{interference}}$ and $\Delta p_{\text{induced}}$, as evidenced by a small axial shift of a weak tunnel shock observed in the body-alone pressure data when the wing is introduced into the flow. This shift was taken into account when fairing the raw experimental pressure curves.

The experimental interference pressure profiles were obtained by a simple subtraction of the faired pressure profiles for the body alone from the faired pressure profiles of the wing-body combination. In this manner, the effect of tunnel flow nonuniformities is eliminated as far as possible.

The zero base for all curves presented herein is the static pressure measured on the body alone. It should

be noted that, although the curves are in effect nondimensionalized for presentation, they apply strictly only for the particular angle of attack used. It has been observed that the pressure distribution on the body, presented in terms of $\beta C_p/\alpha_W$, is affected by the angle of attack of the wing.[5, 6]

(C) Results and Discussion

From the schlieren photograph of the body alone, Fig. 2, the laminar boundary-layer thickness measured at a point 6 in. from the nose is between 0.025 and 0.030 in. Fig. 3 shows a somewhat thicker boundary layer at this position after the wing has been introduced. For comparison, the compressible laminar boundary-layer thickness for 6 in. of flat plate is determined theoretically to be 0.029 in.[9] In subsequent references to the upstream influence of the interference pressure in terms of boundary-layer thicknesses, the thickness will be assumed 0.03 in.

Experimental interference pressure profiles for four representative meridional planes and the corresponding theoretical profiles are plotted in Figs. 6a, 6b, 6c, and 6d. Inasmuch as the theory cannot be applied downstream of the trailing edge Mach helix of the wing, the theoretical pressure was assumed to decrease abruptly to ambient pressure along that helix. All interference pressures were measured on the quadrant of the body above the flat surface of the wing, with the wing fixed at $\pm 8.2°$ angle of attack. Since the model is axially symmetric and the body was maintained at zero angle of attack, the pressure data measured for the two angles of attack of the wing in effect gave the pressure distribution on the body in the presence of a plate-plate wing.

In a comparison of the experimental results with theory, for a particular meridional plane of the body (Fig. 6), two factors affecting the axial position of the wing-body phenomena must be considered: (1) The theoretical pressure discontinuity occurs along the Mach wave helix originating at the linearized position of the wing-body leading- and trailing-edge junctures—i.e., in the plane $\theta = 0°$. Since the wing plane is actually inclined 8.2°, the helices are shifted axially from the linearized position by an amount $X/\beta R = 0.15$. (2) Occurrence of the actual finite pressure jump along the trace of an inclined shock, rather than a Mach wave, introduces a wave-angle error.

(1) *Wing at −8.2° Angle of Attack*

For a negative wing angle of attack, a compression occurs over the flat surface of the wing. In an ideal fluid, the interference pressure coefficient on the body is zero ahead of the Mach helix generated at the leading-edge juncture; the pressure rise at the helix is a discontinuous shock jump, followed by a continuous axial pressure gradient due to the interference potential field. The magnitude of the shock jump at the leading-edge helix is continuously attenuated as the shock moves around the cylinder, diminishing to zero theoretically at the $\theta = 90°$ meridian arc.

Experimentally, with laminar boundary layer on the body, upstream propagation of the pressure disturbance varies from about 30 boundary-layer thicknesses in the $\theta = 10°$ plane to about 60 boundary-layer thicknesses in the $\theta = 90°$ plane. A comparison with the turbulent boundary-layer profiles (Fig. 6) shows the upstream propagation is greater in terms of actual distance for the laminar case, and in terms of the respective boundary-layer thicknesses the laminar propagation is 7 to 10 times that in the turbulent case. In the laminar case the propagation extended to the region of the most forward orifice, and the experimental data did not clearly indicate the maximum extent of the upstream propagation. The values quoted above are therefore conservative. The effect of the character of the boundary layer on the extent of the upstream pressure propagation is in qualitative agreement with experimental results for the interaction of shock waves and boundary layers on a flat surface.[10, 11]

The pressure profiles show a plateau of slightly increased pressure, characteristic of the laminar case, extending upstream from the main shock pressure rise, indicating a bubble of dead air or region of flow separation. At the higher meridians the separation region is more extensive. The china-clay pattern in Fig. 4a indicates separation where the surface is still wet ahead of the Mach helix on the upper part of the body. The variation with θ of the extent of upstream propagation and separation is due in part to the cross flow of the low inertia air in the boundary layer, which results in an accumulation of air along the top of the body. This cross flow is produced by the component of the shock-induced velocity which is normal to the free-stream direction. Figs. 4a and 4b show that the cross flow is stronger in the laminar boundary layer and illustrate the deviation of the flow near the body far ahead of the Mach helix, which is characteristic of the laminar case.

The schlieren photograph, Fig. 3, shows considerable thickening of the laminar boundary layer ahead of point b. The plane portion of the shock wave originating at the wing leading edge is the black line a. The main pressure rise in the top meridional plane of the body commences at point b and continues to point c. As the compressive Mach waves travel outward from the body, they coalesce into a shock wave evidenced by the dark line d. The light region e represents the Prandtl-Meyer expansion at the trailing edge of the wing. The flow overexpands slightly and is recompressed by the shock wave following the Prandtl-Meyer expansion.

The experimental pressure distributions for the laminar case in Figs. 6a, 6b, and 6d exhibit the initial overcompression that has been observed experimentally in investigations of the two-dimensional interaction of a shock wave and the laminar boundary layer on a flat surface.[10, 11] The degree of this overcompression appears to vary with the axial pressure gradient of the pressure jump. No overcompression is noted in the meridional plane $\theta = 60°$, Fig. 6c, where the gradient is relatively weak. The pressure rise associated with the

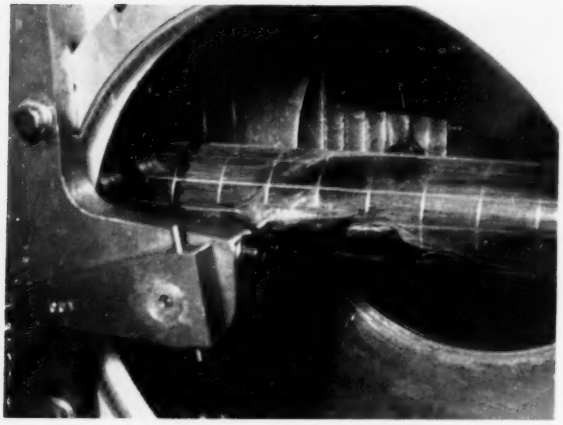

FIG. 1. Model in tunnel test section.

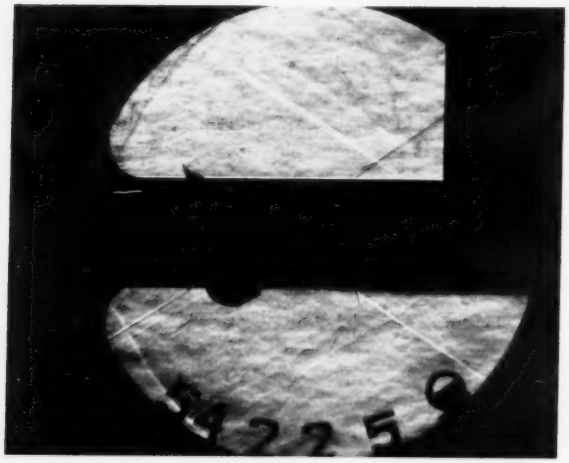

FIG. 2. Schlieren photograph, body alone.

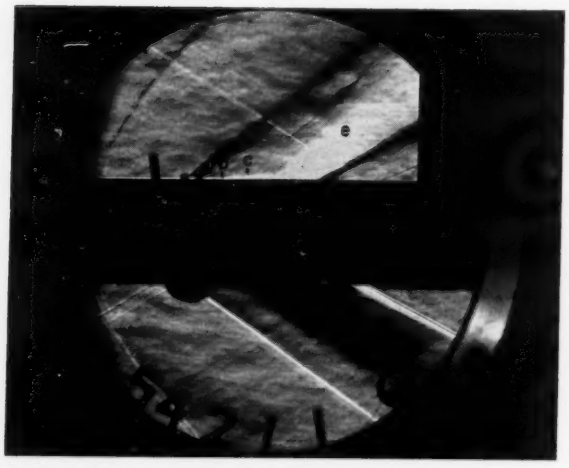

FIG. 3. Schlieren photograph, wing-body combination $\alpha_W = -8.2°$.

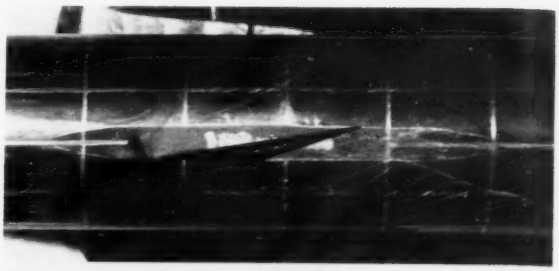

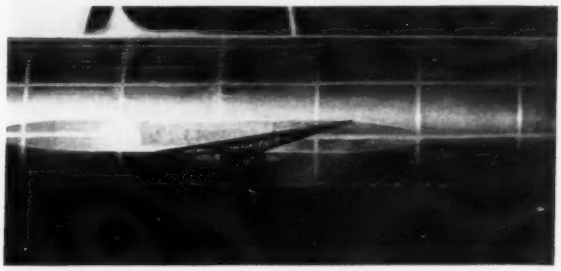

FIG. 4. China-clay photograph, $\alpha_B = 0$, $\alpha_W = -8.2°$.

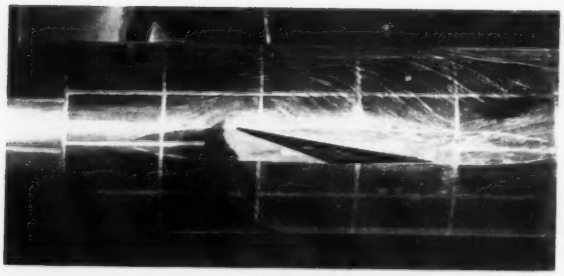

FIG. 5. China-clay photograph, $\alpha_B = 0$, $\alpha_W = +8.2°$.

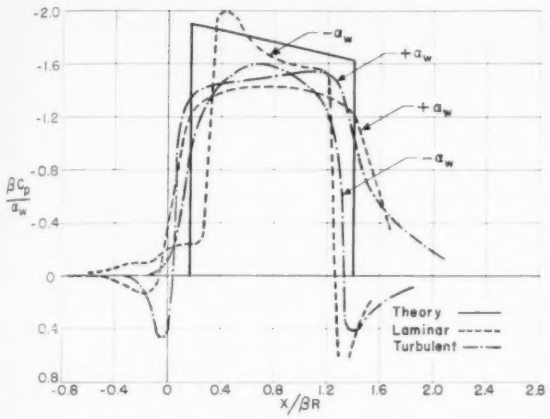

FIG. 6a. Body pressure profiles, $\theta = 10°$.

leading-edge shock occurs later for the laminar boundary layer than for the turbulent boundary layer. It is initiated at about the position of the actual trace of the leading-edge shock on the cylindrical body. Viscous effects result in a pronounced smoothing out of the pressure rise due to the shock.

The experimental maximum pressure coefficient for the laminar case agrees more closely with theory than that for the turbulent boundary layer.

At the trailing-edge expansion, for low values of θ both the laminar and turbulent pressure curves overshoot the ambient pressure and then begin to approach it asymptotically. The pressure behavior downstream of this point is uncertain due to flow nonuniformities and the reflection of the body nose shock which strikes in this region. The large disturbance from the wing-tip and wing support trunion also begin to affect the flow in this region.

(2) *Wing at +8.2° Angle of Attack*

For positive angles of attack an expansion wave originates at the leading edge of the wing. Experimentally, this expansion wave is preceded at small values of θ by a weak shock, probably a continuation of the strong shock wave on the compression side. It is a weaker compression in the laminar case but does not otherwise differ greatly from the turbulent phenomenon.

The upstream propagation of the pressure disturbance in the laminar case varies from about 20 boundary-layer thicknesses in the $\theta = 10°$ plane to about 30 boundary-layer thicknesses in the $\theta = 90°$ plane. This is again greater than the propagation observed with the boundary layer turbulent but somewhat less than for the negative wing angle of attack.

The expansion pressure profiles over the flat surface of the wing are similar for both the laminar and turbulent cases. However, the pressure rise is delayed slightly at the higher values of θ in the laminar case and the peak pressure coefficient is not as great. Due to the fan-like nature of the Prandtl-Meyer expansion, the axial pressure gradient is reduced as θ increases.

The pressure gradient on the body at constant $X/\beta R$ induces cross flow in the boundary layer, illustrated

TABLE 1
Interference Body Lift

	Zero Length Afterbody, lb.	One Chord Length Afterbody, lb.
Linearized theory	0.612	2.993
Laminar boundary layer	0.644	3.014
Turbulent boundary layer	0.991	3.263

by Figs. 5a and 5b. This cross flow is much more pronounced for the laminar boundary layer. The china-clay patterns again show the upstream flow deviation characteristic of laminar boundary-layer interaction, but no separation or pressure plateau is associated with an expansion.

A compression originates at the trailing edge, and the pressures begin to approach the ambient static pressure.

The maximum pressure coefficients over the flat surface of the wing at a positive angle of attack are considerably less than for the wing at negative angle of attack.

The above differences between the effects of interaction of an expansion wave and interaction of a shock wave with a laminar boundary layer have been experimentally observed elsewhere.[5]

(3) *Lift on the Body due to Wing-Body Interference*

The lift force on the body at zero angle of attack due to the presence of a flat-plate wing at an angle of attack was obtained by integrating the body pressure profiles. Since the lift is clearly dependent upon the amount of body downstream of the trailing edge, results were obtained for two different lengths of afterbody: (1) zero length—i.e., the body is assumed to terminate at the trailing edge of the wing; and (2) one chord length. The limitation of one chord length is necessary because of the effects of the disturbances mentioned in Section (C) (1) on the body downstream of this position. The results are presented in Table 1 as the lift force in pounds induced on the body by the wing.

The force on the body with laminar boundary layer slightly exceeds the force predicted by the linearized

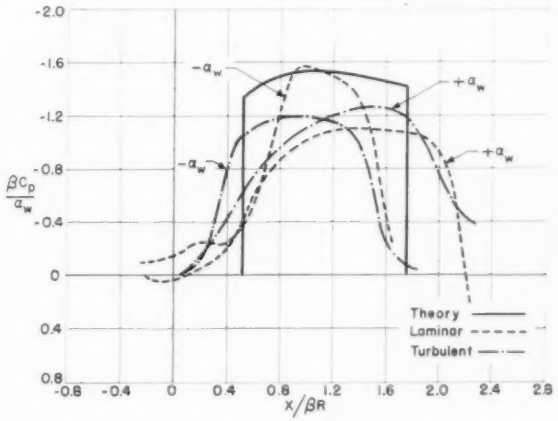

FIG. 6b. Body pressure profiles, $\theta = 30°$.

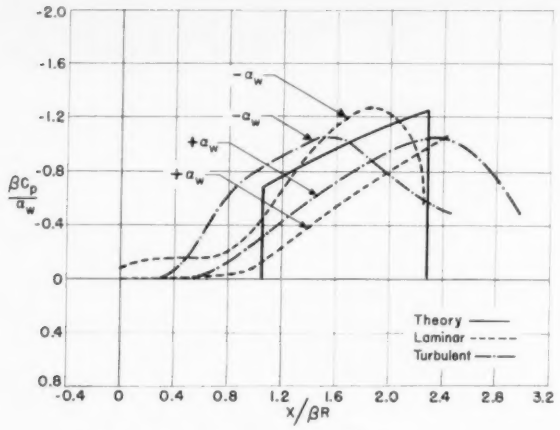

FIG. 6c. Body pressure profiles, $\theta = 60°$.

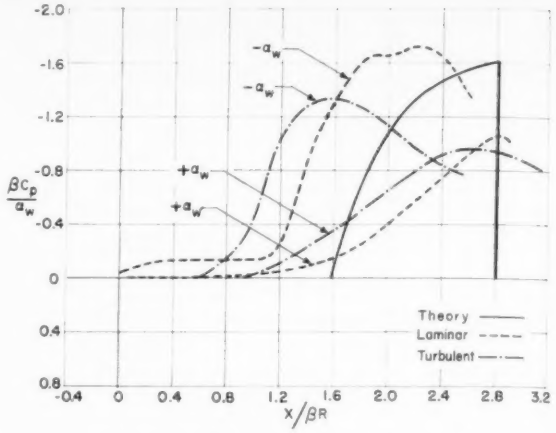

FIG. 6d. Body pressure profiles, $\theta = 90°$.

theory for both lengths of afterbody. In the turbulent case the experimental force exceeds the theoretical value by 62 per cent for zero afterbody and 9 per cent for one chord length afterbody.

The prediction of the interference lift on the body using the linearized theory appears conservative for the lengths of afterbody considered, regardless of the character of the boundary layer.

(D) CONCLUSIONS

With a laminar boundary layer on the fore body of the wing-body combination, the experimental pressure distribution on the body is in good agreement with linearized theory. With a turbulent boundary layer on the forebody the deviation is greater. The linearized inviscid theory[3] appears adequate for the prediction of the body interference pressure distribution.

The singular viscous effects noted for the laminar boundary-layer interaction are: (1) upstream propagation of the pressure disturbance from the wing, as much as 60 boundary-layer thicknesses; (2) local separation of the laminar boundary layer, with a plateau of slightly increased pressure ahead of the shock pressure rise; (3) overcompression associated with sharp axial shock pressure gradients.

Although the viscous effects are strikingly evident in the pressure profiles for the laminar case, their effect on the body loading is not pronounced. For short lengths of afterbody the body loading in the turbulent case may differ substantially from the predicted value.

REFERENCES

[1] Lawrence, H. R., and Flax, A. H., *Wing-Body Interference at Subsonic and Supersonic Speeds—Survey and New Developments*, Journal of the Aeronautical Sciences, Vol. 21, No. 5, pp. 289–324, May 1954.

[2] Phinney, R. E., *Wing-Body Interference; Progress Report No. 4*, University of Michigan, Engineering Research Institute, 1952.

[3] Nielsen, J. N., and Pitts, W. C., *Wing-Body Interference at Supersonic Speeds with an Application to Combinations with Rectangular Wings*, NACA. TN 2677, April, 1952.

[4] Bailey, H. E., and Phinney, R. E., *Final Report, Wing-Body Interference, Part I, Theoretical Investigation*, University of Michigan, Engineering Research Institute, January, 1954.

[5] Pitts, William C., Nielsen, Jack N., and Gionfriddo, Maurice P., *Comparison Between Theory and Experiment for Interference Pressure Field Between Wing and Body at Supersonic Speeds*, NACA TN 3128, April, 1954.

[6] Bailey, H. E., and Phinney, R. E., *Final Report, Wing-Body Interference, Part II, Experimental Investigation of Cylindrical Model*, University of Michigan, Engineering Research Institute, February, 1954.

[7] Bailey, H. E., and Phinney, R. E., *Some Experimental Results on Wing-Body Interference at Supersonic Speeds*, Paper presented at the Second U.S. National Congress of Applied Mechanics, Ann Arbor, Mich., June 14–17, 1954.

[8] Garby, L. C., and Nelson, W. C., *University of Michigan 8 × 13 Inch Intermittent-Flow Supersonic Wind Tunnel*, University of Michigan, Memorandum 59, Engineering Research Institute, June, 1950

[9] Kuethe, A. M., and Schetzer, J. D., *Foundations of Aerodynamics*, p. 301; John Wiley & Sons, Inc., 1950.

[10] Liepmann, H. W., Roshko, A., and Dhawan, S., *On the Reflection of Shock Waves from Boundary Layers*, NACA TN 2334, April, 1951.

[11] Barry, F. W., Shapiro, A. H., and Neumann, E. P., *The Interaction of Shock Waves with Boundary Layers on a Flat Surface*, Journal of the Aeronautical Sciences, Vol. 18, No. 4, pp 229–238, April, 1951.

Analysis of the Plastic Collapse of a Cruciform Column with Initial Twist, Loaded in Compression

J. F. BESSELING*

National Aeronautical Research Institute, Amsterdam, Holland

SUMMARY

The large influence of very small, and therefore unavoidable, imperfections upon the ultimate compressive load of a cruciform column according to the incremental or flow type of mathematical theory of plasticity has been demonstrated by Onat and Drucker.[1] In this paper the process of plastic collapse of a cruciform column with initial twist is further analyzed. In contrast to the model of Onat and Drucker, the flanges are treated here as solid plates. The ultimate compressive stress is determined by a step-by-step procedure, using a simple isotropic flow theory. It is found that collapse is not connected with an ordinary buckling failure, but is caused by a drop in the compressive stress for compressive strains exceeding the critical strain and accompanied by not yet very fastly growing twist. This drop is due to the interaction of compressive strain and shear strain in the plastic stress-strain relations.

SYMBOLS

δ_{ij} = Kronecker delta; $\delta_{ij} = 1$ if $i = j$, $\delta_{ij} = 0$ if $i \neq j$

ϵ_{ij} = strain tensor

ϵ = isotropic strain, $\epsilon = (1/3)(\epsilon_x + \epsilon_y + \epsilon_z)$

e_{ij} = strain deviation tensor, $e_{ij} = \epsilon_{ij} - \epsilon\delta_{ij}$

ϵ_{ij}'', e_{ij}'' = notation ($''$) for permanent strains

σ_{ij} = stress tensor

σ = isotropic stress, $\sigma = (1/3)(\sigma_x + \sigma_y + \sigma_z)$

s_{ij} = stress-deviation tensor

$$s_{ij} = \sigma_{ij} - \sigma\delta_{ij}$$

J_2 = second invariant of the stress tensor

$$J_2 = \frac{1}{2} s_{\alpha\beta} s_{\beta\alpha} \left(= \frac{1}{2}\sum_{\alpha}\sum_{\beta} s_{\alpha\beta} s_{\beta\alpha}, \right.$$

summation convention)

G = elastic modulus of rigidity

Gt = tangent modulus of rigidity

Gs = secant modulus of rigidity

$\zeta = z/h$

$\lambda = h/b$

$A = \sigma_x/3G$

(1) INTRODUCTION

IN THE ELASTIC RANGE a configuration of flat plates, loaded in their plane, becomes unstable at a certain load, the buckling load. For plates with initial deflections the load, at which the deflections start to grow fast, lies close to the buckling load if the initial deflections are small, and this load decreases but slowly for increasing initial deflections. Therefore, the theoretically derived buckling load can be verified experimentally, even if the test specimens are not perfectly plane.

If reaching the ultimate load together with fast growing deflections is taken as a criterion for the buckling load in the plastic range, a large discrepancy is found between the experimental value of the buckling load and the theoretical value, computed by means of the flow theories, which must be considered to be the best founded mathematical theories of plasticity. Onat and Drucker have given an important contribution to the clarification of this paradox. For a simplified model of a cruciform column with nonrestrained ends they demonstrated the large influence of very small initial twist upon the ultimate compressive load according to the flow theory. Subsequently the scope and limitations of the classical buckling theory have been discussed extensively by Hoff[7] and by Drucker and Onat.[8] From reference 8 the important role that imperfections may play in the stability of inelastic systems has become indisputable. In this paper a further analysis will be given of the collapse mechanism for the cruciform column with initial twist. In contrast to the model of Onat and Drucker the cruciform cross section will not be taken as a thin shell of constant thickness, but it will be treated here as having a solid cross section. It will be demonstrated that the collapse mechanism is of a nature entirely different from the ordinary buckling failure. In fact, reaching the ultimate load is not connected with a limit of stability of the untwisted configuration, but with a drop in the compressive stress for increasing compressive strain accompanied by growing twist, caused by the interaction of compressive strain and shear strain in the stress-strain relations for the plastic range. The computations were performed by a step-by-step procedure, using a simple isotropic flow theory.

(2) STRESS-STRAIN RELATIONS

Compression of a cruciform column with initial twist is a process of nonuniform loading. Therefore properly the anisotropic flow theory of reference 3 should be used. However the principal directions of the stress tensor and the value of Lode's coefficient change but slowly and then there is not a pronounced difference between the results of the anisotropic and the isotropic theory. For an understanding of the collapse mechanism the isotropic theory is considered accurate enough to justify the avoidance of the complications of the anisotropic theory. A further simplification of the computations is obtained by approximating the stress-strain curve of the material by two straight portions, the elastic line and the plastic line.

Received November 5, 1954.

* Research Engineer, Structures Department.

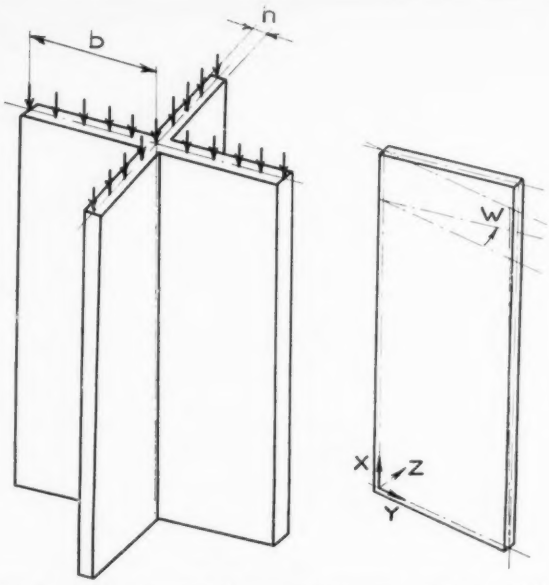

FIG. 1. (*left*) Geometry of cruciform column. FIG. 2. (*right*) Coordinates and deflected shape of flange.

The stress-strain relations of the isotropic flow theory, first given by Prager, are used in the form given in reference 3.

$$\delta s_{ij} = 2G\left[\delta e_{ij} - (1-\mu)\frac{(e_{ij} - e_{ij}'')\,(e_{hk} - e_{hk}'')}{P^2}\,\delta e_{hk}\right] \tag{2.1}$$

if $(e_{hk} - e_{hk}'')\delta e_{hk} > 0$, where

$$P^2 = (e_{ij} - e_{ij}'')\,(e_{ij} - e_{ij}'') = J_2/2\,G^2 \tag{2.2}$$

and

$$\mu = G_t/G \tag{2.3}$$

The initial elasticity limit is defined by a critical value of J_2. The increments of permanent strain follow from

$$\delta e_{ij}'' = (1-\mu)\frac{(e_{ij} - e_{ij}'')\,(e_{hk} - e_{hk}'')}{P^2}\,\delta e_{hk} \tag{2.4}$$

(3) Incremental Relation Between Compressive Strain and the Angle of Twist

The geometry of the cruciform column is given in Fig. 1. As in the paper of Onat and Drucker, the ends are considered to be unrestrained and failure by twisting will occur. The kinematics of the twisting process are described by taking for the small deflection w of a point in the midplane of a flange (see Fig. 2) the expression

$$w = \varphi\, xy/h \tag{3.1}$$

Then each straight line parallel to the axis becomes a helix. According to plate theory the deflection w gives rise to the following strain quantities

$$\left.\begin{aligned} \epsilon_{x_{tw}} &= z[\partial^2(w - w_0)/\partial_x{}^2] = 0 \\ \epsilon_{y_{tw}} &= z\,\frac{\partial^2(w - w_0)}{\partial y^2} = 0 \\ \epsilon_{xy_{tw}} &= e_{xy_{tw}} = \frac{\partial^2(w - w_0)}{\partial_x \partial_y} = (\varphi - \varphi_0)z/h \end{aligned}\right\} \tag{3.2}$$

if $w_0 = \varphi_0\, xy/h$ represents the deflection due to initial twist. To this nonuniform state of deformation is added a state of uniform deformation following from the compression of the column. The total state of deformation is given by the strain quantities

$$\epsilon, \quad \begin{matrix} e_x \\ e_y = -(1/2)e_x, \\ \\ e_z = -(1/2)e_x, \end{matrix} \qquad e_{yx} = (\varphi - \varphi_0)z/h = e_{xy} \tag{3.3}$$

from which the parts

$$\begin{matrix} e_x'' \\ e_y'' = -(1/2)e_x'', \\ e_z'' = -(1/2)e_x'', \end{matrix} \qquad e_{yx}'' = e_{xy}''$$

are permanent.

The state of stress is defined by

$$\sigma = (1/3)\sigma_x, \begin{matrix} s_x = (2/3)\sigma_x, \\ s_y = -(1/3)\sigma_x \\ s_z = -(1/3)\sigma_x \end{matrix} \qquad \tau_{yx} = \tau_{xy} \tag{3.4}$$

It is assumed that the stress distribution may be represented by closed circuits of equal shear stress, following the contour of the cruciform section at a fixed distance. This system of stresses is in equilibrium and is compatible with the stress distribution, which follows by means of the stress-strain relations from the state of strain defined in Eq. (3.3), except for the very outer ends of the flanges, where the lines of equal shear stress had to be closed to circuits in order to restore equilibrium. The assumptions concerning stress and strain are equivalent to considering the solid cruciform as composed of thin concentric shells each of the type Onat and Drucker choose. The shells are connected by the requirement that each suffer the same twist and the same axial compression. (The well-known small deflection theory of elastic thin plates leads to the same stress distribution.)

The external twisting moment due to the compression is given by

$$M_e = 4\int_{-(h/2)}^{h/2}\sigma_x dz \int_0^b \frac{\varphi y}{h}\, y\, dy = \frac{4}{3}\, b^3\, \varphi \int_{-(1/2)}^{1/2}\sigma_x d\zeta \tag{3.5}$$

where

$$\zeta = z/h \tag{3.6}$$

The twisting moment of the internal stresses follows from $(h/b \ll 1)$

$$M_i = 4{\cdot}2b \int_{-(h/2)}^{h/2} \tau_{xy} z dz = 8bh^2 \int_{-(1/2)}^{1/2} \tau_{xy} \zeta d\zeta \tag{3.7}$$

Equating the increments of the external and internal moments and putting

$$\lambda = h/b \tag{3.8}$$

the following equation is obtained

$$6\lambda^2 \int_{-(1/2)}^{1/2} \delta\tau_{xy}\zeta \, d\zeta = \varphi \int_{-(1/2)}^{1/2} \delta\sigma_x \, d\zeta + \delta\varphi \int_{-(1/2)}^{1/2} \sigma_x \, d\zeta \tag{3.9}$$

The stress-strain relations can be written in the form

$$\left.\begin{aligned} \delta\sigma_x &= (3/2)\delta s_x = 3\,G\,\{a_x\delta e_x + a_{xy}\delta e_{xy}\} = 3\,G\,\{a_x\delta e_x + a_{xy}\zeta\delta\varphi\} \\ \delta\tau_{xy} &= 2\,G\,\{b_x\delta e_x + b_{xy}\delta e_{xy}\} = 2\,G\,\{b_x\delta e_x + b_{xy}\zeta\delta\varphi\} \end{aligned}\right\} \tag{3.10}$$

where according to Eqs. (2.1), (2.2), and (3.3)

$$\left.\begin{aligned} a_x &= 1 - (1-\mu)\frac{(3/2)\,(e_x - e_x'')^2}{P^2}; \qquad a_{xy} = -(1-\mu)\frac{2(e_x - e_x'')\,(e_{xy} - e_{xy}'')}{P^2} \\ b_x &= -(1-\mu)\frac{(3/2)\,(e_x - e_x'')\,(e_{xy} - e_{xy}'')}{P^2}; \qquad b_{xy} = 1 - (1-\mu)\frac{2(e_{xy} - e_{xy}'')^2}{P^2} \\ P^2 &= (3/2)\,(e_x - e_x'')^2 + 2\,(e_{xy} - e_{xy}'')^2 \end{aligned}\right\} \tag{3.11}$$

Further, the increments of permanent strain are given by Eq. (2.4)

$$\left.\begin{aligned} \delta e_x'' &= (1 - a_x)\delta e_x - a_{xy}\zeta\delta\varphi \\ \delta e_{xy}'' &= -b_x\delta e_x + (1 - b_{xy})\zeta\delta\varphi \end{aligned}\right\} \tag{3.12}$$

Substitution of Eq. (3.11) into Eq. (3.9) leads to

$$\left[\varphi\int_{-(1/2)}^{1/2} a_x d\zeta - 4\lambda^2\int_{-(1/2)}^{1/2} b_x\zeta d\zeta\right]\delta e_x = \left[4\lambda^2\int_{-(1/2)}^{1/2} b_{xy}\zeta^2 d\zeta - \varphi\int_{-(1/2)}^{1/2} a_{xy}\zeta d\zeta - \sum\left\{\delta e_x\int_{-(1/2)}^{1/2} a_x d\zeta + \delta\varphi\int_{-(1/2)}^{1/2} a_{xy}\zeta d\zeta\right\}\right]\delta\varphi \tag{3.13}$$

By putting

$$\left.\begin{aligned} I_1 &= \int_{-(1/2)}^{1/2} a_x \, d\zeta, \; I_2 = \int_{-(1/2)}^{1/2} a_{xy}\zeta d\zeta, \; I_3 = \int_{-(1/2)}^{1/2} b_x\zeta d\zeta = \frac{3}{4} I_2 \\ I_4 &= \int_{-(1/2)}^{1/2} b_{xy}\zeta^2 d\zeta \qquad A = \frac{\sigma_x}{3G} = \sum\{I_1\delta e_x + I_2\delta\varphi\} \end{aligned}\right\} \tag{3.14}$$

Eq. (3.13) is written as

$$[\varphi\, I_1 - 4\lambda^2 I_3]\delta e_x = [4\lambda^2 I_4 - \varphi\, I_2 - A\,]\delta\varphi \tag{3.15}$$

In the elastic range

$$I_1 = 1, \qquad I_2 = 0, \qquad I_3 = 0, \qquad I_4 = 1/12 \tag{3.16}$$

and for $A = (1/3)\lambda^2$ follows from Eq. (3.15) $\delta\varphi/\delta e_x = \infty$. If $\varphi_0 = 0$ (perfectly straight column) the value of $\delta\varphi/\delta e_x$ becomes indefinite for $A = (1/3)\lambda^2$, which means that the limit of stability is reached. Hence the elastic buckling stress is given by

$$\sigma_{xcr} = 3\,GA = G\,\lambda^2 = G\,(h/b)^2 \tag{3.17}$$

However, for a perfectly straight column in the plastic range only the value of I_1 differs from the values given in Eq. (3.16) according to the expressions (3.11) and (3.14). Therefore, Eq. (3.17) gives also the plastic buckling stress. From experiments it is known, however, that in the plastic range collapse takes place far below the stress given by Eq. (3.17). Onat and Drucker have demonstrated in reference 1 the large influence of very small initial twist upon the ultimate load. In the next paragraph the process of plastic collapse will be analyzed by a step-by-step procedure using Eq. (3.15).

(4) Analysis of the Plastic Collapse by a Step-by-Step Procedure

The dimensions of the column are chosen in accordance with those of the model used in reference 1, where the cruciform cross section is taken as a thin shell of constant thickness. The value of $\lambda = h/b$ is taken

$$\lambda = 0.1\sqrt{3}$$

A cruciform column having a solid cross section with

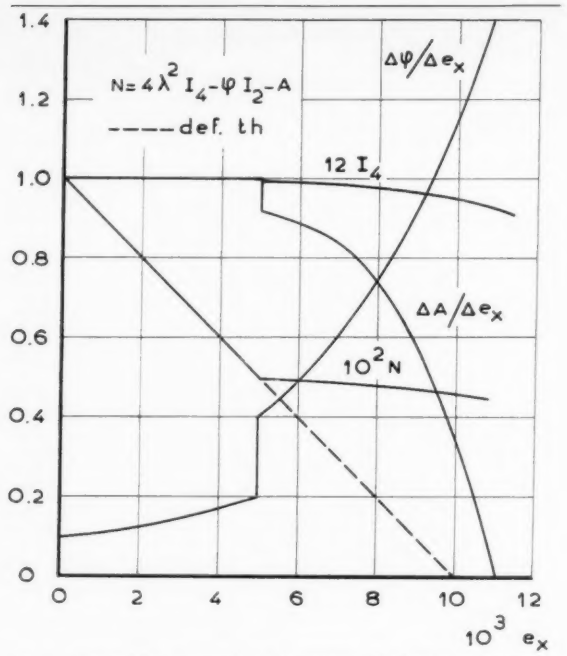

FIG. 3. Quantities, governing the process of plastic collapse, as a function of the compressive strain.

this value of λ has the same buckling stress as the model of reference 1 for $h/b = 0.1$. From Eq. (3.17) the buckling stress is

$$\sigma_{xcr} = G\lambda^2 = 0.030\,G$$

As in reference 1 it is assumed that $\sigma_{xcr} = 2\,\sigma_{xe}$. Thus the elasticity limit lies at

$$\sigma_{xe} = \sigma_{xcr}/2 = 0.015\,G$$

For μ was taken in reference 1

$$\mu = Gt/G = 0.05$$

In order to get a reasonably fast approach of the ultimate load in the step-by-step procedure, the initial twist is taken

$$\varphi_0 = 10^{-3}$$

i.e., a little more than the largest value, considered in reference 1, as (see reference 1)

$$2b\,\vartheta_0 = 2b\,\frac{\varphi_0}{h} = \frac{2}{0.1}\cdot 10^{-3} = 0.02 \text{ rad.} = 98 \text{ min.}$$

Equating M_e [see Eq. (3.5)] and M_t [see Eq. (3.7)] in the elastic range gives the equation

$$\varphi = [\lambda^2/(\lambda^2 - 3e_x)]\varphi_0 \qquad (4.1)$$

At the elasticity limit

$$A = \Sigma\delta e_x = e_x, \qquad e_{xe} = \frac{\sigma_{xe}}{3G} = 5\cdot 10^{-3}$$

and

$$\varphi = \frac{0.03}{0.03 - 0.015}\,10^{-3} = 2\cdot 10^{-3}$$

These are the starting values for the step-by-step procedure. For each successive step the integrals I_1, I_2, and I_4 [see Eq. (3.14)] were computed by means of Simpson's rule, e_x was given an increment $\Delta e_x = 0.5\cdot 10^{-3}$ and $\Delta\varphi$ was computed from Eq. (3.15). After determining ΔA from Eq. (3.14) the procedure was repeated.

The results of the computations are given in Fig. 3. As $\sigma_x = 3\,G\,A$ the ultimate load is reached when $\Delta A \div \Delta e_x = 0$. It is seen in Fig. 3 that then the value of I_4 is but slightly less than the elastic value and the value of $\Delta\varphi/\Delta e_x$ is still small. Hence the plastic collapse of this particular column is not a failure such as that connected with an ordinary buckling process. Such a failure would be marked by the value of

$$N = 4\lambda^2 I_4 - \varphi I_2 - A \qquad (4.2)$$

approaching to zero, thus causing excessive values of $\Delta\varphi/\Delta e_x$, according to Eq. (3.15). In Fig. 3 it is seen, however, that N decreases but slowly beyond the elasticity limit. Therefore the criterion for plastic collapse is not given by $N = 0$, but by

$$\delta A = I_1\delta e_x + I_2\delta\varphi = 0 \qquad (4.3)$$

Beyond the point where $\Delta A/\Delta e_x = 0$, collapse of the column takes place accompanied by deflections growing with increasing velocity. However, as was pointed out above, the failure has but an outer resemblance with the phenomenon of buckling, as this is known in the elastic range.

Fig. 4 contains a plot of σ_x versus e_x. It is seen that the ultimate stress lies only slightly above the elasticity limit.

(5) Discussion of Results

From experiments it is known that for plates loaded in their plane plastic collapse takes place far below the theoretical value of the buckling stress. In fact the ultimate load lies close to the buckling stress calculated either by deformation type theory or by Gerard's rule.[6]

According to the deformation theory the coefficients (3.11) after pure compression are given by

$$\left.\begin{aligned} a_x &= Gt/G, & a_{xy} &= 0 \\ b_x &= 0, & b_{xy} &= Gs/G \end{aligned}\right\} \qquad (5.1)$$

Substitution into Eq. (3.14) gives

$$I_1 = Gt/G, \qquad I_2 = 0, \qquad I_3 = 0, \qquad I_4 = (1/12)Gs/G \qquad (5.2)$$

The buckling stress follows from

$$N = 4\lambda^2 I_4 - A = (1/3)\lambda^2\,Gs/G - (\sigma_x/3G) = 0 \qquad (5.3)$$

Thus, according to the deformation theory, a perfectly straight cruciform column fails by pure torsional buckling at a stress

$$\sigma_{xcr} = Gs\,\lambda^2 \qquad (5.4)$$

Gerard's empirical rule gives for the ultimate stress the same value. The corresponding value of the critical

strain is

$$e_{xcr} = \lambda^2$$

Gerard's rule is purely empirical, but the deformation theory pretends to give an adequate description of the process of plastic buckling, though theoretical objections against the deformation theory[2,3] have been confirmed already by some direct experimental evidence.[4] The calculations of this paper, made with the theoretically sound flow theory, which has been verified by direct experimental evidence, show, however, that the process of plastic collapse may be of a nature entirely different from the pure buckling process, predicted by the deformation theory.

The amount of initial twist of the column, treated in this paper, was taken rather large in order to reach the ultimate load in a reasonable number of steps, but this does not change the nature of the process of collapse. For the chosen value of initial twist the critical strain lies close to the value predicted by Gerard's rule and deformation theory. The ultimate stress lies somewhat below the value $\sigma_{xcr} = Gs\,\lambda^2$, as is seen in Fig. 4.

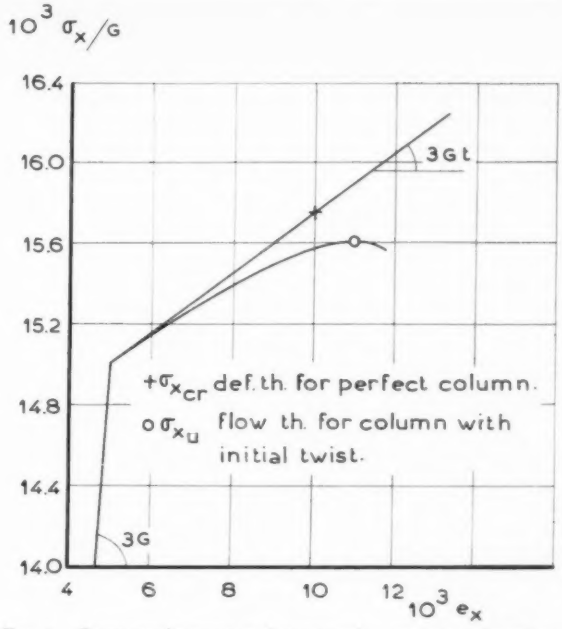

FIG. 4. Stress-strain curve and compressive stress as a function of compressive strain for column with initial twist.

(6) CONCLUSIONS

The analysis of the plastic collapse of a cruciform column with initial twist, given in this paper as a supplement to reference 1, shows that reaching an ultimate load is not connected with an ordinary buckling failure. At a certain critical strain the compressive stress reaches a maximum due to the interaction of compressive strain and shear strain in the plastic stress-strain relations. Increasing compressive strain accompanied by growing twist causes a drop in the compressive stress, the deflections growing initially at no excessive rate. This is in contradiction with the process of collapse as predicted by the deformation theory, while it seems to be in agreement with observations of, for instance, reference 5. For plates loaded in their plane plastic collapse, arising from initial imperfections, can not be treated theoretically in a general way. Therefore, rather than deriving the ultimate load from an imaginary buckling phenomenon, the ultimate load should be computed by empirical rules, like Gerard's rule.[6]

REFERENCES

[1] Onat, E. T., and Drucker, D. C., *Inelastic Instability and Incremental Theories of Plasticity*, Journal of the Aeronautical Sciences, Vol. 20, No. 3, p. 181, March, 1953.

[2] Benthem, J. P., *On the Stress-Strain Relations of Plastic Deformation*, Nat. Aero. Res. Inst., Amsterdam (N.L.L.), Report S.398, 1951.

[3] Besseling, J. F., *A Theory of Plastic Flow for Anisotropic Hardening in Plastic Deformation of an Initially Isotropic Material*, Nat. Aero. Res. Inst., Amsterdam (N.L.L.), Report S.410, 1953.

[4] Peters, R. W., Dow, N. F., and Batdorg, S. B., *Preliminary Experiments for Testing Basic Assumptions of Plasticity Theories*, Proc. of the Soc. for Experimental Stress Analysis, Vol. VII, No. 2, p. 127, 1950.

[5] Besseling, J. F., *On the Buckling Problem in the Plastic Range for Struts and Plates, Part III. Experiments and Non dimensional Buckling Curves*, Nat. Aero. Res. Inst., Amsterdam (N.L.L.), Report S.444, 1955.

[6] Gerard, G., *Secant Modulus Method for Determining Plate Instability Above the Proportional Limit*, Journal of the Aeronautical Sciences, Vol. 13, No. 1, p. 3, January, 1946.

[7] Hoff, N. J., *Buckling and Stability*, J. of the Royal Aero. Soc., January, 1954.

[8] Drucker, D. C., and Onat, E. T., *On the Concept of Stability of Inelastic Systems*, Journal of the Aeronautical Sciences, Vol. 21, No. 8, p. 543, August, 1954.

System Mode Shapes in the Flutter of Compressor Blade Rows*

FRANK LANE†
New York University

Abstract

The problems associated with the prohibitive number of possible system modes for a fluttering compressor or turbine blade row are eliminated by the development that comprises the present report. The existence and uniqueness of extremely simple system flutter modes are proved for blade rows consisting of identical blades equally spaced about a common rotor. These simple system modes, if properly interpreted, have the effect of reducing by a factor of n the number of degrees of freedom necessary to analyze an n-bladed configuration. Stated differently, the system of n blades may be considered, with no loss of generality whatsoever, in terms of a single "equivalent blade." The proof holds under any type of flow and any and all types of interblade coupling, so long as a linear analysis is permissible. Moreover, since it is the flutter-inception point that is of interest in predicting critical velocity or rotational speed, it may well be that the conclusions developed apply even to the onset of stall flutter. Practical application of the method to stall-flutter calculations would, of course, require the availability of aerodynamic stall-flutter coefficients.

The development is carried out first under the assumption of infinite rotor inertia or, in other words, constant rotor velocity. This restriction is then relaxed, and the treatment is expanded to permit torsional oscillations of the rotor itself. It is proved that under certain conditions the assumption of infinite rotor inertia introduces no error whatsoever.

Symbols

A = flutter matrix with infinite rotor inertia assumed
$\tilde{A}$ = flutter matrix with finite rotor inertia
V = relative flow velocity at some reference radius
k = reduced frequency of flutter ($= \omega b/V$) at reference radius
b = semichord length at reference radius
n = number of blades in row
t = time
p = number of degrees of freedom alloted to each blade
q = generalized-coordinate vector excluding rotor deflection
$\tilde{q}$ = generalized-coordinate vector including rotor deflection
q^{Ω} = generalized coordinate associated with rotor deflection
q_{α} = generalized coordinates associated with blade twisting
q_{u} = generalized coordinates associated with blade bending
Ω = rotor angular velocity, rad. per sec.
ω = flutter (circular) frequency
σ_{ν} = argument (radians) of νth of the n nth roots of unity
σ = phase-lag angle between adjacent blades at flutter

Received September 20, 1954.

* The investigation reported in this paper was sponsored by the Wright Air Development Center, Air Research and Development Command, under Contract AF 33(616)-25 with the Research Division, College of Engineering, New York University. Project Director, Chi-Teh Wang, Professor of Aeronautical Engineering.

† Research Associate Professor of Aeronautical Engineering, Daniel Guggenheim School of Aeronautics.

Introduction

The chief contribution of the research reported herein lies in the establishment of a method that permits the linear flutter analysis of configurations characterized by a large number of identical fluttering members and, accordingly, encumbered by a prohibitively large number of degrees of freedom. In order to place this development in true perspective it is necessary to outine the methods by which many-bladed configurations have been flutter analyzed in the past and to indicate wherein the present treatment extends or supersedes this previous research.

With the availability of well-established methods for flutter analysis of single, isolated wings, the first and most obvious method for treating multibladed systems is to ignore all forms of interblade coupling and to proceed under the assumption that each blade flutters just as it would in the absence of all other blades. This approach can be considered as zeroth order approximation and may lead to unconservative estimates of critical flutter velocity.

Turner and Duke,[9] in an investigation of propeller flutter, neglect aerodynamic interaction but dispose of the interblade coupling that arises from the physical connection of the blades of a three-bladed propeller to a common hub by resolving the propeller system mode into "resonant" and "antiresonant" components that are then shown to be uncoupled. This, in turn, allows treatment of a single blade in formulating the flutter problem, all under the assumption of zero aerodynamic interaction between blades. The cumbersome nature of the analysis by resolution into resonant and antiresonant modes (it appears awkward even for as few as three blades) indicates the unsuitability of this approach to systems such as compressors and turbines with many blades. Lilley[2] noted, from experimental observations of the flutter of a series of elastic wings arranged in cascade, that adjacent blades were approximately 180° out of phase when fluttering. This phenomenon was termed "antiphase motion" by Lilley, who recognized immediately that, for the case of zero stagger, a cascade fluttering in antiphase motion is aerodynamically equivalent to a single wing oscillating between parallel walls with its attendant image system. The aerodynamics of the single wing oscillating under the interference of tunnel walls had been studied previously by Reissner[4, 5] and others and is presented in somewhat different form by Lilley[2]

with a view toward obtaining oscillatory air forces for the unstaggered cascade in antiphase motion.

Lilley then applied these air forces to the unstaggered cascade flutter problem for the particular values of elastic and inertial parameters corresponding to his experimental system, under the assumed condition that the system flutter was in antiphase motion, and the agreement between theory and experiment proved excellent. It is to be emphasized that Lilley's observations indicated that, for both staggered and unstaggered cascades, adjacent blades at flutter were *approximately* out of phase and that he derived air forces and solved the cascade flutter problem assuming antiphase motion for only the unstaggered cascade. Previous results for tunnel interference effect on a single oscillating wing also, for obvious reasons, apply only to the unstaggered case. The importance of Lilley's work lies in the fact that he was able to assume in advance the form of the system mode, based on experimental evidence, and hence to determine the oscillatory air forces (including interaction between blades) and proceed with a solution of the flutter problem subject to the restrictions imposed by the antiphase assumption.

Chang and Chu[1] present a derivation of the oscillatory lift and moment acting upon the blades of an unstaggered two-dimensional cascade at zero or very small incidence, under the restrictive assumption that all blades oscillate in phase with one another. This assumed condition permits a solution of the aerodynamics problem by mapping techniques similar to those used by Theodorsen[8] for the fluttering single wing. As will appear evident from calculations to be reported in a subsequent paper, the in-phase assumption is the least conservative one possible with respect to the prediction of critical flutter velocity. In fact, it will appear that critical flutter velocities predicted on the basis of an assumed in-phase motion of all blades will exceed the critical velocity of one of the blades alone, whereas actual blade-row critical flutter velocities are considerably less than that of an isolated blade.

A study of Lilley's paper suggested to the present author the possibility of performing a general investigation of system flutter modes for multibladed systems with the objective of predicting, or at least restricting in advance the form of the system mode which exists at the fluttering condition. We content ourselves here with a somewhat oversimplified statement of the conclusions reached as a result of the investigation. It is proved that a system of identical blades identically supported and equally spaced about a common rotor, whether this rotor be rigid or elastic and of infinite or finite inertia, will flutter in a system mode or at worst in a linear combination of modes, in which all blades oscillate with identical blade modes and in which each blade leads or lags its neighbor by a common phase angle, the value of this angle constituting one portion of the solution of the flutter problem for a particular configuration. The conditions under which this statement is proved are sufficiently general to encompass any type of flow—incompressible, subsonic, supersonic, or even stalling (separating and reattaching boundary layer)—so long as a linear analysis is permissible at the flutter inception point. Moreover, the development permits of all forms of coupling—aerodynamic, elastic, or inertial—between blades. Incidentally, as a consequence of this proof of existence of a simple system flutter mode, it is shown that the antiphase motion observed by Lilley is to be expected for the unstaggered cascade at zero incidence but not necessarily for other configurations. The degree of departure from exact antiphase motion in the case of nonzero stagger or nonzero incidence, or both, must be determined as a result of the flutter calculation for the particular configuration in question.

Analytical Development

(*1*) *Consequences of the Cyclic Characteristics of the Configuration*

In order to keep the explanation from becoming too cumbersome, the details will be developed for a system in which just two degrees of freedom are alloted to each blade (one in torsion q_α and one in bending q_u). The method is, however, equally applicable when any number, p, of degrees is allowed per blade, and, at appropriate points in the development, the method of extending to more coordinates per blade will be indicated. Thus we consider a cyclic system of n blades all identical and identically supported and all equally spaced. By "cyclic" arrangement we mean only to signify the usual propeller, turbine, or compressor configuration wherein the last or nth blade is adjacent to the first blade. We denote by q_α^j, q_u^j, the generalized coordinates corresponding to the torsion and bending modes, respectively, of the jth blade, with (harmonic) time dependence removed, and we arrange the vector of generalized coordinates in the form

$$q = e^{i\omega t} \begin{bmatrix} q_\alpha^1 \\ q_u^1 \\ q_\alpha^2 \\ q_u^2 \\ \cdot \\ \cdot \\ \cdot \\ q_\alpha^n \\ q_u^n \end{bmatrix} \tag{1}$$

where ω is the flutter frequency. We assume initially infinite rotor inertia so that no coordinate is necessary for the rotor itself. Now, under the most general conditions of coupling, the final system of $(2n)$ flutter equations will take the form

$$A\,q = 0 \tag{2}$$

wherein the matrix A must be of cyclic form in its second-order submatrices as a consequence of the cyclic geometry of the configuration. The flutter equation is then of the following form, in expanded notation:

$$\begin{bmatrix} a_1 & b_1 & c_2 & b_2 & c_3 & b_3 & \dots & a_n & b_n \\ c_1 & d_1 & c_2 & d_2 & c_3 & d_3 & \dots & c_n & d_n \\ a_n & b_n & a_1 & b_1 & a_2 & b_2 & \dots & a_{n-1} & b_{n-1} \\ c_n & d_n & c_1 & d_1 & c_2 & d_2 & \dots & c_{n-1} & d_{n-1} \\ a_{n-1} & b_{n-1} & a_n & b_n & a_1 & b_1 & \dots & a_{n-2} & b_{n-2} \\ c_{n-1} & d_{n-1} & c_n & d_n & c_1 & d_1 & \dots & c_{n-2} & d_{n-2} \\ & & \vdots & & & & & & \\ a_2 & b_2 & a_3 & b_3 & a_4 & b_4 & & a_1 & b_1 \\ c_2 & d_2 & c_3 & d_3 & c_4 & d_4 & & c_1 & d_1 \end{bmatrix} \begin{bmatrix} q_\alpha{}^1 \\ q_u{}^1 \\ q_\alpha{}^2 \\ q_u{}^2 \\ q_\alpha{}^3 \\ q_u{}^3 \\ \vdots \\ q_\alpha{}^n \\ q_u{}^n \end{bmatrix} = 0 \tag{3}$$

where elastic, dynamic, and aerodynamic coupling may exist between blades, as well as within a single blade.

Here a_i represents the total effect of the torsion mode in the sth blade upon the torsion mode of the $(s + 1 - i)$th blade, b_i represents the effect of the bending mode in the sth blade upon the torsion mode of the $(s + 1 - i)$th blade, c_i is the effect of the torsion mode in the sth blade upon the bending mode of the $(s + 1 - i)$th blade, and d_i is the total effect of the bending mode in the sth blade upon the bending mode of the $(s + 1 - i)$th blade. The torsion mode of the nth blade affects the bending mode of the second blade in exactly the same way that the torsion mode of the first blade affects the bending mode of the third blade, and so on. It is to be noted that the degrees of freedom (characterized by q_u in bending and q_α in torsion) are taken as the same spanwise or radialwise functions for each blade. In other words, some single bending mode is taken as the bending mode for each blade and some single torsion mode is taken for the torsion mode of all blades. No assumption is made beforehand, however, with regard to the relative magnitude or phasing of the occurrence of the bending and torsion modes in any one or in different blades—i.e., the vector solution q is completely unrestricted.

We now proceed to show, by a study of the determinant $|A|$ of matrix A, that a great deal can be said in advance about the resulting form of q and that, in fact, the problem may be reduced from one requiring $2n$ degrees of freedom to one with only two degrees (in general the reduction is from pn to p degrees). The study of $|A|$ stems from an extension of the special circulant determinant (to which $|A|$ would reduce if we allowed initially only *one* degree of freedom per blade).

Let ω_ρ be the ρth of the n nth roots of unity—i.e.,

$$\omega_\rho = e^{2\pi i(\rho/n)} \tag{4}$$

and define the scalar quantities

$$\left.\begin{aligned} A_j &= (a_1 + a_2\omega_j + a_3\omega_j{}^2 + \dots + a_n\omega_j{}^{n-1}) \\ B_j &= (b_1 + b_2\omega_j + b_3\omega_j{}^2 + \dots + b_n\omega_j{}^{n-1}) \\ C_j &= (c_1 + c_2\omega_j + c_3\omega_j{}^2 + \dots + c_n\omega_j{}^{n-1}) \\ D_j &= (d_1 + d_2\omega_j + d_3\omega_j{}^2 + \dots + d_n\omega_j{}^{n-1}) \end{aligned}\right\} \tag{5}$$

It should be noted that, in view of the fact that

$$\omega_j{}^n = 1 \qquad \text{for all } j$$

we may write A_j, B_j, C_j, D_j equally well in the following form:

$$\left.\begin{aligned} A_j &= (a_1 + a_2\omega_j + a_n\omega_j{}^{-1} + a_3\omega_j{}^2 + a_{n-1}\omega_j{}^{-2} + \dots) \\ B_j &= (b_1 + b_2\omega_j + b_n\omega_j{}^{-1} + b_3\omega_j{}^2 + b_{n-1}\omega_j{}^{-2} + \dots) \end{aligned}\right\}$$
etc. (5a)

Now since the determinant $|A|$ is unaltered in magnitude by adding to any row multiples of the remaining rows, we form new first and second rows ρ_1' and ρ_2' in the following manner (ρ_j denotes the original jth row and ρ_j' the new jth row).

$$\left.\begin{aligned} \rho_1' &= \rho_1 + \omega_j{}^{n-1}\rho_3 + \omega_j{}^{n-2}\rho_5 + \dots + \omega_j\rho_{2n-1} \\ \rho_2' &= \rho_2 + \omega_j{}^{n-1}\rho_4 + \omega_j{}^{n-2}\rho_6 + \dots + \omega_j\rho_{2n} \end{aligned}\right\} \tag{6}$$

This leaves $|A|$ unaltered in magnitude and in the following form (recalling that $(\omega_j)^n = 1$):

$$|A| = \begin{vmatrix} A_j & B_j & \frac{A_j}{\omega_j} & \frac{B_j}{\omega_j} & \frac{A_j}{\omega_j{}^2} & \frac{B_j}{\omega_j{}^2} & \dots & \cdot & \frac{B_j}{\omega_j{}^{n-1}} \\ C_j & D_j & \frac{C_j}{\omega_j} & \frac{D_j}{\omega_j} & \frac{C_j}{\omega_j{}^2} & \frac{D_j}{\omega_j{}^2} & \dots & \cdot & \frac{D_j}{\omega_j{}^{n-1}} \\ a_n & b_n & a_1 & b_1 & a_2 & b_2 & \dots & a_{n-1} & b_{n-1} \\ c_n & d_n & d_1 & d_1 & c_2 & d_2 & \dots & c_{n-1} & d_{n-1} \\ \cdot & \cdot & \cdot & \cdot & \cdot & \cdot & \dots & \cdot & \cdot \\ & & & \text{(Remaining rows unaltered)} & & & & & \\ c_2 & d_2 & c_3 & d_3 & c_4 & d_4 & \dots & c_1 & d_1 \end{vmatrix} \tag{7}$$

Suppose now that we expand the determinant $|A|$ by the Laplace expansion with respect to the first two rows, using $|A|$ in the form (7). We see that all minors of the form

$$\begin{vmatrix} \frac{A_j}{(\omega_j)^s} & \frac{A_j}{(\omega_j)^p} \\ \frac{C_j}{(\omega_j)^s} & \frac{C_j}{(\omega_j)^p} \end{vmatrix} \quad \text{and} \quad \begin{vmatrix} \frac{B_j}{(\omega_j)^s} & \frac{B_j}{(\omega_j)^p} \\ \frac{D_j}{(\omega_j)^s} & \frac{D_j}{(\omega_j)^p} \end{vmatrix}$$

vanish since they are expressible as determinants with identical columns. Moreover, *all nonzero* minors formed from the first two rows contain

$$\Delta_j = \begin{vmatrix} A_j & B_j \\ C_j & D_j \end{vmatrix} \tag{8}$$

as a factor. Thus, since Δ_j is a factor for each of the n

different values of j (corresponding to the n different nth roots of unity), we may express $|A|$ in the product form

$$|A| = K \prod_{j=1}^{n} \Delta_j = K \prod_{j=1}^{n} \begin{vmatrix} A_j & B_j \\ C_j & D_j \end{vmatrix} \tag{9}$$

with K as yet undetermined; in fact K may depend upon the various a's, b's, c's, and d's until we prove otherwise. Now the product (9) is already of order n in any a_j, b_j, c_j, or d_j; hence K cannot depend upon these elements, but must in fact be simply a numerical constant since $|A|$ itself is of order n in each of the a_j, b_j, c_j, d_j. Moreover, since the leading diagonal term of $|A|$ contributes $(a_1)^n \cdot (d_1)^n$ we see immediately that K must be unity. Thus we obtain the expansion of $|A|$ in the particularly simple form

$$|A| = \prod_{j=1}^{n} \Delta_j = \prod_{j=1}^{n} \begin{vmatrix} A_j & B_j \\ C_j & D_j \end{vmatrix} \tag{10}$$

where the product extends over the n nth roots of unity.

At this point we may remark that the initial use of *more* than two degrees of freedom per blade would have led, through similar arguments, to the same form of expansion for $|A|$ except that the factors Δ_j would be of order p instead of order two—i.e.,

$$|A| = \prod_{j=1}^{n} \Delta_j = \prod_{j=1}^{n} \begin{vmatrix} A_{j_{11}} & A_{j_{12}} & \cdots & A_{j_{1p}} \\ A_{j_{21}} & A_{j_{22}} & \cdots & A_{j_{2p}} \\ \cdot & & & \\ \cdot & & & \\ A_{j_{p1}} & A_{j_{p2}} & \cdots & A_{j_{pp}} \end{vmatrix} \tag{11}$$

the elements of these Δ_j being defined in the same manner [see Eq. (5)] as the A_j, B_j, C_j, D_j were defined in the two degree of freedom per blade situation. This is easily seen by remarking that the original $p \times n$ order determinant would be expanded, after Laplace's method, by the first p rows following a process such as Eq. (6) in which, to each of the first p rows were added linear combinations of every pth following row multiplied by a suitable power of ω_j.

(2) *Determination of Critical Flutter Velocity*

Now the flutter problem consists in finding the critical velocity V and corresponding flutter frequency ω such that the determinant $|A|$ vanishes and a nontrivial system mode q is possible as a solution of Eq. (2). The lowest velocity V which causes $|A|$ to vanish and which, with the corresponding value of ω, is consistent with an initially chosen reduced frequency k ($= \omega b / V$) is the critical flutter velocity. The nontrivial vector or vectors q which then satisfy Eq. (2) constitute the system flutter mode or modes. It is to be recalled that the elements a_j, b_j, c_j, d_j, of A involve k and, in compressible flow, the Mach Number M, in such a complicated transcendental form that it is necessary to insert numerical trial values of these parameters, k and M, into A before proceeding with the flutter problem or, alternatively, to include an undetermined parameter in the analysis. We will forget about Mach Number, M, for the present development, assuming that if necessary, the entire process presented herein will be repeated with new trial values of M until a trial value of M and the resulting critical flutter velocity V are consistent with the free-stream sound velocity. Moreover, we mean by b (semichord) V, k, or any other parameter, the value of the parameter at some reference station along the blade span, since in rotating blade systems with radially varying chord the usual definitions of k, V, and b actually vary along a blade. Further, we assume that the velocity V is interchangeable with the rotor velocity Ω, since in general either V, Ω, or the ratio of the two will be fixed in advance.

Returning for convenience, but with no loss of generality, to the case wherein two degrees of freedom are allowed to each blade, we continue the study of the system flutter problem through an examination of the factored form (10) of the flutter determinant, $|A|$. Obviously, if $|A|$ is to vanish, as it must for existence of a nontrivial flutter mode, at least one of the n factors Δ_j must vanish. Hence the scheme which suggests itself at first is the following. Annihilate, in turn, each of the n minors Δ_j by a proper choice of k and subsequent solution for V (call it V_j). This may be performed, for each Δ_j, by the method of successive trial values of k, known as Theodorsen's method[6] or by the method of including an undetermined parameter. Having fixed upon a trial value of k, frequency may be replaced by velocity through the relation

$$\omega = kV/b \tag{12}$$

Then the elements of any Δ_j become complex first degree polynomials in V^2, and the expansion of Δ_j becomes a second (in general pth) degree polynomial in V^2, with complex numerical coefficients. Separating the coefficients into real and imaginary parts, for each Δ_j, we get a pair of simultaneous algebraic equations in V^2. These are then solved respectively for the roots V_R^2, V_I^2 which, in general, will not be the same. New trial values of k are inserted and the roots V^2 may be plotted versus k, until an intersection is obtained—i.e., until some choice of k leads to a *common* solution. $V_R^2 = V_I^2$, for *both* the real and imaginary equations. In case several intersections occur, the solution with the minimum value of V is used, since this will provide the most critical condition for the particular minor Δ_j under consideration. The final critical velocity corresponding to the jth minor Δ_j will be called V_j and the associated k and ω, k_j and ω_j. The process is repeated for each Δ_j, until values of V_j, k_j and ω_j are available for each of the n minors. The minimum V_j then gives the flutter velocity, and the associated k_j provides the flutter frequency ω_j through Eq. (12). If one or more of the Δ_j fails to lead to a physically realizable (real) pair, V_j, ω_j then this index is merely neglected in the comparison to determine the minimum V_j. Summarizing, we have found the velocity V and the associated k and ω which annihilate one (or possibly more than one) of the minors Δ_j and which achieve this annihilation with minimum velocity. This group, k, V, ω would

have been the one arrived at by the far more cumbersome procedure of annihilating the original flutter determinant $|A|$ directly and choosing the annihilating group with minimum velocity.

At this point a tremendous simplification suggests itself for turbine and compressor blade systems with large numbers of blades. For large n, the nth roots of unity approach a condition of density about the unit circle. Thus we replace the preceding process of picking a minimum V_j from among a large set of discrete values by a minimization process with respect to the root angle, σ. In other words, we set equal to zero the general minor

$$\Delta_\sigma = \begin{vmatrix} A_\sigma & B_\sigma \\ C_\sigma & D_\sigma \end{vmatrix} \tag{13}$$

wherein the n discrete values of the nth roots of unity are replaced by the angle σ which is temporarily assumed to be continuously variable between 0 and 2π, and wherein we use an extension of Eq. (5a) to define A_σ, B_σ, C_σ, D_σ:

$$\left.\begin{aligned} A_\sigma &= (a_1 + a_2 e^{i\sigma} + a_n e^{-i\sigma} + a_3 e^{2i\sigma} + a_{n-1} e^{-2i\sigma} + \ldots) \\ B_\sigma &= (b_1 + b_2 e^{i\sigma} + b_n e^{-i\sigma} + b_3 e^{2i\sigma} + b_{n-1} e^{-2i\sigma} + \ldots) \end{aligned}\right\} \tag{14}$$

Now the annihilation of the general minor Δ_σ, leads to the two equations,

$$\left.\begin{aligned} P_R(V^2, k, \sigma) &= 0 \\ P_I(V^2, k, \sigma) &= 0 \end{aligned}\right\} \tag{15}$$

in which P_R, P_I are polynomials in V^2 with coefficients depending transcendentally upon k and upon σ. After insertion of a trial value of k, Eqs. (15) may be solved, respectively, for $V_R{}^2(\sigma)$ and $V_I{}^2(\sigma)$. We shall show subsequently that velocity (and frequency) may be expected to vary smoothly with the angle σ. Thus, to each of several (say ten) values of σ between 0 and 2π we find the value (or, possibly, values) of k which gives consistent roots,

$$V_R{}^2(\sigma) = V_I{}^2(\sigma) \tag{16}$$

The consistent roots $V^2(\sigma)$ and the corresponding values of $k = k(\sigma)$ are then plotted against σ. The flutter condition is found simply by picking the minimum value of $V^2(\sigma_\nu)$ where σ_ν is one of the admissable discrete values of σ.

$$\sigma_\nu = 2\pi\nu/n \tag{17}$$

That is, on the curve (or curves, in case more than one consistent condition exists for some range of values of σ) of V^2 versus σ we find the minimizing value of σ and take the nearest admissable σ_ν with its corresponding V_ν, k_ν as the flutter condition.

The replacement of the problem of annihilation of n determinants Δ_ν by the annihilation of the general minor Δ_σ at a much smaller (than n) number of points and subsequent plotting of annihilating combinations V, k, versus σ to determine the critical flutter condition is justified as follows: referring to Eq. (14) and remarking that the influence of distant blades becomes small rapidly with increasing distance, we see that A_σ, B_σ, C_σ, D_σ and hence also P_R and P_I, take the form of finite complex Fourier series in the angle σ, with rapidly decreasing coefficients for the higher harmonics. Thus it is to be expected that $V^2(\sigma)$ and $k(\sigma)$ will vary smoothly in σ despite the presence of high harmonics (for large n). Indeed, as will be seen subsequently, if the coupling between blades is of an aerodynamic nature only, then for incompressible flow the *infinite* Fourier series corresponding to Eq. (14) are expressible in closed form as smooth (actually analytic) functions of σ for $0 < \sigma < 2\pi$. Hence the plotting process to locate a minimum V and the replacement of the minimizing angle σ by the nearest admissable value σ_ν should be a valid means of obtaining the critical flutter velocity and associated frequency. If the high harmonics occurred with large coefficients then the plotting process and the replacement of the minimizing value of the angle σ by an adjacent admissable value σ_ν would be open to question, but the physical nature of the problem eliminates this difficulty.

Looking at this point in a slightly different light, it seems reasonable to believe that a blade system with n blades, where n is large, will exhibit a critical flutter velocity which differs only slightly from a system with identical blades, identically supported, but $(n + 1)$ in number. This reasoning provides additional support for our contention that $V(\sigma)$ will vary "smoothly" with σ, thereby justifying the minimization process and the replacement of the minimizing angle σ, by its nearest admissable value, σ_ν.

(3) *Determination of the Flutter Mode*

Having determined the critical flutter velocity and the associated values of k, it remains to compute the corresponding flutter mode q. This mode turns out to be very easily described, and in the case where $|A|$ vanishes simply (or doubly in the case of a symmetric blade configuration) to have a very interesting physical relation to the angle σ or σ_ν. Consider the minor Δ_ν which is annihilated by the critical velocity V_ν and the associated k_ν, forgetting, for the present, the possibility of multiple degeneracy—i.e., assume for the present that Δ_ν vanishes simply and that no other Δ_j vanishes upon insertion of $V = V_\nu$, $k = k_\nu$. Then

$$\begin{vmatrix} A_\nu & B_\nu \\ C_\nu & D_\nu \end{vmatrix} = 0 \tag{18}$$

and there exists a nontrivial vector (q_α, q_u) such that

$$\begin{bmatrix} A_\nu & B_\nu \\ C_\nu & D_\nu \end{bmatrix} \begin{bmatrix} q_\alpha \\ q_u \end{bmatrix} = 0 \tag{19}$$

Expanding the elements $A_\nu B_\nu$ etc., and the Eqs. (19), we find

$$\left.\begin{aligned} &(a_1 + a_2\omega_\nu + a_3{\omega_\nu}^2 + \ldots + a_n{\omega_\nu}^{n-1})q_\alpha + \\ &\quad (b_1 + b_2\omega_\nu + b_3{\omega_\nu}^2 + \ldots + b_n{\omega_\nu}^{n-1})q_u = 0 \\ &(c_1 + c_2\omega_\nu + c_3{\omega_\nu}^2 + \ldots + c_n{\omega_\nu}^{n-1})q_\alpha + \\ &\quad (d_1 + d_2\omega_\nu + d_3{\omega_\nu}^2 + \ldots + d_n{\omega_\nu}^{n-1})q_u = 0 \end{aligned}\right\} \tag{20}$$

But these are equivalent to

$$\begin{bmatrix} a_1 & b_1 & a_2 & b_2 & a_3 & b_3 & \cdot\cdot & a_n & b_n \\ c_1 & d_1 & c_2 & d_2 & c_3 & d_3 & \cdot\cdot & c_n & d_n \end{bmatrix} \begin{bmatrix} q_\alpha \\ q_u \\ \omega_\nu q_\alpha \\ \omega_\nu q_u \\ \omega_\nu^2 q_\alpha \\ \omega_\nu^2 q_u \\ \cdot \\ \cdot \\ \omega_\nu^{n-1} q_\alpha \\ \omega_\nu^{n-1} q_u \end{bmatrix} = 0 \tag{21}$$

Or, in other words, the vector

$$q = \begin{bmatrix} q_\alpha \\ q_u \\ \omega_\nu q_\alpha \\ \omega_\nu q_u \\ \cdot \\ \cdot \\ \omega_\nu^{n-1} q_\alpha \\ \omega_\nu^{n-1} q_u \end{bmatrix} \tag{22}$$

is a solution of the first two of the original $2n$ Eqs. (3) under the condition that the minor Δ_ν is annihilated by insertion of the critical flutter velocity. Now multiply both Eqs. (20) through by ω_ν obtaining

$$\left.\begin{aligned} (a_n + a_1\omega_\nu + a_2\omega_\nu^2 + \cdot\cdot + a_{n-1}\omega_\nu^{n-1})q_\alpha + \\ (b_n + b_1\omega_\nu + b_2\omega_\nu^2 + \cdot\cdot + b_{n-1}\omega_\nu^{n-1})q_u = 0 \end{aligned}\right\}$$
$$\left.\begin{aligned} (c_n + c_1\omega_\nu + c_2\omega_\nu^2 + \cdot\cdot c_{n-1}\omega_\nu^{n-1})q_\alpha + \\ (d_n + d_1\omega_\nu + d_2\omega_\nu^2 + \cdot\cdot + d_{n-1}\omega_\nu^{n-1})q_u = 0 \end{aligned}\right\} \tag{23}$$

upon recalling that $(\omega_\nu)^n = 1$.

Eqs. (23) may be rewritten in the form

$$\begin{bmatrix} a_n & b_n & a_1 & b_1 & a_2 & b_2 & \cdot\cdot & a_{n-1} & b_{n-1} \\ c_n & d_n & c_1 & d_1 & c_2 & d_2 & \cdot\cdot & c_{n-1} & d_{n-1} \end{bmatrix} \begin{bmatrix} q_\alpha \\ q_u \\ \omega_\nu q_\alpha \\ \omega_\nu q_u \\ \omega_\nu^2 q_\alpha \\ \omega_\nu^2 q_u \\ \cdot \\ \cdot \\ \omega_\nu^{n-1} q_\alpha \\ \omega_\nu^{n-1} q_u \end{bmatrix} = 0 \tag{24}$$

Thus the vector q of Eq. (22) is also a solution of the third and fourth equations of system (3). By multiplying Eq. (20) by successively higher powers of ω_ν we see that Eq. (22) is indeed a nontrivial solution of the complete original flutter equation. The nontriviality follows from the existence of the nontrivial pair q_α, q_u. Now in the case where insertion of $V = V_\nu$ causes only simple degeneracy of the matrix A, our solution (22) is unique to within an arbitrary multiplicative constant. Moreover the form of the solution (flutter mode) is amazingly simple. q_α, q_u is simply the vector solution to the homogeneous second-degree system (19) which is easily determined once the elements of Δ_ν are available, and this represents the fundamental blade mode. All other blades flutter with *exactly* the same blade mode, with same magnitude of occurrence of this mode (all the powers of ω_ν are of unit magnitude) and with a phase shift equal to the angle σ_ν occurring between successive blades. Thus, as soon as we find the angle, σ_ν, if A is simply degenerate upon insertion of V_ν, we can solve a second (or, in general a pth) order system for the blade mode and immediately write down the system mode solution with no further effort.

Next we consider the possibility of multiple-degeneracy. Multiple-degeneracy of A, it should be noted, implies that upon insertion of the critical flutter velocity $V = V_\nu$, either one of the minors vanishes multiply or several of the minors vanish simply or multiply for a single value of k. If only one minor, Δ_ν is annihilated by the flutter velocity V_ν and if this minor is doubly-degenerate (or possibly multiply-degenerate in the case of p-order minors) then there exist at most two (or possibly more in the p-order case) linearly independent solution vectors $\{q_\alpha, q_u\}$. To each of the linearly independent *blade* modes there corresponds a unique (within a multiplicative constant) *system* mode of precisely the same form as Eq. (22). Hence, in this case, the final system flutter mode is expressible at worst as a linear combination of solutions of the form (22) with different blade modes but equal frequencies and phase shift between blades. If V_ν, k_ν cause the simultaneous vanishing of more than one minor Δ_ν, then to each vanishing minor there corresponds one or more solutions of the form (22). The final system flutter mode will then once again be expressible as a linear combination of solutions of the form (22) with equal frequency

but with the possibility of not only different blade modes but also different phase shift between blades for each of the component vectors.

Of special interest is the symmetrical blade and flow configuration (zero stagger, zero incidence, and symmetrical elastic and dynamic influence) in which at least double-degeneracy will always occur. For in this case,

$$\left.\begin{aligned} a_2 &= a_n,\ a_3 = a_{n-1},\ a_4 = a_{n-2}, && \text{etc.} \\ b_2 &= b_n,\ b_3 = b_{n-1},\ b_4 = b_{n-2}, && \text{etc.} \\ c_2 &= c_n,\ c_3 = c_{n-1},\ c_4 = c_{n-2}, && \text{etc.} \\ d_2 &= d_n,\ d_3 = d_{n-1},\ d_4 = d_{n-2}, && \text{etc.} \end{aligned}\right\} \tag{25}$$

Hence, to any minor Δ_ν a corresponding minor $\Delta_{n-\nu}$ will vanish with the insertion of the velocity V_ν. This is easily seen by introducing Eq. (25) into the defining relations (5) for A_ν, B_ν, C_ν, and D_ν. Under symmetry,

$$\left.\begin{aligned} A_\nu &= \{a_1 + 2a_2 \cos\sigma_\nu + 2a_3 \cos 2\sigma_\nu + \cdots \\ &\quad 2a_{(n+1)/2} \cos[(n-1)/2]\sigma_\nu\} \quad \text{for } n \text{ odd} \\ B_\nu &= \{b_1 + 2b_2 \cos\sigma_\nu + 2b_3 \cos 2\sigma_\nu + \cdots \\ &\quad + 2b_{(n+1)/2} \cos[(n-1)/2]\sigma_\nu\} \quad \text{for } n \text{ odd} \\ &\text{etc.} \end{aligned}\right\} \tag{26}$$

and

$$A_\nu = \{a_1 + 2a_2 \cos\sigma_\nu + \cdots 2a_{n/2} \cos[(n-2)/2]\sigma_\nu + a_{(n+2)/2}\, e^{i n\sigma_\nu/2}\} \quad \text{for } n \text{ even}$$

etc.

and obviously, if V_ν causes Δ_ν to vanish it will also cause $\Delta_{n-\nu}$ to vanish, since

$$\left.\begin{aligned} &\cos 2\pi(m/n)(n-\nu) = \cos 2\pi(m/n)\nu \\ &\text{and} \\ &e^{\pi i(n-\nu)} = e^{\pi i\nu} \qquad \text{for } n \text{ even} \end{aligned}\right\} \tag{27}$$

for all integers m. Hence, if only the two minors Δ_ν and $\Delta_{n-\nu}$ vanish (simply) upon insertion of V_ν, k_ν, then the solution (flutter mode) will be expressible as a linear combination of two modes of the form (22) with identical blade modes and with equal but opposite phase shift between blades. This satisfies our intuitive feeling about the symmetric case, since, with symmetry of flow and configuration, there should be no "preferred direction"—i.e., there is no more reason why the jth blade should *lead* the $(j-1)$th blade by angle σ_ν than *lag* the $(j-1)$th blade by this angle.

It should be noted that there is a possibility of the occurrence of another type of degeneracy which we shall call "quasi-multiple-degeneracy." This situation occurs whenever $|A|$ vanishes with two or more different values of k, each being associated with the same value of V, and when this V is the minimum of all annihilating V's. Physically, this implies that as the critical velocity V is approached, flutter may occur in either of two different modes, each having a different frequency, or in some undetermined linear combination of these two modes. Since the possibility of occurrence of this quasi-multiple-degeneracy is rather remote, we shall not dwell further upon the matter, except to note that there is also the possibility of both multiple- and quasi-multiple-degeneracy occurring simultaneously, with still greater complications.

Finally, the entire preceding discussion with regard to flutter mode is easily generalized to the case in which p degrees of freedom are allowed to each blade. Here the equation corresponding to (19) will possess a nontrivial p-order blade mode, and the process which led up to the system mode (22) is duplicated for the higher order system. Hence again in the simply degenerate case, a single blade mode of p components characterizes all blades, and all blades experience this mode with equal magnitude, equal frequency, and with a common phase-shift angle σ between adjacent blades. Multiply-degenerate cases lead to flutter modes which are expressible as linear combinations of solutions of this type. It is to be emphasized that multiple degeneracy is of no consequence in the determination of the flutter velocity V_ν. Once the minimum $V_\nu = V(\sigma_\nu)$ is found, this is the critical flutter velocity, and the possibility that this V may cause $|A|$ to vanish multiply does not alter this fact.

(4) *Significance of the Flutter Mode*

Having completed the analysis of the multi-bladed system in very general terms, we may now give an interpretation to the results which simplifies tremendously the linear flutter analysis of any blade row. Examination of Eq. (19) or the extension of Eq. (19) to the p-order case, shows that this corresponds actually to a situation in which we solve for the flutter of only one blade when this blade is under a very special form of influence from all other blades; namely, all other blades oscillate with the same *blade* mode, the same magnitude of occurrence of this blade mode, and with a phase shift of (as yet undetermined) angle σ between adjacent blades. Since under multiple-degeneracy the flutter mode is still composed of a linear combination of modes of this type, the present considerations cover the multiply-degenerate case as well.

Keeping the foregoing remarks well in mind, the solution of the flutter problem for a cyclic arrangement of many blades may be performed as follows. Allow only enough degrees, p, of freedom to describe satisfactorily the motion of a *single blade* in flutter. Derive for one blade the air forces experienced by this blade when it oscillates in bending and twisting and all other blades oscillate in the same blade mode with equal magnitude and with a phase shift of some undetermined angle σ between adjacent blades. Do the same for the kinetic and potential energy matrices. It is to be emphasized that *no restriction* is involved in this assumption and that all interblade interference is correctly accounted for. Then solve the flutter problem for this single "equivalent blade" leaving the phase angle σ undetermined. Finally, minimize the flutter velocity with respect to σ to obtain the critical flutter velocity and replace σ by the closest admissable value σ_ν. If one value of σ_ν minimizes V, and if the p order determinant vanishes simply upon insertion of the critical V_ν and σ_ν then the system flutter mode may be written directly

as given by Eq. (22). If the p-order determinant vanishes multiply or if several distinct values of σ_ν give the same minimum value of V for the same k, then, while the system flutter mode cannot be written down expressly, still it is known to be expressible as a linear combination of a finite number of easily determined linearly independent vectors of the form (22). The occurrence of quasi-multiple-degeneracy does not affect the critical velocity V, but does again complicate the flutter mode prediction.

Finally, it should be remarked that a phase shift per blade of angle σ_ν, where $(e^{i\sigma\nu})$ is one of the nth roots of unity, is consistent with the physical nature of an n-bladed system, for it is easily seen that any blade is "in phase with itself" as it certainly must be in actuality. This suggests a further simplification in the problem of obtaining the interference air forces for a blade row with a large number of blades. We merely assume that any blade has an "interference effect on itself" as though it were located n blades away from itself, and this allows us to express the entire interference for all blades in the form of a complex infinite Fourier series in the undetermined angle σ, with coefficients depending upon the blade number multiplied by the gap. In effect we replace the finite number of blades n by an infinite number, and hope that the resulting Fourier series will be recognizable in closed form. In the case of a cascade with or without stagger and with zero or very small flow deflection in incompressible flow, it is indeed the case that the Fourier series may be replaced by a comparatively simple single function of σ, valid for $0 < \sigma < 2\pi$. This will be described in detail in a subsequent report.

(5) *Extension to the Case Where the Rotor May Oscillate in the Rotary Direction*

We now extend our considerations of blade system flutter modes to the situation in which the blade row is mounted upon a rotor of finite moment of inertia. We assume that the rotor is rigidly constrained to remain in its plane of rotation (no axial deflection) but that it is capable of rotary deflection and that, through the effect of the rotor shaft and of other components mounted on this shaft, we can attribute to the rotor a certain spring constant and a damping constant which govern respectively the resistance to angular deflection and rate of deflection. This makes it necessary to introduce an additional degree of freedom q^Ω corresponding to the rotor deflection angle. Let

$$q^\Omega = \bar{q}^\Omega e^{i\omega t}$$

and then drop the bar (−) in further considerations as we have done tacitly in Eq. (1). $q^\Omega e^{i\omega t}$ is the instantaneous angle through which the rotor is deflected away from its equilibrium rotating position Ωt and is considered positive in the same sense as Ω.

Once again we restrict our detailed considerations to the case where two degrees of freedom are allowed to each blade, and again the extension to more degrees is trivial. Again, let $q_\alpha{}^j$, $q_u{}^j$ denote the generalized coordinates (with harmonic time dependence, $e^{i\omega t}$, removed) corresponding to the torsional and flexural degrees of freedom in the jth blade. Now we arrange the complete flutter mode vector (call it $\tilde{q}$) in the form

$$\tilde{q} = \begin{bmatrix} q^\Omega \\ q_\alpha{}^1 \\ q_u{}^1 \\ q_\alpha{}^2 \\ q_u{}^2 \\ \cdot \\ \cdot \\ \cdot \\ q_\alpha{}^n \\ q_u{}^n \end{bmatrix} \tag{28}$$

where, once again, harmonic time dependence has been removed and the q's are simply complex amplitudes. The complete, final system of flutter equations will then be expressible in the simple form

$$\tilde{A}\tilde{q} = 0 \tag{29}$$

wherein $\tilde{A}$ has the following form:

$$\tilde{A} = \begin{bmatrix} \gamma & \delta & \eta & \delta & \eta & \cdots & \delta & \eta \\ \alpha & a_1 & b_1 & a_2 & b_2 & \cdots & a_n & b_n \\ \beta & c_1 & d_1 & c_2 & d_2 & \cdots & c_n & d_n \\ \alpha & a_n & b_n & a_1 & b_1 & \cdots & a_{n-1} & b_{n-1} \\ \beta & c_n & d_n & c_1 & d_1 & \cdots & c_{n-1} & d_{n-1} \\ \alpha & a_{n-1} & b_{n-1} & a_n & b_n & \cdots & a_{n-2} & b_{n-2} \\ \beta & c_{n-1} & d_{n-1} & c_n & d_n & \cdots & c_{n-2} & d_{n-2} \\ & & \cdot & & & & & \\ & & \cdot & & & & & \\ \alpha & a_2 & b_2 & \cdots & \cdots & \cdots & a_1 & b_1 \\ \beta & c_2 & d_2 & \cdots & \cdots & \cdots & c_1 & d_1 \end{bmatrix} \tag{30}$$

The justification for writing $\tilde{A}$ in the form (30) follows immediately from the physical arrangement of the blades upon a rotor. The form of the submatrix obtained by deleting the first row and first column is a direct consequence of the fact that the blades are arranged cyclically about the rotor and the nth blade affects the first blade in precisely the same manner as the first blade affects the second, and so on. It is to be noted that $\tilde{A}$ allows for all types of coupling, aerodynamic, elastic, and dynamic, between the blades and for the influence of the blades upon the rotor and of the rotor upon the blades. The first element γ in the principal diagonal of $\tilde{A}$ includes the rotor inertia, the effective rotor spring constant and the effective rotor damping constant. The alternating form (δ, η, δ, η, ...) of the remainder of the first row follows from the fact that the bending mode in all blades affects the rotor equally, and the torsion mode in all blades affects the rotor equally. Likewise, the first column $\{\alpha, \beta, \alpha, \beta \ldots\}$ reflects the fact that the rotor deflection affects all blade bending modes identically and affects all blade torsion modes identically. Note that no assumptions are implied in the form of $\tilde{A}$ other than the restriction to identical blades, identically supported and equally spaced.

We now proceed in a manner similar, but not identical, to that pursued in the case where the rotor inertia was assumed infinite. Letting ω_ν denote the νth of the n nth roots of unity,

$$\omega_\nu = e^{2\pi i(\nu/n)} \tag{31}$$

and defining A_ν, B_ν, C_ν, D_ν as before—i.e.,

$$\left.\begin{aligned} A_\nu &= (a_1 + a_2\omega_\nu + a_n\omega_\nu^{-1} + a_3\omega_\nu^{2} + a_{n-1}\omega_\nu^{-2} + \dots) \\ B_\nu &= (b_1 + b_2\omega_\nu + b_n\omega_\nu^{-1} + b_3\omega_\nu^{2} + b_{n-1}\omega_\nu^{-2} + \dots) \\ &\text{etc.} \\ \nu &= 0,1,2, \dots (n-1) \end{aligned}\right\} \tag{32}$$

we leave the value of the determinant $|\bar{A}|$ of matrix $\bar{A}$ unchanged by forming new second and third rows as follows (ρ_j denotes an original row and ρ_j', the altered row):

$$\left.\begin{aligned} \rho_2' &= \rho_2 + \rho_4\omega_\nu^{-1} + \rho_6\omega_\nu^{-2} + \rho_8\omega_\nu^{-3} + \dots + \rho_{2n}\omega_\nu \\ \rho_3' &= \rho_3 + \rho_5\omega_\nu^{-1} + \rho_7\omega_\nu^{-2} + \rho_9\omega_\nu^{-3} + \dots + \rho_{2n+1}\omega_\nu \\ \nu &= 1,2,3, \dots (n-1) \end{aligned}\right\} \tag{33}$$

(The value of $|\bar{A}|$ is unchanged by substituting the new rows ρ_2' and ρ_3' for the original rows ρ_2 and ρ_3, since we have merely added to the original rows, linear combinations of succeeding rows). Now making use of the fact that $\omega_\nu^{\,n} = 1$ for all ν and

$$\sum_{p=0}^{n-1} \omega_\nu^{\,p} = \sum_{p=1}^{n} \omega_\nu^{\,p} = \frac{\omega_\nu - \omega_\nu^{\,n+1}}{1 - \omega_\nu} = 0 \qquad \begin{matrix} \text{for } \nu \neq 0 \\ \text{for } \nu \neq n \end{matrix} \tag{34}$$

we may write the determinant $|\bar{A}|$ of matrix $\bar{A}$ in the form

$$\begin{vmatrix}
\gamma & \delta & \eta & \delta & \eta & \delta & \eta & \dots & \delta & \eta \\
0 & A_\nu & B_\nu & \dfrac{A_\nu}{\omega_\nu} & \dfrac{B_\nu}{\omega_\nu} & \dfrac{A_\nu}{\omega_\nu^{\,2}} & \dfrac{B_\nu}{\omega_\nu^{\,2}} & \dots & \dfrac{A_\nu}{\omega_\nu^{\,n-1}} & \dfrac{B_\nu}{\omega_\nu^{\,n-1}} \\
0 & C_\nu & D_\nu & \dfrac{C_\nu}{\omega_\nu} & \dfrac{D_\nu}{\omega_\nu} & \dfrac{C_\nu}{\omega_\nu^{\,2}} & \dfrac{D_\nu}{\omega_\nu^{\,2}} & \dots & \dfrac{C_\nu}{\omega_\nu^{\,n-1}} & \dfrac{D_\nu}{\omega_\nu^{\,n-1}} \\
\alpha & a_n & b_n & a_1 & b_1 & a_2 & b_2 & \dots & a_{n-1} & b_{n-1} \\
\beta & c_n & d_n & c_1 & d_1 & c_2 & d_2 & \dots & c_{n-1} & d_{n-1} \\
\alpha & a_{n-1} & b_{n-1} & . & . & . & . & \dots & . & . \\
\beta & c_{n-1} & d_{n-1} & . & . & . & . & \dots & . & . \\
. & & & & & & & & & \\
. & \multicolumn{9}{l}{\text{[Remaining rows unchanged from original}} \\
. & \multicolumn{9}{l}{\quad \text{form (30)]}}
\end{vmatrix} \tag{35}$$

valid for $\nu = 1,2, \dots (n-1)$

The zero elements in the first column of each of the second and third rows follow directly from relation (34) and from the manner (33) in which the new second and third rows were formed. Note that Eq. (35) is not valid for $\nu = 0$ or $\nu = n$ since Eq. (34) does not hold in these cases. Now we consider the Laplace expansion of $|\bar{A}|$ by its second and third rows, using the form (35) for $|\bar{A}|$. We see immediately that all minors of the form

$$\begin{vmatrix} \dfrac{A_\nu}{\omega_\rho^{\,p}} & \dfrac{A_\nu}{\omega_\nu^{\,s}} \\ \dfrac{C_\nu}{\omega_\nu^{\,p}} & \dfrac{C_\nu}{\omega_\nu^{\,s}} \end{vmatrix} \quad \text{and} \quad \begin{vmatrix} \dfrac{B_\nu}{\omega_\nu^{\,p}} & \dfrac{B_\nu}{\omega_\nu^{\,s}} \\ \dfrac{D_\nu}{\omega_\nu^{\,p}} & \dfrac{D_\nu}{\omega_\nu^{\,s}} \end{vmatrix}$$

vanish due to the fact that they are expressible in terms of determinants with identical columns. The only *non*zero minors which may be formed from the second and third rows of Eq. (35) contain

$$\begin{vmatrix} A_\nu & B_\nu \\ C_\nu & D_\nu \end{vmatrix}$$

as a common factor, for any fixed value of ν. Since this is true for $\nu = 1,2,3, \dots (n-1)$ we see that $|\bar{A}|$ contains the $(n-1)$ factors

$$\Delta_\nu = \begin{vmatrix} A_\nu & B_\nu \\ C_\nu & D_\nu \end{vmatrix} \qquad \nu = 1,2.3 \dots (n-1) \tag{36}$$

Now we perform operation (33), only with $\nu = 0$—i.e., we form new second and third rows as follows (recalling that $\omega_0 = \omega_n = 1$):

$$\left.\begin{aligned} \rho_2' &= \rho_2 + \rho_4 + \rho_6 + \dots + \rho_{2n} \\ \rho_3' &= \rho_3 + \rho_5 + \rho_7 + \dots + \rho_{2n+1} \end{aligned}\right\} \tag{37}$$

The resulting expression for $|\bar{A}|$ [which again is unchanged by the process (37)] is

$$|\bar{A}| = \begin{vmatrix}
\gamma & \delta & \eta & \delta & \eta & \delta & \eta & \dots & \delta & \eta \\
n\alpha & A_0 & B_0 & A_0 & B_0 & A_0 & B_0 & \dots & A_0 & B_0 \\
n\beta & C_0 & D_0 & C_0 & D_0 & C_0 & D_0 & \dots & C_0 & D_0 \\
\alpha & a_n & b_n & a_1 & b_1 & a_2 & b_2 & \dots & a_{n-1} & b_{n-1} \\
\beta & c_n & d_n & c_1 & d_1 & c_2 & d_2 & \dots & c_{n-1} & d_{n-1} \\
\alpha & . & . & . & & & & & & \\
\beta & \multicolumn{9}{l}{\text{remaining rows unaltered from original form}} \\
 & \multicolumn{9}{l}{\quad (30)}
\end{vmatrix} \tag{38}$$

where $A_0 = a_1 + a_2 + a_3 + \ldots + a_n$

$$B_0 = \sum_{r=1}^{n} b_r,\ C_0 = \sum_{r=1}^{n} c_r,\ D_0 = \sum_{r=1}^{n} d_r \quad (39)$$

This time we expand $|\tilde{A}|$, in the form (38), by its first *three* rows. Noting that any third order minors formed from the first three rows vanish if they have two identical columns, we see that the only nonzero minors of order three contain

$$\tilde{\Delta}_0 = \begin{vmatrix} \gamma & \delta & \eta \\ n\alpha & A_0 & B_0 \\ n\beta & C_0 & D_0 \end{vmatrix} \quad (40)$$

as a factor.

Thus we have shown that $|\tilde{A}|$ is expressible in the factored form

$$|\tilde{A}| = K\tilde{\Delta}_0 \left\{ \prod_{\nu=1}^{n-1} \Delta_\nu \right\} \quad (41)$$

where K may contain any of the elements (a_i, b_i, c_i, d_i, γ, α, β, δ, η) of $|\tilde{A}|$ until we prove otherwise—i.e., all we have shown thus far is that each of the factors in the product (41) is indeed a factor of $|\tilde{A}|$. But every term in Eq. (41) is of (total combined) order $(2n + 1)$ in the elements (a_i, b_i, c_i, d_i, γ, δ, α, β, η) of $\tilde{A}$ and, likewise each term in the complete expansion of $|\tilde{A}|$ is of order $(2n + 1)$ in these elements. Thus K must be a constant, independent of these elements. Now we note that the leading diagonal of $|\tilde{A}|$ contributes the term

$$\gamma(a_1)^n(d_1)^n$$

to the expansion of $|\tilde{A}|$, and the coefficient of $\gamma(a_1)^n(d_1)^n$ in Eq. (41) is simply K. Thus

$$K = 1$$

and we have finally

$$|\tilde{A}| = \tilde{\Delta}_0 \left\{ \prod_{\nu=1}^{n-1} \Delta_\nu \right\}$$

or

$$|\tilde{A}| = n \begin{vmatrix} \gamma/n & \delta & \eta \\ \alpha & A_0 & B_0 \\ \beta & C_0 & D_0 \end{vmatrix} \prod_{\nu=1}^{n-1} \begin{vmatrix} A_\nu & B_\nu \\ C_\nu & D_\nu \end{vmatrix} \quad (42)$$

From the factored form (42) of $|\tilde{A}|$ we may draw a host of conclusions concerning the solution of the flutter problem for a blade row mounted on a rotor of finite mass. First we note that as the rotor inertia becomes infinitely large, $|\gamma| \to \infty$, and we have simply

$$|\tilde{A}|_{|\gamma| \to \infty} = \gamma \prod_{\nu=0}^{n-1} \begin{vmatrix} A_\nu & B_\nu \\ C_\nu & D_\nu \end{vmatrix} \quad (43)$$

Hence as $|\gamma| \to \infty$ the problem reduces to the form treated earlier.

Next we see that the product (42) contains "rotor-terms" only in the first factor, all other factors depending only upon the blades. Moreover, these latter factors are identical to those of the infinite-inertia-rotor case. In the determination of critical flutter velocity and frequency we proceed exactly as for the infinite-inertia-rotor case with the reservation that the root angle, σ_ν for $\nu = 0$ becomes exceptional. We may elaborate somewhat on this point. In order for flutter (a nontrivial solution vector $\tilde{q}$) to occur, the determinant $|\tilde{A}|$ must be annihilated by some combination of velocity V and flutter frequency ω (or, alternatively, V and k). This is completely equivalent to the annihilation of one or more of the factors

$$\tilde{\Delta}_0,\ \Delta_1,\ \Delta_2,\ -\ -\ \Delta_{n-1}$$

Thus we determine, for each factor $\tilde{\Delta}_0\Delta_1\Delta_2 \ldots$, the V and k which annihilate this factor (picking the combination with minimum V in case more than one pair, V, k, annihilates any factor) and remark that the flutter condition is given by the pair, V, k, with minimum V. Obviously, if the pair with minimum V corresponds to one of the minors Δ_ν [$\nu = 1,2,3, \ldots (n-1)$] and if the pair k, V which annihilates

$$\Delta_0 = \begin{vmatrix} A_0 & B_0 \\ C_0 & D_0 \end{vmatrix}$$

exhibits larger velocity V than this minimum V_ν, then the flutter frequency and critical velocity for the finite-inertia-rotor are identical to the frequency and velocity for the flutter condition of the infinite-inertia-rotor. Stated differently, if for a given rotor and blade system we solve for the flutter velocity and frequency in two ways, once assuming infinite rotor inertia and once taking proper account of rotor inertia, spring constant, damping and rotor-blade coupling, then we will find exactly the same critical flutter conditions (frequency and velocity) for the two cases, *provided* that Δ_0 is *not* the factor with minimum annihilating velocity in the infinite inertia case *and* $\tilde{\Delta}_0$ is *not* the factor with minimum annihilating velocity in the finite inertia case. If Δ_0 were the factor (under the infinite-inertia-rotor assumption) with minimum annihilating velocity and/or $\tilde{\Delta}_0$ the factor with minimum annihilating velocity in the more exact case of finite rotor inertia, then obviously we can no longer state that the critical flutter velocities and frequencies would be equivalent in the two cases.

Now for the systems with large numbers of blades (and finite rotor inertia) we may proceed in a manner similar (but not identical) to that followed in the infinite-inertia-rotor treatment. Recognizing that the nth roots of unity become dense about the unit circle as n becomes large, once again we annihilate the general minor

$$\Delta_\sigma = \begin{vmatrix} A_\sigma & B_\sigma \\ C_\sigma & D_\sigma \end{vmatrix}$$

where

$$A_\sigma = (a_1 + a_2e^{i\sigma} + a_ne^{-i\sigma} + a_3e^{2i\sigma} + a_{n-1}e^{-2i\sigma} + \ldots)$$

$$B_\sigma = (b_1 + b_2e^{i\sigma} + b_ne^{-i\sigma} + b_3e^{2i\sigma} + b_{n-1}e^{-2i\sigma} + \ldots)$$

etc.

(Again, recalling the smoothness of $V(\sigma)$, $k(\sigma)$, we

need annihilate Δ_σ at only a relatively small number of values of σ.) The annihilating values of $V(\sigma)$ and $k(\sigma)$ are plotted against σ in the range $0 < \sigma < 2\pi$ and the minimum of the discrete set of velocities $V(\sigma_\nu) = V_\nu$, is recorded. Note that we do *not* admit σ_0 (or σ_n) as a possible minimizing value of σ nor do we state at this point that the above-mentioned minimum is the *flutter velocity*. The reason for these statements is, of course, the presence of the factor $\tilde{\Delta}_0$ in the expansion of $|\tilde{A}|$ and the fact that $\tilde{\Delta}_0$ does not fall into the category of Δ_σ as $\sigma \to 0$. Thus, to complete the determination of flutter velocity we find the velocity, V, and reduced frequency k, which annihilate $\tilde{\Delta}_0$ (picking the pair V, k with minimum V if more than one annihilating pair exists) and compare with the minimum V_ν. If the velocity which annihilates $\tilde{\Delta}_0$ *exceeds* the minimum V_ν then V_ν is indeed the critical flutter velocity, and the flutter frequency follows from the reduced frequency k corresponding to the minimizing σ_ν. If the velocity $\bar{V}_0$ which annihilates $\tilde{\Delta}_0$ is less than the minimum of the velocities V_ν then $\bar{V}_0$ is the flutter velocity and the corresponding $k = \bar{k}_0$ gives the flutter frequency.

Up to this point we have said nothing about flutter modes $\bar{q}$ which correspond to the flutter conditions noted above. We proceed now to show that these modes bear a striking resemblance to the modes obtained under the restriction of infinite rotor inertia. Suppose first that the vanishing of one of the $\Delta_\nu[\nu = 1,2, \ldots (n-1)]$ leads to the critical flutter condition and suppose that this Δ_ν vanishes simply upon insertion of the critical k, $V\ (= k_\nu, V_\nu)$ and that no other factor of $|\tilde{A}|$ vanishes with these k, V. Then, with the critical V_ν, k_ν inserted

$$\begin{vmatrix} A_\nu & B_\nu \\ C_\nu & D_\nu \end{vmatrix} = 0$$

and there exists a nontrivial vector $\{q_\alpha, q_u\}$ such that

$$\begin{bmatrix} A_\nu & B_\nu \\ C_\nu & D_\nu \end{bmatrix} \begin{bmatrix} q_\alpha \\ q_u \end{bmatrix} = 0 \tag{44}$$

Expanding Eq. (44), we may write,

$$\left.\begin{aligned} &(a_1 + a_2\omega_\nu + a_3\omega_\nu^2 + \ldots + a_n\omega_\nu^{n-1})q_\alpha + \\ &\quad (b_1 + b_2\omega_\nu + b_3\omega_\nu^2 + \ldots\ldots + b_n\omega_\nu^{n-1})q_u = 0 \\ &(c_1 + c_2\omega_\nu + c_3\omega_\nu^2 + \ldots + c_n\omega_\nu^{n-1})q_\alpha + \\ &\quad (d_1 + d_2\omega_\nu + d_3\omega_\nu^2 + \ldots\ldots + d_n\omega_\nu^{n-1})q_u = 0 \end{aligned}\right\} \tag{45}$$

Now we see from Eq. (45) that the vector

$$\bar{q} = \begin{bmatrix} 0 \\ q_\alpha \\ q_u \\ \omega_\nu q_\alpha \\ \omega_\nu q_u \\ \omega_\nu^2 q_\alpha \\ \omega_\nu^2 q_u \\ \cdot \\ \cdot \\ \cdot \\ \omega_\nu^{n-1} q_\alpha \\ \omega_\nu^{n-1} q_u \end{bmatrix} \tag{46}$$

satisfies the second and third equations of the original flutter equation system (29). Moreover, we see from Eq. (34) that $\bar{q}$, as given by Eq. (46), satisfies the first of Eqs. (29) as well—i.e.,

$$q_\alpha\delta \sum_{p=0}^{n-1} \omega_\nu^p + q_u\eta \sum_{p=0}^{n-1} \omega_\nu^p = 0 \tag{47}$$

Multiplying Eqs. (45) through by ω_ν and recalling that

$$(\omega_\nu)^n = 1$$

we see that

$$\left.\begin{aligned} &(a_n + a_1\omega_\nu + a_2\omega_\nu^2 + a_3\omega_\nu^3 + \ldots)q_\alpha + \\ &\quad (b_n + b_1\omega_\nu + b_2\omega_\nu^2 + b_3\omega_\nu^3 + \ldots)q_u = 0 \\ &(c_n + c_1\omega_\nu + c_2\omega_\nu^2 + c_3\omega_\nu^3 + \ldots)q_\alpha + \\ &\quad (d_n + d_1\omega_\nu + d_2\omega_\nu^2 + d_3\omega_\nu^3 + \ldots)q_u = 0 \end{aligned}\right\} \tag{48}$$

Hence Eq. (46) is a solution of the fourth and fifth of Eqs. (29). Continuing the process—(i.e., multiplying (45) by successively higher powers of ω_ν)—we see that Eq. (46) is indeed a solution of the entire system of flutter Eqs. (29) under the condition that $\Delta_\nu(\nu \neq 0)$ is annihilated by the critical flutter velocity and frequency.

Moreover, since we have stipulated simple degeneracy, Eq. (46) is unique within a multiplicative constant.

Now the solution (46) is of the same form as that obtained under the assumption of infinite rotor inertia with the exception of the additional rotor deflection component which is zero. That is, if the critical flutter condition for the system with rotor of finite inertia corresponds to the vanishing of one of the minors $\Delta_\nu(\nu \neq 0)$ then the flutter mode is one in which all blades oscillate with *identical blade mode* $\{q_\alpha, q_u\}$ at *equal magnitudes* and with a (nonzero) constant phase lag angle $\sigma_\nu(= 2\pi\nu/n)$ between successive blades. Moreover, the rotor does not oscillate but remains unaffected. We can give extra evidence in support of this conclusion, based on Eq. (34). The rotor may be influenced by the blades through some linear combination of blade torsional and flexural displacements, velocities, and accelerations, and hence through some linear combinations of q_α, q_u to which velocity and acceleration may be reduced under harmonic motion. Now, since all blades affect the rotor in the same way and since the blades display a constant nonzero phase lag for the condition where the rotor deflection vanishes, we see that the net torque exerted upon the rotor by the blades at any instant must vanish—i.e.,

$$\left.\begin{aligned} \text{Torque} &= e^{i\omega t} \sum_{1}^{n} (T_\alpha q_\alpha{}^j + T_u q_u{}^j) \\ &= T_\alpha q_\alpha e^{i\omega t} \sum_{j=0}^{n-1} (\omega_\nu)^j + T_u q_u e^{i\omega t} \sum_{j=0}^{n-1} (\omega_\nu)^j \\ &= 0 \qquad \text{for } \nu \neq 0,\ \nu \neq n \end{aligned}\right\} \tag{49}$$

This adds support to our somewhat surprising discovery that $q^\Omega = 0$ in the case where critical flutter corresponds to the vanishing of some Δ_ν with $\nu \neq 0$. Now if the critical V and k cause the simultaneous annihila-

tion of two or more $\Delta_\nu(\nu \neq 0)$ or cause one $\Delta_\nu(\nu \neq 0)$ to vanish multiply, then we know the flutter mode must be expressible as a linear combination of vectors of the form (46) and hence the rotor still exhibits no deflection.

We next discuss the flutter mode for the condition where $\bar{\Delta}_0 = 0$ leads to the critical flutter velocity—i.e., where the V which annihilates $\bar{\Delta}_0$ is the minimum annihilating velocity. Now if the critical velocity and reduced frequency are inserted, then $\bar{\Delta}_0 = 0$ and there exists a nontrivial three-component vector $\{q^\Omega, q_\alpha, q_u\}$ such that

$$\begin{bmatrix} \gamma/n & \delta & \eta \\ \alpha & A_0 & B_0 \\ \beta & C_0 & D_0 \end{bmatrix} \begin{bmatrix} q^\Omega \\ q_\alpha \\ q_u \end{bmatrix} = 0 \tag{50}$$

Expanding Eq. (50) we see that the components q^Ω, q_α, q_u, which we have shown must exist, satisfy the relations

$$\left.\begin{aligned} &\gamma q^\Omega + n\delta q_\alpha + n\eta q_u = 0 \\ &\alpha q^\Omega + (a_1 + a_2 + a_3 + \ldots + a_n)q_\alpha + \\ &\qquad (b_1 + b_2 + b_3 + \ldots + b_n)q_u = 0 \\ &\beta q^\Omega + (c_1 + c_2 + c_3 + \ldots + c_n)q_\alpha + \\ &\qquad (d_1 + d_2 + d_3 + \ldots + d_n)q_u = 0 \end{aligned}\right\} \tag{51}$$

Hence the vector

$$\bar{q} = \begin{bmatrix} q^\Omega \\ q_\alpha \\ q_u \\ q_\alpha \\ q_u \\ \cdot \\ \cdot \\ \cdot \\ q_\alpha \\ q_u \end{bmatrix} \tag{52}$$

where $\{q^\Omega, q_\alpha, q_u\}$ is the solution of Eq. (50), satisfies all $(2n + 1)$ of the original flutter Eqs. (29) and, in case of simple degeneracy, is the unique solution of Eq. (29) to within an undetermined multiplicative constant. Now the solution vector (52) displays in general a *non*zero rotor oscillation q^Ω and a blade system mode with zero phase lag. That is, all blades oscillate with identical blade mode q_α, q_u at equal magnitude (with equal frequency) and all blades are exactly in phase. Moreover, the rotor is no longer unaffected by the blades, but undergoes an oscillation of amplitude $|q^\Omega|$ at the same frequency as that of the blade oscillation. The fact that a nonzero rotor oscillation accompanies the in-phase blade mode is consistent with other considerations, since with $\sigma = 0$, sums of the type (49) are no longer zero, but rather add up to n, the number of blades. Thus all blades exert equal torque upon the rotor with equal frequency and in phase with one another. Obviously under these conditions, the rotor will in general experience a nonzero oscillation. Thus we see that the only difference between the flutter problem for a system with rotor of finite inertia and that for a system with infinite-inertia rotor lies in the zero-phase mode. If the zero-phase mode is not critical in either case, then the results in the two cases are identical. If the zero-phase mode is critical in the infinite-inertia-rotor case then the zero-phase mode occurs with no rotor oscillation. It is difficult to generalize in advance, but if it should turn out, in practice, that the zero-phase mode is seldom or never critical in either the infinite-rotor-inertia or the finite-rotor-inertia case, then there would be little or no need to deal with the rotor at all—i.e., infinite inertia could be assumed at the start and no need would exist for the determination of the elements $(\gamma, \delta, \eta, \alpha, \beta)$. This, however, is merely conjecture and, it must be emphasized, is not to be assumed until definite evidence is available to the effect that $\bar{\Delta}_0 = 0$ and $\Delta_0 = 0$ are seldom or never the critical conditions.

The occurrence of multiple degeneracy will be mentioned only briefly since the considerations involved are similar to those for the infinite-rotor-inertia condition. Again we define true multiple degeneracy as the condition where one pair V, k causes several $(\bar{\Delta}_0, \Delta_\nu)$ to vanish or one of these minors to vanish multiply. Under these conditions the flutter mode will be expressible at worst as some (in general undeterminable) linear combination of modes of the form (46) or (52). If none of the vanishing minors is $\bar{\Delta}_0$, then the flutter mode will exhibit no rotor oscillation. Quasi-multiple degeneracy, the existence of two *equal*, minimum annihilating velocities V corresponding to two *different* reduced frequencies, leads to the possibility of flutter in either of two different frequencies at the single critical flutter velocity.

Now it is important to note that all steps performed up to this point may be generalized to the case where we allow p rather than two degrees of freedom per blade. Once again $|\bar{A}|$ is of circulant-type form with respect to its pth order minors except for the first row and first column which take the respective forms

$$(\gamma, \delta_1, \delta_2, \ldots \delta_p, \delta_1, \ldots \delta_p, \delta_1, \ldots \delta_p \ldots)$$
$$[\gamma, \alpha_1, \alpha_2, \ldots \alpha_p, \alpha_1, \ldots \alpha_p, \alpha_1, \ldots \alpha_p \ldots]$$

Again the replacement of rows 2,3 . . $(p + 1)$ by rows composed of the original row plus multiples of ω_ν times each pth following row leads to a form analogous to form (35) while leaving the value of $|\bar{A}|$ unaltered. Again we expand $|\bar{A}|$ by factors consisting of $(n - 1)$ pth order minors and one $(p + 1)$th order minor. The solution for the critical flutter conditions and modes follows in exactly the same way as for the case with $p = 2$, and the general conclusions with respect to the resulting flutter mode are unchanged.

In summarizing our findings for the case of a blade row mounted on a rotor of finite inertia we may state the following surprising conclusion. If the velocity V_0 which annihilates Δ_0 exceeds the smallest of the velocities V_ν which annihilate the $\Delta_\nu(\nu \neq 0)$ and if the velocity $\bar{V}_0$ which annihilates $\bar{\Delta}_0$ also exceeds the smallest V_ν, then (1) the assumption of infinite rotor inertia causes no error whatsoever, (2) flutter frequency and velocity are the *same* for the infinite-inertia and finite-

inertia rotor conditions, (3) the blade mode and the phase lag between adjacent blades are the same for the two conditions, and (4) the rotor undergoes no oscillatory deflection ($q^{(2)} = 0$). On the other hand, if *either* V_0 or $\bar{V}_0$ is less than the minimum V_ν, then the infinite-inertia assumption leads to an error. If V_0 is less than the minimum V_ν but $\bar{V}_0$ is *not* less than the minimum V_ν then the actual flutter mode (for finite rotor inertia) corresponds to the combination V_ν, k_ν (which was *not* critical in the infinite-rotor-inertia case) and flutter occurs with zero rotor oscillation, blade mode corresponding to Δ_ν, and phase lag σ_ν between blades. If $\bar{V}_0$ is less than the minimum V_ν then flutter (for the finite-rotor-inertia system) occurs with a nonzero rotor deflection ($q^{(2)} \neq 0$) and with a blade mode corresponding to the matrix for which $\bar{\Delta}_0$ is the determinant. Moreover flutter occurs with all blades in phase ($\sigma = 0$).

It is interesting to state one of our results in a slightly different way: if the system leads to a critical flutter mode with nonzero lag between blades under the assumption of infinite rotor inertia—i.e., $V_0 > V_\nu$ for some ν—then there exists a finite value of rotor inertia such that for any value of inertia larger than this finite value the assumption of infinite inertia is exact. We can show this as follows:

Let $V_0 > V_\nu$ where $\begin{cases} V_0 \text{ annihilates } \Delta_0 \\ V_\nu \text{ annihilates } \Delta_\nu \end{cases}$

i.e., V_ν is critical under the assumption of infinite rotor inertia. Now as $|\gamma|$ becomes large

$$\bar{\Delta}_0 \to \gamma \Delta_0$$

Hence $\bar{V}_0$ (the velocity which annihilates $\bar{\Delta}_0$) approaches V_0. Thus, there exists some finite value γ_0 such that for $|\gamma| > |\gamma_0|$, $\bar{V}_0 > V_\nu$ and V_ν is critical.

A final remark may be helpful in the actual process of plotting $V(\sigma)$ or $V^2(\sigma)$ for the case of finite rotor inertia. While $\Delta_0 = 0$ does not actually fall into the scheme of the finite-rotor-inertia case, still, the evaluation of the velocity and reduced frequency, V_0 and k_0, which annihilate A_0, provides useful end-points on the curves $V(\sigma)$ and $k(\sigma)$ for plotting purposes.

References

[1] Chang, Chieh-Chien, and Chu, Wen-Hwa, *Aerodynamic Characteristics of an Oscillating Cascade*, Air Research and Development Command, USAF, (AF 33(038) 12919), September 1, 1952.

[2] Lilley, G. M., *An Investigation of the Flexure-Torsion Flutter Characteristics of Airfoils in Cascade*, Report No. 60, The College of Aeronautics, Cranfield, May, 1952.

[3] Mendelson, A., *Effect of Centrifugal Force on Flutter of Uniform Cantilever Beams at Subsonic Speeds with Application to Compressor and Turbine Blades*, NACA TN 1893, June, 1949.

[4] Reissner, E., *Wind Tunnel Corrections for the Two-Dimensional Theory of Oscillating Airfoils*, Cornell Aeronautical Laboratory Report No. SB-318-S-3, April 22, 1947.

[5] Reissner, E., *Boundary Value Problems in Aerodynamics of Lifting Surfaces in Non-Uniform Motion*, Bulletin of the American Mathematical Society, Vol. 55, No. 9, pp. 825–850, September, 1949.

[6] Scanlan, R. H., and Rosenbaum, R., *Introduction to the Study of Aircraft Vibration and Flutter*, First Edition, p. 266, The MacMillan Company, New York, 1951.

[7] Sisto, F., *Flutter of Airfoils in Cascade*, Doctoral Dissertation, Massachusetts Institute of Technology, 1952.

[8] Theodorsen, T., *General Theory of Aerodynamic Instability and the Mechanism of Flutter*, NACA TR 496, 1934.

[9] Turner, M. J., and Duke, J. B., *Propeller Flutter*, Journal of the Aeronautical Sciences, Vol. 16, No. 6, pp. 323–336, June, 1949.

Interaction of a Shock Wave with a Thermal Boundary Layer

(*Continued from page 22*)

make it desirable to operate the test section at reduced pressure. Since an alternative approach to the problem appears quite promising no serious effort has been made to resolve these difficulties.

The principal mechanism by which the thermal layer disturbs a shock is a change in the local speed of sound. In a sense the change in density which accompanies heating at constant pressure is extraneous to the problem. Prof. Walker Bleakney has suggested that the change in sound speed be produced by allowing gases of different molecular weight to diffuse through one another. In fact, the differential equations for diffusion and heat conduction are the same. A zone of nonuniform gas concentration suitable for experiments analogous to those with a hot or cold plate could be generated by allowing one gas to diffuse slowly through the air above a porous surface for a short time before the shock wave arrives. A light gas corresponds to a hot region and a heavy gas to a cold one. Of the gases readily available hydrogen has the greatest sound velocity and sulfur hexaflouride the lowest. The corresponding extremes of surface temperature would then be 4400°K. and 54°K. An experimental model has been constructed and we hope to report on the results in a subsequent article.

References

[1] Lighthill, M. J., *Reflection at a Laminar Boundary Layer of a Weak Steady Disturbance to a Supersonic Stream, Neglecting Viscosity and Heat Conduction*, Quart. Jour. of Mech. and Appl. Math., Vol. 3, Part 3, p. 303, September, 1950.

[2] Adams, M. C., *On Shock Waves in Inhomogeneous Flow*, Journal of the Aeronautical Sciences, Vol. 16, No. 11, pp. 685–690, November, 1949.

[3] Ribner, H. S., and Moore, F. K., *Unsteady Interaction of Disturbances with a Shock Wave*, 1953 Heat Trans. and Fluid Mech. Inst., also, NACA TN 2864 and 2879.

[4] Chang, C. T., *On the Interaction Between Weak Fluctuating Fields of Sound, Vorticity, and Temperature with an Oscillating Shock*, The Johns Hopkins University, Department of Aeronautics, Preliminary Report, 1953.

[5] Hess, R. V., *The Interaction of a Shock Wave with a Thermal Boundary Layer*, Unpublished.

The Determination of Temperature, Stresses, and Deflections in Two-Dimensional Thermoelastic Problems*

BRUNO A. BOLEY†
Columbia University

SUMMARY

An analytical successive-approximation method for the solution of linear partial differential equations is presented first in general terms, and then applied to the solution of two-dimensional heat and thermal stress problems. The method is applicable when solutions are desired for bars or plates—i.e., for bodies with one dimension small compared to the others. The final expressions given by this procedure for example for the stress σ consist of a number of terms ($\sigma = \Sigma\sigma_i$), where the term σ_i is proportional to the quantity $[\beta^{(2i-1)}\partial^{(2i-1)}T/(\partial x)^{2i-1}]$; β is the ratio of height to length of the bar, and x measures the distance along the span. The first term of the series in that corresponding to the assumption that sections plane before heating remain plane after heating; the solution obtained thus shows that this term provides a good approximation for thermal loadings varying smoothly along the span, and for thin bars. Similar results are obtained for the temperature and the deflections. Explicit formulas for the calculation of stresses and deflections are given. The validity of the Bernoulli-Euler hypothesis of beam-theory is examined. Illustrative examples are presented for all the above developments. The use of the method in problems in which the material properties are functions of the temperature is outlined.

INTRODUCTION AND OUTLINE OF RESULTS

THE ADVENT of high-speed flight has increased the importance of thermal effects in aircraft design and has consequently accentuated the need for practical methods of calculation of temperature, stresses and deflections in many types of structures under a variety of conditions. A great deal of work in this area has been done, and it is useful for the purposes of the present paper to discuss briefly some of the investigations concerning thermal stresses in plates (see, for example, references 1, 2). These invesigations are based on the Bernoulli-Euler hypothesis that sections plane before heating remain plane after heating. Doubts as to the validity of this assumption have however arisen[3] and need clarification. The same type of uncertainty as to the soundness of the Bernoulli-Euler assumption existed in the case of loaded unheated beams, and was resolved by the work of von Kármán[4] and Seewald[5]; the present paper is, in part, an extension of these investigations into the field of thermoelasticity. It considers the effect of heating on beams, and deals specifically with rectangular bars according to the two-dimensional theory of elasticity. The results are of course also valid for plates, if the temperature distribution is independent of one of the coordinates in the plane of the plate, and have been shown in a recent investigation to admit of extension to beams of any cross section. Briefly speaking, one of the principal results obtained is a theory and formulas for the analysis of this type of structure, which establishes the basis for a thermoelastic strength of materials, and can be immediately applied in the same manner as ordinary beam theory in the practical solution of numerous problems. A general summary and description of these results is presented in the remainder of this Introduction; more detailed derivations and illustrations are found in later portions of this paper.

Consider a rectangular beam of height $2c$ and length $2L$, subjected to a temperature distribution $T(x,y)$, where the origin of the coordinates x and y is in the center of the beam (which thus occupies the space $-c \leq y \leq c$, $-L \leq x \leq L$). If the assumption is made that sections plane before heating remain plane after heating[6] the familiar formula for the spanwise normal stress is easily derived:

$$\sigma_x = -\alpha ET + (1/A)\,\alpha E \int T dA + (y/I)\,\alpha E \int Ty dA \tag{1}$$

where α is the coefficient of thermal expansion, E Young's modulus, the limits of integration must be chosen so as to cover the entire cross section, and for a rectangular section of width b the area and moment of inertia are

$$A = 2cb; \qquad I = 2c^3b/3 \tag{1a}$$

Eq. (1) is similar to the formula

$$\sigma_x = (P/A) + (My/I) \tag{2}$$

of strength of materials, which, though also derived on the above-mentioned Bernoulli-Euler assumption concerning plane sections, is known to yield very good results from a practical standpoint even in cases in which this assumption does not hold.[5,6] The reason for the wide range of applicability of this formula may be clarified by an inspection of the more general equation

$$\sigma_x = (P/A) + M(y/I) + (d^2M/dx^2)[(1/2)(y/c)^2 - (3/10)(y/c)] + (\text{terms containing only fourth and higher derivatives of } M) \tag{2a}$$

which has been derived by Seewald.[5] It is then clear

Received November 3, 1954. Revised and received June 8, 1955.

* This work is part of an investigation sponsored by the Wright Air Development Center, U.S. Air Force, under Contract AF 33(616)-2071.

† Associate Professor of Civil Engineering, Institute of Air Flight Structures.

TABLE 1
General Expressions for φ_i and the Corresponding Stresses; $i = 1, 2, 3$

$\int \equiv \int_{-c}^{y}$ $\quad \oint \equiv \int_{-c}^{c}$ $\quad \sigma_{y_i} = \frac{\partial^2 \varphi_i}{\partial x^2}$

i	1	2	3
$\frac{\varphi_i}{\alpha E}$	$-y\int T\,dy + \int Ty\,dy +$ $+\frac{c}{4}\left[1+2\left(\frac{y}{c}\right)+\left(\frac{y}{c}\right)^2\right]\oint T\,dy -$ $-\frac{1}{4}\left[2+3\left(\frac{y}{c}\right)-\left(\frac{y}{c}\right)^3\right]\oint Ty\,dy$	$\frac{\partial^2}{\partial x^2}\left\{\frac{y^2}{c}\int T\,dy - \frac{y^3}{2}\int T\,dy + \frac{y}{2}\int Ty^2\,dy - \frac{1}{6}\int Ty^3\,dy - \right.$ $-\frac{c^2}{24}\left[\left(\frac{y}{c}\right)^2+2\left(\frac{y}{c}\right)^3+\left(\frac{y}{c}\right)^4\right]\oint T\,dy +$ $+\frac{c^2}{40}\left[4\left(\frac{y}{c}\right)+10\left(\frac{y}{c}\right)^2+7\left(\frac{y}{c}\right)^3-\left(\frac{y}{c}\right)^5\right]\oint Ty\,dy -$ $-\frac{c}{8}\left[1+2\left(\frac{y}{c}\right)+\left(\frac{y}{c}\right)^2\right]\oint Ty^2\,dy +$ $\left.+\frac{1}{24}\left[2+3\left(\frac{y}{c}\right)-\left(\frac{y}{c}\right)^3\right]\oint Ty^3\,dy\right\}$	$\frac{\partial^4}{\partial x^4}\left\{\frac{y^5}{120}\int T\,dy - \frac{y^6}{24}\int Ty\,dy + \frac{y^3}{12}\int Ty^2\,dy - \frac{y^2}{12}\int Ty^3\,dy + \frac{y}{24}\int Ty^4\,dy - \frac{1}{120}\int Ty^5\,dy + \right.$ $+c^5\left[\frac{1}{180}-\frac{1}{40}\left(\frac{y}{c}\right)^2+\frac{1}{288}\left(\frac{y}{c}\right)^4-\frac{1}{240}\left(\frac{y}{c}\right)^5-\frac{1}{480}\left(\frac{y}{c}\right)^6\right]\oint T\,dy +$ $+c^4\left[-\frac{1}{1050}\left(\frac{y}{c}\right)+\frac{2}{175}\left(\frac{y}{c}\right)^3+\frac{1}{48}\left(\frac{y}{c}\right)^4+\frac{3}{800}\left(\frac{y}{c}\right)^5-\frac{1}{1120}\left(\frac{y}{c}\right)^7\right]\oint Ty\,dy +$ $+c^3\left[-\frac{1}{48}\left(\frac{y}{c}\right)^2-\frac{1}{24}\left(\frac{y}{c}\right)^3-\frac{1}{48}\left(\frac{y}{c}\right)^4\right]\oint Ty^2\,dy +$ $+c^2\left[\frac{1}{560}\left(\frac{y}{c}\right)+\frac{1}{24}\left(\frac{y}{c}\right)^2+\frac{7}{240}\left(\frac{y}{c}\right)^3-\frac{1}{240}\left(\frac{y}{c}\right)^5\right]\oint Ty^3\,dy -$ $\left.-\frac{c}{56}\left[1+2\left(\frac{y}{c}\right)+\left(\frac{y}{c}\right)^2\right]\oint Ty^4\,dy+\frac{1}{480}\left[2+3\left(\frac{y}{c}\right)-\left(\frac{y}{c}\right)^3\right]\oint Ty^5\,dy\right\}$
$-\frac{\sigma_{z_i}}{\alpha E} = \frac{1}{\alpha E}\frac{\partial^2 \varphi_i}{\partial x\,\partial y}$	$\frac{\partial}{\partial x}\left\{-\int T\,dy + \right.$ $+\frac{1}{2}\left[1+\left(\frac{y}{c}\right)\right]\oint T\,dy -$ $\left.-\frac{3}{4c}\left[1-\left(\frac{y}{c}\right)^2\right]\oint Ty\,dy\right\}$	$\frac{\partial^3}{\partial x^3}\left\{\frac{y^2}{2}\int T\,dy - y\int Ty\,dy + \frac{1}{2}\int Ty^2\,dy - \right.$ $-\frac{c^2}{12}\left[\left(\frac{y}{c}\right)+3\left(\frac{y}{c}\right)^2+2\left(\frac{y}{c}\right)^3\right]\oint T\,dy +$ $+\frac{c}{40}\left[4+20\left(\frac{y}{c}\right)+21\left(\frac{y}{c}\right)^2-5\left(\frac{y}{c}\right)^4\right]\oint Ty\,dy -$ $\left.-\frac{1}{6}\left[1+\left(\frac{y}{c}\right)\right]\oint Ty^2\,dy+\frac{1}{8}\left[1-\left(\frac{y}{c}\right)^2\right]\oint Ty^3\,dy\right\}$	$\frac{\partial^5}{\partial x^5}\left\{\frac{y^4}{24}\int T\,dy - \frac{y^3}{6}\int Ty\,dy + \frac{y^2}{4}\int Ty^2\,dy - \frac{y^3}{6}\int Ty^3\,dy + \frac{1}{24}\int Ty^4\,dy + \right.$ $+c^4\left[\frac{1}{49}\left(\frac{y}{c}\right)+\frac{1}{72}\left(\frac{y}{c}\right)^3-\frac{1}{48}\left(\frac{y}{c}\right)^4-\frac{1}{80}\left(\frac{y}{c}\right)^5\right]\oint T\,dy +$ $+c^3\left[-\frac{1}{1050}+\frac{5}{175}\left(\frac{y}{c}\right)^2+\frac{1}{12}\left(\frac{y}{c}\right)^3+\frac{3}{160}\left(\frac{y}{c}\right)^4-\frac{1}{160}\left(\frac{y}{c}\right)^6\right]\oint Ty\,dy +$ $+c^2\left[-\frac{1}{24}\left(\frac{y}{c}\right)-\frac{1}{8}\left(\frac{y}{c}\right)^2-\frac{1}{12}\left(\frac{y}{c}\right)^3\right]\oint Ty^2\,dy + c\left[\frac{1}{560}+\frac{1}{12}\left(\frac{y}{c}\right)+\frac{7}{80}\left(\frac{y}{c}\right)^2-\right.$ $\left.\left.-\frac{1}{48}\left(\frac{y}{c}\right)^3\right]\oint Ty^3\,dy-\frac{1}{48}\left[1+\left(\frac{y}{c}\right)\right]\oint Ty^4\,dy+\frac{1}{160c}\left[1-\left(\frac{y}{c}\right)^2\right]\oint Ty^5\,dy\right\}$
$\frac{\sigma_{x_i}}{\alpha E} = \frac{1}{\alpha E}\frac{\partial^2 \varphi_i}{\partial y^2}$	$-T+\frac{1}{2c}\oint T\,dy+\frac{3y}{2c^3}\oint Ty\,dy$	$\frac{\partial^2}{\partial x^2}\left\{y\int T\,dy - \int Ty\,dy - \frac{c}{12}\left[1+6\left(\frac{y}{c}\right)+\right.\right.$ $+6\left(\frac{y}{c}\right)^2\Big]\oint T\,dy+\frac{1}{20}\left[10+21\left(\frac{y}{c}\right)-10\left(\frac{y}{c}\right)^3\right]\oint Ty\,dy -$ $\left.-\frac{1}{4c}\oint Ty^2\,dy-\frac{y}{4c^3}\oint Ty^3\,dy\right\}$	$\frac{\partial^4}{\partial x^4}\left\{\frac{y^3}{6}\int T\,dy - \frac{y^2}{2}\int Ty\,dy + \frac{y}{2}\int Ty^2\,dy - \frac{1}{6}\int Ty^3\,dy - \right.$ $-c^3\left[\frac{1}{45}-\frac{1}{24}\left(\frac{y}{c}\right)^2+\frac{1}{12}\left(\frac{y}{c}\right)^3+\frac{1}{16}\left(\frac{y}{c}\right)^4\right]\oint T\,dy + c^3\left[\frac{13}{175}\left(\frac{y}{c}\right)+\frac{1}{4}\left(\frac{y}{c}\right)^2+\right.$ $+\frac{3}{40}\left(\frac{y}{c}\right)^3-\frac{3}{80}\left(\frac{y}{c}\right)^5\Big]\oint Ty\,dy - c\left[\frac{1}{24}+\frac{1}{4}\left(\frac{y}{c}\right)+\frac{1}{4}\left(\frac{y}{c}\right)^2\right]\oint Ty^2\,dy +$ $\left.+\left[\frac{1}{12}+\frac{7}{40}\left(\frac{y}{c}\right)-\frac{1}{12}\left(\frac{y}{c}\right)^3\right]\oint Ty^3\,dy-\frac{1}{48c}\oint Ty^4\,dy-\frac{1}{80c^2}\left(\frac{y}{c}\right)\oint Ty^5\,dy\right\}$

that Eq. (2) holds rigorously only if the bending moment is either independent of x, or varies linearly with that coordinate; if these conditions are not met, Eq. (2a) gives the axial stress either in closed form (if M is a polynomial in x) or in an infinite series in a general case. Most moment distributions encountered in practice, however, are "smooth" (except in the immediate vicinity of concentrated loads)—i.e., their higher spanwise derivatives of M are small, or in other words, M can be expanded in a rapidly convergent power series. Thus in very many practical cases use of the elementary Eq. (2) can be justified on theoretical grounds.

It is shown in this paper that similar statements can be made with regard to the thermal problem and Eq. (1). Consider in fact the expression for σ_x given in Table 1, which can be rewritten in the following nondimensional form:

TABLE 2
Expressions for φ_i and the Corresponding Stresses for Temperature Distributions Independent of y

i	1	2	3
$\frac{\varphi_i}{\alpha E}$	0	$-\frac{1}{24}\left(y^2-c^2\right)^2\frac{d^2T}{dx^2}$	$\frac{1}{360}\left(y^2-c^2\right)^2\left(y^2-3c^2\right)\frac{d^4T}{dx^4}$
$\frac{\sigma_{z_i}}{\alpha E} = -\frac{1}{\alpha E}\frac{\partial^2 \varphi_i}{\partial x\,\partial y}$	0	$\frac{y}{6}\left(y^2-c^2\right)\frac{d^3T}{dx^3}$	$-\frac{y}{180}\left(y^2-c^2\right)\left(7c^2-3y^2\right)\frac{d^5T}{dx^5}$
$\frac{\sigma_{x_i}}{\alpha E} = \frac{1}{\alpha E}\frac{\partial^2 \varphi_i}{\partial y^2}$	0	$-\frac{1}{6}\left(3y^2-c^2\right)\frac{d^2T}{dx^2}$	$\frac{1}{180}\left(15y^4-30y^2c^2+7c^4\right)\frac{d^4T}{dx^4}$
$\frac{\sigma_{x_i}}{\alpha E} = \frac{1}{\alpha E}\frac{\partial^2 \varphi_i}{\partial x^2}$	0	$-\frac{1}{24}\left(y^2-c^2\right)^2\frac{d^4T}{dx^4}$	$\frac{1}{360}\left(y^2-c^2\right)^2\left(y^2-3c^2\right)\frac{d^6T}{dx^6}$

$$\frac{\sigma_x}{\alpha E} = \left\{-T + \oint Td\eta + 12\eta \oint T\eta\,d\eta\right\} + \beta^2\frac{\partial^2}{\partial(x/L)^2}\left\{4\eta\int Td\eta - 4\int T\eta d\eta - (1/6)(1+12\eta+24\eta^2)\oint Td\eta + (2/5)(5+21\eta-40\eta^3)\oint T\eta d\eta - 2\oint T\eta^2 d\eta - 8\eta\oint T\eta^3 d\eta\right\} + \{\text{terms containing only fourth and higher derivatives of } T \text{ with respect to } x\} \quad (3)$$

where

$$\eta = y/(2c); \qquad \beta = (c/L) \quad (3a)$$

and the remainder of the notation is defined in Table 1. The first term of Eq. (3) is the same as the right-hand side of Eq. (1) put in nondimensional form; in the other terms the higher derivatives of T with respect to x appear in exactly the same manner as the derivatives of M in Eq. (2a). The previous discussion concerning the validity of Eq. (2) therefore applies to Eq. (1) as well, provided that the temperature is substituted for the bending moment, and in particular it follows that Eq. (1) can be used in practice for any smooth temperature distribution.

The nondimensional form employed in Eq. (3) furthermore shows that, for a given temperature distribution, convergence will be improved [and thus a closer approximation will be provided by Eq. (1)] as the aspect ratio β decreases.

Attention should be brought at this point to an exception to the above statements which arises only in the

thermal problem. Consider in fact a temperature distribution independent of y; then the expressions of Table 1 reduce to those of Table 2, which shows that Eq. (1) yields a zero value for σ_x. Obviously then the second term of the expansion—i.e., that proportional to $(\partial^2 T/\partial x^2)$—will be predominant and cannot be neglected. The same situation will arise when the temperature is of the form

$$T = F_1(x) + yF_2(x) \tag{3b}$$

The discussion presented in the section "Calculation of Deflections" shows that the Bernoulli-Euler hypothesis holds only if T is independent of the span, as may be expected from the fact that shear stresses (see Table 1) do not arise in this case. In addition it is shown there that an expansion in terms of successively higher derivatives of T in the manner of Eq. (3) is possible also in case of the curvature $(1/\rho)$ of the beam, so that the approximate formula

$$EI(1/\rho) = \iint \alpha ET y \, dy \tag{4}$$

can be expected to have the same range of validity as the familiar equation

$$EI(1/\rho) = M \tag{4a}$$

of strength of materials. These results are analogous to those obtained by von Kármán[4] who showed that the curvature of a loaded beam can also be expressed in a series whose terms are proportional to successively higher derivatives of M.

The results discussed above thus constitute an extension into thermal problems of the fundamental work in beam theory done by von Kármán and Seewald. These investigators derived their results with the aid of an integral transform technique, and then expanded the bending moment distribution into a Taylor series along the span. This technique has the advantage that it can be used to examine the behavior in the vicinity of discontinuities such as are introduced by concentrated loads, but it becomes very cumbersome in the derivation of the particular results needed here. It was noticed, however, that these results could be derived by a step-by-step solution of the governing differential equation; and, furthermore, that such a procedure was of a very general character and could be applied to other linear partial differential equations as well. The method is discussed therefore in general terms in the section which follows, and then applications to the solution of the heat equation and of the thermoelastic equations with variable mechanical properties are discussed. In particular, it may be pointed out that the solution of the heat-conduction problem for a beam with thermal boundary conditions varying along the span can be expressed in a series whose terms contain successively higher derivatives (of the quantity specified in the boundary condition); thus for smooth variations formulas for the temperature distribution valid to the same degree of approximation as Eq. (1) can be readily obtained. The use of the above-mentioned step-by-step solution procedure in the various problems of interest here is outlined in Table 3. An example of the solution of a heat-conduction problem with this method is presented below; the derivation of the formulas of Tables 1 and 2 can be carried out without difficulty with the equations of Table 3 and is therefore not presented. (Additional details may be found in reference 9.)

The author wishes to express his appreciation to Prof. Jerome H. Weiner for his valuable contributions to the developments presented in this report, to Emanuel S. Diamant and Irwin S. Tolins for their work on the preliminary phases of the investigation, and to C. C. Chao and F. H. T. Liu for their assistance in the final portions of the work.

Method of Solution

Let the solution be required of a differential equation of any order n of the form

$$(D_{YT} + D_{XYT} + D_{XT})z = F(x, y, t) \tag{5}$$

where z is the dependent variable, and where the linear partial differential operator $(D_{YT} + D_{XYT} + D_{XT})$ has been divided in three parts chosen so that no derivatives with respect to x appear in D_{YT}, none with respect to y in D_{XT}, and only terms containing both such derivatives appear in D_{XYT}. Let the solution be desired for the range $y_1(x) \leq y \leq y_2(x)$; $x_1(y) \leq x \leq x_2(y)$; $t \geq 0$; and assume the boundary and initial conditions to be of the form:

$$\sum_{j=0}^{n-1} k_j \frac{\partial^j z}{\partial y^j} = X_{1,2}(x, t) \qquad \text{when } y = y_{1,2}(x) \tag{5a}$$

$$\sum_{j=0}^{n-1} k_j' \frac{\partial^j z}{\partial x^j} = Y_{1,2}(y, t) \qquad \text{when } x = x_{1,2}(y) \tag{5b}$$

$$\sum_{j=0}^{n-1} k_j'' \frac{\partial^j z}{\partial t^j} = f_0(x, y) \qquad \text{when } t = 0 \tag{5c}$$

where the k's are constants. A method of solution of Eq. (5) under these boundary conditions will now be outlined; it will be useful when solutions are desired for a thin strip—i.e., when $(y_2 - y_1) \ll (x_2 - x_1)$. Let the solution of Eq. (5) be written in the form

$$z(x, y, t) = \sum_{i=0}^{\infty} z_i(x, y, t) \tag{6}$$

where the z_i functions are to be determined as indicated below. Substitution into Eq. (5) gives

$$(D_{YT} + D_{XYT} + D_{XT})(z_0) + D_{YT}(z_1) + \sum_{i=2}^{\infty} [D_{YT}(z_i) + (D_{XYT} + D_{YT})z_{i-1}] = F(x, y, t) \tag{6a}$$

It is therefore clear that Eq. (6a), and therefore also Eq. (5), will be satisfied if the z_i functions are chosen so as to satisfy the following relations:

$$D_{YT} z_1 = F_1(x, y, t) \tag{7a}$$

$$D_{YT}(z_i) = -(D_{XYT} + D_{XT})z_{i-1} + F_i(x, y, t) \qquad i = 2, 3, 4 \ldots \tag{7b}$$

$$(D_{YT} + D_{XYT} + D_{XT})\, z_0 = 0 \tag{7c}$$

TABLE 3
Equations for the Solution of the Heat and Thermal Stress Problems

PROBLEM	TEMPERATURE DISTRIBUTION	STRESS DISTRIBUTION	
		CONSTANT PROPERTIES	VARIABLE PROPERTIES
DIFFER. EQUAT.	$\kappa \nabla^2 T = \frac{\partial T}{\partial t}$ (Ref. 8)	$\nabla^4 \varphi = -\alpha E \nabla^2 T$ (Ref. 14)	$\frac{\partial^2}{\partial y^2}\left(\frac{\partial^2 \varphi}{E \partial y^2} - \frac{\nu}{E}\frac{\partial^2 \varphi}{\partial x^2}\right) + \frac{\partial^2}{\partial x^2}\left(\frac{\partial^2 \varphi}{E \partial x^2} - \frac{\nu}{E}\frac{\partial^2 \varphi}{\partial y^2}\right) + 2\frac{\partial^2}{\partial x \partial y}\left(\frac{1+\nu}{E}\frac{\partial^2 \varphi}{\partial x \partial y}\right) = -\nabla^2(\alpha T)$
BNDRY COND.	Depend on particular problem	$\sigma_y = \tau = 0$ when $y = \pm c$; $\oint \sigma_x dy = \oint \tau dy = \oint \sigma_x y dy = 0$ (satisfied automat'lly)	
z	T	φ	
D_{YT}	$\kappa \frac{\partial^2}{\partial y^2} - \frac{\partial}{\partial t}$	$\frac{\partial^4}{\partial y^4}$	$\frac{\partial^2}{\partial y^2}\left(\frac{1}{E}\frac{\partial^2}{\partial y^2}\right)$
D_{XT}	$\kappa \frac{\partial^2}{\partial x^2}$	$\frac{\partial^4}{\partial x^4}$	$\frac{\partial^2}{\partial x^2}\left(\frac{1}{E}\frac{\partial^2}{\partial x^2}\right)$
D_{XYT}	0	$2\frac{\partial^4}{\partial x^2 \partial y^2}$	$2\frac{\partial^2}{\partial x \partial y}\left(\frac{1}{E}\frac{\partial^2}{\partial x \partial y}\right) - \frac{\partial^2(\nu/E)}{\partial x^2}\frac{\partial^2}{\partial y^2} - \frac{\partial^2(\nu/E)}{\partial y^2}\frac{\partial^2}{\partial x^2} - 2\frac{\partial^2(\nu/E)}{\partial x \partial y}\frac{\partial^2}{\partial x \partial y}$
F	0	$-\alpha E \nabla^2 T$	$-\nabla^2(\alpha T)$
F_1	0	$-\alpha E(\partial^2 T/\partial y^2)$	$-\partial^2(\alpha T)/\partial y^2$
F_2	0	$-\alpha E(\partial^2 T/\partial x^2)$	$-\partial^2(\alpha T)/\partial x^2$
$F_i\ (i>2)$	0	0	
SOLUTION FROM ($i \neq 0$):	EQS. (7a)–(7b)	EQS. (7e)–(7g)	
z_0 FROM	EQ. (8) or EQ. (11)	Stresses are self-equilibrating (see bdry cond.); hence it follows from eqs. (8) and (8a) that $\varphi_0 = 0$	

NOTE: $\nabla^2 = \frac{\partial^2}{\partial x^2} + \frac{\partial^2}{\partial y^2}$; $\nabla^4 = \nabla^2(\nabla^2)$; $\sigma_x = \frac{\partial^2 \varphi}{\partial y^2}$, $\sigma_y = \frac{\partial^2 \varphi}{\partial x^2}$, $\tau = -\frac{\partial^2 \varphi}{\partial x \partial y}$

where the F_i functions can be chosen in any convenient manner, provided, of course, that

$$F = \sum_{i=1}^{\infty} F_i \tag{7d}$$

The manner in which the portions z_i of the variable z are defined is not unique; for example, if they are chosen so as to satisfy the following relations:

$$D_{YT} z_1 = F_1(x, y, t) \tag{7e}$$

$$D_{YT} z_2 = D_{XYT} z_1 + F_2(x, y, t) \tag{7f}$$

$$D_{YT} z_i = -D_{XYT} z_{i-1} - D_{XT} z_{i-2} + F_i(x, y, t) \qquad i = 3, 4, 5 \ldots \tag{7g}$$

$$(D_{YT} + D_{XYT} + D_{XT}) z_0 = 0 \tag{7h}$$

it is easily seen that Eq. (5) will again be satisfied. Other manners of defining the z_i functions can of course be devised; the individual functions z_i will be different in each case, but their sum will be the same. In the solutions presented in the following sections (see Table 3) the functions z_i will be defined in such a manner that each contains derivatives with respect to x of a single order only; thus in the solution of the heat equation the first of the methods just described will be employed, while for the determination of the stresses the second was used. In any case, both the system (7a)–(7c) or the system (7e)–(7h) have certain characteristics in common, which will now be discussed.

Solution of (7a) and (7b), or of (7e), (7f), and (7g) is evidently simpler than that of Eq. (5), since no derivatives with respect to x appear in the left-hand sides of these equations, and therefore the role of this independent variable has been reduced to that of a parameter. However, it is possible to satisfy with each function $z_i (i \neq 0)$ individually only conditions (5a) and (5c); the function z_0 must then be chosen so as to satisfy homogeneous boundary conditions in place of Eqs. (5a) and (5c), as well as

$$\sum_{j=0}^{n-1} k_j' \frac{\partial^j z_0}{\partial x^j} = Y_{1,2}(y, t) - \sum_{i=1}^{\infty} \sum_{j=0}^{n-1} k_j' \frac{\partial^j z_i}{\partial x^j}$$

at $x = x_{1,2}(y)$ (7i)

Clearly the exact determination of z_0 is, in general, as difficult as the solution of the original problem; fortunately it is possible in the case of a thin-strip to obtain an approximate and at the same time adequate expression for this quantity.

Consider first an infinite narrow strip, that is the case of $x_{1,2} = \mp \infty$. Conditions (5b) would then ordinarily be replaced by the requirement that z and some of its derivatives remain finite at $x = \pm \infty$, and will be automatically satisfied if this requirement is consistent with the behavior at infinity of the functions F, X_1, and X_2. In this case then $z_0 = 0$.

In the case of a long but finite strip, one may write $(y_2 - y_1) \ll (x_2 - x_1)$, and an approximation to z_0 is the solution of

$$D_{XT} z_0 = 0 \tag{8}$$

with

$$\sum_{j=0}^{n-1} k_j' \frac{\partial^j z_0}{\partial x^j} = \frac{1}{y_2 - y_1} \int_{y_1}^{y_2} \left[Y_{1,2} - \sum_{i=1}^{\infty} \sum_{j=0}^{n-1} k_j' \frac{\partial^j z_i}{\partial x^j} \right] dy$$

when $x = x_{1,2}$ (8a)

The resulting expression for z_0 will then be independent of y. The error introduced by this approximation can be found by solving Eqs. (7c) or (7h) under boundary condition (7i). Comparison of Eqs. (7i) and (8a) shows that the average correction to the quantity on the left-hand side of these equations is zero. The actual general determination of this error is again a task of the same difficulty as the solution of the original equation; but in the problems of temperature and stress distribution the error is negligible except in short distances [of the order of $(y_2 - y_1)$] at each end of the strip. In the stress problem this follows from Saint-Venant's principle[6]; in the heat problem it is intuitively clear that an analogous principle will hold. As an example, the temperature T in a semi-infinite strip of height $(y_2 - y_1) = (2c)$ due to a suddenly applied "self-equilibrating" heat input $Q = Q_0 \cos(\pi y / c)$ at $x = 0$ can be verified

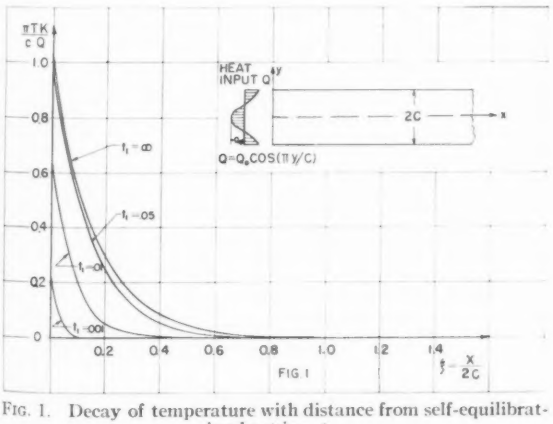

FIG. 1. Decay of temperature with distance from self-equilibrating heat input.

to be

$$[TK/(2cQ)] = -\int_0^{t_1} (1/\pi t_1)^{1/2} \exp[-4\pi^2 t_1 - x^2/(16c^2 t_1)]\, dt_1 \tag{9}$$

or, in a form more suitable for calculation:

$$(2\pi KT/cQ) = e^{-\pi x/c} \{1 + \text{erf}[2\pi\sqrt{t_1} - x/(4c\sqrt{t_1})]\} - e^{\pi x/c} \{1 - \text{erf}[2\pi\sqrt{t_1} + x/(4c\sqrt{t_1})]\} \tag{9a}$$

where the nondimensional time $t_1 = \kappa t/4c^2$, and where κ is the thermal diffusivity of the material. A plot of these expressions, shown in Fig. 1, clearly indicates that only a limited region is appreciably affected by the heat applied.*

The solution of Eq. (5) has thus been reduced to that of Eqs. (7a), (7b) [or Eqs. (7e), (7f), and (7g)] and (8), together with the appropriate boundary conditions; application of these equations in the specific problems of interest here is considered and illustrated in Table 3 and in the examples which follow with reference to a rectangular region defined by

$$-c \le y \le c; \qquad -L \le x \le L: \qquad \beta = (c/L) \ll 1 \tag{9b}$$

Temperature Determination—Example

Let it be desired to find the temperature distribution in the rectangular bar defined by Eq. (9b), when heat is applied to the side $y = +c$ at the rate

$$Q = Q_0 q(\xi); \quad \xi = x/2c \tag{10}$$

all other edges being insulated. For the time being this heat application is assumed to be suddenly started at $t_1 = 0$, and to be continued thereafter at a constant rate; other types of time variation are considered later. The equations for the functions T_i are easily found from Table 3; the boundary conditions are

$$K \frac{\partial T_1}{\partial y} = \begin{cases} Q & \text{when } y = c \\ 0 & \text{when } y = -c \end{cases} \tag{10a}$$

$$\partial T_i/\partial y = 0 \qquad \text{when } y = \pm c \qquad i \ge 2 \tag{10b}$$

The function T_1 is then readily found to be[8]

$$\frac{T_1 K}{2cQ_0} = q(\xi) f(t_1, \eta) = q(\xi) \left\{ t_1 + \frac{1}{2}\left(\eta + \frac{1}{2}\right)^2 - \frac{1}{6} - \frac{2}{\pi^2} \sum_{n=1}^{\infty} \frac{(-1)^n e^{-n^2\pi^2 t_1}}{n^2} \cos n\pi\left(\eta + \frac{1}{2}\right) \right\} \tag{10c}$$

The other functions T_i can then be determined in a straightforward manner (see reference 9); the result is

* It is interesting to note in this connection a difference in Saint-Venant's principle in the stress and heat problems, when used with transient disturbances. It was poiated out in reference 7 that Saint-Venant's principle holds in dynamical problems only if the loads are applied sufficiently slowly: that this restriction is not necessary in the heat problem is illustrated in Fig. 1. The different behavior in the two cases arises from the different character (hyperbolic and parabolic, respectively) of the governing differential equations of the two transient problems.

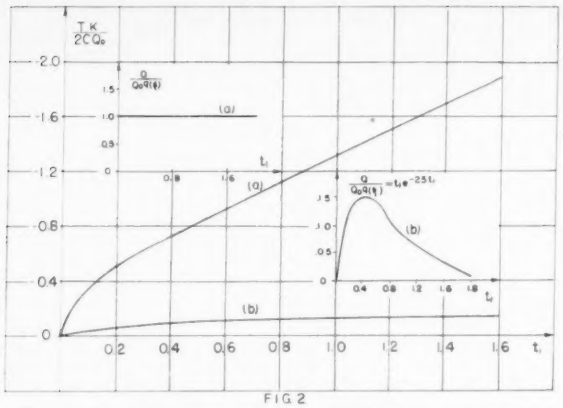

FIG. 2

FIG. 2. Variation of temperature with time at $\xi = 0$, $\eta = 1/2$, for (a) suddenly applied heat input and (b) heat input varying according to Eq. (13).

$$\frac{T_2K}{2cQ_0} = q''(\xi)\left\{\frac{t_1^2}{2} - \frac{[\eta + (1/2)]^4}{24} + \frac{[\eta + (1/2)]^2}{12} - \frac{7}{360} - \frac{2}{\pi^4}\sum_{n=1}^{\infty}\frac{(-1)^n e^{-n^2\pi^2 t_1}}{n^4}(1 + n^2\pi^2 t_1) \times \cos n\pi\,[\eta + (1/2)]\right\} \quad (10d)$$

$$\frac{T_3K}{2cQ_0} = q''''(\xi)\left\{\frac{t_1^3}{6} + \frac{[\eta + (1/2)]^6}{720} - \frac{[\eta + (1/2)]^4}{144} + \frac{7[\eta + (1/2)]^2}{720} - \frac{31}{15120} - \frac{2}{\pi^6}\sum_{n=1}^{\infty}\frac{(-1)^n e^{-n^2\pi^2 t_1}}{n^6} \times [1 + n^2\pi^2 t_1 + n^4\pi^4 t_1^2/2]\cos n\pi\,[\eta + (1/2)]\right\} \quad (10e)$$

and so forth. Note that primes indicate differentiation with respect to ξ. It may be noticed that, in general, T_i is proportional to the $2(i - 1)$th derivative of q with respect to ξ; thus it is clear that, if q is a polynomial, only a finite number of T_i functions will exist and so no question of convergence arises. Thus T_1 represents the entire solution if $q(\xi)$ is a polynomial of the first degree at most; $(T_1 + T_2)$ if $q(\xi)$ is a polynomial of the third degree at most; and so forth. For q functions other than polynomials no such simple results can be obtained; but certainly if the function is sufficiently "smooth"—i.e., if its higher derivatives decrease sufficiently fast—good convergence will be obtained.

The quantity T_0 still remains to be determined; it is the solution of the equation

$$\kappa(\partial^2 T_0/\partial x^2) = (\partial T_0/\partial t) \quad (11)$$

together with the appropriate boundary condition given by Eq. (8a). If, for example, the ends $x = \pm L$ are insulated, the pertinent solution is

$$T_0 = (1/\beta)\int_0^{t_1}\int_{-(1/2)}^{(1/2)}\left\{f(t_1\beta^2, -\xi\beta)\left(\sum_{i=1}^{\infty} T_i'\right)_{\xi=-(1/2\beta)} - f(t_1\beta^2, +\xi\beta)\left(\sum_{i=1}^{\infty} T_i'\right)_{\xi=+(1/2\beta)}\right\} d\eta\, dt_1 \quad (11a)$$

where dots indicate differentiation with respect to t_1 and f is given by Eq. (10c).

In order to proceed with the determination T_0 it is impractical to leave $q(\xi)$ in general terms; therefore a specific example was chosen—namely,

$$q(\xi) = 1 + (q_0)\beta(\xi + 2\beta\xi^2); \qquad \xi \le (1/2\beta) \quad (12)$$

where q_0 is a constant. Then Eq. (11a) yields, after some manipulation,

$$\frac{T_0K}{2CQ_0} = q''(\xi)\left\{-\frac{t_1^2}{2} + \frac{t_1}{4\beta^2}\left(\frac{1}{6} - \xi\beta - 2\xi^2\beta^2\right) - \frac{1}{96\beta^4}\left(\frac{7}{60} - 3\xi\beta - 2\xi^2\beta^2 + 4\xi^3\beta^3 + 4\xi^4\beta^4\right) - \frac{1}{2\beta^4\pi^4}\sum_{n=1}^{\infty}\frac{[3(-1)^n + 1]}{n^4}e^{-n^2\pi^2\beta^2 t_1} \times \cos\left[n\pi\left(\xi\beta + \frac{1}{2}\right)\right]\right\} \quad (12a)$$

In this case q is a polynomial of the second degree and therefore $T_i = 0$ for i larger than 2.

The variation with time of the temperature as given by the above formulas at $x = 0$ and $y = c$ is plotted in nondimensional form in Fig. 2. The values $q_0 = -(1/2)$ and $\beta = 1/5$ were chosen for the numerical example. Also shown on the same figure is the temperature at the same point due to a heat input Q^* varying with time according to the law

$$Q^*(\xi, t_1) = Q_0 q(\xi)\, t_1 e^{-\alpha t_1} \quad (13)$$

where α is a nondimensional parameter chosen here a equal to 2.5. A plot of Eq. (13) is shown in the inset of Fig. 2. The temperature T^* due to Q^* is, from Duhamel's formula,[10]

$$T^* = \int_0^{t_1} T(t^*)\frac{\partial Q^*}{\partial t_1}(\xi, t^* - t_1)dt^* \quad (13a)$$

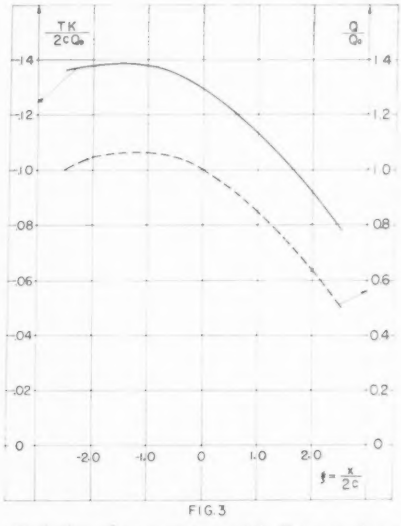

FIG. 3

FIG. 3. Variation of temperature with distance along the span at $\eta = 1/2$, $t_1 = 0.05$ for suddenly applied heat input $Q = Q_0(1 - 0.1\,\xi - 0.04\,\xi^2)$.

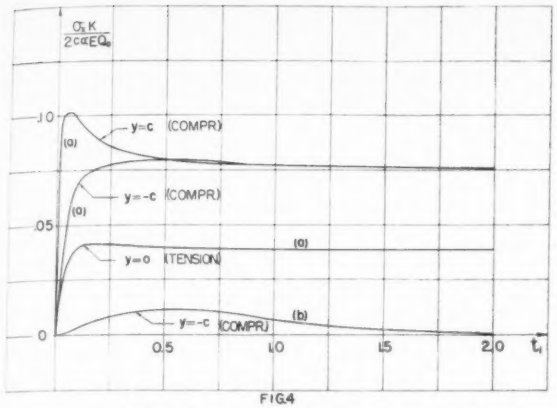

FIG.4

FIG. 4. Variation of stress σ_x with time at $\xi = 0$ and various values of η, for (a) suddenly applied heat input and (b) heat input varying according to Eq. (13).

where $T(t_1)$ is the temperature previously calculated for heating suddenly applied. The integration indicated in Eq. (13a) was carried out numerically.

An example of the variation of the temperature along the span of the bar is presented in Fig. 3, in which a nondimensional plot of temperature against ξ for $y = c$ and $t_1 = 0.05$ may be found. Again $\beta = 1/5$ and $q_0 = -(1/2)$.

Stress Distribution—Example

The stresses arising in a rectangular bar under the heat input of Eq. (10) can now be calculated by direct use of the formulas of Tables 1 and 2. The temperature is given by Eqs. (10c)–(10e); direct substitution gives (for example, for the stress σ_x) the expression

$$[\sigma_x K/(2c\alpha EQ_0)] = q(\xi)\left\{\frac{1}{24} - \frac{\eta^2}{2} + \frac{2}{\pi^2} \times \sum_{n=1}^{\infty} \frac{(-1)^n}{n^2} e^{-n^2\pi^2 t_1} \cos\left[n\pi\left(\eta + \frac{1}{2}\right)\right] - 48\,\eta S_4'\right\} + q''(\xi)\left\{t_1\left(\frac{1}{24} - \frac{\eta^2}{2}\right) + \frac{\eta^4}{12} - \frac{\eta^2}{24} + \frac{7}{2880} + S_4'\left[16\eta^3 - \left(\frac{12}{5} + 48t_1\right)\eta\right] - 96\eta S_6' + \frac{2}{\pi^4}\sum_{n=1}^{\infty}\frac{(-1)^n e^{-n^2\pi^2 t_1}}{n^4}(2 + n^2\pi^2 t_1)\cos\left[n\pi\left(\eta + \frac{1}{2}\right)\right]\right\} \quad (14)$$

where $$S_i' = \sum_{n=1,3,5,\ldots}^{\infty} [e^{-n^2\pi^2 t_1}/(n^i\pi^i)]$$

Some details of the derivation of Eq. (14) may be found in reference 9. To the above expression for the stress must now be added the stress due to the temperature T_0 of Eq. (12a). This portion of the temperature is independent of y and therefore Table 2 applies; the result:

$$\frac{\sigma_x K}{2c\alpha EQ_0} = T_0''\left\{\frac{1}{24} - \frac{\eta^2}{2}\right\} + T_0''''\left\{\frac{\eta^4}{12} - \frac{\eta^2}{24} + \frac{7}{2880}\right\} + \ldots \quad (14a)$$

The expression of Eq. (14) is exact if q is that given by Eq. (12), while Eq. (14a) contains even in this case an infinite number of terms. Numerical calculations showed, however, that the series contained in the latter equation is very rapidly convergent, and that, in fact, even the first term provides a reasonable approximation. Some numerical results are presented in Figs. 4 and 5 both for suddenly applied heat [see Eq. (10)], and for heat application following Eq. (13).

Figs. 3 and 5 show the variation of temperature and stress, respectively, with the distance along the span; also shown in these figures is the variation along the span of the applied heat Q according to Eq. (11). Inspection of the calculations from which these results were obtained shows that, as indicated in the Introduction, the first terms of the expression for these quantities—i.e., T_1 and φ_1—are of paramount importance, while even the second term may be neglected.

Calculation of Deflections

The deflections of the bar considered in the previous developments are easily calculated from the stresses given in Table 1. The displacements in the x and y directions are respectively denoted by u and v and must satisfy the equations[6]

$$\left.\begin{aligned} E(\partial u/\partial x) &= \sigma_x - \nu\sigma_y + \alpha ET \\ E(\partial v/\partial y) &= \sigma_y - \nu\sigma_x + \alpha ET \\ E[(\partial u/\partial y) + (\partial v/\partial x)] &= 2(1+\nu)\tau \end{aligned}\right\} \quad (15)$$

The desired result is easily obtained by substituting in Eq. (15) the expressions for the stresses in terms of the stress function of Table 1, and integrating the first and second of Eqs. (15) with respect to x and y respectively. The arbitrary functions (respectively of y and x) arising during this process are then adjusted so as to satisfy the last of Eq. (15). The final result is

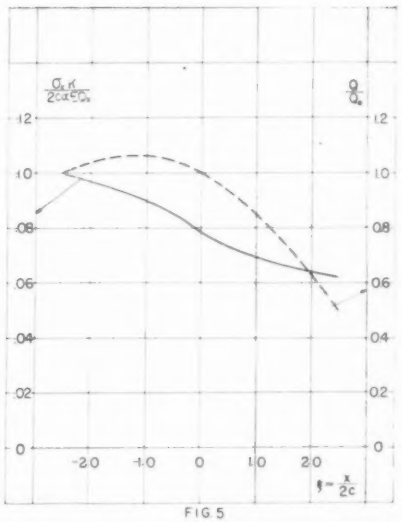

FIG.5

FIG. 5. Variation of stress σ_x with distance along the span at $\eta = 1/2$, $t_1 = 1$ for suddenly applied heat input $Q = Q_0(1 - 0.1\,\xi - 0.04\,\xi^2)$

$$\frac{u}{\alpha} = \{c_1 + c_2 y\} + \int_{-L}^{x} \left\{ \frac{1}{2c} \int_{-c}^{c} T\,dy + \frac{3y}{2c^3} \int_{-c}^{c} T\,y\,dy \right\} dx + \frac{\partial}{\partial x} \left\{ (1+\nu) \left[\int_{-c}^{y} T\,dy - \int_{-c}^{y} T\,y\,dy \right] - \frac{c}{2} \int_{-c}^{c} T\,dy \left[\frac{1}{6} + \frac{\nu}{2} + (1+\nu)\frac{y}{c} + \left(1 + \frac{\nu}{2}\right)\left(\frac{y}{c}\right)^2 \right] + \frac{1}{2} \int_{-c}^{c} T\,y\,dy \left[1 + \nu + \left(\frac{21}{10} + \frac{3\nu}{2}\right)\left(\frac{y}{c}\right) - \left(1 + \frac{\nu}{2}\right)\left(\frac{y}{c}\right)^3 \right] - \frac{1}{4c} \int_{-c}^{c} T y^2\,dy - \frac{y}{4c^3} \int_{-c}^{c} T y^3\,dy \right\} + \ldots \quad (16a)$$

and

$$\frac{v}{\alpha} = \{c_3 - c_2 x\} + \int_{-L}^{x} \int_{-L}^{x} \left\{ \frac{3}{2c^3} \int_{-c}^{c} T\,y\,dy \right\} dx\,dx + \left\{ (1+\nu) \int_{-c}^{y} T\,dy - \frac{1}{2} \int_{-c}^{c} T\,dy \left[1 + \nu + \nu \frac{y}{c} \right] + \frac{1}{c} \int_{-c}^{c} T\,y\,dy \left[\frac{7}{20} + \frac{3\nu}{4} - \frac{3\nu}{4}\left(\frac{y}{c}\right)^2 \right] + \frac{1}{4c^3} \int_{-c}^{c} T y^3\,dy \right\} + \ldots \quad (16b)$$

Both the right-hand sides of Eqs. (16a) and (16b) contain successively higher derivatives of the temperature with respect to x, and therefore will converge under conditions similar to those mentioned in the Introduction. The rigid body displacements of first bracket in each of the above expressions depend on the constants c_1, c_2, and c_3, which are to be determined from the boundary conditions of the problem. The next bracket represents a contribution due entirely to the function φ_1 of Table I. This portion, in the case of the displacement u, is linear in y, and therefore follows the assumption that sections plane before heating remain plane after heating, and may be seen to be rigorously valid only for temperature distributions which are independent of the distance along the span. Eq. (16a) can also be used to estimate the error in any elementary theory developed on the basis of the Bernoulli-Euler hypothesis. The corresponding term for the displacement v depends upon the integral $\int_{-c}^{c} T\,y\,dy$, which plays in fact a role similar to that of the bending moment in elementary beam theory. It is interesting in this connection to calculate the average curvature; it is

$$\frac{d^2 v_{av.}}{dx^2} = \left\{ \frac{3}{2c^3} \int_{-c}^{c} \alpha T y\,dy \right\} + \left\{ -\frac{3}{20c} \int_{-c}^{c} \alpha \frac{\partial^2 T}{\partial x^2}\,y\,dy + \frac{1}{4c^3} \int_{-c}^{c} \alpha \frac{\partial^2 T}{\partial x^2}\,y^3\,dy \right\} + \ldots \quad (17)$$

and is therefore expressible in the form discussed in the Introduction [see Eqs. (4)].

Stress Distribution—Variable Properties

In all the above developments it has been assumed that the mechanical properties of the material are independent of the temperature. However, this was not found to be the case in an experimental investigation conducted by the NACA,[11, 12] which led to the following approximate formulas for the variation of the modulus of elasticity E, the shear modulus G and the coefficient of thermal expansion α for 75S-T6 aluminum alloy:

$$\left.\begin{aligned} E &= E_0 - (1470T + 15.17T^2) \\ G &= G_0 - (1440T + 4.87T^2) \\ \alpha &= \alpha_0 + 3.52 \times 10^{-9} T \end{aligned}\right\} \quad (18)$$

In these expressions the subscript 0 indicates the properties at $T = 0$. The values $E_0 = 10.5 \times 10^6$ lbs. per sq.in., $G_0 = 4.0 \times 10^6$ lbs. per sq.in., and $\alpha_0 = 12.52 \times 10^{-6}/°\text{F}$. are suggested for the above material.[12]

Examination of Eqs. (18) shows a considerable variation of material properties with temperature. The variation of α provides no new difficulties, since it merely changes the right-hand side of the governing equation (Table 3) and therefore corresponds to a different applied temperature function. The variation of E and G (and therefore ν), on the other hand, requires use of the equation given in Table 3, which, though still linear, has variable coefficients. Considerable doubt has been recently thrown, however, on the correctness of the variation of E and G as obtained above, and the opinion has been expressed[13] that a more critical interpretation of the experimental evidence might reveal that the moduli of elasticity vary very little, the apparent variation being due to a neglect of the viscoelastic effects. This problem can not be dealt with here; nevertheless it is shown below how the general method employed throughout this paper is applicable to the present equation as well. It will then remain for future research to determine the type of problem in which such a solution is of importance.

The solution of the problem can be found without difficulty with the aid of Table 3. The function φ_1, for example, is

$$\varphi_1 = \int_{-c}^{y} \int_{-c}^{y} (-\alpha E T + c_1 E y + c_2 E)\,dy\,dy \quad (19)$$

where the values of c_1 and c_2 required to satisfy the boundary conditions are

$$c_1 = \frac{\left(\int_{-c}^{c} E\,y\,dy\right)\left(\int_{-c}^{c} \alpha E T\,dy\right) - \left(\int_{-c}^{c} E\,dy\right) \times \left(\int_{-c}^{c} \alpha E T\,y\,dy\right)}{\left(\int_{-c}^{c} E\,y\,dy\right)^2 - \left(\int_{-c}^{c} E\,dy\right)\left(\int_{-c}^{c} E\,y^2\,dy\right)} \quad (19a)$$

$$c_2 = \frac{\left(\int_{-c}^{c} E\,y\,dy\right)\left(\int_{-c}^{c} \alpha E T\,y\,dy\right) - \left(\int_{-c}^{c} E\,y^2 dy\right) \times \left(\int_{-c}^{c} \alpha E T\,dy\right)}{\left(\int_{-c}^{c} E\,y\,dy\right)^2 - \left(\int_{-c}^{c} E\,dy\right)\left(\int_{-c}^{c} E\,y^2\,dy\right)} \qquad (19b)$$

Note that c_1 and c_2 are functions of x if T (and therefore E) vary along the span. With these quantities the first terms of the expressions for the stresses may be derived. In particular, it is interesting to note that the first term of the stress σ_x is

$$\sigma_{x_1} = -\alpha E T + c_1 E\,y + c_2 E \qquad (19c)$$

and has therefore the same form as that given in Table 1 and could be obtained on the basis of the Bernoulli-Euler assumption. Of course the constants c_1 and c_2 are different here from those of Table 1, though they become identical (and this is true of all corresponding expressions in the developments for variable and constant properties) if E is taken to be constant. As in the case of constant properties [see the discussion preceding Eq. (3b)] the stress given by Eq. (19c) is zero if Eq. (3b) holds.

In the case of constant properties, the expression for σ_x analogous to Eq. (19c) was found to be exact for temperature distributions with $\partial^2(\alpha T)/\partial x^2 = 0$. In the present case, however, it will be seen φ_2 contains terms of the type $\partial\ (\alpha T)/\partial x$; hence $\varphi_1(i \geq 2)$ will vanish, and Eq. (19) will be exact, only for temperature distributions independent of the span.

References

[1] Tsien, H. S., *Similarity Laws for Stressing Heated Wings*, Journal of the Aeronautical Science, Vol. 20, No. 1, p. 1, 1953.

[2] Pell, W. H., *Thermal Deflections of Anisotropic Thin Plates*, Quart. Appl. Math., Vol. 4, p. 27, 1946.

[3] Sokolnikoff, J. S. and Sokolnikoff, E. F., *Thermal Stresses in Elastic Plates*, Trans. Am. Math. Soc., Vol. 45, p. 235, 1939.

[4] von Kármán, T., *Ueber die Grundlagen der Balkentheorie*, Abh. Aerodynam. Inst., Tech. Hochschule Aachen, Vol. 7, p. 3, 1927.

[5] Seewald, F., *Die Spannungen und Formanderungen von Balken mit rechteckigem Querschnitt*, Abh. Aerodynam. Inst., Tech. Hochschule Aachen, Vol. 7, p. 11, 1927.

[6] Timoshenko, S., and Goodier, J. N., *Theory of Elasticity*, Second Ed. McGraw-Hill Book Co., New York, 1951.

[7] Boley, Bruno A., *The Application of Saint-Venant's Principle in Dynamical Problems*, Journal of Applied Mechanics, Vol. 22, No. 2, June 1955.

[8] Carslaw, H. S., and Jaeger, J. C., *Conduction of Heat in Solids*, Clarendon Press, Oxford, England, 1947.

[9] Boley, Bruno A., *The Determination of Temperature, Stresses and Deflections in Two-Dimensional Thermo-elastic Problems*, W.A.D.C. Tech. Rep. 54–424.

[10] Churchill, R. V., Modern Operational Mathematics in Engineering, p. 193, McGraw-Hill Book Co., New York, 1944.

[11] Heimerl, G. J., and Roberts, W. M., *Determination of Plate Compressive Strengths at Elevated Temperatures*, NACA TN 960, 1950.

[12] Heldenfels, R. R., *The Effect of Non-uniform Temperature Distributions on the Stresses and Distortions of Stiffened Shell Structures*, NACA TN 2240, 1950.

[13] Freudenthal, A. M., *On Inelastic Thermal Stresses in Flight Structures*, Paper presented at 22nd Annual Meeting, 1954, Institute of the Aeronautical Sciences, Preprint No. 429.

[14] Hetényi, M., *Handbook of Experimental Stress Analysis*, p. 755, John Wiley and Sons, New York, 1950.

An Investigation on Fully Developed Turbulent Flows . . .

(*Continued from page 34*)

(g) An agitation of radial movements near the outer wall and a suppression of such movements near the inner wall can be speculated as the explanation of the experimental fact that the integral scales L_ϕ and L_r are larger at the outer wall than at the inner wall. (See Figs. 23 and 24).

(h) The distribution of U shows that both $d(Ur)/dr$ and $d(U/r)/dr$ are much larger at the outer wall than at the inner wall. The consequent larger turbulence production at the outer wall explains the larger turbulence intensity there (Fig. 7).

References

[1] Wattendorf, F. L., *A Study of the Effect of Curvature on Fully Developed Turbulent Flow*, Proc. Roy. Soc., Vol. 148, pp. 565–598, 1935.

[2] Laufer, J., *Investigation of a Turbulent Flow in a Two-Dimensional Channel*, NACA TN 2123, July, 1950.

[3] Wislicenus, G. F., and Yeh, H., *A Program of Research in the Field of Turbulent Flow in Ducts, in a Space of Revolution, and in Turbomachinery*, Nonr 248(33) Report I-8, Department of Mechanical Engineering, The Johns Hopkins University, December, 1952.

[4] Eskinazi, S., *An Investigation of Fully Developed Turbulent Flow in a Curved Channel*, Nonr 248(33) Report I-20, Department of Mechanical Engineering, The Johns Hopkins University, August, 1954.

[5] Corrsin, S., *Interpretation of Viscous Terms in the Turbulent Energy Equation*, Journal of the Aeronautical Sciences, Reader's Forum, Vol. 20, No. 12, p. 853, December, 1953.

[6] Eskinazi, S., *Fully Developed Flow in Curved Parallel Channel*, Nonr 248(33) Progress Report I-10, Department of Mechanical Engineering, The Johns Hopkins University, April, 1953.

[7] Kovasznay, L. S. G., *Development of Turbulence Measuring Equipment*, NACA TN 2839, January, 1953.

[8] Townsend, A. A., *Measurement of Double and Triple Correlation Derivatives in Isotropic Turbulence*, Proc. Cambridge Phil Soc., Vol. 43, pt. 4, pp. 560–570, October, 1947.

[9] Clauser, F. H., *Turbulent Boundary Layers in Adverse Pressure Gradients*, Journal of the Aeronautical Sciences, Vol. 21, No. 2, pp. 91–108, February, 1954.

[10] Laufer, J., *The Structure of Turbulence in Fully Developed Pipe Flow*, NACA TN 2954, June, 1953.

[11] Yeh, H., *Influence of Curvature in Turbulent Channel Flows*, Seminar given in Meeting on Internal Fluid Mechanics, Department of Mechanical Engineering, The Johns Hopkins University, May 25, 1954.

[12] Rotta, J., *Statistische Theorie für Nichthomogener Turbulenz*, Zeit. für Physik, Vol. 129, pp. 547–572, 1951.

[13] Rayleigh, J. W. S., *On the Dynamics of Revolving Fluids*, Proc. Roy. Soc., Vol. 6A, pp. 148–154, 1916.

Compressibility Effects on Secondary Flows*

H. G. LOOS†

California Institute of Technology

SUMMARY

The method of W. R. Hawthorne for the calculation of the secondary vorticity is generalized for compressible flow. It is shown that in the linearized theory (small vorticity) the influence of compressibility upon the secondary vorticity is due to (1) the entropy gradient in the approaching flow and (2) the compression of the fluid during the turning of the flow. The analysis is applied to the secondary vorticity which generates in a cascade or bend if the approaching flow has a boundary layer with a Prandtl Number equal to unity and has been developed along an insulated wall.

For a cascade with a passage cross section which increases linearly with the turning angle and at the exit is 1.4 times the entrance cross-section area, the compressibility correction, to be applied upon the secondary vorticity, amounts to 24 per cent for a cascade entrance Mach Number of 0.8.

The problem of determination of the secondary flow downstream of the cascade, which is associated with a given secondary vorticity, is the same for compressible and incompressible flow

SYMBOLS

$\boldsymbol{q}$	=	velocity vector
$\boldsymbol{\omega}$	=	vorticity vector
ω_σ	=	vorticity component in stream direction
ω_n	=	vorticity component normal to streamline
ρ	=	density
T	=	temperature
S	=	entropy
c_p	=	specific heat at constant pressure
R	=	radius of curvature of streamline
ϑ	=	flow angle
M	=	Mach Number
γ	=	ratio of specific heats
ϕ	=	angle between centripetal acceleration and the vector $q \times (c_p \text{ grad } T - T_0 \text{ grad } S)$
ϵ	=	small parameter
f_1, f_2	=	correction factors

INTRODUCTION

THE STUDY OF ROTATIONAL FLOWS is of considerable importance for the understanding and analysis of three-dimensional flows in turbomachines. A most interesting aspect of rotational flows is the development of a vorticity component in the stream direction (secondary vorticity), due to a curvature of the streamlines in the presence of a vorticity component normal to the stream direction. The development of the secondary vorticity has been studied by H. B. Squire and K. G. Winter in reference 1 and by W. R. Hawthorne in reference 2 for incompressible fluids.

Received November 4, 1954.

* This work was carried out under the sponsorship of the Office of Scientific Research, Air Research and Development Command, and represents a portion of an investigation into secondary flow in axial compressors, performed at The Daniel and Florence Guggenheim Jet Propulsion Center, California Institute of Technology.

† Research Fellow in Jet Propulsion.

In modern turbojet propulsion plants, the Mach Number of the flow entering the compressor is usually so high that a study of the influence of the compressibility on the secondary flow seems desirable. Another case where such an investigation might be of interest is the secondary flow in a turbine, following a combustion chamber. There we can expect appreciable temperature gradients, caused by the combustion process.

In the present investigation, the method of Hawthorne[2] to derive an expression for the secondary vorticity is generalized for compressible flows. An application to cascades, approached by a flow with a boundary layer, developed along an insulated wall and with a Prandtl Number equal to unity, is given, and an estimate of the compressibility effects on the secondary vorticity is made. Some attention is given to the integration problem in compressible flow for the secondary motion far downstream from a cascade with a given vorticity field.

THE LINEARIZED EQUATION FOR THE SECONDARY VORTICITY

Let $\boldsymbol{q}$ denote the velocity vector, $\boldsymbol{\omega}$ the vorticity vector, ω_σ the component of the vorticity in the direction of $\boldsymbol{q}$ and ρ the density of the fluid. The vorticity vector may be resolved into its components in the flow direction and perpendicular to it,

$$\boldsymbol{\omega} = \frac{\omega_\sigma}{\rho q}\,\rho\boldsymbol{q} + \frac{(\boldsymbol{q} \times \boldsymbol{\omega}) \times \boldsymbol{q}}{q^2}$$

The divergence of the vorticity vanishes, hence

$$\frac{\omega_\sigma}{\rho q}\,\text{div}\,(\rho\boldsymbol{q}) + \rho\boldsymbol{q}\cdot\text{grad}\,\frac{\omega_\sigma}{\rho q} + \text{div}\,\frac{(\boldsymbol{q} \times \boldsymbol{\omega}) \times \boldsymbol{q}}{q^2} = 0 \quad (1)$$

For steady flow, $\text{div}\,(\rho\boldsymbol{q}) = 0$ and Eq. (1) reduces to

$$\rho\boldsymbol{q}\cdot\text{grad}\,\frac{\omega_\sigma}{\rho q} = -\text{div}\,\frac{(\boldsymbol{q} \times \boldsymbol{\omega}) \times \boldsymbol{q}}{q^2} \quad (2)$$

The equations of motion require that

$$\begin{aligned}\boldsymbol{q} \times \boldsymbol{\omega} &= c_p \text{ grad } T_0 - T \text{ grad } S \\ &= c_p \text{ grad } T_0 - T_0 \text{ grad } S + (1/2c_p)q^2 \text{ grad S}\end{aligned}$$

where T_0 is the stagnation temperature and S the entropy. This relation substituted in Eq. (2) gives

$$\begin{aligned}\rho\boldsymbol{q}\cdot\text{grad}(\omega_\sigma/\rho q) = &-\text{div}\,\{(1/q^2)\,[(c_p \text{ grad } T_0 - T_0 \\ &\text{grad } S) \times \boldsymbol{q}]\} \\ &-(1/2c_p)\,\text{div}\,(\text{grad } S \times \boldsymbol{q}) \quad (3)\end{aligned}$$

We use the identities

$$\begin{aligned}\operatorname{div}(\operatorname{grad} S \times \boldsymbol{q}) &= \operatorname{curl}\operatorname{grad} S\cdot\boldsymbol{q} - \operatorname{grad} S\cdot\operatorname{curl}\boldsymbol{q}\\ &= -\boldsymbol{\omega}\cdot\operatorname{grad} S\end{aligned}$$

$$\begin{aligned}\operatorname{div}\{(1/q^2)\,[\boldsymbol{q}\times(c_p\operatorname{grad}T_0 - T_0\operatorname{grad}S)]\} &= [\operatorname{grad}(1/q^2)]\cdot[\boldsymbol{q}\times(c_p\operatorname{grad}T_0 - T_0\operatorname{grad}S)] +\\ &\quad (1/q^2)\operatorname{div}[\boldsymbol{q}\times(c_p\operatorname{grad}T_0 - T_0\operatorname{grad}S)]\end{aligned}$$

and

$$\begin{aligned}\operatorname{div}[\boldsymbol{q}\times(c_p\operatorname{grad}T_0 - T_0\operatorname{grad}S)] &= (c_p\operatorname{grad}T_0 - T_0\operatorname{grad}S)\cdot\operatorname{curl}\boldsymbol{q} - \boldsymbol{q}\cdot\operatorname{curl}(c_p\operatorname{grad}T_0 - T_0\operatorname{grad}S) =\\ &\quad (c_p\operatorname{grad}T_0 - T_0\operatorname{grad}S)\cdot\boldsymbol{\omega} - c_p\boldsymbol{q}\cdot\operatorname{curl}\operatorname{grad}T_0 + \boldsymbol{q}\cdot(\operatorname{grad}T_0\times\operatorname{grad}S) + \boldsymbol{q}\cdot(T_0\operatorname{curl}\operatorname{grad}S) =\\ &\quad (c_p\operatorname{grad}T_0 - T_0\operatorname{grad}S)\cdot\boldsymbol{\omega} + \boldsymbol{q}\cdot(\operatorname{grad}T_0\times\operatorname{grad}S)\end{aligned}$$

Then Eq. (3) may be written

$$\begin{aligned}\rho\boldsymbol{q}\cdot\operatorname{grad}(\omega_\sigma/\rho q) &= [\operatorname{grad}(1/q^2)]\cdot[\boldsymbol{q}\times(c_p\operatorname{grad}T_0 - T_0\operatorname{grad}S)] +\\ &\quad (1/q^2)\,[(c_p\operatorname{grad}T_0 - T_0\operatorname{grad}S)\cdot\boldsymbol{\omega} + \boldsymbol{q}\cdot(\operatorname{grad}T_0\times\operatorname{grad}S)] + (1-2c_p)\boldsymbol{\omega}\cdot\operatorname{grad}S \quad (4)\end{aligned}$$

With the identity

$$\operatorname{grad}(1/q^2) = -(1/q^4)\operatorname{grad}q^2 = -(1/q^4)\,[2(\boldsymbol{q}\cdot\nabla)\boldsymbol{q} + 2\boldsymbol{q}\times\operatorname{curl}\boldsymbol{q}]$$

the first term on the right-hand side of Eq. (4) becomes

$$[\operatorname{grad}(1/q^2)]\cdot[\boldsymbol{q}\times(c_p\operatorname{grad}T_0 - T_0\operatorname{grad}S)] = -(1/q^4)\,[2(\boldsymbol{q}\cdot\nabla)\boldsymbol{q} + 2\boldsymbol{q}\times\boldsymbol{\omega}]\cdot[\boldsymbol{q}\times(c_p\operatorname{grad}T_0 - T_0\operatorname{grad}S)] \quad (5)$$

The vector $(\boldsymbol{q}\cdot\nabla)\boldsymbol{q}$ is easily recognized as the acceleration vector for steady flow. For a flow of an inviscid fluid, the stagnation temperature T_0 and the entropy S are constant along streamlines, so that the vector $c_p\operatorname{grad}T_0 - T_0\operatorname{grad}S$ is perpendicular to the vector $\boldsymbol{q}$. Also, $\boldsymbol{q}\times(c_p\operatorname{grad}T_0 - T_0\operatorname{grad}S)$ is perpendicular to $\boldsymbol{q}$ so that in the product $[(\boldsymbol{q}\cdot\nabla)\boldsymbol{q}]\cdot[\boldsymbol{q}\times(c_p\operatorname{grad}T_0 - T_0\operatorname{grad}S)]$ only the centripetal acceleration gives a contribution. If ϕ is the angle between the centripetal acceleration and the vector $\boldsymbol{q}\times(c_p\operatorname{grad}T_0 - T_0\operatorname{grad}S)$, then we have

$$[(\boldsymbol{q}\cdot\nabla)\boldsymbol{q}]\cdot[\boldsymbol{q}\times(c_p\operatorname{grad}T_0 - T_0\operatorname{grad}S)] = (q^3/R)\cos\phi\,|c_p\operatorname{grad}T_0 - T_0\operatorname{grad}S|$$

where R is the radius of curvature of the streamline. The product $(\boldsymbol{q}\times\boldsymbol{\omega})\cdot[\boldsymbol{q}\times(c_p\operatorname{grad}T_0 - T_0\operatorname{grad}S)]$ in Eq. (5) can be expanded as

$$q^2[\boldsymbol{\omega}\cdot(c_p\operatorname{grad}T_0 - T_0\operatorname{grad}S)] - [\boldsymbol{q}\cdot(c_p\operatorname{grad}T_0 - T_0\operatorname{grad}S)](\boldsymbol{\omega}\cdot\boldsymbol{q}) = q^2\boldsymbol{\omega}\cdot(c_p\operatorname{grad}T_0 - T_0\operatorname{grad}S)$$

because $\boldsymbol{q}$ and $c_p\operatorname{grad}T_0 - T_0\operatorname{grad}S$ are perpendicular. Use of these relations in Eq. (4) yields

$$\begin{aligned}\rho\boldsymbol{q}\cdot\operatorname{grad}(\omega_\sigma/\rho q) &= (-2/qR)\cos\phi\,|c_p\operatorname{grad}T_0 - T_0\operatorname{grad}S| - (2/q^2)\boldsymbol{\omega}\cdot(c_p\operatorname{grad}T_0 - T_0\operatorname{grad}S) +\\ &\quad (1/q^2)\,[(c_p\operatorname{grad}T_0 - T_0\operatorname{grad}S)\cdot\boldsymbol{\omega} + \boldsymbol{q}\cdot(\operatorname{grad}T_0\times\operatorname{grad}S)] + (1-2c_p)\boldsymbol{\omega}\cdot\operatorname{grad}S\end{aligned}$$

and after combining the terms on the right-hand side, one finds

$$\rho\boldsymbol{q}\cdot\operatorname{grad}(\omega_\sigma/\rho q) = (-2/qR)\cos\phi\,|c_p\operatorname{grad}T_0 - T_0\operatorname{grad}S| + (1/c_p)\boldsymbol{\omega}\cdot\operatorname{grad}S + (1/q^2)\boldsymbol{q}\cdot(\operatorname{grad}T_0\times\operatorname{grad}S) \quad (6)$$

Integration of Eq. (6) along a streamline gives

$$\left.\frac{\omega_\sigma}{\rho q}\right|_1^2 = -\int_1^2\frac{2}{\rho q^2 R}\cos\phi\,|c_p\operatorname{grad}T_0 - T_0\operatorname{grad}S|\,d\sigma + \int_1^2\left[\frac{1}{\rho q^3}\boldsymbol{q}\cdot(\operatorname{grad}T_0\times\operatorname{grad}S) + \frac{1}{\rho q c_p}\boldsymbol{\omega}\cdot\operatorname{grad}S\right]d\sigma \quad (7)$$

where $d\sigma$ is a line element of the streamline.

If grad T_0 and grad S have the same direction—i.e., if the stagnation temperature and the entropy are constant on the same surfaces—then the last integral in Eq. (7) vanishes.

Eq. (7) does not express the secondary vorticity ω_σ explicitly, because the integrands depend on $\boldsymbol{\omega}$. On the other hand, Eq. (7) lends itself very easily to the application of a perturbation procedure.

Expand all fields of interest in a power series in the small parameter ϵ,

$$\begin{aligned}\boldsymbol{q} &= \boldsymbol{q}^{(0)} + \epsilon\,\boldsymbol{q}^{(1)} + \ldots,\\ \boldsymbol{\omega} &= \epsilon\,\boldsymbol{\omega}^{(1)} + \ldots,\\ T_0 &= T_0^{(0)} + \epsilon\,T_0^{(1)} + \ldots,\\ S &= S^{(0)} + \epsilon\,S^{(1)} + \ldots,\\ \rho &= \rho^{(0)} + \epsilon\,\rho^{(1)} + \ldots,\end{aligned}$$

$$\begin{aligned}\phi &= \phi^{(0)} + \epsilon\,\phi^{(1)} + \ldots,\\ R &= R^{(0)} + \epsilon\,R^{(1)} + \ldots,\end{aligned}$$

where $\boldsymbol{q}^{(0)}$ is chosen such that it fulfills the equations of motion and continuity, that curl $\boldsymbol{q}^{(0)} = 0$, and that the corresponding stagnation temperature and entropy, $T_0^{(0)}$ and $S^{(0)}$, are constant.

Introduction of these power series expansions in Eq. (7) and separation of the different powers of ϵ gives for the first-order perturbation

$$\left.\frac{\omega_\sigma^{(1)}}{\rho^{(0)}q^{(0)}}\right|_1^2 = -\int_1^2\frac{2}{\rho^{(0)}q^{(0)2}R^{(0)}}\cos\phi^{(0)}\,|c_p\operatorname{grad}T_0^{(1)} - T_0^{(0)}\operatorname{grad}S^{(1)}|\,d\sigma \quad (8)$$

If the zeroth-order field is known together with the first-order perturbations of the flow conditions

at point 1, then the first-order solution for the secondary vorticity can be calculated with Eq. (8) for all other points on the same streamline of the zeroth-order flow. This calculation involves the knowledge of grad $T_0^{(1)}$ and grad $S^{(1)}$, which can be derived from the given flow perturbation at point 1 and the fact that both $T_0^{(1)}$ and $S^{(1)}$ are constant along the zeroth-order streamlines.

If the infinitesimal change in flow angle $d\vartheta = d\sigma/R$ is introduced, Eq. (8) can be written in a somewhat more convenient form,

$$\frac{\omega_\sigma^{(1)}}{\rho^{(0)}q^{(0)}} = -2\int_1^2 \frac{\cos\phi^{(0)}}{\rho^{(0)}q^{(0)^2}} \left| c_p \text{ grad } T_0^{(1)} - T_0^{(0)} \text{ grad } S^{(1)} \right| d\vartheta \quad (9)$$

A comparison with the formula of Hawthorne[2] shows that the compressibility has two effects: (1) the entropy distribution of the approaching flow is in general nonuniform and this gives rise to an additional secondary vorticity generation; and (2) the streamwise density variations in the region where the secondary vorticity develops modifies this vorticity generation.

Eq. (9) is valid when grad T_0 and grad S are small. It is possible, however, to apply the small perturbation technique under less restrictive assumptions. When $|c\rho \text{ grad } T_0 - T_0 \text{ grad } S|$ is small, but if not both grad T_0 and grad S are small, then the angle between the vectors grad T_0 and grad S should be small, or one of these vectors is small. In both cases, (grad $T_0 \times$ grad S) in Eq. (7) is a small vector and $\boldsymbol{\omega}\cdot$grad S is a small number, so that ω_σ is also small and the perturbation procedure is applicable if the second integral in Eq. (7) is properly taken into account. As in most cases where the perturbation procedure is at all applicable, both grad T_0 and grad S are small; we shall only consider this case and use Eq. (9) as a linearized equation. We can express this equation in a more convenient form by writing

$$|c_p \text{ grad } T_0 - T_0 \text{ grad } S| = |c_p \text{ grad } T_0 - T \text{ grad } S - (T_0 - T_1) \text{ grad } S|$$

and

$$(T_0 - T)/\gamma RT = (1/2c_p)(q^2/c^2) = (1/2c_p)M^2$$

or

$$T_0 - T = [(\gamma - 1)/2]M^2T$$

so that

$$|c_p \text{ grad } T_0 - T_0 \text{ grad } S| = |c_p \text{ grad } T_0 - T \text{ grad } S - [(\gamma - 1)/2]M^2T \text{ grad } S| = |\boldsymbol{q} \times \boldsymbol{\omega} - [(\gamma - 1)/2]M^2T \text{ grad } S|$$

Therefore, we may write

$$\frac{\omega_\sigma^{(1)}}{\rho^{(0)}q^{(0)}}\Bigg|_1^2 = -2\int_1^2 \frac{\cos\phi^{(0)}}{\rho^{(0)}q^{(0)^2}} \left| \boldsymbol{q} \times \boldsymbol{\omega} - \frac{\gamma - 1}{2} M^{(0)^2}T^{(0)^2} \text{ grad } S^{(1)} \right| d\vartheta \quad (10)$$

Application to Compressible Boundary-Layer Flow

Consider a three-dimensional boundary layer with free flow streamlines which are almost straight over a considerable length and show an appreciable lateral curvature in a fairly small length interval. Then, in the region where the free flow streamlines are almost straight, the boundary-layer flow may be considered as two-dimensional. In the region where the turning of the flow takes place, however, there is a certain part of the boundary layer where inertial forces dominate the viscous forces. This part of the boundary layer is the outer part, where the gradient and the curvature of the velocity profile is small. Also, in about the same "layer," the conditions for applicability of the linearized theory hold. Close to the wall the results of the linearized theory for inviscid flow have no significance because of the large viscous forces, the no-slip condition for the cross flow, and the magnitude of the velocity gradients.

If the boundary layer is not too thick we may assume that $\partial p/\partial y = 0$ if y is the distance to the wall. Then

$$|\text{grad } S| = \left|\frac{\partial S}{\partial y}\right| = \frac{c_p}{T}\left|\frac{\partial T}{\partial y}\right|$$

so that the correction term in Eq. (10) can be written

$$\frac{\gamma - 1}{2} M^{(0)^2}T^{(0)}|\text{grad } S^{(1)}| = \frac{\gamma - 1}{2} M^{(0)^2}c_p \left|\frac{\partial T}{\partial y}\right|$$

Hence we may write

$$|\boldsymbol{q} \times \boldsymbol{\omega} - \frac{\gamma - 1}{2} M^{(0)^2}T^{(0)} \text{ grad } S^{(1)}| = q\omega_n + \frac{\gamma - 1}{2} M^{(0)^2}c_p \left|\frac{\partial T}{\partial y}\right|$$

where ω_n is the component of the vorticity normal to $\boldsymbol{q}$.

If the Bernoulli surfaces are at a constant distance from each other (for instance, parallel planes or coaxial cylinders), then ω_n and $\partial T/\partial y$ are constant in the inviscid flow, so that the factor

$$\left(q\omega_n + \frac{\gamma - 1}{2} M^{(0)^2}c_p \left|\frac{\partial T}{\partial y}\right|\right)$$

can be put in front of the integral in Eq. (10). The angle ϕ between the centripetal acceleration and the vector $\boldsymbol{q} \times (c_p \text{ grad } T_0 - T_0 \text{ grad } S)$ is 0 or π, depending on the orientation of the centripetal acceleration. More precisely, $\cos\phi = 1$, if the curvature vector, $\boldsymbol{q}$, and the vector normal to the wall pointing towards the fluid form a right-hand system, and $\cos\phi = -1$ if they form a left-hand system. The sign of $\cos\phi$ can also be taken into account by giving $d\vartheta$ a sign. Let $d\vartheta$ be positive if the streamline curves away from the vorticity vector and negative if it curves toward the vorticity vector. Then, Eq. (10) may be expressed as

$$\left.\frac{\omega_\sigma^{(1)}}{\rho^{(0)}q^{(0)}}\right|_1^2 = -2\left(q\omega_n + \frac{\gamma-1}{2}M^{(0)^2}c_p\left|\frac{\partial T_1}{\partial y}\right|\right)\times \int_1^2 \frac{d\vartheta}{\rho^{(0)}q^{(0)^2}} \quad (11)$$

where the index 1 refers to the position just upstream of the cascade.

For a laminar or turbulent boundary layer with Prandtl Number equal to unity along an insulated wall, the energy in the boundary layer is constant. Thus,

$$c_p\left|\frac{\partial T_1}{\partial y}\right| = \left|-q_1\frac{\partial q_1}{\partial y}\right| = q_1\,\omega_{n1}$$

and Eq. (11) becomes

$$\left.\frac{\omega_\sigma^{(1)}}{\rho^{(0)}q^{(0)}}\right|_1^2 = -2q_1^{(0)}\,\omega_{n1}^{(0)}\left(1+\frac{\gamma-1}{2}M^{(0)^2}\right)\times \int_1^2 \frac{d\vartheta}{\rho^{(0)}q^{(0)^2}} \quad (12)$$

If the mass flow density $\Theta = \rho q/\rho^* q^*$ is introduced, where the star refers to the critical condition, we have

$$\int_1^2 \frac{d\vartheta}{\rho q^2} = \frac{1}{\rho_1 q_1^2}\int_1^2 \frac{d\vartheta}{(\Theta/\Theta_1)\,(q/q_1)}$$

The ratios's q/q_1 and Θ/Θ_1 can be related to the Mach Number

$$\frac{q}{q_1} = \frac{M}{M_1}\left\{\frac{2+(\gamma-1)M_1^2}{2+(\gamma-1)M^2}\right\}^{1/2},$$

$$\frac{\Theta}{\Theta_1} = \frac{M}{M_1}\left\{\frac{2+(\gamma-1)M_1^2}{2+(\gamma-1)M^2}\right\}^{\frac{\gamma+1}{2(\gamma-1)}}$$

From the last equation it follows that

$$\frac{2+(\gamma-1)M_1^2}{2+(\gamma-1)M^2} = \left(\frac{\Theta}{\Theta_1}\frac{M}{M_1}\right)^{\frac{2(\gamma-1)}{\gamma+1}}$$

so that the equation for q/q_1 becomes

$$q/q_1 = (M/M_1)\,[(\Theta/\Theta_1)\,(M/M_1)]^{\frac{\gamma-1}{\gamma+1}}$$

Thus,

$$\int_1^2 \frac{d\vartheta}{\rho q^2} = \frac{1}{\rho_1 q_1^2}\times \int_1^2 \frac{d\vartheta}{(\Theta/\Theta_1)\,(M/M_1)\,[(\Theta/\Theta_1)\,(M/M_1)]^{\frac{\gamma-1}{\gamma+1}}} = \frac{1}{\rho_1 q_1^2}\int_1^2 \frac{d\vartheta}{[(\Theta/\Theta_1)^\gamma\,(M/M_1)]^{\frac{2}{\gamma+1}}} \quad (13)$$

If $M_1 \ll 1$, we find as an approximation

$$\frac{M}{M_1} \simeq \frac{\Theta}{\Theta_1}\left\{1+\frac{\gamma+1}{4}M_1^2\left[\left(\frac{\Theta}{\Theta_1}\right)^2-1\right]\right\}$$

which, inserted in the integral (13) gives

$$\int_1^2 \frac{d\vartheta}{\rho q^2} = \frac{1}{\rho_1 q_1^2}\left\{\left(1+\frac{1}{2}M_1^2\right)\int_1^2 \frac{d\vartheta}{(\Theta/\Theta_1)^2} - \frac{1}{2}M_1^2(\vartheta_2-\vartheta_1)\right\} \quad (14)$$

If A is the normal cross-section area of the passage, the continuity equation may be written

$$\overline{\Theta A} = \overline{\Theta_1 A_1}$$

where $\bar{\Theta}$ denotes the average mass flow density through the corresponding cross section of the passage. If furthermore, the relative variation $[(\Theta-\bar{\Theta})/\bar{\Theta}]$ is small, we may replace Θ by $\bar{\Theta}$ in Eq. (14) so that

$$\int_1^2 \frac{d\vartheta}{\rho q^2} = \frac{1}{\rho_1 q_1^2}\left\{\left(1+\frac{1}{2}M_1^2\right)\int_1^2\left(\frac{A}{A_1}\right)^2 d\vartheta - \frac{1}{2}M_1^2(\vartheta_2-\vartheta_1)\right\}$$

and the expression (12) for the secondary vorticity becomes

$$\left.\frac{\omega_\sigma^{(1)}}{\rho^{(0)}q^{(0)}}\right|_1^2 = -2\frac{\omega_{n1}^{(1)}}{\rho_1^{(0)}q_1^{(0)}}\left(1+\frac{\gamma-1}{2}M_1^{(0)^2}\right)\times \left\{\left(1+\frac{1}{2}M_1^{(0)^2}\right)\int_1^2\left(\frac{A}{A_1}\right)^2 d\vartheta - \frac{1}{2}M_1^{(0)^2}(\vartheta_2-\vartheta_1)\right\} \quad (15)$$

It is clear that in a diverging and curved passage, the form between the brackets in Eq. (15) is greater than $\int_1^2\left(\frac{A}{A_1}\right)^2 d\vartheta$ while the reverse is true for a converging channel. This means that in a compressor cascade the compressibility effects on the secondary flow are more severe than in a turbine cascade.

In order to evaluate the influence of compressibility on the generation of secondary vorticity, we will assume that $\omega_{\sigma 1} = 0$ and write Eq. (15) in the form

$$\omega_{\sigma 2} = -2\frac{A_1}{A_2}\,\omega_{n_1}\left[\int_1^2\left(\frac{A}{A_1}\right)^2 d\vartheta\right] f_1 f_2 \quad (16)$$

where

$$f_1 = 1 + [(\gamma-1)/2]M_1^2 \quad (17)$$

and

$$f_2 = 1 + \frac{1}{2}M_1^2\left[1 - \frac{\vartheta_2-\vartheta_1}{\int_1^2\left(\frac{A}{A_1}\right)^2 d\vartheta}\right] \quad (18)$$

The factor f_1 is independent of the cascade geometry and is plotted in Fig. 1. The factor f_2 depends not only on the entrance Mach Number, but also upon the cascade geometry. As an example, let us consider a cascade with a passage cross section which varies linearly with the turning angle, such that $A_2/A_1 = 1.4$. For this diverging passage, we have

$$\frac{A}{A_1} = 1 + 0.4\frac{\vartheta-\vartheta_1}{\vartheta_2-\vartheta_1}$$

Then the factor f_2 becomes

$$f_2 = 1 + (1/2)\,(1-0.69)M_1^2 = 1 + 0.16M_1^2$$

The factor f_2, together with the product $f_1 f_2$ is plotted in Fig. 1. The value of $f_1 f_2$ is 1.24 for $M_1 = 0.8$ so that for this entrance Mach Number the compressibility

correction for the secondary vorticity is 24 per cent.

The Secondary Flow far Downstream of the Cascade

The next question to consider concerns the effect of compressibility on the integration problem of the secondary flow—i.e., the problem of determination of the secondary flow associated with a given secondary vorticity field. Because of the mathematical complications involved in the calculation of a three-dimensional secondary flow, the analysis is restricted to the flow far downstream of the cascade. There, we have a secondary vorticity ω_s, which, in the linearized theory, is independent of the streamwise coordinate x and varies in a known way with the perpendicular coordinates y, z.

If the components of the secondary flow in x, y, z directions are u, v, w respectively, and u/U, v/U, w/U are small compared with unity, where U denotes the main downstream flow velocity, then it is clear that only u gives a first-order contribution to the pressure field, while v and w only contribute to the second-order pressure perturbation. The flow far downstream of the cascade has "settled down," so that, in this region, the first-order pressure field is constant. Hence, the first-order continuity equation reduces to

$$(\partial v/\partial y) + (\partial w/\partial z) = 0$$

for positions far downstream of the cascade. Then, for given secondary vorticity ω_s, the velocity components v, w must fulfill the equation

$$(\partial w/\partial y) - (\partial v/\partial z) = \omega_s$$

Clearly, the problem of determination of v and w is the same as for incompressible flow. It should be emphasized, however, that this is only true for the linearized analysis and far downstream of the cascade.

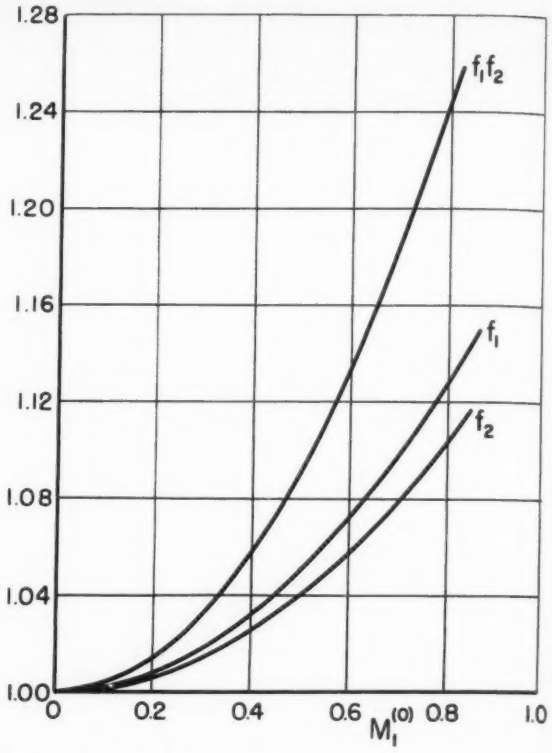

FIG. 1. Compressibility correction factors for secondary vorticity.

References

[1] Squire, H. B., and Winter, K. G., *The Secondary Flow in a Cascade of Airfoils in a Nonuniform Stream*, Journal of the Aeronautical Sciences, Vol. 18, No. 4, pp. 271–277, April, 1951.

[2] Hawthorne, W. R., *Secondary Circulation in Fluid Flow*, Proc. of the Royal Society of London, Series A, Vol. 206, No. A 1086, May, 1951.

Changes of Address

Since the Post Office Department does not as a rule forward magazines to forwarding addresses, it is important that the Institute be notified of changes in address 30 days in advance of publishing date to ensure receipt of every issue of the JOURNAL and REVIEW.

Notices should be printed legibly and sent directly to:

Institute of the Aeronautical Sciences, Inc.

2 East 64th Street, New York 21, New York

Readers' Forum

BRIEF REPORTS of investigations in the aeronautical sciences and discussions of papers published in the JOURNAL are presented in this special department. Entries must be restricted to a maximum of 1,300 words or the equivalent of one JOURNAL page including formulas and illustrations. Publication is completed as soon as possible after receipt of the material. The Editorial Committee does not hold itself responsible for the opinions expressed by the correspondents.

Contents

Effects of Pressure Gradient and Heat Transfer on the Stability of the Compressible Laminar Boundary Layer ..... NORMAN M. SHAPIRO 81

Graphical Aids for Frequency Response Analysis ..... HOMER D. ECKHARDT 83

On the Role of Reynolds Stresses in Stability Theory ..... J. T. STUART 86

Generalized Crippling Analysis of Formed Sections ..... GEORGE GERARD 88

The Transonic Flow Hydraulic Analogy ..... R. A. A. BRYANT 90

The Forces on the General Slender Body of Elliptic Cross Section in Supersonic Flow ..... H. PORTNOY 91

The Lift of a Blowing Wing in a Parallel Stream ..... D. A. SPENCE 92

A Note on Methods for the Determination of Transient Stresses ..... J. W. MAR, T. H. H. PIAN, AND J. M. CALLIGEROS 94

Double and Triple Correlations Behind a Heated Grid ..... A. L. KISTLER, V. O'BRIEN, AND S. CORRSIN 96

Effects of Pressure Gradient and Heat Transfer on the Stability of the Compressible Laminar Boundary Layer

Norman M. Shapiro

Research Division, Ordnance Missile Laboratories, Redstone Arsenal, Huntsville, Ala.

June 7, 1955

LOW'S PUBLICATION[1] of an accurate method for calculating the flow characteristics of compressible laminar boundary layers with heat-transfer and small pressure gradients has made possible the calculation, by the approximate formula of Lees,[2] of the minimum critical (neutral) Reynolds Number of thin airfoils with heat transfer. Calculations of minimum critical Reynolds Numbers for flat plates with variable wall-to-free-stream temperature ratio have been given by Van Driest,[3] for insulated airfoils by Lees,[4] Weil,[5] and Laurmann,[6] and Low[7] has determined the cooling requirements for complete stability for several pressure gradients.

Low's solution for the laminar boundary layer is obtained by a method of perturbation on the flat-plate solution of Chapman and Rubesin.[8] A linear viscosity-temperature relationship is assumed and results are tabulated for a Prandtl Number of 0.72 and an isothermal wall. Van Driest's calculations indicate that the assumption of a linear viscosity-temperature relationship introduces considerable error into the stability calculations for free-stream Mach Numbers greater than 3. For this reason, the present calculations have been limited to Mach Numbers of 3 and below. However, it will be seen that the effect of pressure gradient on minimum critical Reynolds Number decreases with increasing Mach Number in the regions far removed from complete stability.

Lee's formula for minimum critical Reynolds Number becomes, in Low's notation,

$$Re_{x,cr} = \left\{ \frac{25[t^*(c)]^2 C}{c^4 \sqrt{1 - M_e^2(1-c)^2}} \left(\frac{u^{*\prime}}{t^*} \right)_w \right\}^2 \frac{p_e^*}{4C} \tag{1}$$

The quantity c is the phase velocity of the disturbance divided by u_e and is the quantity which simultaneously satisfies the following equations:

$$V = \frac{-\pi c u_e^* u^{*\prime}(0)}{(t_w^*)^2} \left[\frac{t^{*2}}{(u^{*\prime})^2} \left(\frac{u^{*\prime\prime}}{u^{*\prime}} - \frac{2t^{*\prime}}{t^*} \right) \right]_c \tag{2}$$

$$V = \frac{0.580(1+\lambda)}{1 - 0.960\,\lambda + 0.570\,\lambda^2} \tag{3}$$

where λ, the wave length of the disturbance, is obtained from

$$\lambda = \frac{u^{*\prime}(0) I t^*(\eta_c)}{u_e^* t_w^* c} - 1 \tag{4}$$

The starred quantities p^*, t^*, and u^* in Eqs. (2) to (4) refer to local values of pressure, temperature, and velocity divided by their respective reference quantities. They may be determined from references 1 and 7 once the Mach Number, wall temperature ratio, and pressure gradient have been prescribed. Derivatives are

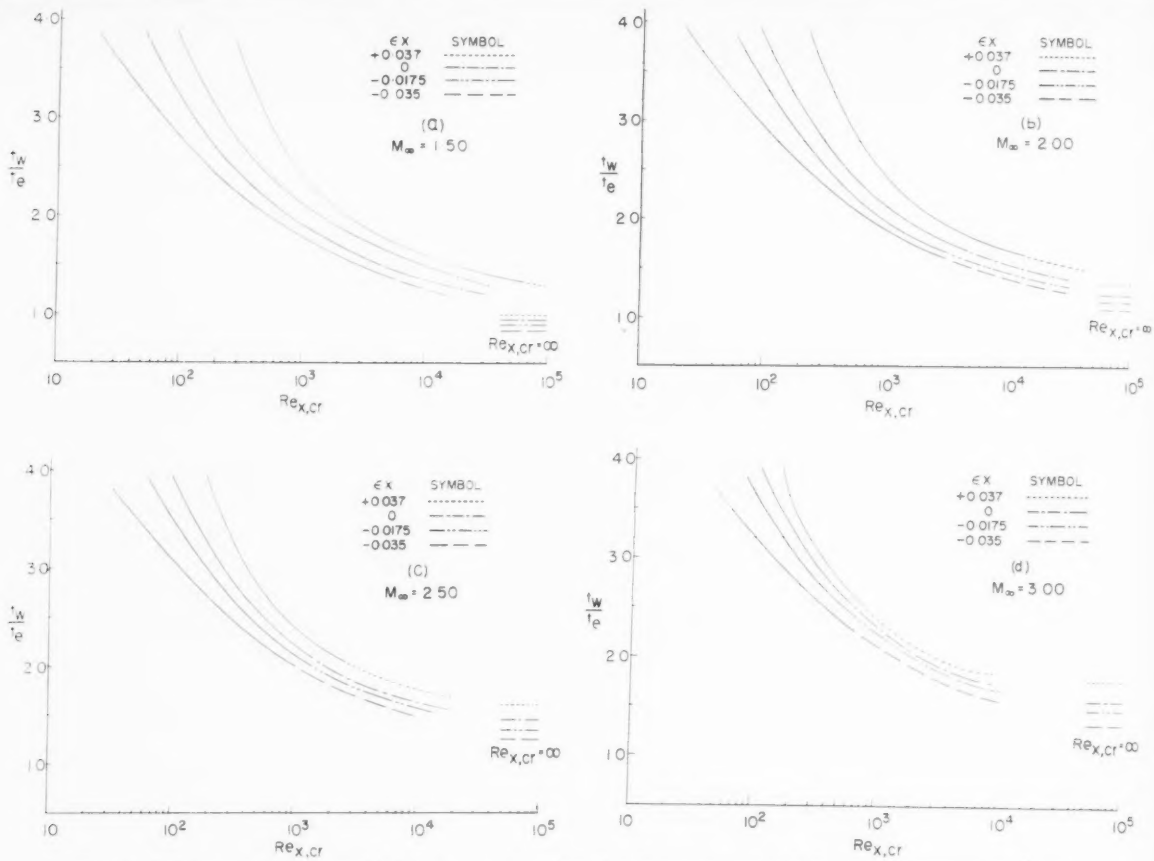

FIG. 1. Minimum critical Reynolds Number as a function of wall temperature ratio for several pressure gradients.

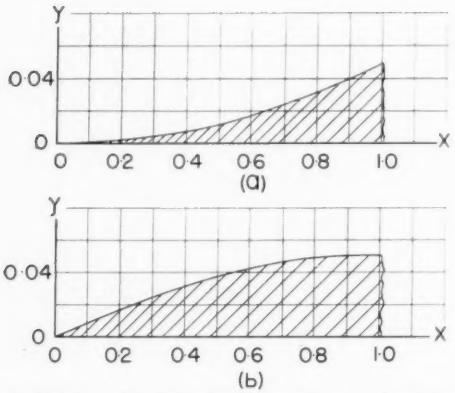

FIG. 2. Airfoils with (a) adverse pressure gradient and (b) favorable pressure gradient.

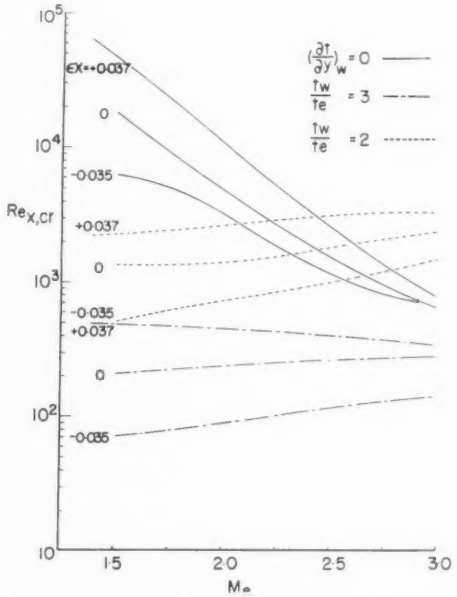

FIG. 3. Minimum critical Reynolds Number as a function of Mach Number.

taken with respect to the characteristic variable, η, which is also defined in reference 1. Subscripts e, r, and w refer to conditions at the edge of the boundary layer, reference conditions, and wall conditions, respectively. The constant, C, in the viscosity-temperature relationship is defined by

$$C = \sqrt{t_w/t_r}\ [(t_r + 216°\text{R.})/(t_w + 216°\text{R.})] \quad (5)$$

$$It^*(\eta_e) = \int_0^{\eta_e} t^*(\xi)\, d\xi \quad (6)$$

The velocity at the edge of the boundary layer, u_e, is related to a reference velocity, u_r, by

$$(u_e/u_r) = u_e^* = 1 + \epsilon x \quad (7)$$

which leads to a pressure gradient parameter $(x/u_r)(du_e/dx) = \epsilon x$. The reference velocity[1] is determined by the free-stream Mach Number and the coordinates of the particular airfoil under consideration, and ϵ is a small quantity which is a measure of the shape and magnitude of the velocity distribution at the outer edge of the boundary layer.

Eqs. (2) and (3) have been solved for $\epsilon x = -0.035$, -0.0175, 0, and $+0.037$ for several free-stream Mach Numbers and wall temperature ratios. The results are presented in Fig. 1. Negative values of ϵx indicate unfavorable pressure gradients, and positive values indicate favorable pressure gradients.

The pressure gradients used in the examples are typical of those that might be encountered on the constant pressure gradient airfoils of reference 1 which are shown in Fig. 2. Since ϵx varies with distance along an airfoil with a constant pressure gradient, the minimum critical Reynolds Number for a particular value of ϵx can be applied at only one point on the airfoil.

The wall temperature ratios investigated included both heated walls (indicated by solid curves) and cooled walls (dashed portions of curves). Also shown on Fig. 1 are the wall temperature ratios required for complete stability (infinite Reynolds Numbers).

It can be seen from Fig. 1 that effects of heating or cooling on minimum critical Reynolds Number are considerably stronger than the effects of the small but conventional pressure gradients considered here. The rapid increase in minimum critical Reynolds Number with small changes in temperature as infinite Reynolds Numbers are approached, which indicates radical changes in the boundary layer near complete stability, has already been noted by Van Driest.[3]

In Fig. 3 some of the present data are plotted as a function of Mach Number for two wall temperature ratios and for zero heat transfer. Laurmann has pointed out that an unfavorable pressure gradient produces a decrease in stability with increasing Mach Number for an insulated wall. The present data show the same trend for an insulated wall but show the opposite effect for flows with heat transfer. The decrease in pressure gradient effectiveness with increasing Mach Number can also be seen in Fig. 3.

It should be noted that the present calculations are restricted to the effects of two-dimensional disturbances. Dunn and Lin[9] have recently considered the effects of three-dimensional disturbances and found that these disturbances can be more destabilizing than two-dimensional disturbances at supersonic Mach Numbers. In addition, they have obtained improved viscous solutions of the stability equation which are more accurate than those of reference 2 for calculating minimum critical Reynolds Numbers at supersonic Mach Numbers. These solutions, however, are only accurate for minimum critical Reynolds Number up to a Mach Number of 2 and do not significantly change the values of wall temperature ratios required for completely stability of two-dimensional disturbances.

References

[1] Low, George M., *The Compressible Laminar Boundary Layer with Heat Transfer and Small Pressure Gradient*, NACA TN No. 3028, October, 1953.

[2] Lees, Lester, *The Stability of the Laminar Boundary Layer in a Compressible Fluid*, NACA TR No. 876, 1947.

[3] Van Driest, E. R., *Calculation of the Stability of the Laminar Boundary Layer in a Compressible Fluid on a Flat Plate with Heat Transfer*, Journal of the Aeronautical Sciences, Vol. 19, No. 12, p. 801, December, 1952.

[4] Lees, Lester, *Stability of Supersonic Boundary Layers with a Pressure Gradient*, Princeton University, Aeronautical Engineering Laboratory, Report No. 167, 1950.

[5] Weil, Herschel, *Effect of Pressure Gradient on Stability and Skin Friction in Laminar Boundary Layers in Compressible Fluids*, Journal of the Aeronautical Sciences, Vol. 18, No. 5, p. 311, May, 1951.

[6] Laurmann, J. A., *Stability of the Compressible Laminar Boundary Layer with an External Pressure Gradient*, The College of Aeronautics, Cranfield, Report No. 48, September, 1951.

[7] Low, George M., *Cooling Requirements for Stability of Laminar Boundary Layer with Small Pressure Gradient at Supersonic Speeds*, NACA TN No. 3103, March, 1954.

[8] Chapman, Dean R., and Rubesin, Morris W., *Temperature and Velocity Profiles in the Compressible Laminar Boundary Layer with Arbitrary Distribution of Surface Temperature*, Journal of the Aeronautical Sciences, Vol. 16, No. 9, p. 547, September, 1949.

[9] Dunn, D. W., and Lin, C. C., *On the Stability of the Laminar Boundary Layer in a Compressible Fluid—Part I*, Massachusetts Institute of Technology, Department of Mathematics, December, 1953.

Graphical Aids for Frequency Response Analysis

Homer D. Eckhardt*

Aviation Systems Laboratory, Radio Corporation of America, Waltham, Mass.

July 1, 1955

In the investigation of the behavior of closed loop dynamic systems by means of "frequency response" methods, it is often desirable to obtain plots of the logarithm of the amplitude ratio of of the frequency response of a system versus the phase angle of that response as a function of frequency.[1] For brevity, such plots are often referred to as "gain-phase" plots. Further, during the evolution of the design of such a dynamic system, it is often desired to obtain further gain-phase plots which differ from a previous gain-phase plot only by the addition, elimination, or slight modification of a very few simple dynamic elements in the system being investigated.

Gain-phase plots are commonly obtained either by plotting from tables of experimental data, or from tables of computed data, or by cross-plotting from plots of amplitude ratio and phase angle versus frequency. The modified gain-phase plots are ordi-

* Formerly, Research Engineer, Flight Control Laboratory, Massachusetts Institute of Technology, where this paper was prepared.

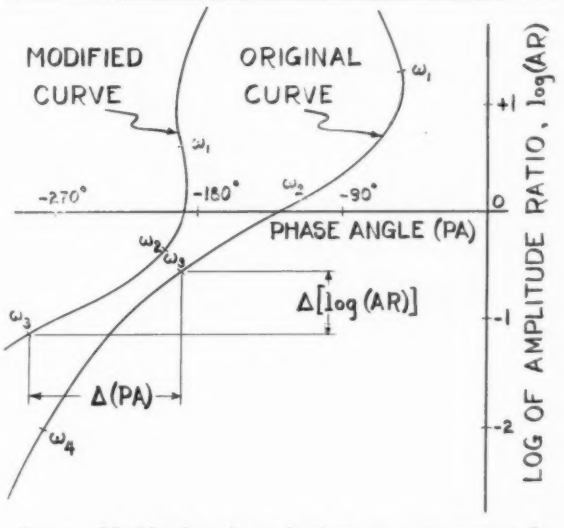

FIG. 1. Modification of a gain-phase curve to account for the cascading of a modifying transfer function with the original transfer function.

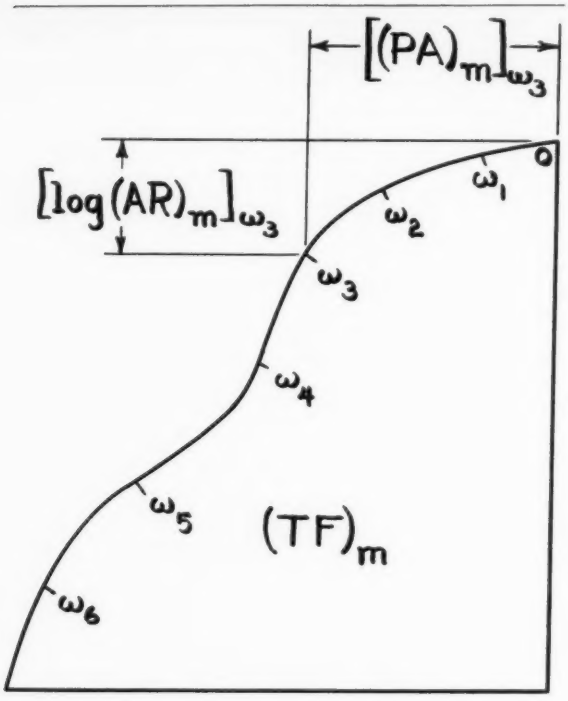

FIG. 2. Possible configuration of a template for use in modifying a gain-phase plot to account for the cascading of a transfer transfer function $(TF)_m$ with the original transfer function.

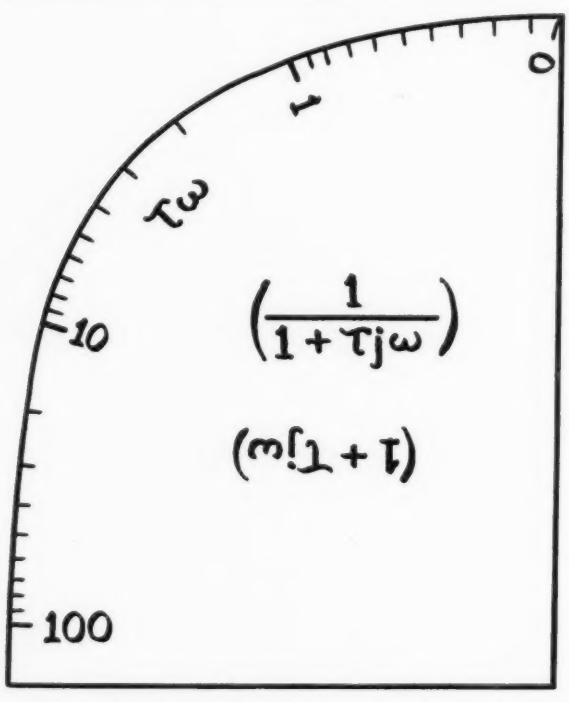

FIG. 4. A form of a template for use in modifying a gain-phase plot to account for the cascading of an element whose transfer function is $[1/(1 + \tau j\omega)]$ or $(1 + \tau j\omega)$.

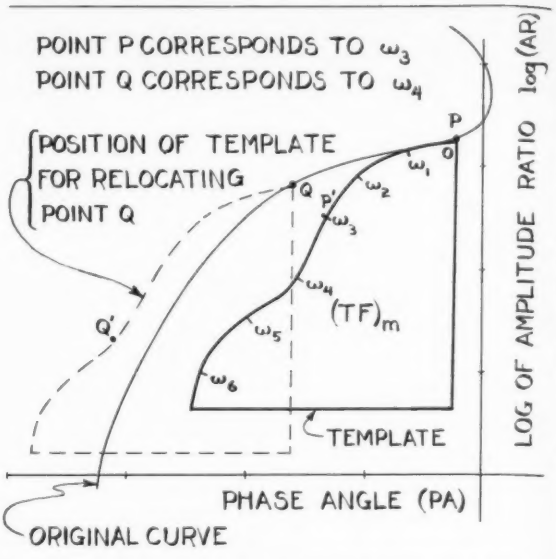

FIG. 3. Use of a template to modify a gain-phase curve graphically.

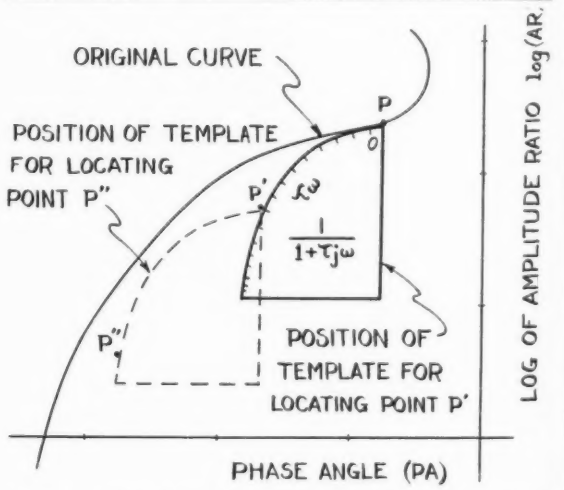

FIG. 5. Use of a template for the transfer function $[1/(1 + \tau j\omega)]$ to modify a gain-phase curve to account for the cascading of an element whose transfer function contains complex roots.

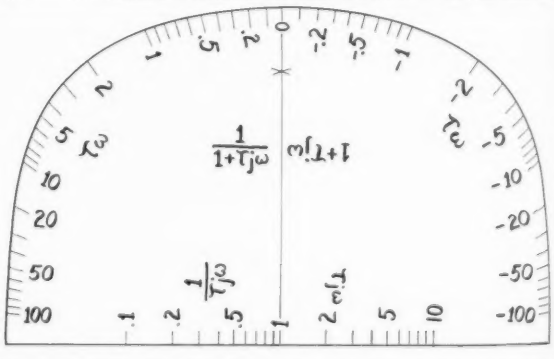

FIG. 6. A template for the direct construction or modification of gain-phase diagrams involving any linear transfer functions.

narily obtained by performing additional computations in the original table or by suitably modifying the plots of amplitude ratio and phase angle versus frequency and then from this new data plotting a new gain-phase plot. If the need for recourse to these tables or curves of amplitude ratio and phase angle versus frequency could be eliminated and a simple graphical method for directly modifying the original gain-phase curve could be devised, much work and opportunity for error could be removed from frequency response analysis.

To visualize the graphical system presently used by the author[2] for this direct modification, consider a fragment of a gain-phase curve as shown in Fig. 1.

In Fig. 1, the original gain-phase curve which is to be modified has been plotted and values of frequency, ω, in rad. per sec. have been indicated at appropriate intervals along the curve.

Note now that, if the curve is to be modified by the cascading of a new transfer function with the original transfer function, in general each point on the original curve will be moved to a new position, which position will be determined by the phase shift and amplitude ratio of the modifying transfer function at the frequency corresponding to the point being moved. For instance in the case of point P at frequency ω_2 in Fig. 1, the shift in phase has been by an amount $\Delta(PA)$ and since a logarithmic amplitude ratio scale has been used, the amplitude ratio shift has been $\Delta[\log (AR)]$, where $\Delta(PA)$ and $\Delta[\log (AR)]$ are a phase shift and log of an amplitude ratio respectively associated with the modifying transfer function. To see the manner in which this occurs, consider the three transfer functions $(TF)_o$ and $(TF)_m$ and $(TF)_r$, all at a given value of frequency where the subscripts o, m, and r indicate original, modifying, and resulting, respectively.

$$(TF)_o = (AR)_o e^{j(PA)o}$$
$$(TF)_m = (AR)_m e^{j(PA)m}$$
$$(TF)_r = (AR)_r e^{j(PA)r}$$

Then if $(TF)_o(TF)_m = (TF)_r$, it can be seen that

$$(AR)_r e^{j(PA)r} = (AR)_o(AR)_m e^{j[(PA)o + (PA)m]}$$

Then
$$(PA)_r = (PA)_o + (PA)_m$$
$$(AR)_r = (AR)(AR_o)_m$$

or
$$\log (AR)_r = \log (AR)_o + \log (AR)_m$$

Thus it can be seen that the cascading of transfer functions results in the addition of the phase shifts and the addition logs of their amplitude ratios. These additions correspond to the additions of linear distances on a plot of the form shown in Fig. 1.

Consider then that a template is cut in the shape of the gain-phase plot of the new modifying transfer function as shown in Fig. 2. Consider also an original curve as shown in Fig. 3 which is to be modified by the cascading of $(TF)_m$. Then, by placing the point marked 0 on the template on the point P as shown in Fig. 3 and aligning the template axes parallel to the axes of Fig. 3, a point P′ may be located on the modified curve by placing a mark next to the point labeled ω_2 on the template. To relocate a second point, Q, the point marked 0 on the template is placed at Q, and the new point Q′ is located by placing a mark next to ω_4 on the template. Obviously, the whole modified curve may then be located in this way by repeating the above procedure at points corresponding to the other frequencies of interest.

Ordinarily, a template for a particular modifying transfer function would have limited use unless that same transfer function were to be used repeatedly in a problem. There are, however, several simple transfer functions which are frequently used and whose frequency scales may be nondimensionalized simply. One such function is that which is expressed in Laplace form as $1/(1 + \tau p)$ and in frequency response form as $1/(1 + \tau j\omega)$ where τ is a real time constant and ω is a real frequency. A template for the phase and amplitude increments of the frequency response of this transfer function would appear much as in Fig. 4 where the scales on the edge of the template are of $\tau\omega$ instead of the dimensional ω.

Now if a transfer function is expressed as

$$(TF)_a = (AR)_a e^{j(PA)a}$$

and if a second transfer function $(TF)_b$ is its reciprocal,

$$(TF)_b = 1/(TF)_a$$

then

$$(AR)_b e^{j(PA)b} = [1/(AR)_a] e^{-j(PA)a}$$

or

$$(AR)_b = [1/(AR)_a] \quad \text{or} \quad \log (AR)_b = -\log (AR)_a$$
$$(PA)_b = -(PA)_a$$

Then it can be seen that the phase shift and log of the amplitude ratio of the transfer function $(1 + \tau j\omega)$ at any given frequency will be equal to the negatives of the phase shift and log of amplitude ratio respectively of the transfer function $[1/(1 + \tau j\omega)]$. From this fact it may be deduced that the template of Fig. 4 can be rotated in the plane of the page by 180° for use in connection with the transfer function $(1 + \tau j\omega)$. Another simple template may be developed for the pair of transfer functions $(\tau j\omega)$ and $(1/\tau j\omega)$.

It is apparent then that by the use of templates of the above described form, the gain-phase diagram of any linear transfer function can be modified directly and graphically to account for cascading in series with the given transfer function an element having a transfer function in the Laplace form $(1 + \tau p)$, $[1/(1 + \tau p)]$, τp, or $(1/\tau p)$. It may also be noted that this modified or resulting gain-phase curve may be further modified in the same manner as was the original curve in order to account for the cascading of a second element having a transfer function in Laplace form $(1 + \tau p)$, $[1/(1 + \tau p)]$, τp, or $(1/\tau p)$. Realizing then, that this modification procedure can be repeated as often as desired, consider the case wherein the original transfer function is taken to be unity. The gain-phase plot of such a transfer function is merely a point. Then by successively modifying the gain-phase plot of this transfer function by use of the templates described herein, a gain-phase plot representing the frequency response of any transfer function whose Laplace form is as follows may be constructed.

$$(TF) = 1\left[\frac{p^q(1 + \tau_1 p)(1 + \tau_2 p) \ldots (1 + \tau_m p)}{p^r(1 + \tau_{(m+1)} p)(1 + \tau_{(m+2)} p) \ldots (1 + \tau_n p)}\right]$$

where all of the τ's are real.

The poles and zeros of any transfer function of this type lie on the real axis when plotted in the complex p plane.

It is desirable to circumvent the restrictions imposed above by the requirement that poles and zeros in the transfer function must lie on the real axis in the complex p plane. To develop a method for handling those transfer functions which have complex poles and zeros, note that those poles or zeros always appear in conjugate pairs and that in the factored form of the transfer function each pair is represented by a factor which may be written in the Laplace form as

$$(p^2/\omega_n^2) + 2\zeta(p/\omega_n) + 1$$

where ω_n is positive and real and $-1 < \zeta < +1$.

In the frequency response form this factor may be expressed as

$$(j\omega/\omega_n)^2 + 2\zeta(j\omega/\omega_n) + 1$$

This factor may be factored to give

$$\zeta^2\left[1 + j\left(\frac{\omega}{\zeta\omega_n} + \frac{\sqrt{1 - \zeta^2}}{\zeta}\right)\right]\left[1 + j\left(\frac{\omega}{\zeta\omega_n} - \frac{\sqrt{1 - \zeta^2}}{\zeta}\right)\right]$$

which may be expressed as

$$\zeta^2(1 + \tau_1 j\omega)(1 + \tau_2 j\omega)$$

where
$$\tau_1\omega = (\omega/\zeta\omega_n) + (\sqrt{1 - \zeta^2}/\zeta)$$
$$\tau_2\omega = (\omega/\zeta\omega_n) - (\sqrt{1 - \zeta^2}/\zeta)$$

From this it is seen that the factor representing a pair of complex poles or zeros can be treated in a manner quite similar to two real poles or zeros but that the τ's involved are not constant.

A procedure which may be followed in modifying a gain-phase curve to account for the cascading with the original transfer func-

tion of a transfer function having a pair of complex roots in the complex p plane is as follows. Referring to Fig. 5, the curve is to be modified to account for the cascading of an additional transfer function

$$\frac{K_m}{[(j\omega/\omega_n)^2 + 2\zeta(j\omega)/\omega_n) + 1]}$$

As seen above, this modifying transfer function may be written as

$$\frac{K_m}{\zeta^2(1 + \tau_1 j\omega)(1 + \tau_2 j\omega)}$$

To relocate the point P in Fig. 5, the template for $1/(1 + \tau j\omega)$ is positioned as shown in Fig. 5 with the point O on the point P and knowing the frequency ω corresponding to point P, and the values of ζ and ω_n, the appropriate value of $\tau_1\omega$ is quite easily computed and a point P′ is located next to that value of $\tau\omega$ on the template scale. Then the template is repositioned as shown by dashed lines such that its point O is on the point P′ just plotted and again, knowing ω, ζ, and ω_n, the value of $\tau_2\omega$ is computed and a point P'' is plotted next to that value of $\tau\omega$ on the template scale. This point P″ is then the relocated position of point P. This procedure may be repeated at as many points of the original curve as desired and the modified curve is faired through the double-primed points.

Note now that the transfer function which has been cascaded is

$$\frac{1}{(1 + \tau_1 j\omega)(1 + \tau_2 j\omega)} = \left\{\frac{K_m}{[(j\omega/\omega_n)^2 + 2\zeta(j\omega/\omega) + 1]}\right\}\left(\frac{\zeta^2}{K_m}\right)$$

Thus, it must be remembered that when a final open loop gain, K_{OL}, is chosen for the modified system on the basis of this gain-phase diagram, that gain is

$$K_{OL} = K_O(K_m/\zeta^2)$$

where K_O is the total gain of the system, exclusive of this modifying transfer function.

At first glance, it appears that the computations of $\tau_1\omega$ and $\tau_2\omega$ are inconvenient but when it is realized that ζ and ω_n are constants for a given pair of complex poles or zeros, it becomes apparent that

$$\tau_1\omega = (\omega/k_1) + k_2$$

$$\tau_2\omega = (\omega/k_1) - k_2$$

where k_1 and k_2 are easily computed constants.

It will be noted that the value of $\tau_2\omega$ is negative at low frequencies and will become positive at higher frequencies. To provide for this, the template for $1/(1 + \tau j\omega)$ and $(1 + \tau j\omega)$ should be extended to negative values of $\tau\omega$. An alternative procedure is to note that at any given frequency, the phase angle associated with $(1 - \tau j\omega)$ is the negative of the phase angle associated with $(1 + \tau j\omega)$ and that their amplitude ratios are the same. Then if a suitable transparent template has been made for $(1 + \tau j\omega)$, this template need only be rotated 180° about a line of constant phase and used in this reversed position for the negative value of $\tau\omega$. The same effect may be obtained by using the template in its usual attitude but on the back side of the plotting paper when negative $\tau\omega$'s are encountered.

Conclusions

The author has found that a single template of the form shown in Fig. 6 can be used to construct graphically a gain-phase plot for a system resulting from the cascading of any linear transfer function whose factors are known, with a transfer function whose gain-phase plot has already been made, and to perform this graphical construction quickly and easily directly on the original gain-phase plot.

Obviously, the construction of any gain-phase plot, the transfer function for which is known in factored form, becomes merely a special case of the above procedure.

References

[1] James, H. M., Nichols, N. B., and Phillips, R. S. (Ed.), *Theory of Servomechanism*, Vol. 25, Radiation Laboratory Series; McGraw-Hill Book Company, Inc., New York, 1947.

[2] Markusen, D. L., and Graves, M. H., *Attenuation and Phase Characteristics of Linear Systems*, Minneapolis-Honeywell Aeronautical Report AR 2426-R6, December 20, 1951.

On the Role of Reynolds Stresses in Stability Theory*

J. T. Stuart

National Physical Laboratory, Department of Scientific and Industrial Research, Aerodynamics Division, Teddington, England

June 20, 1955

Recently Pai[1] advanced an argument which, on the assumptions implied, shows that two-dimensional parallel flows are stable against periodic disturbances of finite magnitude. This conclusion contradicts the work of Meksyn and Stuart,[2] who have shown theoretically that pressure flow between parallel planes is unstable for both finite and infinitesimal disturbances. Since the difference between the conclusions of these two papers is a fundamental one involving the interpretation of the role of the Reynolds stresses in finite-disturbance theory, it is important to show exactly how the discrepancy arises. An additional reason for emphasizing it is that other authors[3,4] have argued in favor of universal stability in a similar way. On grounds of the simplicity of its mathematics, attention is mainly focussed on Pai's paper, for then the physical ideas are more easily discussed.

Consider a two-dimensional flow between parallel planes, x being the distance parallel to the planes and y the distance normal to them, u and v being the corresponding velocity components. Let p denote pressure, ρ density, ν kinematic viscosity, and t time. Then the Navier-Stokes equations are

$$\frac{\partial u}{\partial t} + u\frac{\partial u}{\partial x} + v\frac{\partial u}{\partial y} = -\frac{1}{\rho}\frac{\partial p}{\partial x} + \nu\left(\frac{\partial^2 u}{\partial x^2} + \frac{\partial^2 u}{\partial y^2}\right) \quad (1)$$

$$\frac{\partial v}{\partial t} + u\frac{\partial v}{\partial x} + v\frac{\partial v}{\partial y} = -\frac{1}{\rho}\frac{\partial p}{\partial y} + \nu\left(\frac{\partial^2 v}{\partial x^2} + \frac{\partial^2 v}{\partial y^2}\right) \quad (2)$$

$$(\partial u/\partial x) + (\partial v/\partial y) = 0 \quad (3)$$

The mean motion in this case is $u = \bar{u}(y)$, $v = 0$; that is, the flow is independent of distance downstream. Consider a finite disturbance u', v' of the mean flow; thus $u = \bar{u} + u'$, $v = v'$, where

$$u = \bar{u} + u' = \bar{u}(y, t) + u_1'e^{i\alpha x} + u_2'(y, t)e^{2i\alpha x} + \ldots + \bar{u}_1'e^{-i\alpha x} + \bar{u}_2'(y, t)e^{-2i\alpha x} + \ldots \quad (4)$$

$$v = v' = v_1'e^{i\alpha x} + v_2'(y, t)e^{2i\alpha x} + \ldots + \bar{v}_1'(y, te)^{-i\alpha x} + \bar{v}_2'(y, t)e^{-2i\alpha x} + \ldots \quad (5)$$

(the symbol $\sim$ denotes a complex conjugate).

This is a harmonic disturbance of wave length $2\pi/\alpha$, and is the type of perturbed flow examined by Meksyn and Stuart. Now in laminar flow and in laminar flow perturbed by an infinitesimally small disturbance, the mean motion is controlled by viscous stresses and pressure gradients, and its equation is

$$0 = -(1/\rho)(\partial\bar{p}/\partial x) + \nu(\partial^2\bar{u}/\partial y^2) \quad (6)$$

Now when the flow is perturbed by a *finite* disturbance, momentum is transferred by the finite fluctuations and a system of stresses, known as the Reynolds stresses, results. With these stresses accounted for, the equations of mean motion are

$$\frac{\partial\bar{u}}{\partial t} + \overline{u'\frac{\partial u'}{\partial x}} + \overline{v'\frac{\partial u'}{\partial y}} = -\frac{1}{\rho}\frac{\partial\bar{p}}{\partial x} + \nu\frac{\partial^2\bar{u}}{\partial y^2} \quad (7)$$

$$\overline{u'\frac{\partial v'}{\partial x}} + \overline{v'\frac{\partial v'}{\partial y}} = -\frac{1}{\rho}\frac{\partial\bar{p}}{\partial y} \quad (8)$$

where a bar above a quantity denotes an average with the dis-

* This work has been carried out as part of the research program of the National Physical Laboratory, and this paper is published by permission of the Director of the Laboratory.

tance x. The argument of reference 1 is based on Eq. (6) even for finite disturbances and therefore assumes implicitly that only viscous stresses and pressure gradient affect the mean motion, which is not correct. The effect of this on the disturbance Eqs. (10) and (11) is noted later.

In the case of neutral traveling waves the average with distance is equivalent to an average in time, but with damped or amplified oscillations an exponential dependence on time remains. Since the quantities $\overline{u'^2}$, $\overline{v'^2}$ $\overline{u'v'}$ are independent of x, the Reynolds stresses in Eqs. (7) and (8) may be written $(\partial/\partial y)(\overline{u'v'})$ and $(\partial/\partial y)(\overline{v'^2})$ respectively, when use is made of the equation of continuity. The dependence of $\bar{u}$ on t is retained because if the disturbance is amplifying or decaying, the mean motion also suffers modifications in order to maintain the energy balance; this point is referred to again later.

By subtraction of Eq. (7) from Eq. (1) and Eq. (8) from Eq. (2), the equations for the perturbation motion are found without approximation to be

$$\frac{\partial u'}{\partial t} + \bar{u}\frac{\partial u'}{\partial x} + v'\frac{\partial \bar{u}}{\partial y} + X_1 = -\frac{1}{\rho}\frac{\partial p'}{\partial x} + \nu\left(\frac{\partial^2 u'}{\partial x^2} + \frac{\partial^2 u'}{\partial y^2}\right) \quad (9)$$

$$\frac{\partial v'}{\partial t} + \bar{u}\frac{\partial v'}{\partial x} + X_2 = -\frac{1}{\rho}\frac{\partial p'}{\partial y} + \nu\left(\frac{\partial^2 v'}{\partial x^2} + \frac{\partial^2 v'}{\partial y^2}\right) \quad (10)$$

$$(\partial u'/\partial x) + (\partial v'/\partial y) = 0, \quad (11)$$

where

$$X_1 = u'\frac{\partial u'}{\partial x} + v'\frac{\partial u'}{\partial y} - \overline{u'\frac{\partial u'}{\partial x}} - \overline{v'\frac{\partial u'}{\partial y}} \quad (12)$$

$$X_2 = u'\frac{\partial v'}{\partial x} + v'\frac{\partial v'}{\partial y} - \overline{u'\frac{\partial v'}{\partial x}} - \overline{v'\frac{\partial v'}{\partial y}} \quad (13)$$

The disturbance equations of reference 1 differ from these because they do not include the averaged quadratic qualities of X_1 and X_2. It is important to note that X_1 and X_2 are harmonic in x of wave length $2\pi/\alpha$, as are all the other terms in the disturbance equations, whereas the disturbance equations of reference 1 wrongly include (nonharmonic) terms which should be in the mean-motion equations.

Now let us consider the energy contained within a volume bounded by the planes $y = \pm h$, and by $x = 0$ and $2\pi/\alpha$. Then the balance of energy within this volume yields in the usual way

$$\frac{\partial E_1}{\partial t} = \frac{\partial}{\partial t}\iint \frac{1}{2}\rho(u'^2 + v'^2)dx\,dy = -\iint \rho u'v'\frac{\partial \bar{u}}{\partial y}\,dx\,dy - \mu\iint\left(\frac{\partial v'}{\partial x} - \frac{\partial u'}{\partial y}\right)^2 dx\,dy \quad (14)$$

where E_1 denotes the energy of the disturbance contained in the volume. Pai obtains this relation correctly, because the quadratic terms, X_1 and X_2, of the disturbance equations integrate out. In the first integral on the right-hand side, $u'v'$ may be replaced by $\overline{u'v'}$ because only the mean terms contribute to the integral. The left-hand side of the above energy relation gives the rate of increase of the disturbance energy within the volume. On the right-hand side, the first integral gives the rate of transfer of energy from the mean flow to the disturbance, while the second integral, which is necessarily always positive, represents the viscous dissipation of energy. If the first integral is negative, energy is transferred to the disturbance and if it is greater than the dissipation, instability results. Now by multiplying Eq. (9) by $\bar{u}$, integrating throughout the domain and using the incomplete version of X_1 (without the averaged terms), Pai obtains

$$+\iint \rho u'v'\frac{\partial \bar{u}}{\partial y}\,dx\,dy = \rho\frac{\partial}{\partial t}\iint \bar{u}u'dx\,dy - \mu\iint u'\frac{\partial^2 \bar{u}}{\partial y^2}dx\,dy \quad (15)$$

He then points out that, since u' is a harmonic function of x, the integrals (linear in u') on the right-hand side are zero. Thus, he concludes that the energy-supply integral $\iint \rho u'v'(\partial\bar{u}/\partial y)dx\,dy$ is zero. However, if we use the complete expression for X_1 and follow a similar procedure we obtain

$$-\iint \rho\bar{u}X_1 dx\,dy = \rho\iint \bar{u}\frac{\partial u'}{\partial t}\,dx\,dy - \mu\iint u'\frac{\partial^2 \bar{u}}{\partial y^2}dx\,dy \quad (16)$$

Since X_1 is a harmonic function of x, as is u', this relation is merely the identity $0 \equiv 0$, and no information is obtained about the energy-supply integral. Consequently, in general,

$$\iint \rho u'v'\frac{\partial \bar{u}}{\partial y}\,dx\,dy \neq 0. \quad (17)$$

From his deduction that this integral *is* zero, Pai concludes that the flow is stable because the rate of increase of disturbance energy Eq. (14) is then negative and is accounted for by the viscous dissipation. The analysis given above shows this conclusion to be fallacious. Particular values of the energy-supply integral above have been calculated by Meksyn and Stuart[2] for finite and infinitesimal disturbances, and that the energy-supply is nonzero is confirmed both by their work and by that of others.

As a matter of interest, the mean-motion energy equation may be evaluated as

$$\frac{\partial E_0}{\partial t} = \frac{\partial}{\partial t}\iint \frac{1}{2}\rho\,\bar{u}^2\,dx\,dy = +\iint \rho u'v'\frac{\partial \bar{u}}{\partial y}\,dx\,dy - \iint \bar{u}\frac{\partial \bar{p}}{\partial x}\,dx\,dy - \mu\iint\left(\frac{\partial \bar{u}}{\partial y}\right)^2 dx\,dy, \quad (18)$$

where E_0 is the energy contained within the mean flow.

The left-hand side represents the rate of increase of the mean-flow energy. On the right-hand side, the first term gives the energy transfer to the disturbance (and is the complement of the energy-supply integral in the disturbance energy equation), the second term gives the work done by the pressure gradient to maintain the motion, and the third integral gives the viscous dissipation of the mean flow. For a neutral oscillation, both $\partial E_0/\partial t$ and $\partial E_1/\partial t$ are zero and the work done by the pressure gradient balances the dissipation of kinetic energy by the mean flow and by the disturbance; thus

$$-\iint \bar{u}\frac{\partial \bar{p}}{\partial x}\,dx\,dy = \mu\iint\left[\left(\frac{\partial \bar{u}}{\partial y}\right)^2 + \left(\frac{\partial v'}{\partial x} - \frac{\partial u'}{\partial y}\right)^2\right]dx\,dy \quad (19)$$

for a mean flow and neutral finite disturbance. The statement in reference 1 that two-dimensional flows are stable is thus seen to arise from an incomplete analysis of the mutual interdependence of the mean and harmonic terms in the nonlinear system of equations. To put it in a more descriptive physical way, neither the deformation of the mean flow by the Reynolds stress of the disturbance, nor the effect of the *modification* of the mean flow on the disturbance flow are taken into account.

In a paper dealing with the stability of flow in a circular pipe, Thomas[3] makes the same implicit assumption as Pai. His argument that the flow in a pipe is always stable against finite or infinitesimal disturbances is similarly invalidated. In this case the question of stability or instability for infinitesimal disturbances is still open, although the work of Pretsch and Sexl suggests stability. The case of a finite disturbance has not been treated theoretically.

Another approach to the problem has been used by Theodorsen[4] who bases his treatment of the stability of two-dimensional flows against two-dimensional disturbances on the rate of change of the integral of the square of the vorticity. The vorticity ω in a two-dimensional flow is given by

$$(\partial\omega/\partial t) + u(\partial\omega/\partial x) + v(\partial\omega/\partial y) = \nu\nabla^2\omega \quad (20)$$

or alternatively by

$$(\partial\omega/\partial t) + \boldsymbol{q}\cdot\nabla\omega = \nu\nabla^2\omega \quad (21)$$

where $\boldsymbol{q}$ is the velocity (u, v).

It is assumed in reference 3 that the mean motion of the Orr-Sommerfeld flow is given by

$$\nabla^2\bar{\omega} = 0 \tag{22}$$

where the bar denotes average with distance x; thus the mean value of the quadratic disturbance terms is neglected. The terms omitted represent the vorticity transfer between mean motion and disturbance motion by a process of convective stretching of vorticity, and if they are accounted for, the mean vorticity equation reads

$$(\partial\bar{\omega}/\partial t) + \overline{\boldsymbol{q}'\cdot\nabla\omega'} = \nu\nabla^2\bar{\omega} \tag{23}$$

where the dependence of $\bar{\omega}$ on t is retained to show any decay of the vorticity of the mean flow. As before, a prime denotes the perturbation. By consideration of the integral of the square of the total vorticity for the volume considered earlier, we obtain

$$W = \frac{\partial}{\partial t}\int\int\frac{1}{2}\omega^2 dx\,dy = \nu\int\int(\omega'\nabla^2\omega' + \bar{\omega}\nabla^2\bar{\omega})dx\,dy \tag{24}$$

the quadratic terms of integrating out for a periodic disturbance. Theodorsen sets $\nabla^2\bar{\omega} = 0$ as mentioned earlier, and obtains

$$W = \nu\iint\omega'\nabla^2\omega' dx\,dy \tag{25}$$

Apart from omitting the term $\bar{\omega}\nabla^2\bar{\omega}$ in the vorticity integral (24), Theodorsen also states that Eq. (25) represents *dissipation* of vorticity and therefore concludes that two-dimensional Orr-Sommerfeld flows are stable for two-dimensional disturbances of finite or infinitesimal amplitude. However, Eq. (25) does not represent only decay of vorticity, for, with the periodic disturbance mentioned earlier, Eqs. (4) and (5), Eq. (25) may be written

$$\int\int\omega'\nabla^2\omega' dx\,dy = \int_x\left[\frac{\partial}{\partial y}\left(\frac{\partial u'}{\partial y}\right)^2\right]_{y=h} dx - \int\int\left[\left(\frac{\partial\omega'}{\partial x}\right)^2 + \left(\frac{\partial\omega'}{\partial y}\right)^2\right]dx\,dy \tag{26}$$

The first integral is assumed to be positive on physical grounds, since it represents the *generation* of vorticity at the walls; the second integral gives the decay of vorticity within the volume due to viscous action. It appears that the integral giving the vorticity generation was not accounted for in the conclusion given in reference 3.

Eq. (24) may be rewritten in mean and disturbance parts ($W = \bar{W} + W'$) for the periodic disturbance Eqs. (4) and (5) in the form

$$\bar{W} = \frac{\partial}{\partial t}\int\int\frac{1}{2}\bar{u}^2\,dx\,dy = -\int\int\bar{\omega}\,\overline{\boldsymbol{q}'\cdot\nabla\omega'}\,dx\,dy + \nu\int_x\left[\frac{\partial}{\partial y}\left(\frac{\partial\bar{u}}{\partial y}\right)^2\right]_{y=h} dx - \nu\int\int\left[\left(\frac{\partial\bar{\omega}}{\partial x}\right)^2 + \left(\frac{\partial\bar{\omega}}{\partial y}\right)^2\right]dx\,dy \tag{27}$$

$$W' = \frac{\partial}{\partial t}\int\int\frac{1}{2}\omega'^2 dx\,dy = \int\int\bar{\omega}\overline{\boldsymbol{q}'\cdot\nabla\omega'}\,dx\,dy + \nu\int_x\left[\frac{\partial}{\partial y}\left(\frac{\partial u'}{\partial y}\right)^2\right]_{y=h} dx - \nu\int\int\left[\left(\frac{\partial\omega'}{\partial x}\right)^2 + \left(\frac{\partial\omega'}{\partial y}\right)^2\right]dx \tag{28}$$

On the right-hand sides of Eqs. (27) and (28), the first integral represents the convective vorticity transfer between mean and disturbance flows, the second integral the generation of vorticity at the boundary, and the third integral the dissipation of vorticity within the volume. On addition of Eqs. (27) and (28) and use of Eq. (26) and its mean-vorticity analog, Eq. (24) is again obtained. Eqs. (27) and (28) illustrate the physical processes contributing to the growth or decay of a disturbance in a fluid, and a conclusion of stability or instability does not appear possible without proper solution of the equations of motion. In this connection, the work of Meksyn and Stuart[2] is relevant; and their conclusion is that pressure flow between parallel planes is unstable for finite disturbances.

References

[1] Pai, S. I., *On the Stability of Parallel Flows with Respect to Periodic Disturbances*, Journal of the Franklin Institute, Vol. 259, No. 3, p. 197, March, 1955.

[2] Meksyn, D., and Stuart, J. T., *Stability of Viscous Motion Between Parallel Planes for Finite Disturbances*, Proc. Roy. Soc., Series A, Vol. 208, p. 517, 1951.

[3] Thomas, T. Y., *Qualitative Analysis of the Flow of Fluid in Pipes*, American Journal of Mathematics, Vol. 64, p. 754, 1942.

[4] Theodorsen, T., *Mechanism of Turbulence*, Proc. of Second Midwestern Conf. on Fluid Mechanics, Ohio, 1952.

Generalized Crippling Analysis of Formed Sections

George Gerard

Assistant Director, Research Division, College of Engineering, New York University

July 1, 1955

Introduction

THE PURPOSE of this note is to report briefly on a new method of crippling analysis of formed sections. This method has resulted from work sponsored by the National Advisory Committee for Aeronautics and is presented in detail in a report submitted to the NACA.

Most crippling methods in current use involve subdivision of the cross section of the formed section into a series of plates[1] or angle sections.[2] The crippling stress of the section is obtained as a weighted average of the crippling stresses of the subdivided elements.

The method described herein is empirical in nature, as are the other methods, but does not require the subdivision of the cross section into elements. The geometric parameters required for the analysis are the developed length-thickness ratio, A/t^2, and the number of corners of the cross section. In a sense, the method is a generalization of the work of Schuette,[3] Gallaher,[4] and Needham[2] on formed Z and channel sections.

Symbols

A = cross-sectional area, in.^{2}
b_w = web width, in.
c = number of corners
E = elastic modulus, lbs. per sq. in.
f = cladding thickness as a fraction of total plate thickness
t = thickness, in.
$\bar{\eta}$ = cladding reduction factor; $\bar{\eta} = \dfrac{1 + 3(\sigma_{cl}/\sigma_{cr})f}{1 + 3f}$
σ_{cl} = cladding yield stress, ksi
σ_{cr} = buckling stress, ksi
σ_{cy} = compressive yield stress, ksi
$\bar{\sigma}_{cy}$ = compressive yield stress of formed corner, ksi
$\bar{\sigma}_f$ = crippling stress, ksi

Equal Flange Z and Channel Elements

In order to demonstrate the method of analysis, a large mass of test data[3, 4] on equal flange Z and channel formed sections is shown in Fig. 1. The following relations gave a good fit to the test data:

(a) For $\bar{\sigma}_f/\sigma_{cy} \leq 2(t/b_w)^{1/3}$

$$\bar{\sigma}_f/\sigma_{cy} = \beta[(t^2/A)\,(\bar{\eta}E/\sigma_{cy})^{1/3}]^{0.75} \tag{1}$$

(b) For $\bar{\sigma}_f/\sigma_{cy} > 2(t/b_w)^{1/3}$

$$\bar{\sigma}_f = \sigma_{cr} \tag{2}$$

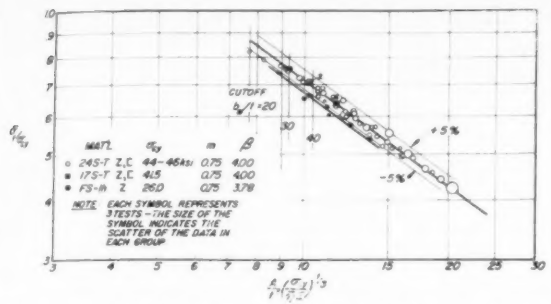

FIG. 1 Generalized crippling analysis of formed Z and channel sections.

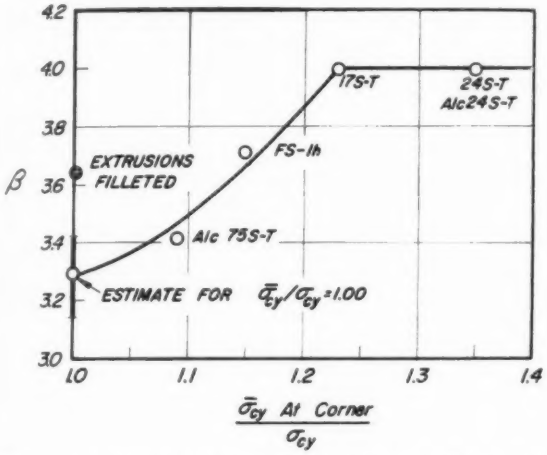

FIG. 2. Variation of the generalized crippling coefficient with the increased corner properties.

SHAPE	t	a	b	c
E1	0.0252"	1.991"	0.653"	0.961"
E2	0.0253	1.032	0.492	0.844
E3	0.0504	2.141	0.418	1.028
E4	0.0255	1.213	0.408	0.935

t
0.025"
0.040
0.064

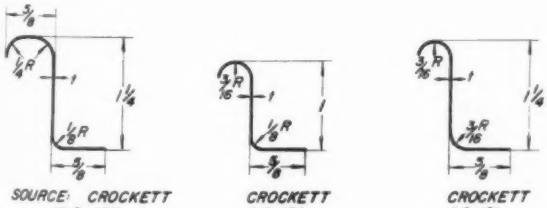

t
0.025"
0.040

FIG. 3. Dimensions of two-corner formed sections used for analysis.

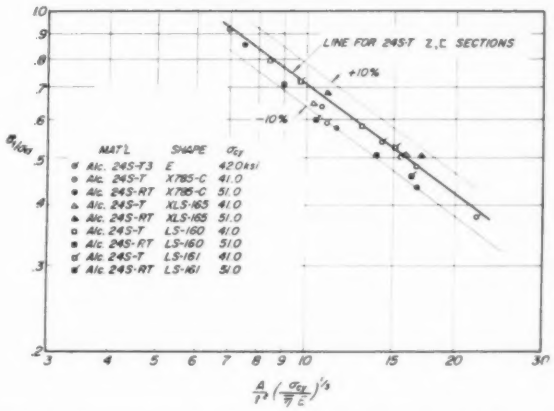

FIG. 4 Generalized crippling analysis of two-corner formed sections.

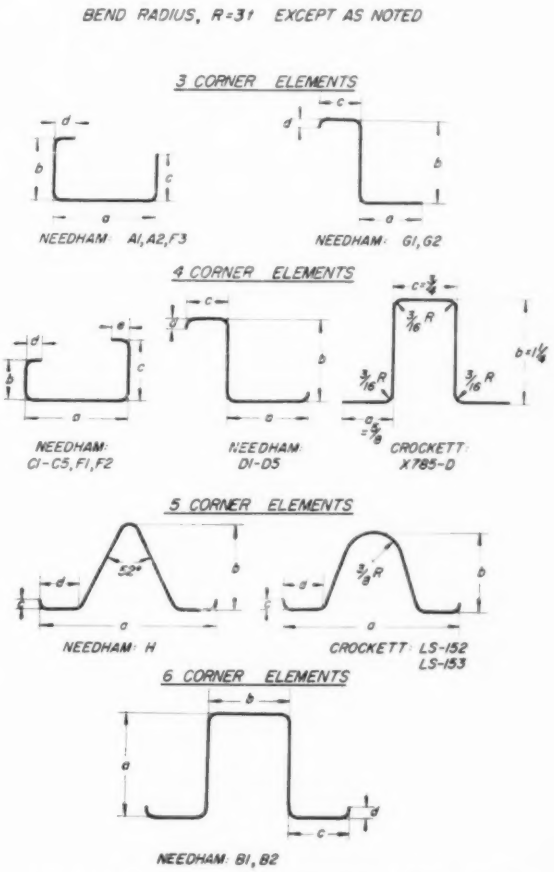

FIG. 5. Multicorner formed sections used for analysis

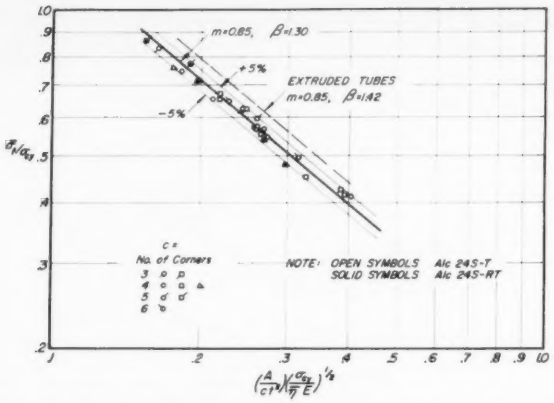

FIG. 6. Generalized crippling analysis of multicorner formed sections.

The value of the generalized crippling coefficient, β, depends upon the increased yield properties, $\bar{\sigma}_{cy}$, in the corners of formed sections. The variation of β as a function of $\bar{\sigma}_{cy}/\sigma_{cy}$ for equal flange Z and channel sections is shown in Fig. 2.

TWO-CORNER ELEMENTS

Available test data on two-corner elements shown in Fig. 3 were correlated according to the parameters of Eq. (1). The test data are shown in Fig. 4 from which it can be observed that Eq. (1) for equal flange Z and channel sections is in good agreement with other two-corner elements.

MULTICORNER ELEMENTS

Elements with three or more corners generally tend to behave in a manner similar to that of a thin-walled tube. The multicorner elements shown in Fig. 5 were correlated according to

$$\bar{\sigma}_f/\sigma_{cy} = \beta[(ct^2/A)\,(\bar{\eta}E/\sigma_{cy})^{1/2}]^{0.85} \qquad (3)$$

with the results shown in Fig. 6. It can be observed that good agreement exists.

With the limited test data available, it was not possible to establish a variation of β with $\bar{\sigma}_{cy}/\sigma_{cy}$ for multicorner sections. Also, it was not possible to establish a suitable cutoff for Eq. (3). However, beyond $\bar{\sigma}_f/\sigma_{cy} = 3/4$, Eq. (2) is probably of sufficient accuracy for most cases.

CONCLUDING REMARKS

The publication of these results is intended to stimulate further checks of the generalized analysis with the extensive test data available in the test reports of the aircraft industry. It is hoped that such data can be made available to the author for inclusion in later reports. Aside from the simplicity of the method, further verification can result in a substantial reduction of crippling tests both at room and elevated temperatures. It is to be noted that this method of analysis applies equally well to extruded sections by using appropriate value of β in Eqs. (1) and (3).

REFERENCES

[1] Crockett, H. B., *Predicting Stiffener and Stiffened Panel Crippling Stresses*, Journal of the Aeronautical Sciences, Vol. 9, No. 13, pp. 501–509, November, 1942.

[2] Needham, Robert A., *The Ultimate Strength of Aluminum-Alloy Formed Structural Shapes in Compression*, Journal of the Aeronautical Sciences, Vol. 21, No. 4, pp. 217–229, April, 1954.

[3] Schuette, E. H., *Observations of the Maximum Average Stress of Flat Plates Buckled in Edge Compression*, NACA TN 1625, February, 1949.

[4] Gallaher, G. L., *Plate Compressive Strength of FS-1h Magnesium Alloy Sheet and a Maximum Strength Formula for Magnesium-Alloy and Aluminum-Alloy Formed Sections*, NACA TN 1714, October, 1948.

The Transonic Flow Hydraulic Analogy

R. A. A. Bryant
Lecturer in Mechanical Engineering,
The New South Wales University of Technology, Sydney, Australia
July 6, 1955

THE PURPOSE OF THIS NOTE is to comment briefly on a recent article by Fleddermann and Stancil.[1] As stated by these authors, there is a continued interest in the hydraulic analogy, and work is currently being carried out in several countries.

It is a simple matter to demonstrate that a mathematical analogy exists for unsteady rotational gas flow without shocks; as soon as shock phenomena are included in the analogy, however, it is necessary to pay particular attention to the conditions under which a physical analogy can be obtained from this mathematical analog. In fact, as has already been implied by Laitone,[2] it is not possible to construct an exact physical analogy to satisfy the mathematical analog at all Mach Numbers.

A mathematical study has recently been made here to re-evaluate the validity of the analogy and bring to light those factors needing particular attention when carrying out physical research with the water table. Besides the conditions mentioned by Laitone, we found that shock phenomena have a very important effect on the downstream flow. It is well known that in passing through a curved shock an originally irrotational gas flow becomes rotational downstream of the shock; no exact quantitative relationship could be demonstrated between the vorticity distributions in the two cases. In fact, it is doubtful whether much more than an overall qualitative correspondence can exist since curl $\underset{\sim}{V}$ in the physical water flow will have finite components not normal to the plane of the water surface whereas in the gas flow curl $\underset{\sim}{V}$ will, by assumption, always be normal to the flow plane.

From the work carried out here, it appears that the use of the water table for studying transonic phenomena, must be based on an a priori assumption of validity. Consequently one is continually faced with the problem of verifying experimental results by correlating them with either gas dynamics or analytical data; this situation has to be overcome before the water table can be accepted as a satisfactory research tool, and, as a result, current work on the analogy should be aimed at explaining experimental discrepancies. Fleddermann and Stancil,[1] while endeavoring to make a plausible explanation of some experimental results, have apparently failed to realize that the water flow downstream of the bow wave *Must* be physically different from the corresponding gas flow, as has already been mentioned.

Furthermore, in making their comparison with Guderley's theory they have tacitly assumed that their method of transferring water table results is satisfactory. This is not the case since their Eq. (1) does not take into account the discontinuity conditions existing across the bow wave and is not accurate due to the general adoption of the square of the water depth ratio for the pressure ratio in the hydraulic gas.[3] The equations given by Harleman and Ippen (page 6 of reference 3) are also in error in this respect and require modification to take into account state changes across the bow wave. Unless such modifications are made it is fruitless to proceed further with the explanation of experimental discrepancies.

It should be noted that, in transferring the pressure coefficients from the hydraulic gas to air as outlined by Crossley and Harleman,[4] a stretching factor must be introduced when considering points in the flow outside the boundaries. Such stretching is also applicable to the shock geometry so that a complete transformation of the whole flow field is brought about in changing from $\gamma = 2$ to $\gamma = 1.4$. Also, the pressure coefficients in the stagnation zone cannot be transferred as the method does not then apply.

REFERENCES

[1] Fleddermann, Richard G., and Stancil, Robert T., *Wedge Pressure*

Coefficients in Transonic Flow by Hydraulic Analogy, Journal of the Aeronautical Sciences, Readers' Forum, Vol. 22, No. 4, pp. 271–273, April, 1955.

[2] Laitone, E. V., *A Study of Transonic Gas Dynamics by the Hydraulic Analogy*, Journal of the Aeronautical Sciences, Vol. 19, No. 4, pp. 265–272, April, 1952.

[3] Harleman, Donald R. F., and Ippen, Arthur T., *Mémoires sur la Mécanique des Fluides offerts à Dimitri Riabouchinsky à l'occasion de son Jubilé Scientifique*, "The Range of Application of the Hydraulic Analogy in Transonic and Supersonic Aerodynamics": Publications Scientifiques et Techniques du Ministère de l'air.

[4] Crossley, Harry, E., and Harleman, Donald R. F., *Studies on the Validity of the Hydraulic Analogy to Supersonic Flow*, Massachusetts Institute of Technology Hydrodynamics Laboratory, T.R. No. 11, December, 1952.

The Forces on the General Slender Body of Elliptic Cross Section in Supersonic Flow

H. Portnoy*
Imperial College of Science and Technology, University of London, England
July 7, 1955

Introduction

Special cases of the slender body of elliptic cross section have been dealt with by Ward,[1] Fraenkel,[2] and Kahane and Solarski.[3] Ward considered a smooth pointed body, whose surface near the base was that of an elliptic cylinder, and did not consider the thickness problem in detail. Fraenkel considered a body with elliptic sections of constant eccentricity, having their major axes parallel, but allowed a finite number of discontinuities in longitudinal profile slope spaced well apart, while Kahane and Solarski investigated a smooth, pointed symmetrical body whose elliptic sections could have a variation of eccentricity along the axis, and whose incidence was zero.

In the present note, the results of reference 4 are applied to the case of a slender body with a finite number of well-spaced discontinuities, and having elliptic sections which may have varying eccentricities, and may be displaced and rotated in any manner.

The work of reference 4 reduced the problem of finding the forces on any slender body with a finite number of discontinuities in longitudinal profile slope, to one of finding a two-dimensional harmonic potential $\phi_h = Re(w)$ in planes just before and just after each discontinuity. Let Ox, Oy, Os be a right-handed system of axes with Os lying in the direction of the undisturbed stream, and with O at the center of area of the nose section of the body. Let ν denote the normal to a section of the body in a plane s = constant, τ the circumferential variable, $d\nu/ds$ the streamwise slope, $S(s)$ the body cross-sectional area at the station of the plane, and t the body thickness parameter. Then ϕ_h must satisfy the boundary conditions

$$\partial\phi_h/\partial\nu = d\nu/ds \tag{1}$$

and

$$\lim_{r\to\infty}\left(\phi_h - \frac{S'(s)}{2\pi}\log r\right) = 0 \tag{2}$$

in its plane.

The Harmonic Potential ϕ_h

Consider a cross section of the body at some station s (see Fig. 1). Let the x_1- and y_1-axes be the principal axes of the cross section, so that

$$z = -g(s)e^{i\eta(s)} + z_1 e^{i\psi(s)} \tag{3}$$

where

$$z = x + iy \qquad z_1 = x_1 + iy_1$$

and let the surface of the body be defined by

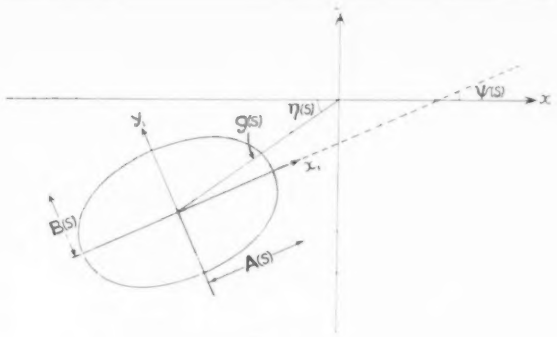

Fig. 1.

$$x_1 = A(s)\cos u + O(t^3)$$
$$y_1 = B(s)\sin u + O(t^3)$$

i.e., by

$$z = -ge^{i\eta} + e^{i\psi}(A\cos u + iB\sin u) + O(t^3) \tag{4}$$

Now for a body defined parametrically in the form

$$x = x(u, s) \qquad y = y(u, s) \qquad \text{or} \qquad z = z(u, s)$$

it is readily shown, by considering the direction ratios, that if u increases counterclockwise,

$$\frac{d\nu}{ds} = \frac{x_s y_u - y_s x_u}{(x_u^2 + y_u^2)^{1/2}} = Im\,\frac{\bar{z}_s z_u}{|z_u|}$$

Hence, in the present case,

$$\frac{d\nu}{ds} = Im\,\{[-g'e^{-i\eta} + i\eta' g e^{-i\eta} - i\psi' e^{-i\psi}(A\cos u - iB\sin u) + e^{-i\psi}(A'\cos u - iB'\sin u)]\,[e^{i\psi}(-A\sin u + iB\cos u)]\,[A^2\sin^2 u + B^2\cos^2 u]^{-1/2}\}$$

$$= \left[\frac{S'}{2\pi} + C\cos u + D\sin u + I\cos 2u + J\sin 2u\right][A^2\sin^2 u + B^2\cos^2 u]^{-1/2} \tag{5}$$

where

$$\left.\begin{aligned} S'(s) &= \pi(AB' + A'B) = (d/ds)(\pi AB)\\ C(s) &= -B[g'\cos(\psi - \eta) + \eta' g\sin(\psi - \eta)]\\ D(s) &= -A[-g'\sin(\psi - \eta) + \eta' g\cos(\psi - \eta)]\\ I(s) &= (1/2)(A'B - AB') = (1/2)B^2(d/ds)(A/B)\\ J(s) &= (1/2)\psi'(A^2 - B^2) \end{aligned}\right\} \tag{6}$$

If we now make the transformation

$$\left.\begin{aligned} z_1 &= \zeta + \frac{A^2(\sigma) - B^2(\sigma)}{4\zeta}\\ s &= \sigma \end{aligned}\right\} \tag{7}$$

where $\zeta = \lambda e^{i\mu}$, then on the body

$$\lambda = \lambda_b = \frac{A + B}{2} \qquad \mu = u$$

$$\left|\frac{dz_1}{d\zeta}\right| = \frac{1}{\lambda_b}(A^2\sin^2\mu + B^2\cos^2\mu)^{1/2} \tag{8}$$

and the boundary condition on the body becomes

$$\frac{\partial\phi_h}{\partial\lambda} = \frac{d\nu}{ds}\left|\frac{dz_1}{d\zeta}\right| = \frac{1}{\lambda_b}\left\{\frac{S'}{2\pi} + C\cos\mu + D\sin\mu + I\cos 2\mu + J\sin 2\mu\right\}$$

Hence the solution is

* The author would like to express his sincere thanks to L. E. Fraenkel, who supervised this work, for his assistance.

$$\left.\begin{aligned}\phi_h &= Re\left\{\frac{S'}{2\pi}\log\zeta - \lambda_h\frac{(C+iD)}{\zeta} - \frac{1}{2}\lambda_h{}^2\frac{(I+iJ)}{\zeta^2}\right\}\\ &= \frac{S^1}{2\pi}\log\lambda - \frac{\lambda_h}{\lambda}(C\cos\mu + D\sin\mu) - \\ &\qquad \frac{1}{2}\frac{\lambda_h{}^2}{\lambda^2}(I\cos 2\mu + J\sin 2\mu)\end{aligned}\right\} \quad (9)$$

The Drag Force

The expression for the drag found in reference 4 is

$$\frac{D}{(1/2)\rho U^2} = \frac{1}{2\pi}{}^*\int_{\sigma=0-}^{l+}\int_{s=0-}^{l+}\log\frac{1}{|s-\sigma|}\,dS'(s)dS'(\sigma) + \sum_{i=0}^{m}\left\{\frac{1}{2\pi}(\Delta S_i')^2\log\frac{2}{\beta} + \oint_{C_i}\left[(\phi_h)_{s=e_i-}\left(\Delta\frac{dv}{ds}\right)_i - (\Delta\phi_h)_i\left(\frac{dv}{ds}\right)_{s=e_i+}\right]d\tau\right\} + O(t^3) \quad (10)$$

where * denotes the finite part of the double Stieltjes integral; l is the total length of the body; $\beta = \sqrt{(M^2-1)}$; ρ and U are the free-stream density and velocity respectively, and $s = e_i$ is the position of a discontinuity, where $e_0 = 0$ and $e_m = l$. Also, C_i represents the body contour at $s = e_i$ (the body radius being continuous in our case), and

$$\Delta f_i = (f)_{s=e_i+} - (f)_{s=e_i-}$$

Since the same "ζ" transformation applies for $(\phi_h)_{s=e_i+}$ and $(\phi_h)_{s=e_i-}$, and since

$$\frac{dv}{ds}\delta\tau = \frac{\partial\phi_h}{\partial v}\delta\tau = \frac{\partial\phi_h}{\partial\lambda}\left|\frac{d\zeta}{dz_1}\right|\left|\frac{dz_1}{d\zeta}\right|\lambda_h\delta\mu = \frac{\partial\phi_h}{\partial\lambda}\lambda_h\delta\mu,$$

$$\oint_{C_i}\left[(\phi_h)_{s=e_i-}\left(\Delta\frac{dv}{ds}\right)_i - (\Delta\phi_h)_i\left(\frac{dv}{ds}\right)_{s=e_i+}\right]d\tau$$

$$= \int_0^{2\pi}\left[(\phi_h)_{\sigma=e_i-}\left(\Delta\frac{\partial\phi_h}{\partial\lambda}\right)_i - (\Delta\phi_h)_i\left(\frac{\partial\phi_h}{\partial\lambda}\right)_{\sigma=e_i+}\right]_{\lambda=\lambda_h}\lambda_h d\mu$$

$$= \frac{(\Delta S_i')^2}{2\pi}\log\left(\frac{2}{A+B}\right)_{s=e_i} + \pi\left[(\Delta C_i)^2 + (\Delta D_i)^2 + \frac{1}{2}(\Delta I_i)^2 + \frac{1}{2}(\Delta J_i)^2\right] \quad (11)$$

The drag is immediately obtained on substituting Eq. (11) in Eq. (10).

The Complex Lateral Force

As the profile radius is continuous here, the expression for the complex lateral force $F(s) = X(s) + iY(s)$ up to a station s, far downstream of a discontinuity is, by reference 4,

$$[F(s)/(1/2)\rho U^2] = 4\pi a_1(s) + 2(d/ds)\,[z_g(s)S(s)] + O(t^4) \quad (12)$$

where a_1 is the coefficient of z^{-1} in the series form of w, $[\phi_h = Re(w)]$, and z_g is the complex coordinate of the center of area of the section.

In the present instance,

$$z_g = -ge^{i\eta}. \quad (13)$$

By using Eqs. (3) and (7), we obtain

$$\zeta = e^{-i\psi}(z + ge^{i\eta}) + O(1/z)$$

and so substitution in Eq. (9) gives

$$\phi_h = Re\left\{\frac{S^1}{2\pi}\log z + \left[\frac{S'}{2\pi}ge^{i\eta} - \lambda_b e^{i\psi}(C+iD)\right]\frac{1}{z} + O(1/z^2)\right\}$$

hence

$$[F(s)/(1/2)\rho U^2] = 4\pi[(S'/2\pi)ge^{i\eta} - \lambda_b e^{i\psi}(C+iD)] - 2S'ge^{i\eta} - 2S(g' + ig\eta')e^{i\eta} + O(t^4)$$

If we put

$$g' + ig\eta' = \alpha_e(s\,e^{i\delta(s)} \quad (14)$$

where α_e is the "equivalent incidence" at station s, we obtain

$$-4\pi\lambda_b e^{i\psi}(C+iD) = 2e^{i\psi}\,\alpha_e S\,[e^{i(\eta+\delta-\psi)} + (B/A)\cos(\eta+\delta-\psi) + i(A/B)\sin(\eta+\delta-\psi)]$$

and hence

$$[F(s)/(1/2)\rho U^2] = 2\alpha_e S e^{i\psi}\,[(B/A)\cos(\eta+\delta-\psi) + i(A/B)\sin(\eta+\delta-\psi)] + O(t^4) \quad (15)$$

The corresponding force coefficients are best found in the directions of the principal axes of the section at station s. Thus, if $C_{X_1}(s) = X_1(s)/(1/2\rho U^2 S(s)$, etc.,

$$C_{X_1}(s) = 2\alpha_e(B/A)\cos(\eta+\delta-\psi) + O(t^2);$$
$$C_{Y_1}(s) = 2\alpha_e(A/B)\sin(\eta+\delta-\psi) + O(t^2) \quad (16)$$

If we put $s = l$ in Eq. (15) we obtain the total complex force on the body, and similarly $s = l$ in Eq. (16) gives the total force coefficients in the directions of the base axes.

The Complex Moment

In reference 4 the following is obtained:

$$M_z = M_x + iM_y = i\left[lF(l-) - \int_0^l F(s)\,ds\right] + O(t^4) \quad (17)$$

where moments are positive in the sense of a right-handed coordinate system. Here we have

$$\frac{M_z}{(1/2)\rho U^2} = lS(l\,e^{i\psi(l)}\,[iC_{X_1}(l) - C_{Y_1}(l)] - \int_0^l e^{i\psi(s)}S(s)[iC_{X_1}(s) - C_{Y_1}(s)]\,ds + O(t^4) \quad (18)$$

The Pressure Coefficient

The general expression for the pressure coefficient on the body is too complicated to be useful. In any particular case C_p may be calculated, far downstream of a discontinuity, using

$$C_p \sim -2\left(\frac{\partial\phi_h}{\partial\sigma} + \frac{\partial\phi_h}{\partial\lambda}\frac{\partial\lambda}{\partial s} + \frac{\partial\phi_h}{\partial\mu}\frac{\partial\mu}{\partial s}\right)_{\lambda=\lambda_h} - \left[\left(\frac{\partial\phi_h}{\partial\lambda}\right)^2 + \frac{1}{\lambda_h{}^2}\left(\frac{\partial\phi_h}{\partial\mu}\right)^2\right]\left|\frac{d\zeta}{dz_1}\right|^2_{\lambda=\lambda_h} - 2b_0'$$

where

$$b_0'(s) = \frac{1}{2\pi}\left[S''(s)\log\frac{\beta}{2} - \int_{\sigma=0-}^{s}\log(s-\sigma)dS''(\sigma) - \sum_{j=0}^{i}\Delta S_j'\frac{1}{s-e_j}\right] \quad \text{for} \quad e_i < s < e_{i+1} \quad (19)$$

References

[1] Ward, G. N., *Supersonic Flow past Slender Pointed Bodies*, Quart. J. Mech. and Applied Math., Vol. 2, No. 1, pp. 75–97, March, 1949.

[2] Fraenkel, L. E., *Supersonic Flow past Slender Bodies of Elliptic Cross-Section*, Aero. Res. Council Rep. 15166, 1952 (to be published as R & M 2954).

[3] Kahane, A., and Solarski, A., *Supersonic Flow about Slender Bodies of Elliptic Cross-Section*, Journal of the Aeronautical Sciences, Vol. 20, No. 8, pp. 513–521, August, 1953.

[4] Fraenkel, L. E., and Portnoy, H., *Supersonic Flow past Slender Bodies with Discontinuous Profile Slope*, Aeronautical Quarterly, Vol. 6, No. 2, pp. 114–124, May, 1955.

The Lift of a Blowing Wing in a Parallel Stream

D. A. Spence
Royal Aircraft Establishment, Farnborough, England

July 18, 1955

H. B. Helmbold[1] has derived downwash equations which relate the vorticity distribution on a thin airfoil with a

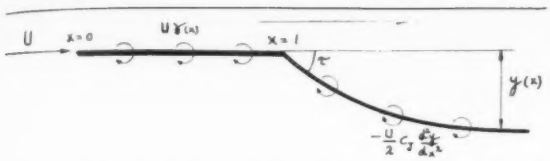

FIG. 1. Linearized representation of thin airfoil with deflected jet. U is the undisturbed stream velocity, $y(x)$ is the deflection ($+ve$ downwards) of the jet below the chord line. The airfoil extends from $x = 0$ to $x = 1$.

narrow high-velocity jet issuing from its trailing edge to the slope and curvature of the jet. We outline here the solution of these equations, for the lift induced on a thin uncambered wing at zero incidence when a thin jet, of momentum flux M, issues at a small downward angle τ from its trailing edge. This is slightly different from Helmbold's case of a wing at some incidence α, with a jet emerging tangentially at the trailing edge, but is governed by the same equations. In fact, the general case (incidence α, deflection τ) may be solved by the present method.

Downwash Equations

Defining a jet momentum coefficient $C_J = M/(1/2)\rho U^2$, the vortex strength ($+ve$ clockwise) per unit length may be written $U\gamma(x)$ on the air-foil, and may be shown to be $-(U/2)C_J(d^2y/dx^2)$ on the jet.

The downwash at a point x is therefore

$$-\frac{U}{2\pi}\int_0^1 \frac{\gamma(\xi)d\xi}{\xi - x} + \frac{UC_J}{4\pi}\int_1^\infty \frac{y''(\xi)d\xi}{\xi - x}$$

For x on the air-foil, the downwash is zero. For $x > 1$, it is $U(dy/dx)$. Thus we form the equations

$$\frac{1}{\pi}\int_0^1 \frac{\gamma(\xi)d\xi}{\xi - x} - \frac{1}{\pi}\frac{C_J}{2}\int_1^\infty \frac{y''(\xi)d\xi}{\xi - x} = 0 \quad (0 < x < 1) \tag{1}$$

$$-2(dy/dx) \quad (1 < x) \tag{2}$$

Reduction to Single Equation

The appropriate solution of Eq. (1) is

$$\gamma(x) = -\frac{C_J}{2}\frac{1}{\pi^2}\left(\frac{1-x}{x}\right)^{1/2}\int_0^1 \frac{d\xi}{\xi - x}\left(\frac{\xi}{1-\xi}\right)^{1/2} \times \int_1^\infty \frac{y''(\eta)}{\eta - \xi}\,d\eta \tag{3}$$

$$= -\frac{C_J}{2}\frac{1}{\pi^2}\left(\frac{1-x}{x}\right)^{1/2}\int_1^\infty \frac{y''(\eta)}{\eta - x}\,d\eta \times \int_0^1 \left(\frac{1}{\xi - x} - \frac{1}{\xi - \eta}\right)\left(\frac{\xi}{1-\xi}\right)^{1/2} d\xi \tag{4}$$

Now the following results hold

$$\frac{1}{\pi}\int_0^1 \frac{d\xi}{\xi - \sigma}\left(\frac{\xi}{1-\xi}\right)^{1/2} = 1 \quad (0 < \sigma < 1) \tag{5}$$

$$= 1 - \left(\frac{\sigma}{\sigma - 1}\right)^{1/2} \quad (\sigma > 1) \tag{6}$$

$$\frac{1}{\pi}\int_0^1 \frac{d\xi}{\xi - \sigma}\left(\frac{1-\xi}{\xi}\right)^{1/2} = -1 \quad (0 < \sigma < 1) \tag{7}$$

$$= -1 + \left(\frac{\sigma - 1}{\sigma}\right)^{1/2} \quad (\sigma > 1) \tag{8}$$

Thus using Eqs. (5) and (6)

$$\gamma(x) = -\frac{C_J}{2}\frac{1}{\pi}\left(\frac{1-x}{x}\right)^{1/2}\int_1^\infty \left(\frac{\eta}{\eta - 1}\right)^{1/2}\frac{y''(\eta)}{\eta - x}\,d\eta \tag{9}$$

Thus for $x > 1$, the left-hand side of Eq. (2) is*

$$-\frac{C_J}{2}\frac{1}{\pi^2}\int_0^1 \left(\frac{1-\xi}{\xi}\right)^{1/2}\frac{d\xi}{\xi - x}\int_1^\infty \left(\frac{\eta}{\eta - 1}\right)^{1/2}\frac{y''(\eta)}{\eta - \xi}\,d\eta - \frac{C_J}{2}\int_1^\infty \frac{y''(\xi)d\xi}{\xi - x}$$

$$= -\frac{C_J}{2}\frac{1}{\pi^2}\int_1^\infty \left(\frac{\eta}{\eta - 1}\right)^{1/2}\frac{y''(\eta)}{\eta - x}\,d\eta \int_0^1 \left(\frac{1-\xi}{\xi}\right)^{1/2} \times \left\{\frac{1}{\xi - x} - \frac{1}{\xi - \eta}\right\} d\xi - \frac{1}{\pi}\frac{C_J}{2}\int_1^\infty \frac{y''(\xi)d\xi}{\xi - x}$$

$$= -\frac{C_J}{2}\frac{1}{\pi}\left(\frac{x-1}{x}\right)^{1/2}\int_1^\infty \left(\frac{\eta}{\eta - 1}\right)^{1/2}\frac{y''(\eta)}{\eta - x}\,d\eta, \text{ using Eq. (8)}$$

$$= -2u'(x), \quad \text{by Eq. (2).} \tag{10}$$

Solution in Fourier Series

The governing equation, for the slope of the jet, is thus

$$\frac{C_J}{4}\frac{1}{\pi}\left(\frac{x-1}{x}\right)^{1/2}\int_1^\infty \left(\frac{\eta}{\eta - 1}\right)^{1/2}\frac{y''(\eta)}{\eta - x}\,d\eta = y'(x) \tag{11}$$

This may be solved by recognizing the logarithmic singularity in y'' at the trailing edge (cf. the spanwise loading on a wing with a part-span flap).

In order to construct a solution we may put

$$y'(x) = (4/C_J)\tan\tau\,[(1/\pi)F(x) + G(x)] \tag{12}$$

where

$$F(x) = -(2/x^{1/2})\log(x - 1) + 2\log[(x^{1/2} - 1)/(x^{1/2} + 1)] \tag{13}$$

$$F'(x) = (1/x^{3/2})\log(x - 1) \tag{14}$$

For this function,

$$\frac{1}{\pi}\left(\frac{x-1}{x}\right)^{1/2}\int_1^\infty \left(\frac{\eta}{\eta - 1}\right)^{1/2}\frac{F'(\eta)}{\eta - x}\,d\eta = \frac{\pi}{x^{3/2}} \tag{15}$$

Thus Eq. (11) becomes

$$\frac{1}{\pi}\left(\frac{x-1}{x}\right)^{1/2}\int_1^\infty \left(\frac{\eta}{\eta - 1}\right)^{1/2}\frac{G'(\eta)d\eta}{\eta - x} + \frac{1}{x^{3/2}} = \frac{4}{C_J} \times \left[\frac{1}{\pi}F(x) + G(x)\right] \tag{16}$$

This is now an equation for $G(x)$. To solve it, introduce a trigonometrical variable θ by means of

$$x = 1/\cos^2(\theta/2) \tag{17}$$

and seek a solution for which

$$\frac{d}{d\theta}G(\theta) = \sin\frac{\theta}{2}\sum_{n=0}^{\infty} A_n \cos n\theta \tag{18}$$

With $G(\theta)$ so defined, the Cauchy integral on the left of Eq. (16) becomes a standard form, and the equation is found to be

$$-A_0 \sin\frac{\theta}{2}\cos^2\frac{\theta}{2} - \cos^3\frac{\theta}{2}\sum_{n=1}^{\infty} A_n \sin n\theta + \cos^3\frac{\theta}{2} = \frac{4}{C_J}\frac{1}{\pi}F(\theta) + \frac{4}{C_J}\left(\cos\frac{\theta}{2}\sum_{n=0}^{\infty}\frac{2}{4n^2 - 1}A_n \cos n\theta + \sin\frac{\theta}{2}\sum_{n=1}^{\infty}\frac{4n}{4n^2 - 1}A_n \sin n\theta\right) \tag{19}$$

From this may be derived a series of linear equations for a finite set of the coefficients $A_0, A_1, A_2, \ldots$, either (1) by satisfying the equation at pivotal points $\theta = (m\pi/N)$, $m = 0, 1, 2, \ldots N$, or (2) by operating on the equation with

$$\int_0^\pi \cos\frac{\theta}{2}\cos m\theta\,d\theta, \qquad \text{for } m = 0, 1, 2, \ldots$$

i.e., by expressing each side as a Fourier cosine series and equating coefficients. Satisfactory results have been obtained by the former method, using six equations—points spaced at 30° in-

* I am indebted to Alan Billington of the Aeronautical Research Laboratories, Melbourne, Australia, for introducing me to this method of reduction.

tervals. The coefficients converged rapidly. For $C_J = 0.4$, it was found that $A_0 = -0.189$, $A_1 = 0.942$, $A_2 = -0.248$, $A_3 = 0.206$, $A_4 = -0.124$, and $A_5 = 0.065$.

Lift and Chordwise Loading

The total circulation is

$$\Gamma = U\int_0^1 \gamma(x)dx - \frac{C_J}{2}U\int_1^\infty y''(x)dx \tag{20}$$

By a series of manipulations similar to those of Eqs. (3) to (10), it is found that

$$\Gamma = -\frac{UC_J}{2}\int_1^\infty \left(\frac{\eta}{\eta-1}\right)^{1/2} y''(\eta)d\eta \tag{21}$$

$$= -2\pi U A_0 \tan\tau \tag{22}$$

This is the total lift, and includes that developed on the jet—$C_J \sin\tau$—which produces an equal lift on the internal ducting. Thus the lift involves A_0 only. This would be expected from the form of $y'(x)$. When the A_n satisfy Eq. (19), then

$$y'(x) = -\tan\tau\left(\cos^3\frac{\theta}{2} - A_0\sin\frac{\theta}{2}\cos^2\frac{\theta}{2} - \cos^3\frac{\theta}{2}\times\sum_{n=1}^{\infty}A_n\sin n\theta\right) \tag{23}$$

Since $(1/x) = \cos^2(\theta/2)$, the leading term for large x is $(A_0\tan\tau/x)$, corresponding to the above circulation.

Thus

$$C_L = -4\pi A_0\tan\tau \tag{24}$$

The chordwise vortex distribution may be shown to satisfy

$$\frac{\gamma(x)}{2\tan\tau} = -\frac{1}{\pi}\frac{\log(1-x)}{x^{3/2}} - \frac{1}{\pi}\left(\frac{1-x}{x}\right)^{1/2}\times\int_0^\pi \frac{\cos^2\frac{\theta}{2}\sum_{n=0}^{\infty}A_n\cos n\theta d\theta}{1-x\cos^2\frac{\theta}{2}} \tag{25}$$

for $0 < x < 1$. Putting $x = \cos^2(\phi/2)$ on the wing, this is

$$\frac{\gamma(x)}{2\tan\tau} = -\frac{1}{\pi x^{3/2}}\log(1-x) - \frac{1}{x^{1/2}}\times\left\{\frac{A_0}{1+\sin(\phi/2)} + \sum_{n=1}^{\infty}\frac{A_n}{[1+\sin(\phi/2)]^2}\left[\frac{1-\sin(\phi/2)}{1+\sin(\phi/2)}\right]^{n-1}\right\} \tag{26}$$

Thrust and Suction at Leading and Trailing Edges

Coefficients for the suction forces developed at the ends may be defined. At the leading edge a thrust of the amount given by

$$C_{SL}\,(\text{say}) = (\pi K^2/2)\tan^2\tau \tag{27}$$

is developed, where $K\tan\tau$ is the coefficient of the term $(1/x^{1/2})$ in the expression for $\gamma(x)$, i.e.,

$$K = (2/\pi) - [A_0 + (A_1/2)] \tag{28}$$

The total thrust on the wing is C_J; of this $C_J\cos\tau$ develops on the internal surface, C_{SL} at the leading edge, and the balance of the horizontal forces is brought about by a suction drag, given by

$$C_{ST}\,(\text{say}) \doteq (\pi K^2 - C_J)(\tau^2/2)$$

which develops at the trailing edge. The logarithmic singularity at the trailing edge is insufficient to produce a finite suction force, and it follows, as had been implicitly assumed in specifying the problem, that $C_{ST} = 0$. Hence, $\pi K^2 = C_J$, which may be verified for the results quoted above.

Reference

[1] Helmbold, H. B., *The Lift of a Blowing Wing in a Parallel Stream*, Journal of the Aeronautical Sciences, Vol. 22, No. 5, p. 341, May, 1955.

A Note on Methods for the Determination of Transient Stresses

J. W. Mar, T. H. H. Pian, and J. M. Calligeros
Aeronautical Engineering Department, Massachusetts Institute of Technology, Cambridge, Mass.
July 10, 1955

THE CLASSICAL METHOD[1] for the determination of dynamic stresses under a given transient disturbance is based upon the equations of motion which use the displacements of the normal modes as the so-called normal generalized coordinates.

$$M_r\ddot{\xi}_r + M_r\omega_r^2\xi_r = \Xi_r^D(t) + \Xi_r^M(\xi_1,\ldots,\dot{\xi}_1,\ldots,\ddot{\xi}_1,\ldots) \tag{1}$$

where

$r = 1, \ldots, m$ = rigid body modes
$r = m+1, \ldots n$ = deformation modes
$\Phi_r(x)$ = the mode shape of the rth mode
$\Xi_r^D(t)$ = the generalized force corresponding to the prescribed disturbing force
Ξ_r^M = the generalized force corresponding to the motion dependent forces

The displacement at x is given by

$$w(x) = \sum_{r=1}^{n}\Phi_r(x)\,\xi_r(t) \tag{2}$$

where $\xi_r(t)$ is the normal coordinate.

In a problem of this kind, the number of normal coordinates which are used to describe the system must be kept to some small number in order to make the solution of the normal equations of motion tractable.

There is still considerable labor involved in obtaining the transient stresses even after the major task of solving the equations of motion have been completed. Three methods are presently available for the determination of the transient stresses for systems which include motion-dependent forces. These shall be referred to as the force summation, mode displacement and mode acceleration methods, respectively. The force summation method is the most laborious to use but also contains the most accurate representation of all the forces, as will be demonstrated. The mode displacement method is the easiest to use but is not as accurate. The mode acceleration method as presented in the form given in references 1 and 2 is also laborious to use, but yields accuracy comparable to the force summation method. This note presents an alternative version of this last method and points out that in this version the mode acceleration method is actually very easy to apply. An analysis of the interrelations of the three different methods is also given.

The force summation method obtains the stress of a given point in the structure by superimposing the stresses due to the external disturbing forces, the inertia forces, and the motion-dependent forces. Such an analysis assumes the three types of forces to be statically applied at each instant of time. The normal coordinates, $\xi_r(t)$, are utilized to obtain the displacements, $w(x,t)$; velocities, $\dot{w}(x,t)$; and accelerations, $\ddot{w}(x,t)$; from which the inertia forces and the motion-dependent forces are obtained. It should be noted that the method which was referred to as mode acceleration method in reference 3 is actually the force summation method according to the definition in this note.

The mode displacement method obtains the transient stress merely by the superposition of the contributions from the normal modes which are used to represent the system and can be expressed as

$$\sigma_i = \sum_{r=m+1}^{n} A_i^{(r)}\xi_r(t) \tag{3}$$

where

σ_i = stress at point i
$A_i^{(r)}$ = stress at point i due to a unit displacement of the rth normal mode

The mode acceleration method is best explained by the following manipulation. Note that the equation of motion can be rearranged into the form

$$\xi_r(t) = (\Xi_r{}^D/M_r\omega_r{}^2) + (\Xi_r{}^M/M_r\omega_r{}^2) - (\ddot{\xi}_r/\omega_r{}^2) \qquad (4)$$

If this is substituted into Eq. (3) there results

$$\sigma_i = \sum_{r=m+1}^{n} A_i{}^{(r)} \frac{\Xi_r{}^D}{M_r\omega_r{}^2} + \sum_{r=m+1}^{n} A_i{}^{(r)} \frac{\Xi_r{}^M}{M_r\omega_r{}^2} - \sum_{r=m+1}^{n} A_i{}^{(r)} \frac{\ddot{\xi}_r}{\omega_r{}^2} \qquad (5)$$

It is recognized that the first term is the stress resulting from the static application of the external forces and hence it can be more completely obtained by elementary means than by a superposition of contributions from the normal modes. Thus, the mode acceleration method can be expressed as

$$\sigma_i = (\sigma_i)_{\text{static}} + \sum_{r=m+1}^{n} A_i{}^{(r)} \frac{\Xi_r{}^M}{M_r\omega_r{}^2} - \sum_{r=m+1}^{n} A_i{}^{(r)} \frac{\ddot{\xi}_r}{\omega_r{}^2} \qquad (6)$$

The term involving $\Xi_r{}^M$ is extremely laborious to calculate and, for example, it will contain convolution integrals when unsteady aerodynamics are important. For this reason, the mode acceleration method in this version is not practical for problems which contain motion-dependent forces as was stated in reference 1.

It should be recognized, however, that the normal equation of motion can be rearranged in the form

$$\xi_r - (\Xi_r{}^D/M_r\omega_r{}^2) = (\Xi_r{}^M/M_r\omega_r{}^2) - (\ddot{\xi}_r/\omega_r{}^2) \qquad (7)$$

If this is substituted into Eq. (6), there results the alternative version of the mode acceleration method.

$$\sigma_i = (\sigma_i)_{\text{static}} + \sum_{r=m+1}^{n} A_i{}^{(r)} \left(\xi_r - \frac{\Xi_r{}^D}{M_r\omega_r{}^2} \right) \qquad (8)$$

In this form, no new quantities need to be calculated since $\Xi_r{}^D$ the prescribed function which disturbs the system and ξ_r has already been calculated.

Obviously, if an infinite number of normal coordinates are used, the various methods will all yield the same answer.

An illustration of the difference between the force summation and mode acceleration methods is shown by considering a cantilever beam under a transient load $P(x)f(t)$. When the damping force due to motion can be considered as viscous the equations of motion are given by Eq. (1), in which

$$\Xi_r{}^D(t) = \int_0^l P(x)\Phi_r(x)dx \cdot f(t) \qquad (9)$$

$$\Xi_r{}^M = -\sum_{s=1}^{n} \frac{qa}{U} \int_0^l c(x)\Phi_r(x)\Phi_s(x)\, dx\, \dot{\xi}_s \qquad (10)$$

where q is the dynamic pressure, U the wind velocity, a the slope of lift curve, and $c(x)$ the local chord.

By using the mode acceleration method, the shear at x is given by

$$S(x) = [S(x)]_{\text{static}} - \sum_{r=1}^{n} A_r(x) \sum_{s=1}^{n} \frac{qa}{U} \int_0^l c(x)\Phi_r(x)\Phi_s(x)\, dx\, \dot{\xi}_s + \sum_{r=1}^{n} A_r(x) \frac{\ddot{\xi}_r}{\omega_r{}^2} \qquad (11)$$

where $A_r(x)$ is given by

$$A_r(x) = \omega_r{}^2 \int_x^l m(x)\Phi_r(x)dx \qquad (12)$$

By using the force summation method, the shear at x is given by

$$S(x) = [S(x)]_{\text{static}} - \sum_{r=1}^{n} (qa/U) \int_x^l c(x)\Phi_r(x)\, dx\dot{\xi}_r + \sum_{r=1}^{n} \int_x^l m(x)\Phi_r(x)\, dx\, \ddot{\xi}_r \qquad (13)$$

It can be seen that the difference between Eqs. (11) and (13) lies only in the second term. It can be proved, in fact, that

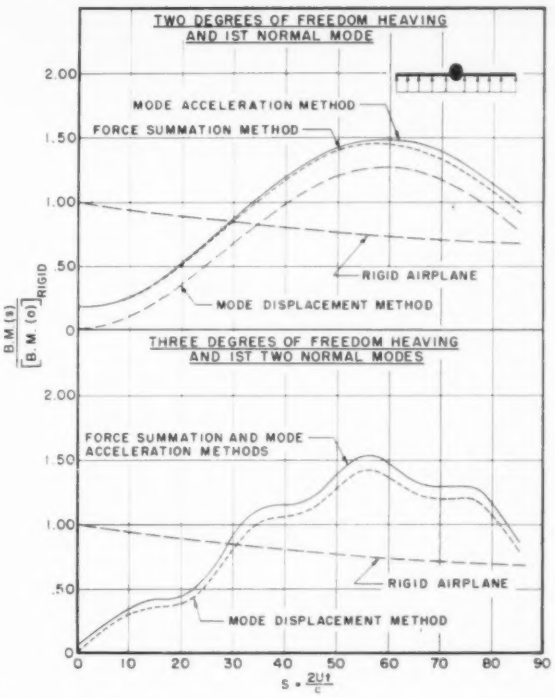

FIG. 1. Time history of bending moment at wing root due to unit step gust load.

$$\sum_{s=1}^{n} \frac{qa}{U} \int_x^l c(x)\Phi_s(x)\, dx\, \dot{\xi}_s = \sum_{r=1}^{\infty} \frac{A_r(x)}{M_r\omega_r{}^2} \sum_{s=1}^{n} \frac{qa}{U} \times \int_0^l c(x)\, \Phi_r(x)\, \Phi_s(x)\, dx\, \dot{\xi}_s \qquad (14)$$

by expanding the damping force $(qa/U)\, c(x)\Phi_s(x)\dot{\xi}_s$ into a series of normal loadings each having a distribution proportional to the inertia loading in the vibration mode. This is a clear indication that the force summation method given by Eq. (13) will lead to a more complete solution than that given by the mode acceleration method. It should also be noted that the two methods become the same when the generalized forces are independent of the motion of the system.

A comparison of the three different methods has been made on an idealized wing which consists of a uniform beam with a center mass to represent the fuselage. The disturbing function is a step-function gust loading uniformly distributed along the span. Two cases have been considered: in case A the heaving mode and the first vibration mode were chosen as the normal coordinates, and in case B the heaving mode and the first two vibration modes were chosen as the normal coordinates. The time histories of the bending moment at the wing root obtained by the three methods are shown in Fig. 1. It can be seen that the result by the force summation and mode acceleration methods are quite close together. In fact, in case B where two vibration modes are used, the two methods are indistinguishable from each other.

REFERENCES

[1] Bisplinghoff, R. L., Isakson, G., and Pian, T. H. H., *Methods in Transient Stress Analysis*, Journal of the Aeronautical Sciences, Vol. 17, No. 5, pp. 259–270, May, 1950.

[2] Bisplinghoff, R. L., Ashley, H., Halfman, R. L., and Mar, J. W., *Notes on a Survey Course in Aeroelasticity*, Department of Aeronautical Engineering, Massachusetts Institute of Technology, 1952. (See also, *Aeroelasticity*, Bisplinghoff, R. L., Ashley, H., and Halfman, R. L., to be published by Addison-Wesley.)

[3] Pian, T. H. H., and Winter, P. H., *Effect of Structural Flexibility on Aircraft Loading—Estimation of the Dynamic Overstress in Straight Wing Airplanes*, AFTR 6358, Part XVI, February, 1954.

Double and Triple Correlations Behind a Heated Grid

A. L. Kistler,* V. O'Brien,† and S. Corrsin‡
School of Engineering, The Johns Hopkins University, Baltimore, Md.
August 3, 1955

HOT-WIRE MEASUREMENTS have been made of some statistical properties of the (approximately isotropic) turbulence and temperature fluctuation fields downstream of a heated grid set perpendicular to a uniform air stream. The grid is 1-in. mesh of 1/4-in. wood dowel; heat is introduced by a 1-in. mesh network of #18 nichrome wire mounted just upstream of and aligned with grid dowels. The mean air speed is 14 ft. per sec. and the mean temperature rise in the air stream is 5° C.

Although the resulting temperature field is not satisfactorily uniform (the mean temperature has a standard deviation of 10 per cent about its spatial average in the central 70 per cent area of the air stream), some of the characteristic results may merit reporting.

A primary result is the relative decay rate of velocity and temperature fluctuations (u' and ϑ' respectively**). This difference, arising in essence from the vector-scalar difference between the two fields was discussed analytically in reference 1. The faired curve of Fig. 1 indicates a slower decay for the scalar field, apparently approaching quantitative agreement with the prediction,[1] $(d\vartheta'/\vartheta')/(du'/u') \simeq 3/5$, in the downstream region. A slightly modified analysis has been given in reference 2.

A comparison of temperature autocorrelation with longitudinal velocity autocorrelation is given in Fig. 2:

$$m(\xi) \equiv \frac{\overline{\vartheta(x)\vartheta(x+\xi)}}{\overline{\vartheta'(x)\vartheta'(x+\xi)}}; \qquad f(\xi) \equiv \frac{\overline{u(x)u(x+\xi)}}{\overline{u'(x)u'(x+\xi)}}$$

Most noteworthy is the rough equality of vertex curvatures and of general extent, hence of "microscales" and "integral scales." The latter is doubtless associated with the equality of thermal and momentum mesh sizes in the grid.

Fig. 3 illustrates the general resemblance of pertinent triple correlation coefficients,

$$k(\xi) \equiv \frac{\overline{u^2(x)u(x+\xi)}}{\overline{u'^2(x)u'(x+\xi)}}; \qquad p(\xi) \equiv \frac{\overline{u(x)\vartheta(x)\vartheta(x+\xi)}}{\overline{u'(x)\vartheta'(x)\vartheta'(x+\xi)}}$$

which enter the equations for f and m respectively.[1, 3]

This work is being supported by the National Advisory Committee for Aeronautics. Measurements with improved equipment are in progress.

References

[1] Corrsin, S., *The Decay of Isotropic Temperature Fluctuations in an Isotropic Turbulence*, Journal of the Aeronautical Sciences, Vol. 18, No. 6, pp. 417–423, June 1951.

[2] Kistler, A. L., O'Brien, V., and Corrsin, S., *Preliminary Measurements of Turbulence and Temperature Fluctuations Behind a Heated Grid*, NACA Res. Memo. 54D19, June, 1954.

[3] von Karman, T., and Howarth, L., *On the Statistical Theory of Isotropic Turbulence*, Proc. Roy. Soc. (London), A, Vol. 164, No. 917, January, 1938.

* Now, Pvt., U.S. Army, Ballistics Research Lab., Aberdeen Proving Ground.

† Aeronautics Dept.

‡ Chairman, Mechanical Engineering Dept.

** The prime denotes root mean square value. u is in the mean flow (x) direction.

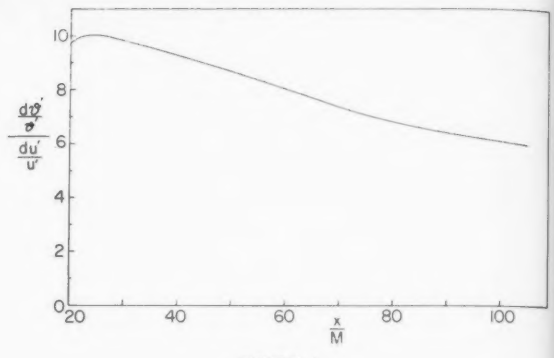

FIGURE 1

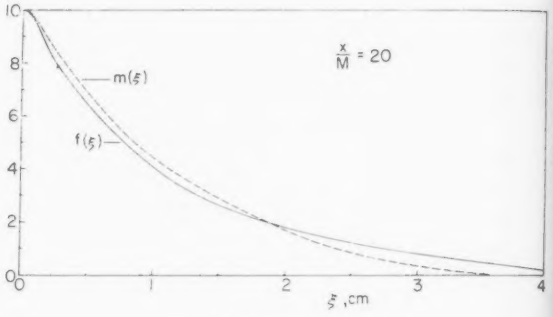

FIGURE 2

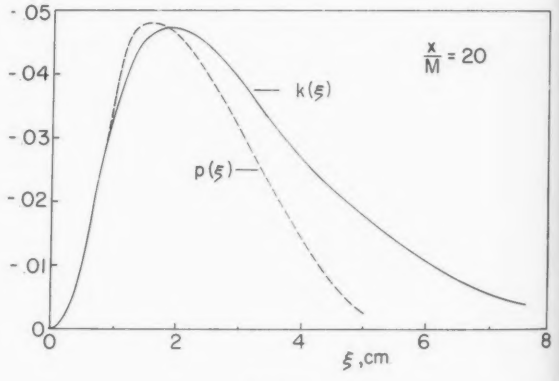

FIGURE 3

4

8